Tes. 023

Enhanced Solubility and Transport in Membrane/Copolymer Barrier Systems for Containment of Aromatics in Contaminated Groundwater

by

William Roy Haulbrook

Submitted to the Department of Chemical Engineering
in partial fulfillment of the requirements for the degree of
Doctor of Philosophy in Chemical Engineering

at the

MASSACHUSETTS INSTITUTE OF TECHNOLOGY

June 1993

Author .....
Department of Chemical Engineering
April 27, 1993

Certified by .....
Jefferson W. Tester
Professor of Chemical Engineering
Thesis Supervisor

Accepted by .....
Robert E. Cohen
Chairman, Committee for Graduate Students

Enhanced Solubility and Transport in Membrane/Copolymer Barrier Systems for Containment of Aromatics in Contaminated Groundwater

by
William Roy Haulbrook

Submitted to the Department of Chemical Engineering
on April 27, 1993 in partial fulfillment of the requirements
for the degree of Doctor of Philosophy in Chemical Engineering

Abstract

Effective management of groundwater contaminant plume migration needs new approaches that reduce or eliminate the inefficiencies of current treatment / containment methods such as pump-and-treat and concrete barrier containment. The system proposed in this work consists of hollow fiber membrane bundles, containing a copolymer solution, implanted directly into the aquifer of concern. Hydrophobic contaminant diffuses through the membrane and is solubilized by the amphipathic copolymer. The copolymer is retained within the membrane tube, and the contaminant-saturated copolymer solution may be intermittently flushed for copolymer regeneration and/or waste incineration. The system takes advantage of the high molecular weight (i.e. 1,000,000 g/mol), high organic solubilization capacity, non-toxicity, and low cost of the copolymer as well as the long-term nature of groundwater contaminant plume migration. The proposed system filters the contaminant from the groundwater as the plume slowly moves past the treatment area.

The objectives of this thesis were threefold -- first, to quantify the enhanced solubilization of several aromatic compounds in solutions of N-vinylpyrrolidone/styrene copolymer (NVPS); second, to measure the transmembrane diffusion rates of aromatic solute through polysulfone membrane into copolymer solution; and third, to demonstrate and model the proposed aromatic solute extraction system on a lab scale.

Values of polymer-water partition coefficient, K_{pw}, were obtained for systems of NVPS copolymer and the aromatic solutes toluene, naphthalene, and phenanthrene from solubility experiments. K_{pw} is defined as the mass of solute in polymer per mass polymer divided by the mass of solute in water per mass water. Values of log K_{pw} obtained were 3.39 ± 0.04, 3.38 ± 0.01, and 4.69 ± 0.02 (to a 95% confidence level) for toluene, naphthalene, and phenanthrene, respectively, in aqueous NVPS solution. A relationship between log K_{pw} and log K_{ow}, octanol-water partition coefficient, based on a Flory-Huggins activity coefficient model was proposed to extend predictive analysis to other solute-polymer systems.

Transmembrane diffusion rates of naphthalene and phenanthrene were determined from transport experiments with anisotropic polysulfone ultrafiltration membranes. Careful experimental set-up insured negligible transmembrane convection effects. Transport of solute from the exterior to the interior of the membrane tubes was determined by on-line concentration measurements using UV-VIS spectrophotometry. Values of total membrane resistance, R_{tot}, were determined from experiments using two different membranes. Measured values of R_{tot} agreed well with modeled values. The major source of molecular diffusive resistance was posed in all cases by the membrane support stucture, not the membrane skin itself. Although its pores are far more restricitve to diffusion than the support layer pores, the membrane skin layer posed negligible resistance due to its thinness (the skin layer was 0.1 to 0.2-μm thick, the support layer was 0.275-mm thick). The resistance posed by the interior and exterior fluid boundary layers was modeled in addition to the above membrane resistances.

The proposed groundwater solute extraction system was modeled on a laboratory scale using the solutes, copolymer, and membranes that were characterized in the solubility and transport experiments. The lab-scale extraction experiments involved a constant-temperature tank filled with Ottawa sand, designed to allow a constant, slow flow of aqueous solution from end to end. The tank dimensions were 50 cm length, 38 cm width, and 30 cm depth. One experiment demonstrated the decrease in naphthalene concentration of solution in a rectangular well in which the proposed extraction system operated. An aqueous solution of constant, saturated naphthalene concentration continuously flowed through the pre-naphthalene-saturated tank. The well naphthalene concentration was monitored via on-line UV-VIS spectrophotometry. A model for the decreased well concentration was posed. Another experiment demonstrated the movement of a naphthalene plume through and around a cylindrical well. Both the mixed well concentration and the 2-D concentration profile behind the well was modeled as a function of time, and concentration predictions agreed well with experimental data.

Finally, designs of various full-scale system applications were modeled to determine system feasibility. It was concluded that the proposed membrane/ copolymer system is a more effective contaminant barrier for contaminated aquifers with lower groundwater velocity, higher contaminant hydrophobicity, and higher soil organic carbon fraction. The modeled case studies show the proposed system is a promising means of contaminant remediation and containment for a wide variety of contaminated aquifers. Areas of further work needed for process development were suggested.

Thesis Supervisor: Professor Jefferson W. Tester

Title: Professor of Chemical Engineering

Acknowledgements

I thank my advisor, Professor Jefferson W. Tester, for his generous intellectual support during the completion of this project. I thank my committee members Professors William M. Deen, T. Alan Hatton, and Philip M. Gschwend for their support and guidance. I also appreciate the assistance of Jefferey L. Feerer and Patricia Hurter in this project. Also, thank you Phil Marrone, Gabe Worley, and the rest of the Thermo Group for providing interest in this work.

I thank Rev. Dr. Samuel Bombara and his family as well as the congregation of St. Paul Evangelical Church for their emotional and spiritual support throughout my stay in Boston.

I especially thank my family for their encouragement. This thesis is dedicated to them -- my brother Bob Haulbrook, and my father and mother, Roy and Hattie Haulbrook.

Table of Contents

List of Figures

List of Tables

1. Summary / Digest

1.1. Introduction

The world is faced today with a myriad of organic, metallic and radioactive chemical wastes. Many early disposal practices are now deemed inadequate, and chemical waste containment and remediation is becoming a necessity as more cases of groundwater contamination become apparent. The technology at present is underdeveloped, and remediation times and costs seem overwhelming. The Department of Energy has estimated the cost of remediation of the United States' contaminated nuclear weapons production sites alone at $130 billion, and remediation will take about 50 years (Crawford, 1989). These bleak figures prompt a movement to newer, less expensive, and more efficient technologies for hazardous waste site containment and remediation. This paper describes a new concept in hazardous waste site containment and remediation. The concept involves an aqueous amphipathic copolymer solution in hollow fiber membrane tubes placed in wells in the contaminated aquifer. Since the remediation takes place directly in the aquifer, the system allows cleanup without removal of contaminated soil to a treatment facility. The proposed technique offers containment of organic chemical waste and long-term, passive removal of the waste.

Figure 1-1 is a schematic of the proposed system. It shows a cross-sectional view of a region of contamination in an aquifer. As in many contaminated groundwater situations, it is important, first, to provide *containment* of the plume to prevent contaminant leaching to drinking water or irrigation supplies.

Figure 1-1: Proposed Barrier Concept

Cross-Sectional View

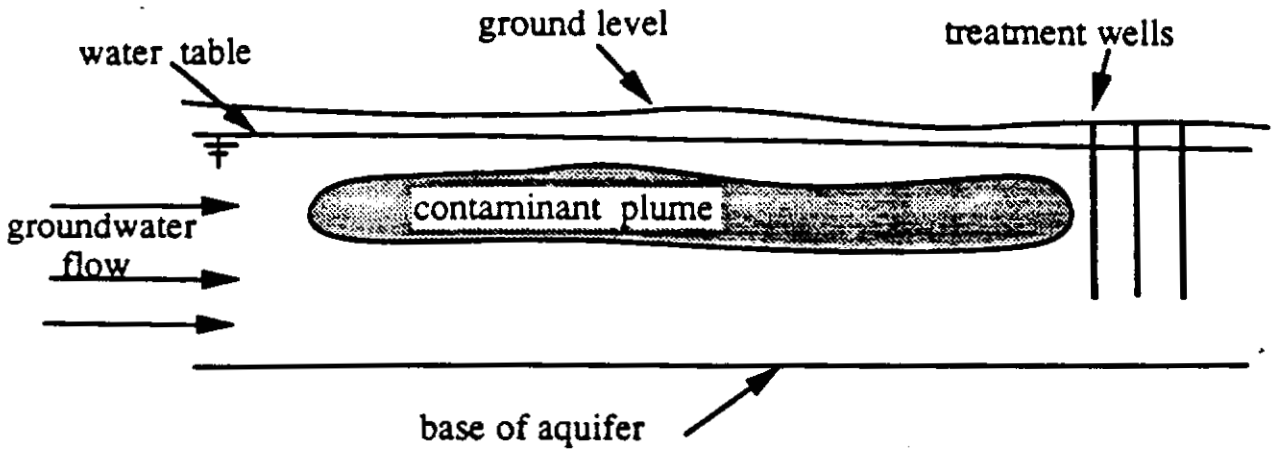

Overhead View

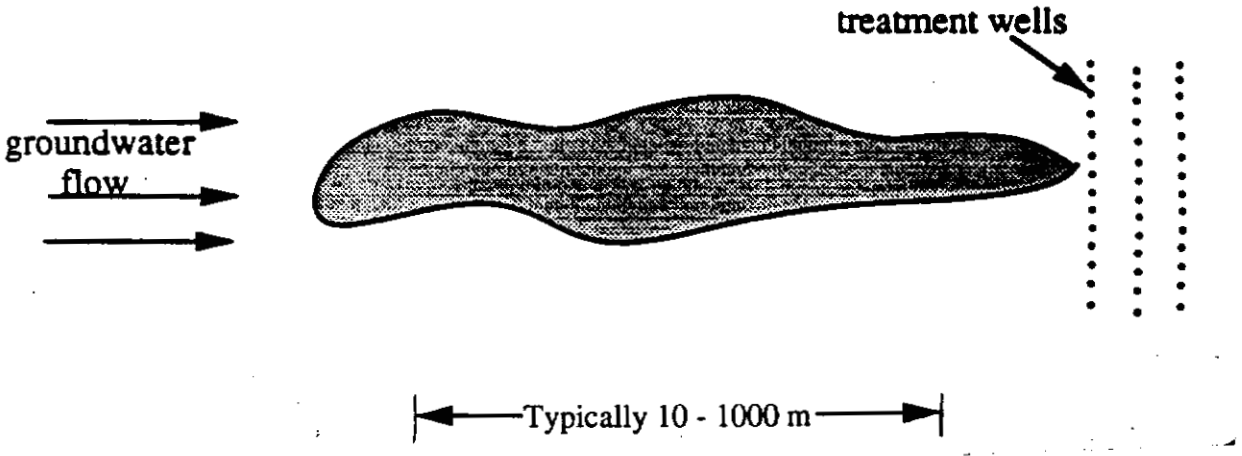

As pictured, the plume is located in the water-saturated region of the aquifer (below the water table) and is assumed to contain dissolved or suspended organic contaminant. In the case of a chemical spill of pure organic liquid (such as gasoline), there is generally a layer of the pure organic floating on the water table. This layer is most easily removed by pumping, but leaching of the organic to the groundwater up to that organic species' solubility in water will have taken place. Even though most organics have low solubility in water (such as PAH's and pesticides), many remain toxic at even lower levels. For example, the organic pesticies endrine, lindane, and toxaphene have water solubilities 0.2, 7, and 3 mg/L, respectively; but they are hazardous to human health at much lower concentrations – 0.0002, 0.004, and 0.005 mg/L, respectively (Freeze and Cherry, 1979).

The treatment wells in Figure 1-1 are cylindrical monitoring-type wells from 2 to 6 inches in diameter. These wells are arranged in lines perpendicular to the direction of groundwater flow. In the case of non-unidirectional groundwater flow, the wells would be arranged in such a way as to intercept all of the passing contaminant. A variation of the system replaces the cylindrical wells with a long, rectangular well extending perpendicularly to the direction of groundwater flow.

Figure 1-2 shows a cross-section of one of the treatment wells from Figure 1-1. Inside each well is placed a bundle of hollow fiber membrane tubes (each approximately 1 mm in diameter) filled with an aqueous, macromolecular copolymer solution. Contaminant travels through the membrane wall via molecular diffusion and adsorbs to hydrophobic sites of the copolymer. The

Figure 1-2 : Proposed Process -- Single Well Cross-Section

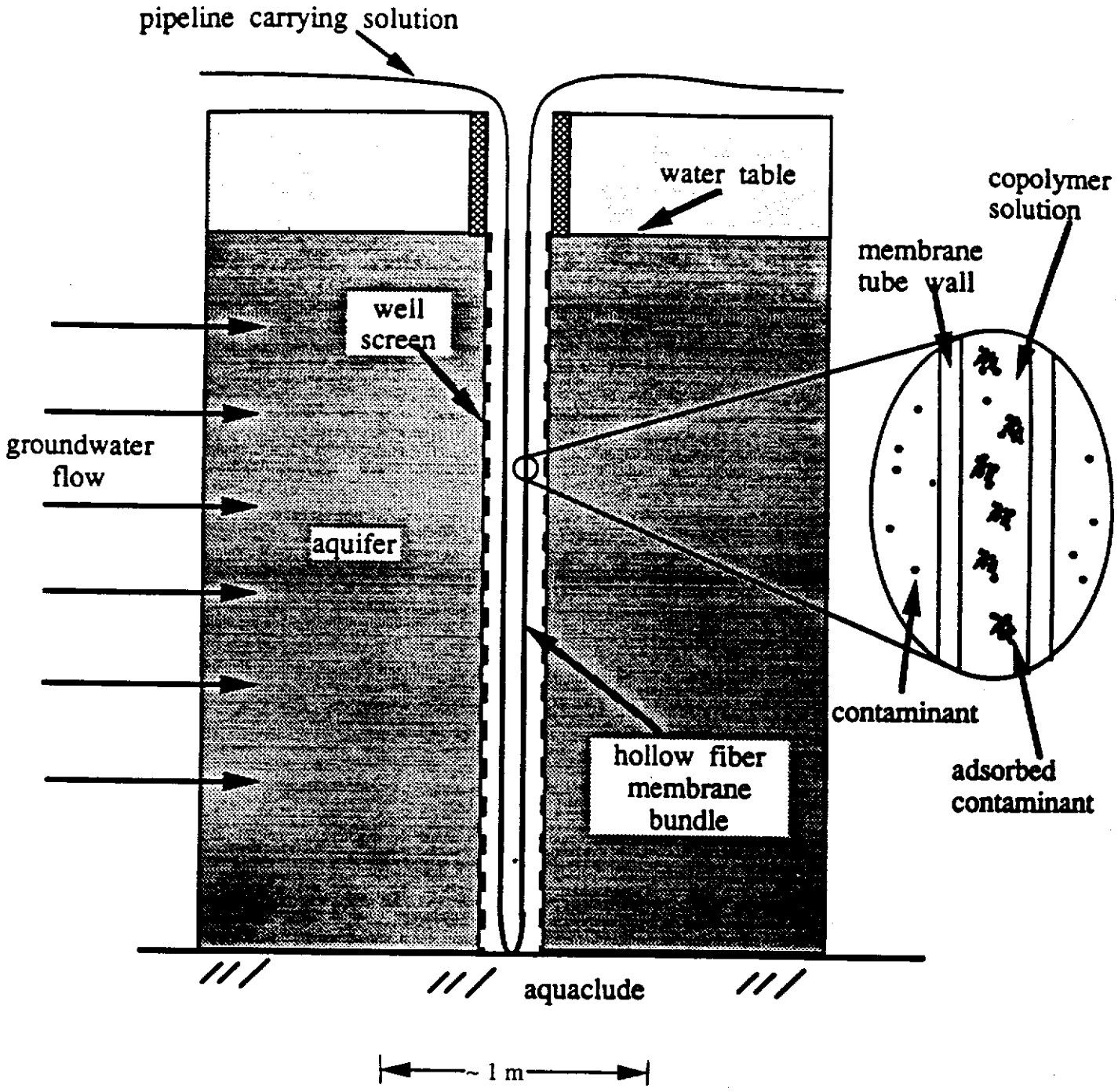

copolymer effectively enhances the solubilization of the organic species in aqueous solution. The copolymer solution may be recirculated intermittently when it becomes sufficiently loaded with contaminant for copolymer regeneration or waste incineration. The pore size of the membrane is chosen large enough to allow passage of contaminant into the copolymer solution, but small enough to prevent passage of copolymer out of the membrane interior. Contaminant removal takes place passively as the plume slowly moves through the cleanup area. In this way, immediate containment of the contaminant plume is achieved as is eventual removal of the contaminant. Intermittent replacement (i.e. monthly) of the copolymer solution is the only required operational procedure following installation.

Operating specifications to be determined for such a system include copolymer and membrane type, membrane average pore size, copolymer concentration, well spacing and configuration, and membrane configuration in each individual well. Factors affecting the optimum choices for the above specifications include groundwater flowrate and flow direction (governed by aquifer properties such as conductivity and hydraulic gradient), contaminant type and properties (solubility, molecular diffusion coefficient in water, molecular weight), and remediation requirements. These factors and operating specifications are discussed in this work.

The membranes used in this work are Supelco's polysulfone ultrafiltration membranes. The membranes used are anisotropic and have nominal molecular weight cutoffs of 2000 and 50,000 g/mol. The membrane skins are 0.1 - 0.2μm thick and are bound to a membrane support structure 0.275mm thick. Membranes best suited to the groundwater remediation system are those that are

sufficiently resistant to microbial attack, chemical degradation, and fouling. Work is currently being done to develop coatings which make industrial ultrafiltration membranes more resistant to fouling (Brink and Romijn, 1990, and Nystrom, 1989). This is a topic of concern in ultrafiltration technologies as well, where harsh environments are often encountered.

The copolymer used was N-vinylpyrrolidone/styrene (NVPS), a high molecular weight (3.4 million g/mol) random-structured copolymer, supplied by Scientific Polymer Products, Inc. The basic molecular backbone and structure is depicted in Figure 1-3. NVPS is nontoxic and has both hydrophobic and hydrophilic properties. Thus, it is an effective organic solubilizer, and it forms a stable suspension in water. The key features of the copolymer chosen for the system are its hydrophobicity (organic-solubilization capacity) and its molecular weight. The latter attribute is important since membrane pore size must be considerably less than the size of the copolymer molecule to prevent leakage.

Figure 1-3: Structure of Copolymer, N-Vinylpyrrolidone/styrene (NVPS)
A random sequential arrangement of ring structures x and y on the copolymer chain with x to y weight ratio of 60:40 is depicted.

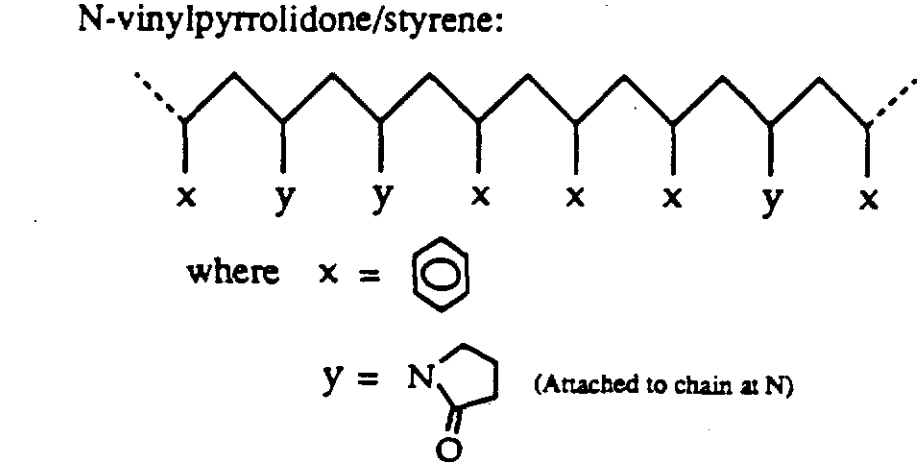

The hydrophobic model organic compounds used in this study were toluene (99.8% pure), naphthalene (99+% pure), and phenanthrene (98% pure). Toluene was obtained from Aldrich Chemical Company, Inc., and the naphthalene and phenanthrene were obtained from Sigma Chemical Company. These chemicals were used without further purification.

1.2. Thesis Objectives and Approach

The objectives of this thesis are threefold. The first two objectives involve the experimental and theoretical study of fundamental phenomena -- solubility and diffusive transport -- important to the remediation system proposed in Section 1.1. The third objective addresses a lab-scale demonstration of the proposed system.

The first objective of this work was to quantify the enhanced solubilization of three aromatic compounds -- toluene, naphthalene, and phenanthrene -- in aqueous amphipathic copolymer solution. Solubility experiments were conducted and a thermodynamic analysis was completed. The results tell how well contaminant may be concentrated in copolymer solutions used in the proposed process.

The second objective dealt with characterization of the rate of molecular diffusive transport of the aromatic solutes through anisotropic hollow fiber membranes into an aqueous copolymer solution. Diffusive transport experiments were conducted and a scaling analysis to determine controlling mechanisms was carried out. The results tell how quickly the contaminant

diffuses through the membrane and into the copolymer solution used in the proposed process. A comparison of experimental and modeled results gives insight into what parameters could be altered to decrease mass transfer resistance, and increase the performance of the proposed remediation system.

The third objective was the demonstration of the proposed system on a laboratory scale. The extraction of solute from an aqueous naphthalene plume moving through a model soil matrix was demonstrated in two different experimental configurations. Data from the solubility and transport experiments were used as inputs in the theoretical modeling of the laboratory-scale experiments. Finally, a copolymer/membrane remediation system was developed and evaluated for hypothetical contaminated aquifers.

1.3. Enhanced Solubility of Aromatics in Amphipathic Copolymer Solution

Experiments were performed to quantify the enhanced solubility of three aromatic solutes -- toluene, naphthalene, and phenanthrene -- in aqueous solutions of N-vinylpyrrolidone/ styrene copolymer. A thermodynamic analysis was used to develop a methodology for generalizing the results so that the solubilization capacities of NVPS and other copolymers could be estimated for various hydrophobic compounds of interest.

Since organics tend to adsorb onto solid surfaces such as the containers used in concentration measurements, careful handling techniques must be employed. 25-mL glass flasks were filled with aqueous NVPS copolymer

solutions of known concentration and about 8 g of either solid naphthalene or phenanthrene. Other 25-mL glass flasks were filled with aqueous NVPS solution and about 10 mL of liquid toluene. Very low headspace was allowed in the flasks (< 2 mL). The flasks were covered, shaken, and allowed to equilibrate at 23.0 ± 0.1°C in a constant-temperature water bath.

Solution concentrations of naphthalene, phenanthrene, and toluene were determined by absorbance measurements from a Perkin-Elmer Lambda 3B UV/VIS spectrophotometer, using quartz Suprasil cells. Measurements were made at maximum absorbance wavelengths for each compound: 276 nm (2760 Å) for naphthalene, 293 nm for phenanthrene, and 261 nm for toluene. Extinction coefficients for the solutes and NVPS copolymer were measured at the above wavelengths so that the concentration of all species in solution could be determined.

The saturated equilibrium concentrations of toluene, naphthalene, and phenanthrene in solutions of NVPS are given in Table 1-1 and are plotted in Figure 1-4 as a function of NVPS to water weight ratio. Each concentration measurement for a solute is given as a multiple of the solute's saturated concentration in pure water at 23.0°C (Table 1-2). For example, a solution with an NVPS to water weight ratio of 0.04 will solubilize about 100 times the naphthalene, or about 2000 times the phenanthrene that an equal amount of pure water will solubilize. Figure 1-4 shows a linear relationship between the solute concentration and the NVPS to water ratio for each of the three solutes. Such linear equilibrium relationships have been observed for systems of solid solute partitioning between two immiscible liquids (Prausnitz et al., 1986).

Table 1-1 : Saturated Concentrations of Solutes in Aqueous NVPS Solutions

Toluene		Naphthalene		Phenanthrene	
g NVPS / g water	$C/C_{w,sat}$	g NVPS / g water	$C/C_{w,sat}$	g NVPS / g water	$C/C_{w,sat}$
.0069	19.0	.0051	13.9	.0100	366
.0104	25.1	.0101	25.9	.0211	1020
.0197	46.6	.0152	38.9	.0316	1530
.0234	47.6	.0205	51.1	.0416	2020
.0243	59.0	.0256	62.1	.0531	2710
.0406	89.9	.0309	78.6	.0652	3150
.0793	204.5	.0362	87.9		
		.0416	99.8		
		.0472	110.7		

C = solute concentration in NVPS solution

$C_{w,sat}$ = saturated concentration of solute in pure water
(= constant for each solute at system temperature and pressure, given in Table 1-2)

$C/C_{w,sat}$ = factor of solute concentration "enhancement" provided by the NVPS

Figure 1-4 : Enhanced Solubility of Phenanthrene, Naphthalene, and Toluene in Aqueous NVPS Solution as a Function of NVPS:Water Weight Ratio

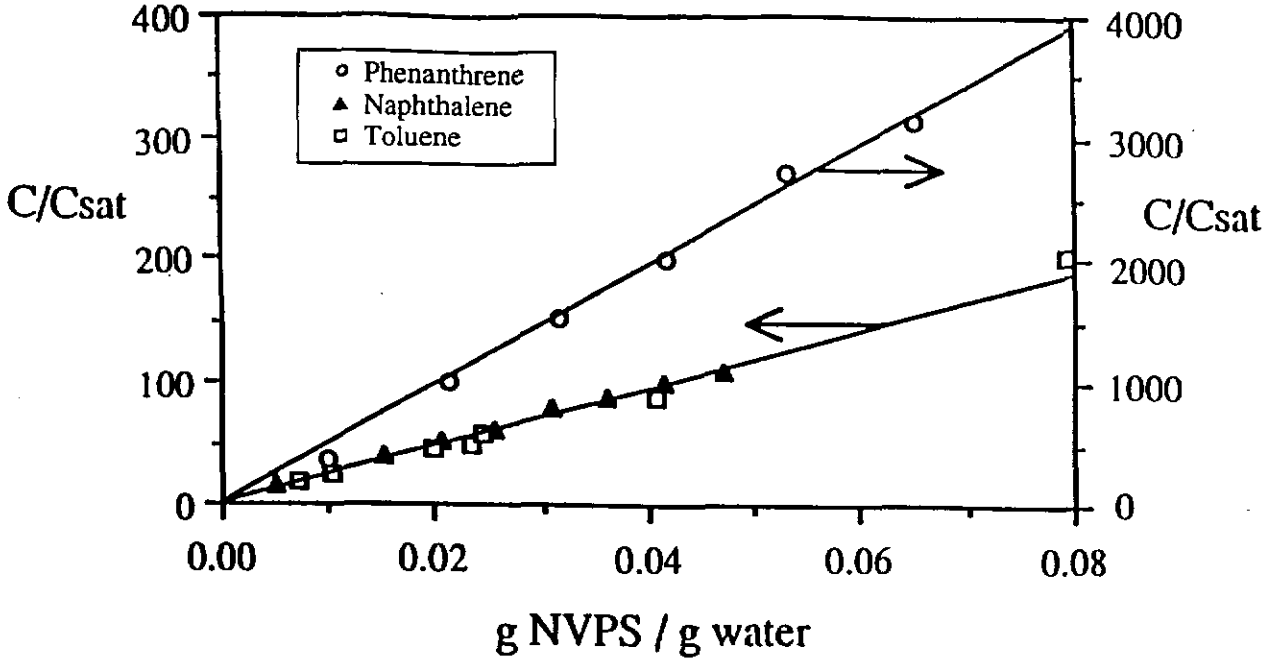

Table 1-2: Comparison of Surfactant Partition Coefficients for Model Solutes

Solute	Water Solubility Csat, (mg/L)	Log K_{ow} (conc. ratio)	Log K_{pw} (NVPS) (this work)	Log K_{sw} (P103)	Log K_{sw} (Brij 30)	Log K_{sw} (Igepal CA-720)	Log K_{sw} (Tergitol NP-10)	Log K_{sw} (Triton X-1000)
Toluene	627	2.73	3.39 ± .04	----	----	----	----	----
Naphthalene	31.2	3.37	3.38 ± .01	3.31	3.29	3.02	2.99	3.10
Phenanthrene	1.29	4.46	4.69 ± .02	4.60	4.27	4.07	4.14	4.16
Sources:	(*a*, *b*)	(*c*)	(*this work*)	(*d*)	(*e*)	(*e*)	(*e*)	(*e*)

(a) Bohon and Claussen, 1951
(b) May et al., 1978
(c) Hansch and Leo, 1979
(d) Hunter and Hatton, 1992
(e) Edwards et al., 1991

A surfactant-water partition coefficient may be derived for each solute-surfactant system, and because the saturation behavior is linear, each partition coefficient will be constant. The overall amount of solute in the solution is divided into solute associated with the water and polymer pseudophases. Here, a pseudophase is defined as one of two separate interspersed phases. The water and polymer pseudophases are intimately mixed on an approximately 1-μm size scale as a microemulsion, but remain chemically and physically distinct below this size level. The concentration basis defined as follows is used to express the partitioning of solute between these two pseudophases:

$$\frac{C}{C_{w,sat}} = \frac{C_w + C_p}{C_{w,sat}} = \frac{C_w}{C_{w,sat}} + \frac{C_p}{C_{w,sat}} \qquad (1\text{-}1)$$

where C = g solute per ml solution, C_p = g solute in "polymer" pseudophase per ml solution, C_w = g solute in "water" pseudophase per ml solution, and $C_{w,sat}$ = g solute in pure water at saturation per mL water. K_{pw} and NVPS to water weight ratio are defined as follows:

$$K_{pw} \equiv \frac{\text{g solute in NVPS polymer / g polymer}}{\text{g solute in water / g water}} \qquad (1\text{-}2)$$

$$M \equiv \frac{\text{g NVPS}}{\text{g water}} \qquad (1\text{-}3)$$

Then for $C_w \equiv C_{w,sat}$, the relationship between measured solute concentration and NVPS to water weight ratio becomes the following:

$$\frac{C}{C_{w,sat}} = 1 + K_{pw} M \qquad (1\text{-}4)$$

Values of K_{pw} for NVPS-water partitioning for the three solutes are given in Table 1-2 with 95% confidence intervals given.

Values from the literature of $\log_{10} K_{sw}$, surfactant-water partition coefficient, with the same concentration basis as K_{pw} are shown in Table 1-2 for a variety of surfactants with naphthalene and phenanthrene solutes. The organic solubilization capacity of the NVPS copolymer compares well with that of the widely-used surfactants. Table 1-2 also lists values of $\log_{10} K_{ow}$, the octanol-water partition coefficient, for the solutes defined for an octanol-water binary as follows:

$$K_{ow} = \frac{\text{g solute in octanol-rich phase / mL octanol}}{\text{g solute in water-rich phase / mL water}} \qquad (1\text{-}5)$$

Thermodynamic analysis of two-phase equilibrium was used to predict the relationship between K_{pw} and K_{ow} for the solute-water-NVPS systems, as follows:

$$\log K_{pw} = \log K_{ow} + \log \gamma_i^o + \log v_o - \log \gamma_i^{*p} - \log \left(\frac{MW_{sol}}{1000}\right) - \log R_p \qquad (1\text{-}6)$$

where v_o is the molar volume of pure octanol at system temperature and pressure [L/mol]; γ_i^o is the activity coefficient of solute i in the octanol-rich phase of an octanol-water binary in equilibrium with solid solute; γ_i^{*p} is the activity coefficient of solute i in the polymer-rich phase calculated on a *weight fraction* basis; MW_{sol} is the molecular weight of the solute [g/mol]; and R_p is the ratio of

polymer mass to polymer *phase* mass [g/g]. Another expression for K_{pw} was derived as well:

$$\log K_{pw} = \log v_w - \log \gamma_i^{*p} + \log \gamma_i^{w} - \log \frac{MW_{sol}}{1000} - \log R_p \qquad (1\text{-}7)$$

where v_w is the molar volume of pure water at system temperature and pressure [L/mol], and γ_i^w is the activity coefficient of solute i in the water-rich phase of the water-polymer binary. Estimates for K_{pw} from Equations 1-6 and 1-7 are within about a factor of two of the experimental K_{pw} values (Table 1-3)-- very reasonable agreement considering estimated error of parameters.

Table 1-3: Activity Coefficients and Other Parameter Inputs for Equations 1-6 and 1-7: NVPS-Solute-Water Systems

Solute	Log Kow [a]	Log γ_i^o	Log γ_i^w	Log γ_i^{*p}	Log $\frac{MWsol}{1000}$	Log P	Log K_{pw} (Equ. 1- 7)	Log K_{pw} (Equ. 1-6)	Log K_{pw} (measured)
Toluene	2.73	0.34 [b]	3.99	0.17	-1.04	-0.41	3.53	3.55	3.39
Naphthalene	3.37	0.53 [c]	4.93	0.41	-0.89	-0.03	3.70	3.61	3.38
Phenanthrene	4.46	0.82 [c]	6.43	0.41	-0.75	-0.03	5.06	4.85	4.69

Constants: $\log_{10} v_o = -0.80$

$\log_{10} v_w = -1.74$

v_i [=] L/mol

(a) Values taken from Hansch and Leo, 1979.
(b) Value taken from Thomas et al., 1982.
(c) Values estimated using UNIFAC/UNIQUAC method (Lyman et al., 1990).

1.4. Transmembrane Diffusion of Organic Solute in Aqueous Solution

Fundamental to the efficacy of the proposed barrier/remediation system is the speed at which contaminant can diffuse through the membrane into the copolymer solution. Figure 1-5 shows a schematic diagram of a transmembrane transport experiment involving transfer of solute from an exterior aqueous solution to an interior aqueous, copolymer solution. This set-up more closely demonstrates the proposed groundwater contaminant barrier system, since solute diffuses into a copolymer solution. Initially, an aqueous, copolymer solution is introduced to the interior of a membrane tube of volume V_t at zero solute concentration. The exterior solution is maintained at a constant, saturated solute concentration. Molecular diffusive transport from the exterior to the interior is allowed until the copolymer solution has an aqueous pseudophase concentration equal to the exterior phase concentration. The governing equation and initial conditions for this experiment are as follows:

Governing Equation:

$$V_t \frac{dC_{int,aq}}{dt} = -\frac{A_t}{R_{tot}}(C_{ext} - C_{int,aq}) - MK_{pw}V_t\frac{dC_{int,aq}}{dt} \qquad (1\text{-}8)$$

Initial Conditions:

$$C_{int,aq}(t=0) = 0 \qquad (1\text{-}9)$$

$$C_{ext} = C_{sat} = \text{constant at all time t} \qquad (1\text{-}10)$$

where V_t is the membrane tube interior volume [cm^3]; $C_{int,aq}$ is the interior aqueous pseudophase solute concentration [g/cm^3]; C_{ext} is the exterior solution solute concentration [g/cm^3]; C_{sat} is the saturated concentration of solute in

Figure 1-5 : Schematic Diagram of Transmembrane Transport Experiment -- Solute Transport Into Copolymer Solution

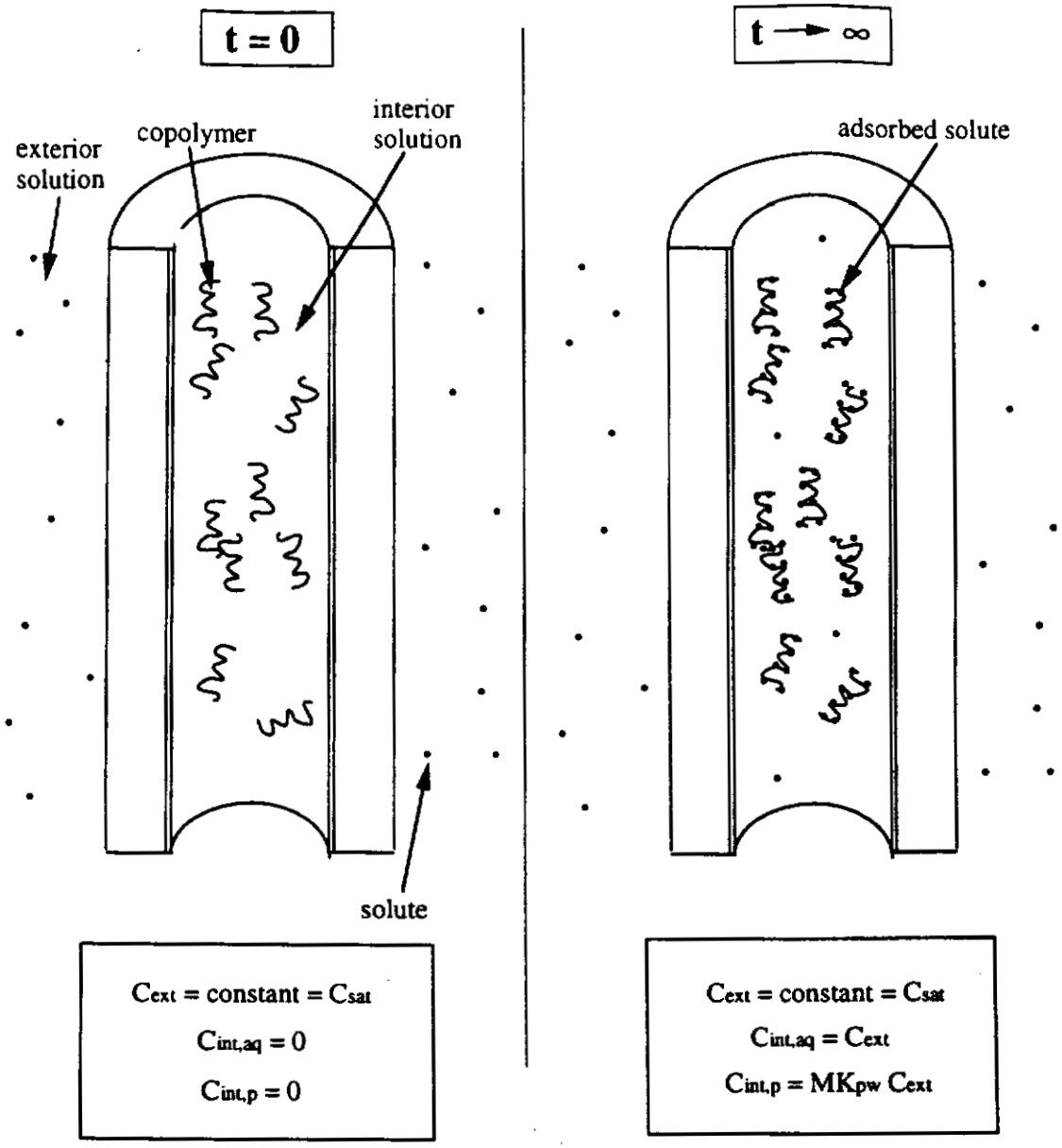

Note: Not to scale.

water [g/cm^3]; A_t is the membrane tube surface area [cm^2], R_{tot} is the overall membrane tube resistance [s/cm]; M is the ratio of polymer to water mass in the interior copolymer solution [g/g], and K_{pw} is the polymer-water partition coefficient of the solute [dimensionless]. The governing equation follows from a mass balance on the interior *aqueous pseudophase*. The term on the left-hand side of Equation 1-8 is the accumulation of solute in this phase, the first term on the right-hand side is the net transport of solute into this phase, and the second term on the right-hand side is a "reaction" term describing the transfer of solute out of the interior aqueous pseudophase and into the interior polymer pseudophase. The measured interior phase solute concentration is the sum of the solute's concentration in the two pseudophases:

$$C_{int} = C_{int,aq} + C_{int,p} \tag{1-11}$$

where C_{int} is the measured interior concentration [g/cm^3 solution]; $C_{int,aq}$ is the solute concentration in the aqueous pseudophase [g/cm^3 solution]; and $C_{int,p}$ is the solute concentration in the polymer pseudophase [g/cm^3 solution]. Assuming equilibrium exists between the pseudophases, we may solve Equation 1-8 with respect to 1-9 and 1-10 for measured interior solution concentration, C_{int}, as follows:

$$\frac{C_{int}}{C_{sat}} = (1 - e^{-Bt})\,(1 + M\,K_{pw}) \tag{1-12}$$

$$\text{where } B = \frac{A_t}{V_t R_{tot}(1 + M\,K_{pw})}.$$

Equation 1-12 can be expressed as follows:

$$\Omega(t) = \frac{1}{R_{tot}} t \qquad (1\text{-}13)$$

$$\text{where} \quad \Omega(t) = -\ln \left[1 - \frac{C_{int}/C_{ext}}{(1 + M K_{pw})} \right] / b \ ,$$

$$b = \frac{A_t}{V_t(1 + M K_{pw})}$$

Values of $\Omega(t)$ can be graphed with time t to obtain R_{tot} for a given system. The experimental R_{tot} values can then be compared to values predicted from literature correlations. The experimental set-up for all diffusion experiments in this work is shown in Figure 1-6. The system consists of a membrane tube cartridge through which solution is pumped both interior and exterior to the hollow membrane fibers, teflon-lined piston-diaphragm pumps which are used to transport the fluid, and a PAH column through which the exterior-side solution is passed to keep the solution saturated with organic solute. When a given parcel of solution is not in transit through the membrane or PAH column, it resides in the interior or exterior soluton reservoir. The solutions in these glass flasks are sealed from the surrounding air and are well-mixed by magnetic stirrers. Side-streams from both the interior and exterior solution lines are sent through quartz flow cells in the UV/VIS spectrophotometer for on-line concentration measurement. Then the solutions are returned to their respective storage reservoirs.

Normalized naphthalene concentration, $\Omega(t)$, from Equation 1-13 are plotted versus time in Figure 1-7 for the naphthalene runs using both the 2000 and 50,000 molecular-weight-cutoff membranes. Slopes and corresponding resistances are shown in Table 1-4. Normalized concentrations from the

Figure 1-6 : Diffusion Experiment Set-Up

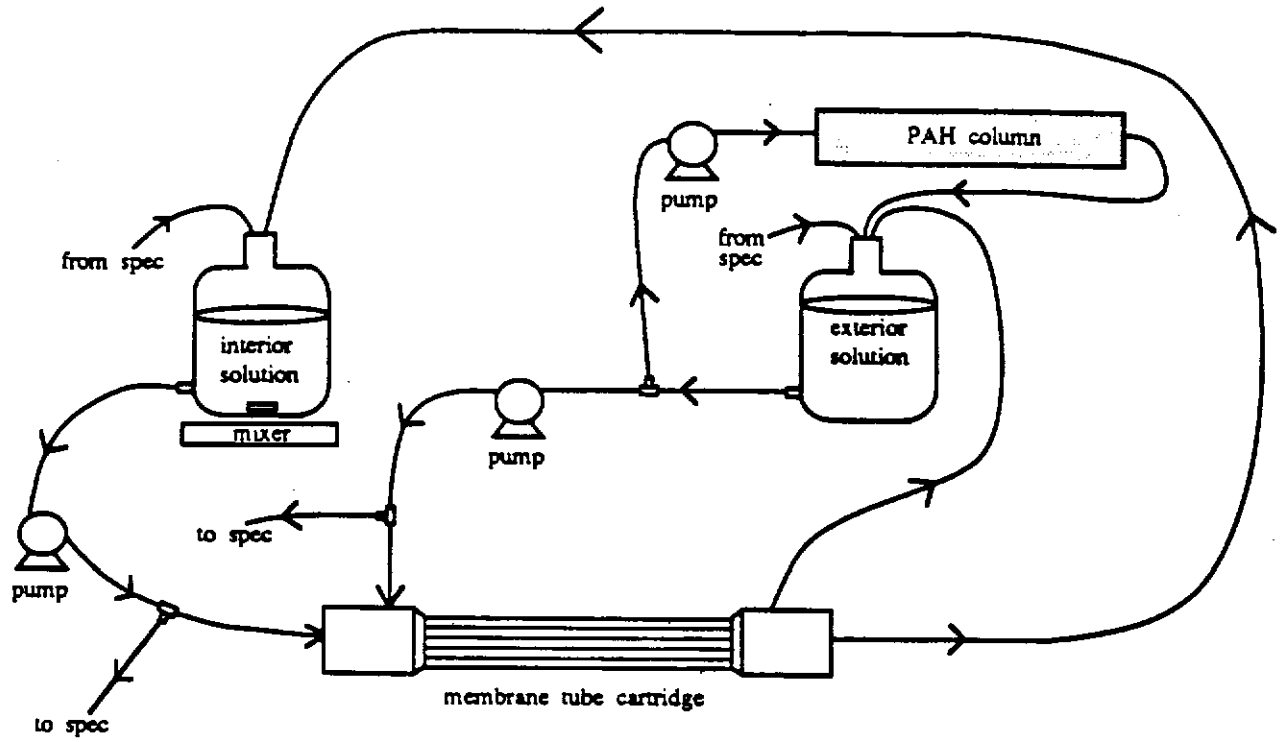

Figure 1-7 : Naphthalene Diffusion Through 2K and 50K MW Cutoff Membranes Into NVPS Copolymer Solution -- Normalized Data

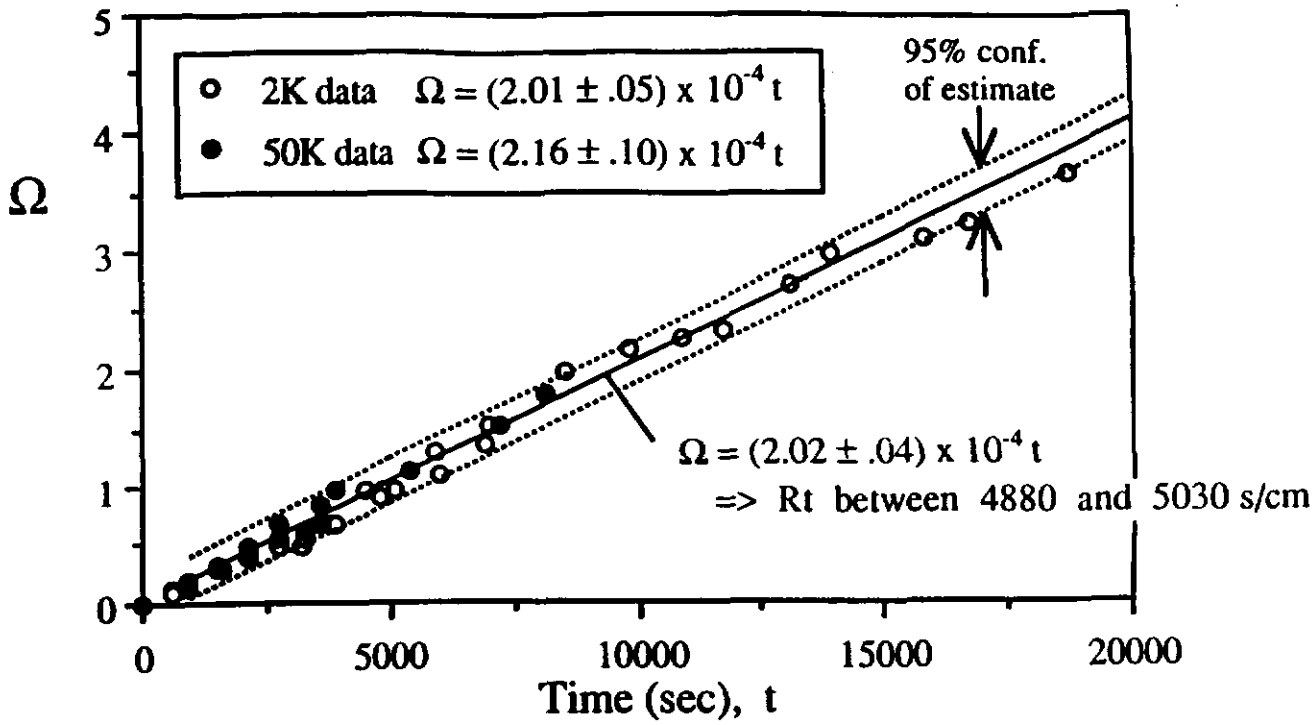

Figure 1-8 : Phenanthrene Diffusion Through 2K and 50K MW Cutoff Membranes Into NVPS Copolymer Solution -- Normalized Data

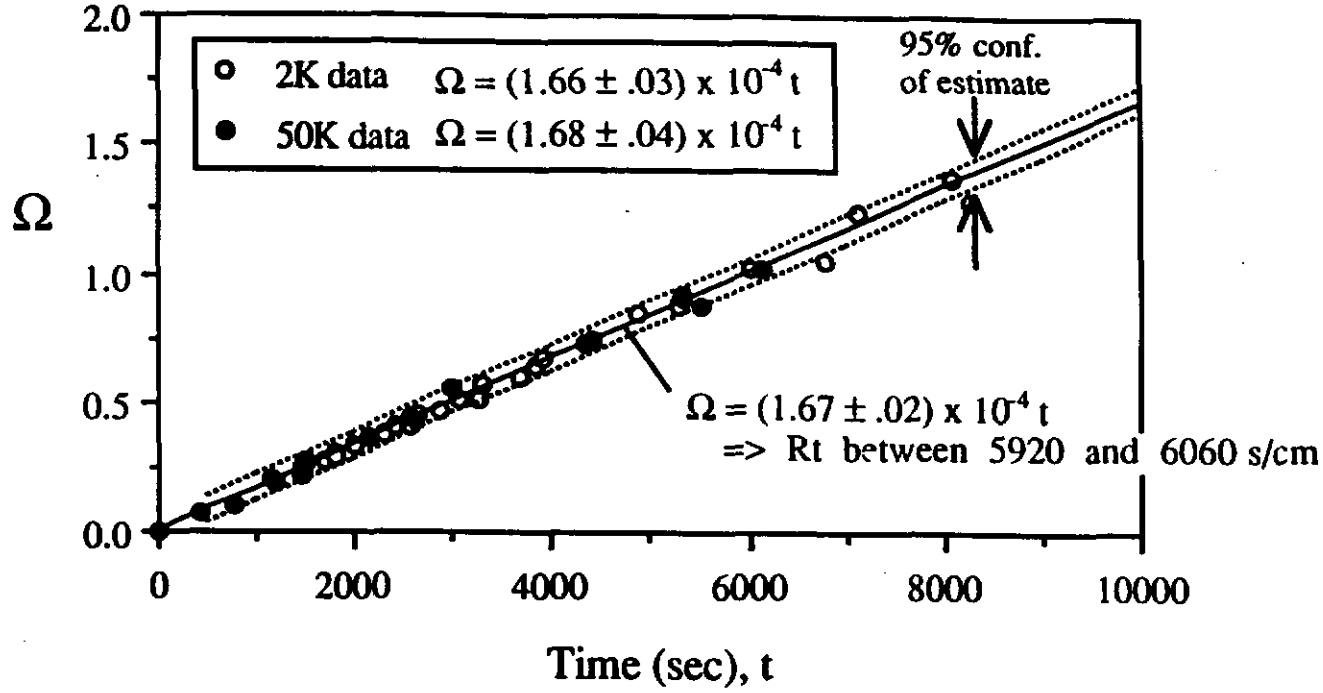

$$\Omega = -\ln\left(1 - \frac{C_{int}/C_{sat}}{1 + M K_{pw}}\right) / b$$

Table 1-4: Slopes of Normalized Concentration Versus Time Plots

Solute	Membrane MW Cutoff	Slope of Ω vs. t	R_{tot} (s/cm)
Naphthalene	2000	$(2.01 \pm 0.05) \times 10^{-4}$ cm/s	4980 ± 120
Naphthalene	50,000	$(2.16 \pm 0.10) \times 10^{-4}$ cm/s	4630 ± 210
Naphthalene	Pooled Data	$(2.02 \pm 0.04) \times 10^{-4}$ cm/s	4950 ± 100

All variations in $d\Omega/dt$ and R_{tot} cited to 95% confidence.

Table 1-5: Slopes of Normalized Concentration Versus Time Plots

Solute	Membrane MW Cutoff	Slope of Ω vs. t	R_{tot} (s/cm)
Phenanthrene	2000	$(1.66 \pm 0.03) \times 10^{-4}$ cm/s	6020 ± 100
Phenanthrene	50,000	$(1.68 \pm 0.04) \times 10^{-4}$ cm/s	5950 ± 140
Phenanthrene	Pooled Data	$(1.67 \pm 0.02) \times 10^{-4}$ cm/s	5990 ± 70

All variations in $d\Omega/dt$ and R_{tot} cited to 95% confidence.

phenanthrene runs are plotted versus time in Figure 1-8 and corresponding resistances are shown in Table 1-5.

The modeled resistance ($R_{tot} = \frac{1}{d\Omega/dt}$) approximates the measured overall resistance for both the naphthalene and phenanthrene diffusive transfer experiments with less than 10% error. This is within the collective error of model inputs for these experiments. The dominant resistance is the membrane support layer. The experimental data reflect the fact that phenanthrene has a slightly lower diffusivity in water than naphthalene; since D_{AB}(phen.) < D_{AB}(naph.), the overall resistance for phenanthrene transport is greater than for naphthalene transport. The model also shows that the resistance of the membrane skin layer is negligible compared to overall resistance. This explains the negligible difference between the experimentally-measured resistances using the 2000 and 50,000 MW membranes. The membranes were identical except for their skin layers.

1.5. Aquifer Simulator Experiments

The basic purpose of the aquifer simulator experiments was to demonstrate the removal of naphthalene from water flowing through a lab-scale soil matrix by means of the proposed membrane/copolymer system. The rectangular well experiment demonstrates the removal of naphthalene from a pre-contaminated aquifer. The cylindrical well experiment demonstrates the interception of naphthalene from a plume moving through a previously-uncontaminated soil matrix.

The goal of the well-mixed rectangular well experiment was to demonstrate and model the removal of naphthalene from a pre-contaminated lab-scale aquifer with a constant contaminant source using the proposed membrane/copolymer system. Figure 1-9 shows the soil tank set-up used in the rectangular well experiment. Sections 3 and 5 were filled with Ottawa sand. The entire tank was filled with distilled water and flow was initiated through the tank by maintaining constant water levels in sections 2 and 6 such that the level in section 2 was slightly above (by about 0.1 cm) the level of section 6. The overall flowrate through the tank was 0.419 cm^3/s, and remained constant throughout the experiment. The seepage velocity of the water through the soil corresponding to this volumetric flowrate was 4.0 cm/hr (0.067 cm/s). The tank was kept at 23.0°C by means of an externally insulated, constant temperature bath. The liquid in section 2 was continuously saturated with naphthalene by pumping through a column filled with solid naphthalene. The naphthalene concentration of the fluid in both section 2 and the well (section 4) was determined by on-line UV-VIS spectrophotometry absorbance readings at 276-nm wavelength. The well concentration increased to saturated concentration as naphthalene reached the well. The membrane/copolymer system was placed in the well prior to the naphthalene saturation of the well, but copolymer solution had not been circulated through the interior of the membrane tubes. This allowed for the naphthalene to adsorb to all materials in the well area before the experimental run began. Any measured decrease, then, in the measured well concentration after the interior copolymer solution began circulating through the membrane would be due to naphthalene transport through the membrane into the copolymer solution, not adsorption onto a surface newly-introduced to the well fluid.

Figure 1-9: Groundwater Flow Simulator

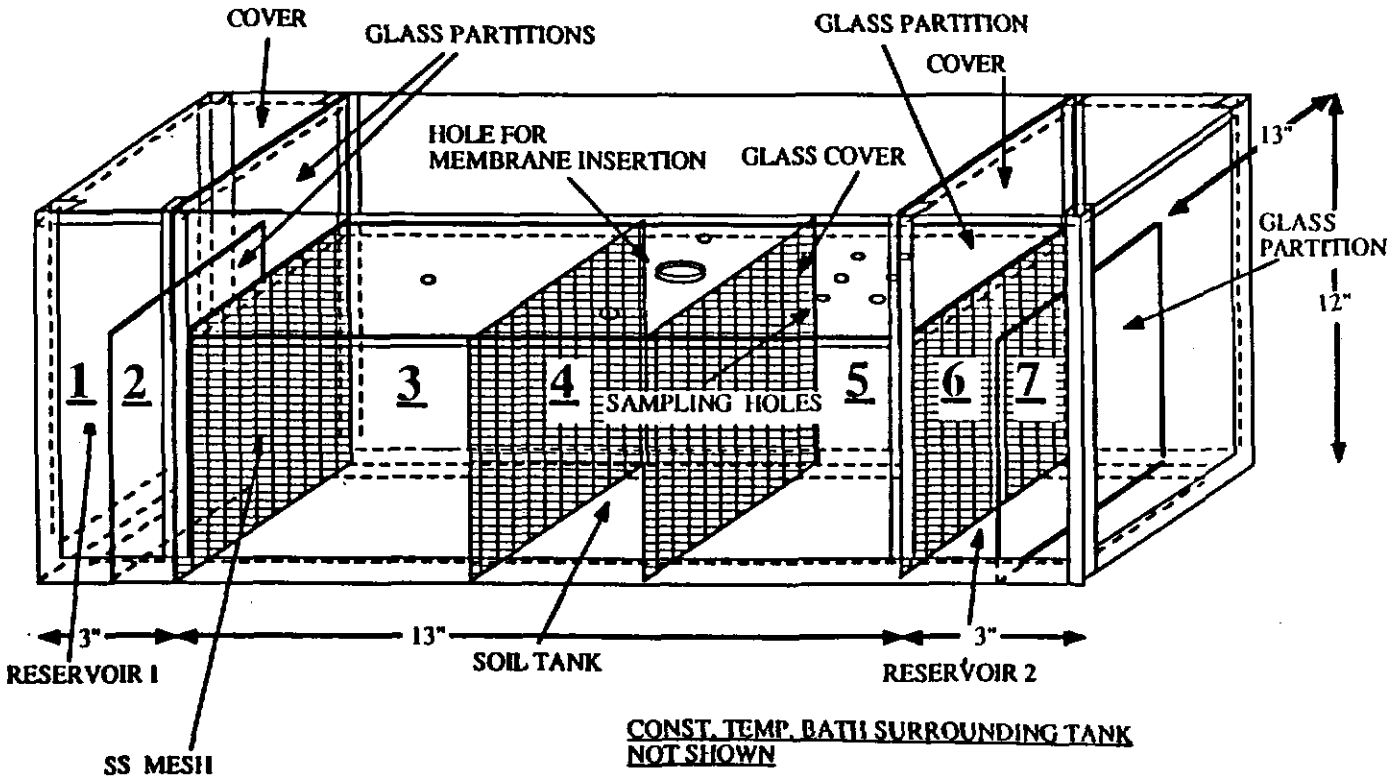

The governing equations for the well solution naphthalene concentration consists of two mass balances -- one on the membrane interior solution and one on the well solution:

Membrane Tube Interior Mass Balance:

$$V_t \frac{dC_{int,aq}}{dt} = \frac{A_t}{R_{tot}} (C_{well} - C_{int,aq}) - MK_{pw}V_t \frac{dC_{int,aq}}{dt} \qquad (1\text{-}14)$$

Well Mass Balance:

$$V_w \frac{dC_{well}}{dt} = Q (C_o - C_{int,aq}) - \frac{NA_t}{R_{tot}} (C_{well} - C_{int,aq}) \qquad (1\text{-}15)$$

where V_t is the membrane tube interior volume [cm^3]; V_w is the well volume [cm^3]; A_t is the membrane tube surface area [cm^2]; R_{tot} is the overall membrane tube resistance [s/cm]; M is the polymer to water mass ratio (in copolymer solution) [g/g]; K_{pw} is the polymer-water partition coefficient of solute [dimensionless]; Q is the fluid flow rate into the well [cm^3/s]; N is the number of membrane tubes; C_o is the solute concentration of fluid entering the well [g/cm^3]; $C_{int,aq}$ is the interior aqueous pseudophase solute concentration [g/cm^3]; and C_{well} is the solute concentration of the well fluid [g/cm^3]. The initial conditions are as follows:

Initial Conditions:

$$C_{well}(t=0) = C_o \tag{1-16}$$

$$C_{int,aq}(t=0) = 0 \tag{1-17}$$

The solution using Equations 1-14 to 1-17 is as follows:

$$\frac{C_{well}}{C_{sat}} = \frac{\alpha}{a_1 - a_2}\left(e^{-a_1\tau} - e^{-a_2\tau}\right) + 1 \tag{1-18}$$

where $\alpha = \dfrac{NA_t}{QR_{tot}}$; $\beta = \dfrac{A_t V_w}{QR_{tot}V_t(1 + MK_{pw})}$;

$a_1 = \dfrac{a - \sqrt{a^2 - 4\beta}}{2}$; $a_2 = \dfrac{a + \sqrt{a^2 - 4\beta}}{2}$;

$a = 1 + \alpha + \beta$; $\tau = \dfrac{t}{V_w/Q}$.

Figure 1-10 shows the experimental results of the well-mixed rectangular well experiment. The well concentration decreases as naphthalene diffuses into the copolymer solution.

Using the experimentally-determined membrane diffusive resistance, R_{tot} = 5000 s/cm, the model predicts a bigger concentration decrease than was seen experimentally. The data is more closely predicted using an R_{tot} between 15,000 and 20,000 s/cm in the Equation 1-18 model. This significantly higher R_{tot} is probably due to the dynamic desorption of naphthalene adsorbed to the solid surfaces in the well and not a change in support/membrane resistance.

Figure 1-10 Rectangular Well Experiment -- Naphthalene Concentration of Well Fluid

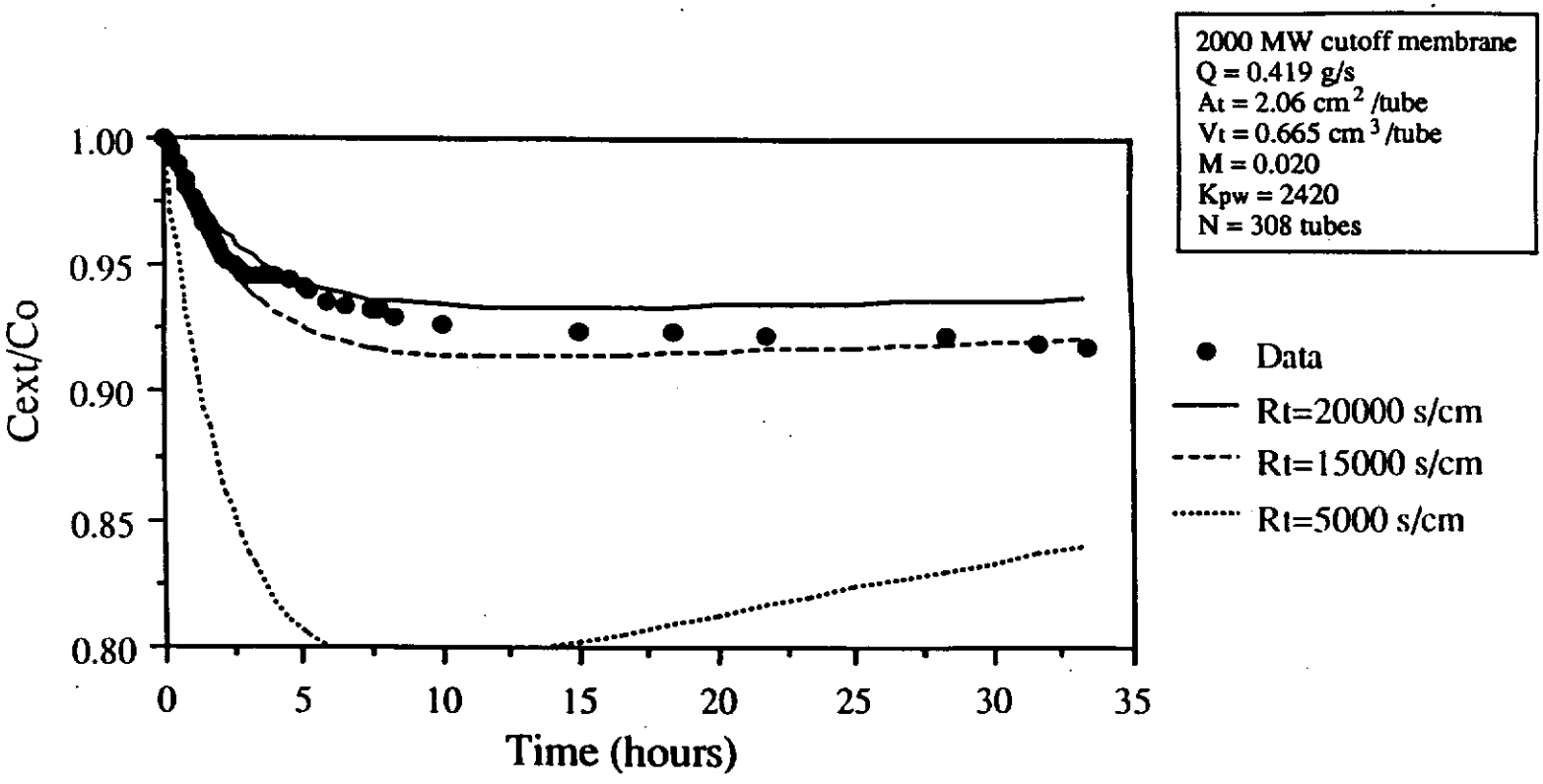

The goals of the 2-D cylindrical well experiment were to experimentally demonstrate the decreased concentration plume of solute leaving a cylindrical membrane/copolymer system treatment well, to model the well's naphthalene concentration as a function of time, and to model the plume profile as a function of length, width, and time.

The domain for the 2-D experiment modeling is shown in Figure 1-11. The modeling scheme is divided into two parts. First, the well concentration, $C_{well}(t)$, is modeled analytically as a function of time given an experimentally-determined functional form for incoming fluid concentration $C_o(t)$. Secondly, the naphthalene concentration of the region behind the well is solved for numerically using $C_{well}(t)$ and $C_o(t)$ as boundary conditions. The governing equation, boundary conditions, and initial conditions used to determine the 2-D naphthalene concentration profile in the domain $0 \le x \le L$, $0 \le y \le W$ in Figure 1-11 are as follows:

$$\frac{\partial C}{\partial t} + u_x(x,y)\frac{\partial C}{\partial x} + u_y(x,y)\frac{\partial C}{\partial y} = D_x\frac{\partial^2 C}{\partial x^2} + D_y\frac{\partial^2 C}{\partial y^2} - \frac{\rho_b}{n}K_d\frac{\partial C}{\partial t} \qquad (1\text{-}19)$$

$$\frac{\partial C}{\partial y} = 0 \quad \text{at } y=W \qquad (1\text{-}20)$$

$$\frac{\partial C}{\partial y} = 0 \quad \text{at } y=0 \qquad (1\text{-}21)$$

$$\frac{\partial C}{\partial x} = 0 \quad \text{at } x=L \qquad (1\text{-}22)$$

$$C(t) \text{ is known along } x=0 \qquad (1\text{-}23)$$

$$C(x,y) = 0 \text{ at } t=0 \text{ for all } x, y \qquad (1\text{-}24)$$

where $u_i(x,y)$ is the i component of velocity [cm/s]; D_i is the dispersion coefficient in the i direction [cm^2/s]; K_d is the solute soil-water partition coefficient [(g/g)/(g/mL)]; ρ_b is the soil bulk density [g/cm^3]; n is the aquifer porosity [dimensionless]; and C is solute concentration of aqueous solution in the domain, a function of x, y, and t [g/cm^3]. Functional values of $u_x(x,y)$ and $u_y(x,y)$ were obtained from the flow field solution shown in Figure 1-12. The domain in Figure 1-11 was discretized, and nodal equations written using an explicit finite difference approximation of Equation 1-19. The discretization used was found to provide a stable, convergent solution over the problem domain.

Figure 1-11: 2-D Cylindrical Well Experiment -- Modeling

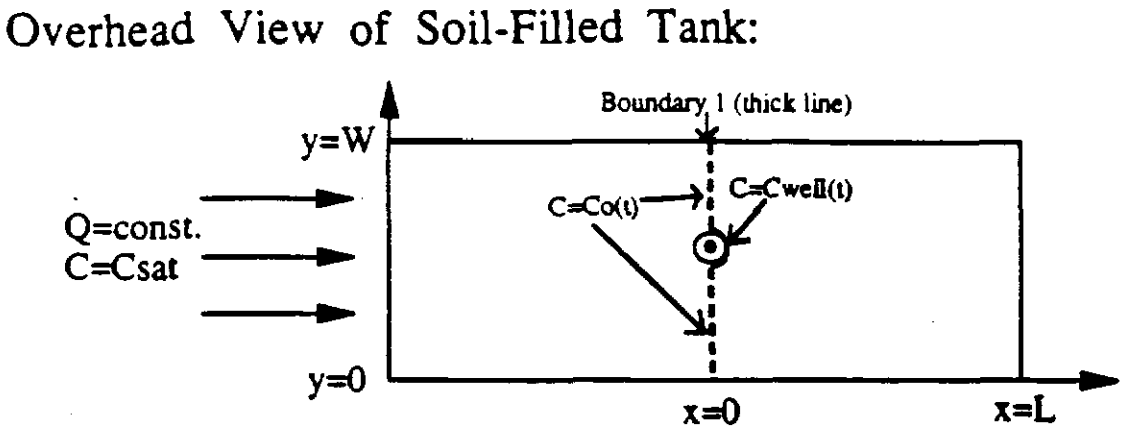

Figure 1-12: Solution for Flow Field About a Cylindrical Well

Velocity Field

$$q_I = [\, q_x(1 + \frac{R^2}{r^2}) \cos\phi \,] e_r - [\, q_x(1 - \frac{R^2}{r^2}) \sin\phi \,] e_\phi$$

Streamfunction

$$\psi = q_x \left(r + \frac{R^2}{r} \right) \sin\phi$$

Graph of Streamlines

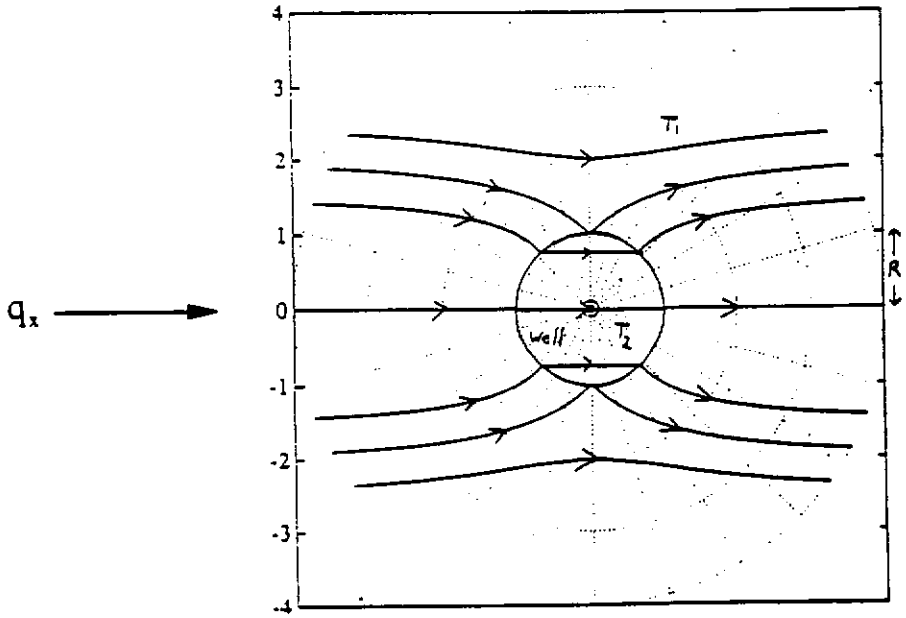

A graphical representation of the well concentration solution and plume profile at t = 2 hours using the experimental input parameters is shown in Figure 1-13. The contour plot shows that fluid concentration is diminished by the presence of the treatment well up to a width twice the diameter of the well. The slight "bulge" in solution concentration along the center of the well is due to the flow field solution shown in Figure 1-12. The seepage velocity in the x-direction at the middle of the well is faster than the velocity at the far sides of the well; hence, the concentration "dips" on each side of the well.

The naphthalene concentration of solution samples at various positions in the tank were measured off-line at t = 2 hours. These values are shown superimposed over the modeled concentration profile in Figure 1-14. The data values agree with modeled concentration values within 20% for all points. Note the data plot shows the "bulge" at the center of the well seen previously in the model. The data support the conclusions of the scaling analysis -- namely, that the decreased concentration plume leaving a cylindrical treatment well has a width about twice the diameter of the well.

Figure 1-13: 2-D Well Experiment Model Output
2-D Concentration Profile at t = 2 hours

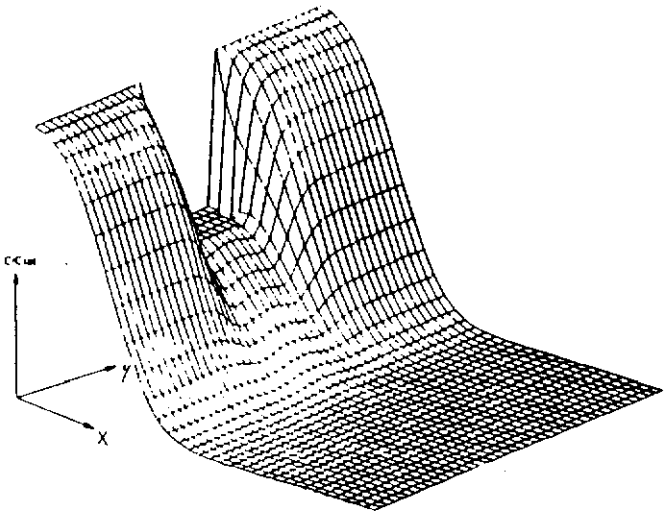

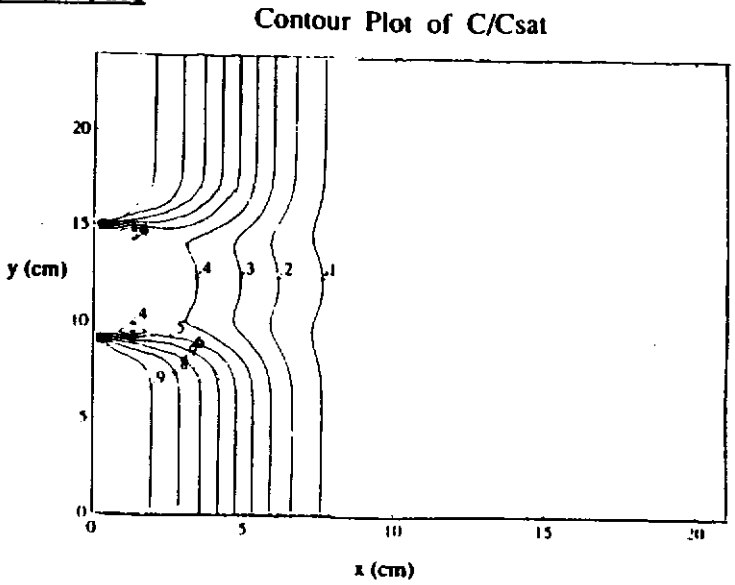

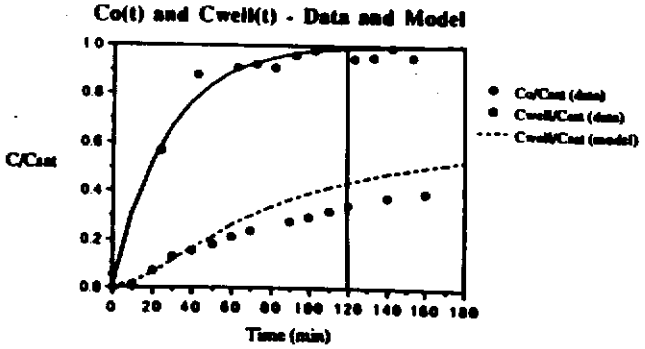

Input Parameters - Base Case

1. Well volume = 573.4 cm^3
2. Tube volume = 0.667 cm^3
3. Seepage velocity = 0.001038 cm/s
4. K_{pw} = 2420
5. M = 0.00362 (mass ratio NVPS:water in interior soln.)
6. R_{tot} = 5000 s/cm
7. Number of tubes = 300
8. Surface area of tube = 2.06 cm^2
9. Domain width = 12.0 cm x 2
10. Domain length = 21.0 cm
11. Retardation coefficient R_d = 1.4
12. Dispersion coef., x-dir., D_x = 0.000394 cm^2/s
13. Dispersion coef., y-dir., $D_y = 0.5\ D_x$
14. Time step length = 10 s
15. Number of time steps taken = 720
16. Porosity = 0.38
17. Well depth = 27.0 cm

Figure 1-14: 2-D Well Experiment Concentration Data at t = 2 hours

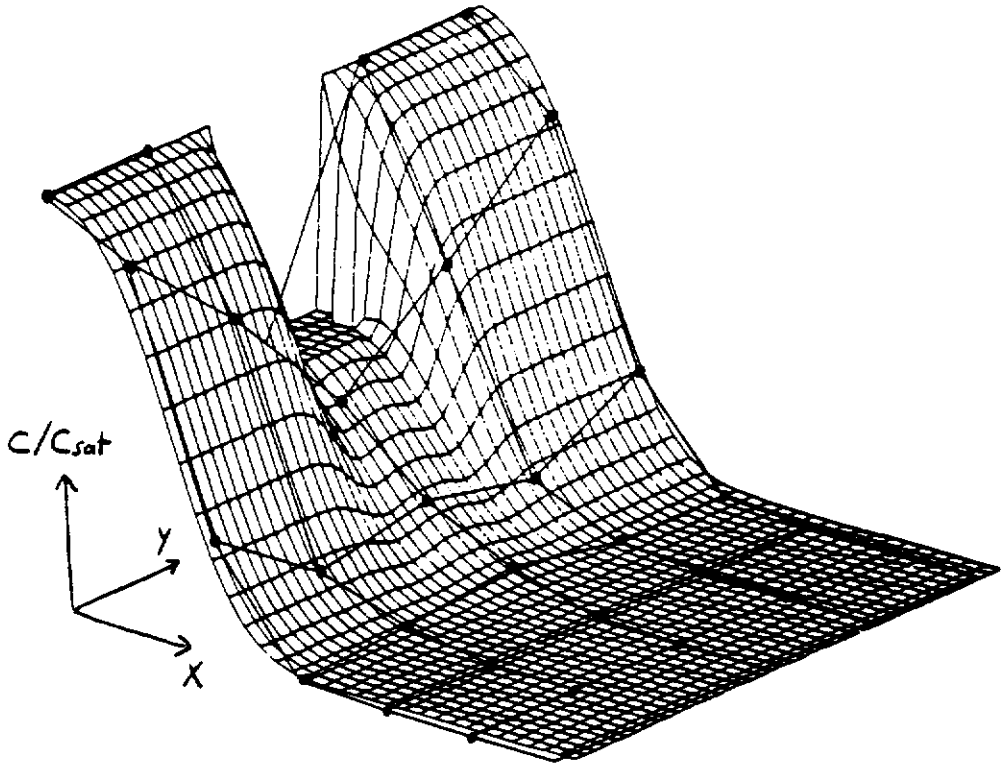

1.6. Hypothetical Full-Scale System Application

A hypothetical contaminated aquifer is shown in Figure 1-15. Figure 1-16 shows the solution of C_{well}/C_o for the case of both naphthalene and phenanthrene contamination of the hypothetical well in Figure 1-15 with given inputs. The resistance, R_{tot}, and partition coefficient, K_{pw}, for each case is as determined in the lab-scale experiments. The effective contaminant velocity into the well, $u_{eff} = u_x/R_d$, is chosen as 2cm/day. The number of membrane tubes in the well is 600 per square-foot of the wall area; this corresponds to an approximately 1.4-inch diameter bundle of the 0.5-mm-ID polysulfone membranes per foot of well length. In Figure 1-16, the solute concentration in the well initially decreases over a time period of one or two days, the concentration stays low for an interval of 10 to 30 days, then the concentration increases as the copolymer becomes saturated with solute. Thus, Figure 1-16 demonstrates a workable containment system where copolymer solution is replaced every 10 to 30 days. Increasing the number of membrane tubes used in the well results in decreasing the minimum concentration reached, and thus enhancing the efficiency of the system.

1.7. Conclusions and Recommendations

(1) Quantification of enhanced solubilization for three model aromatics:

The first objective of this work was to quantify the enhanced solubilization of three aromatic compounds -- toluene, naphthalene, and phenanthrene – in aqueous amphipathic copolymer solution. The amphipathic copolymer used was N-vinylpyrrolidone/styrene (NVPS), a high molecular weight (3.4 million g/mol) random-structured copolymer (Figure 1-3). The experiments showed

Figure 1-15: Cross-Section of Hypothetical, Rectangular Treatment Well

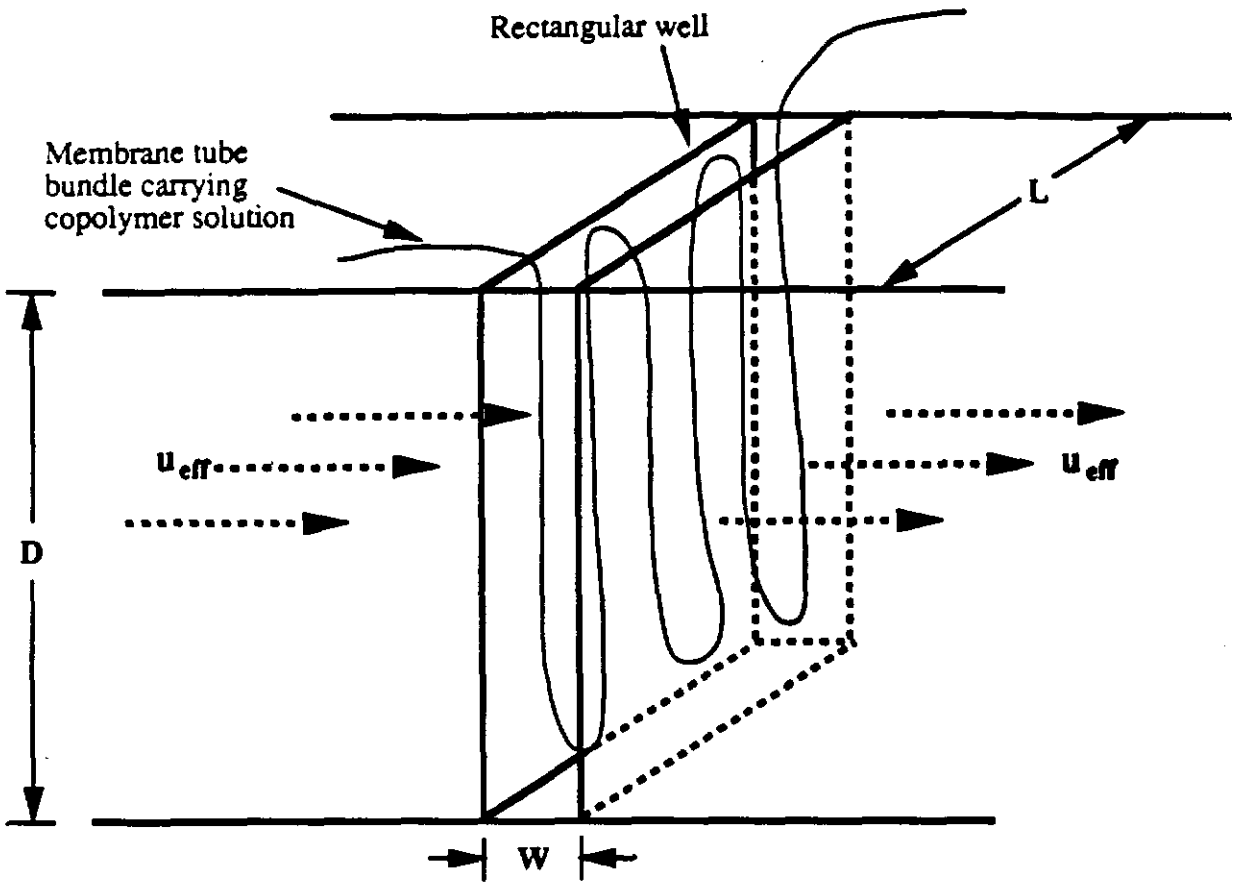

Well Properties

Wall area of the well = D x L
Well width = 6 inches
Well volume = 14,158 cm^3/ ft^2 wall area
Initial contaminant concentration in well = C_o

Membrane Tube Properties

Tube surface area, A = 4.788 cm^2/ ft^2 wall area
Tube volume, V = 0.0598 cm^3 / ft^2 wall area
Nominal MW Cutoff = 50,000 (average pore diameter = 50 Å)
Transmembrane molecular diffusive resistance = R_{tot} [s/cm]

Copolymer Solution Properties

Type copolymer = N-vinylpyrrolidone/styrene
Tube interior soluion polymer:water weight ratio, M = 0.20
Polymer-water partition coefficient K_{pw}(naphthalene) = 2420
Polymer-water partition coefficient K_{pw}(phenanthrene) = 49,100

Aquifer Properties

Porosity, n=0.50
Effective solute transport rate = u_{eff} [cm/s]
Contaminant concentration of fluid entering well = C_o

Figure 1-16: C_{well}/C_o Versus Time in a Rectangular Well

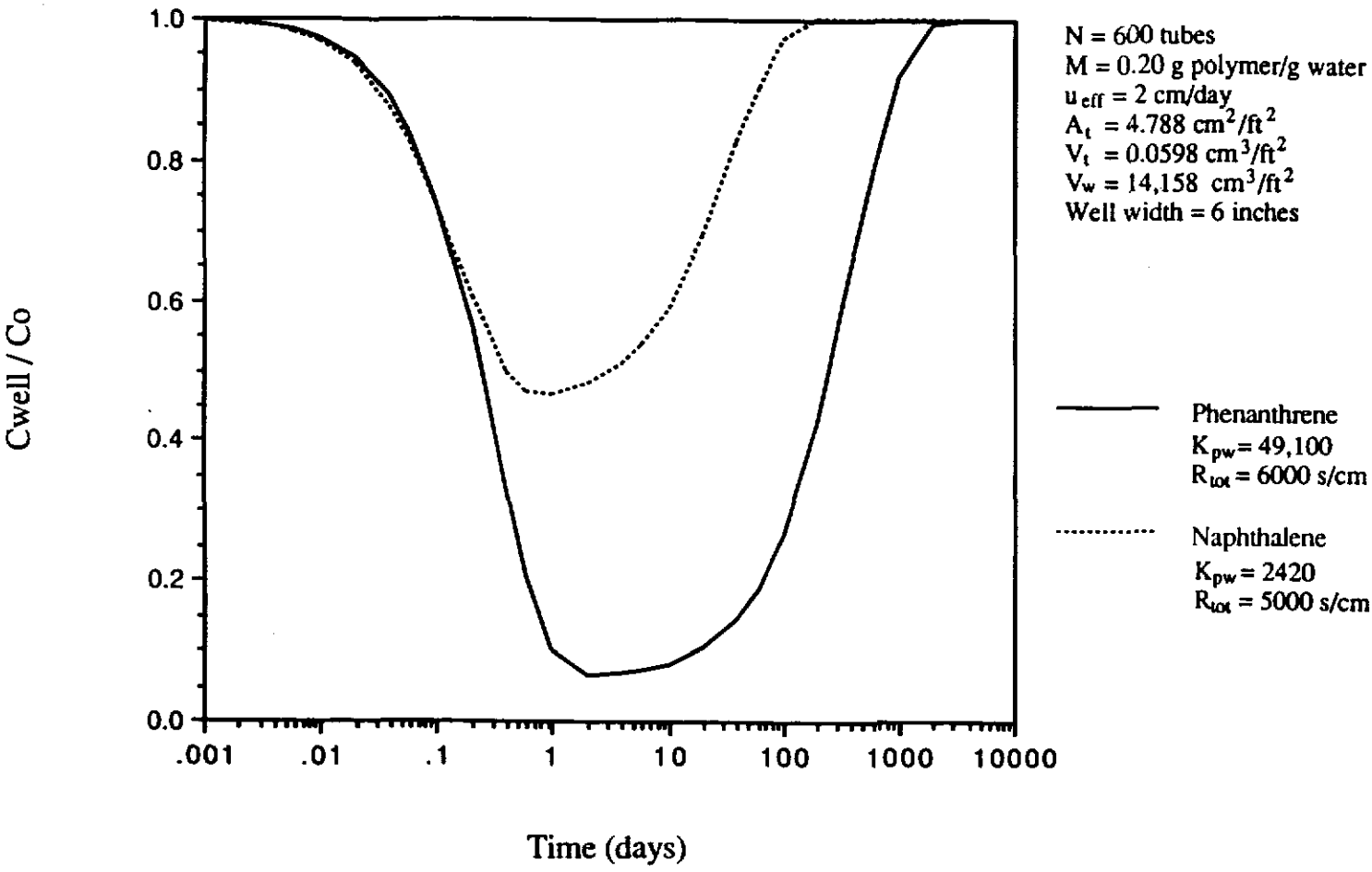

there is evidence of greatly enhanced solubilization of the organics in aqueous NVPS solution. Constant values of K_{pw} were determined from equilibrium data at 23.0°C for the three solutes in NVPS solutions, and are as follows:

$$\log K_{pw} \text{ (toluene)} = 3.39 \pm 0.04 \quad (1\text{-}25)$$

$$\log K_{pw} \text{ (naphthalene)} = 3.38 \pm 0.01 \quad (1\text{-}26)$$

$$\log K_{pw} \text{ (phenanthrene)} = 4.69 \pm 0.02 \quad (1\text{-}27)$$

The deviations given correspond to the 95% confidence interval of the data set. These values of partition coefficient for NVPS systems compare favorably to partition coefficients for other, lower molecular weight surfactant systems (Table 1-2).

(2) Total mass transfer resistance measurements and modeling:

Values of R_{tot} were obtained from the diffusion data for the polysulfone membrane tubes (each tube has 0.1-0.2μm-thick skin layer bound to a 0.275mm-thich support structure), as follows:

Table 1-6: Measured Membrane Resistances

Solute	Membrane MW Cutoff	R_{tot} (s/cm)
Naphthalene	2000	4980 ± 120
Naphthalene	50,000	4630 ± 210
Naphthalene	Pooled Data	4950 ± 100
Phenanthrene	2000	6020 ± 100
Phenanthrene	50,000	5950 ± 140
Phenanthrene	Pooled Data	5990 ± 70

The variances shown are 95% confidence intervals determined from the data fits. The experimental values for R_{tot} correspond very closely to the independently-predicted resistances for the experimental systems.

The membrane skin layer resistance to solute transmembrane molecular diffusion was much less than the resistance posed by the thicker membrane support structure for the systems studied here. This statement is supported by both the resistance data and the resistance models. Therefore, using a thinner support structure can significantly decrease the resistance to transmembrane solute diffusion, thus increasing system efficiency.

(3) Demonstration of the proposed system on a laboratory scale:

The third objective of this work was the demonstration of the proposed membrane/copolymer remediation system on a laboratory scale. The extraction of solute from an aqueous naphthalene plume moving through a soil matrix was demonstrated in two types of system set-ups -- one with a rectangular well, and one with a cylindrical well.

In the rectangular well experiment, the capture of naphthalene from an *initially naphthalene-saturated* lab-scale aquifer was demonstrated experimentally, and well concentration was modeled as a function of time. The match of the well concentration data with the modeled values was affected by desorption of naphthalene from well surfaces.

In the cylindrical well experiment, the capture of naphthalene from an *initially clean* lab-scale aquifer was demonstrated experimentally and well concentration was modeled as a function of time. Also, the naphthalene

concentration of the plume leaving the cylindrical treatment well was modeled as a function of time and two-dimensional space. Well concentration data agreed well with model predictions. The 2-D concentration data also agreed well with model predictions. The modelled 2-D concentration profile of the plume leaving the well was more strongly influenced by the velocity field solution than by the soil dispersion coefficients. Thus, for groundwater flow through a cylindrical well of diameter D, the decreased concentration plume has width approximately 2 times the diameter.

Recommended future work related to this thesis includes the development of the proposed system from lab scale to field scale. The effects on the proposed remediation system of naturally-occurring humic substances, multicomponent-contaminant systems, and membrane fouling and degradation should be investigated before implementation of the proposed system on a field scale. The application of the proposed system to cases where contaminated groundwater is actively pumped is another possible area of research.

A study of the improvement of transmembrane diffusion rates and system efficiency should be undertaken; of concern is the minimum required thickness of the membrane support structure for system durability. Membranes with thinner support structures have the potential for improving system efficiency significantly.

Further solubilization studies of systems using NVPS and like copolymers should be undertaken. This study has shown NVPS is a very effective organic solubilizer (compared with currently-used surfactants), and it is available in extremely high molecular weights (over 3 million g/mol). This allows for great

flexibility in filtration techniques for solute separation. Thus, the use of NVPS and similar amphipathic copolymers as easily-separable organic filtrants should be investigated for organic solute systems not studied in this work. Also, studies of ways to regenerate organic-saturated NVPS and like copolymers would be important in improving the cost efficiency of a proposed organic filtration system. Possible regeneration techniques include solvent extraction and organic solute evaporation. The latter of these may be a feasible means of removing volatile organics from the copolymer.

1.8. References for Chapter 1.

Bohon, Robert L. and Claussen, W. F., "The Solubility of Aromatic Hydrocarbons in Water," **JACS**, Vol. 73, 1951, pp.1571-1578.

Brink, L. E. S. and Romijn, D. J., "Reducing the Protein Fouling of Polysulfone Surfaces and Polysulfone Ultrafiltration Membranes: Optimization of the Type of Presorbed Layer," **Desalination**, Vol. 71, 1990, pp.209-233.

Crawford, Mark, "DOE Calls in the Labs for Defense Waste Cleanup," **Science**, Vol. 246, 1989, pp.24-25.

Edwards, D. A.,; Luthy, R. G.; Liu, Z., "Solubilization of Polycyclic Aromatic Hydrocarbons in Micellar Nonionic Surfactant Solutions," **Env. Sci. Tech.**, Vol. 25, 1991, pp.127-133.

Freeze, R. Allan and Cherry, John A., **Groundwater**, Prentice Hall, Inc.: Englewood Cliffs, N.J., 1979.

Hansch, C. and Leo, A., **Substituent Constants for Correlation Analysis in Chemistry and Biology**, Wiley: New York, N. Y., 1979.

Hurter, P. N. and Hatton, T. A., "Solubilization of Polycyclic Aromatic Hydrocarbons by Poly(ethylene oxide-propylene oxide) Block Copolymer Micelles: Effects of Polymer Structure," **Langmuir**, Vol. 8, 1992, pp.1291-1299.

Lyman, W. J.; Reehl, W. F.; and Rosenblatt, D. H., **Handbook of Chemical Property Estimation Methods**, American Chemical Society: Washington, D. C., 1990.

May, Willie E.; Wasik, Stanley P.; and Freeman, David H., "Determination of the Solubility Behavior of Some Polycyclic Aromatic Hydrocarbons in Water," **Analytica Chemistry**, Vol. 50, 1978, pp.997-1000.

Nystrom, Marianne, "Fouling of Unmodified and Modified Polysulfone Ultrafiltration Membranes by Ovalbumin," **Journal of Membrane Science**, Vol. 44, 1989, pp.183-196.

Prausnitz, J. M.; Lichtenthaler, R. N.; and deAzevedo, E. G., **Molecular Thermodynamics of Fluid-Phase Equilibrium**, Prentice-Hall, Inc.: Englewood Cliffs, N. J., 1986.

Thomas, E. R.; Newman, B. A.; Long, T. C.; Wood, D. A.; Eckert, C. A., "Limiting Activity Coefficients of Nonpolar and Polar Solutes in Both Volatile and Nonvolatile Solvents by Gas Chromatography," **J. Chem. Eng. Data**, Vol. 27, 1982, p.399.

2. Introduction

2.1. Background

The world is faced today with a myriad of organic, metallic and radioactive chemical wastes. Many early disposal practices are now deemed inadequate, and chemical waste containment and remediation is becoming a necessity as more cases of groundwater contamination become apparent. The technology at present is underdeveloped, and remediation times and costs seem overwhelming. The Department of Energy has estimated the cost of remediation of the United States' contaminated nuclear weapons production sites alone at $130 billion, and remediation will take about 50 years (Crawford, 1989). These bleak figures prompt a movement to newer, less expensive, and more efficient technologies for hazardous waste site containment and remediation. This thesis describes a new concept in hazardous waste site containment and remediation. The concept involves an aqueous amphipathic copolymer solution in hollow fiber membrane tubes placed in wells in the contaminated aquifer. Since the remediation takes place directly in the aquifer, the system allows cleanup without removal of contaminated soil to a treatment facility. The proposed technique offers containment of organic chemical waste and long-term, passive removal of the waste. Current methods for remediation and containment of contaminated aquifers are briefly discussed below.

One of the most widely-used methods for contaminated aquifer remediation is the *pump-and-treat* process. This process works by extracting contaminated groundwater by pumping, and treating it with a suitable technique such as solvent extraction or carbon adsorption, to remove the contaminant

before reinjecting the water into the soil. Factors such as high contaminant binding to organic material of the aquifer and large pumping requirements make this method inefficient, particularly for removing hydrophobic, sparingly water-soluble contaminants such as polycyclic aromatic hydrocarbons (PAH's) (James and Sanning, 1989, and MacKay and Cherry, 1989).

Contaminant concentrations on soil can be orders of magnitude higher than their concentrations in the surrounding liquid water phase due to preferential partitioning. This effect is primarily due to the attraction of hydrophobic organic contaminant to the organic components of the soil. The use of surfactants such as sodium dodecylsulfate to facilitate transfer of soil-adsorbed contaminants into a mobile aqueous phase is under investigation for application to pump-and-treatment-type processes (Valsaraj and Thibodeaux, 1989 and Edwards et al., 1991)

The goal of the treatment part of the pump-and-treat process is the concentration of the organic contaminant into an easily-mobilized phase. As mentioned, current methods of liquid waste concentration include *carbon adsorption* and *solvent extraction*. In carbon adsorption, organic contaminant is filtered from water passing through an activated carbon bed. Bulk handling and pumping concerns have made this technique unattractive for some applications (Ackerman, 1983). The solvent extraction technique attempts to remove the organic contaminant by contacting the contaminated water with an organic solvent, allowing the organic contaminant to preferentially partition into the organic phase. The use of traditional solvents such as benzene and toluene in this technique is not favorable, since counter-contamination of the water with solvent may be a problem (Mackay and Medir, 1983). More desirable routes of

aqueous waste separation and concentration which employ nontoxic, easily separable compounds are currently under investigation. One such process proposed by Prof. T. Alan Hatton at MIT involves ultrafiltration with high molecular weight copolymer surfactants (Hurter and Hatton, 1992).

Off-site *incineration* of soil to remove contaminant is also a widely-used aquifer treatment method, especially in cases where there is a high degree of adsorption of organic contaminant to the soil. Soil is excavated and moved off-site to an incinerator, where organic is vaporized from the soil.

Supercritcal water oxidation as a means of treating organics in aqueous wastes and soils is currently under development at MIT (Tester et al., 1993). The process makes use of the enhanced solubility of organics and oxygen in water at supercritical conditions (T > 374°C and P > 220 bar). The organic contaminant is oxidized readily at temperatures in the 400° to 600°C range since both the organic component and oxygen are in the same phase and the kinetics are relatively fast. *Bioremediation* (also called biorestoration) is a relatively new *in-situ* cleanup procedure based on the stimulation of natural microbial degradation processes that occur in the soil (Staps, 1989). *High pressure soil washing* as an on-site technique was used in Berlin by Kloeckner Umuelttechnik to remove organics and heavy metals (James and Sanning, 1989). The concept behind *thermal heating* is the extraction of contaminants from *in-situ*-heated soil by evaporation. *Steam injection* is a related technique which involves the volatilizaton of organics and other contaminants by injecting steam into the aquifer. A treatment technique proposed for on-site use at the Wide Beach Superfund site in the U. S. is *chemical treatment* with the substance potassium polyethylene glycol (KPEG). KPEG causes a change in the structure of PCB's (polychlorinated biphenyls) (James and

Sanning, 1989). *Electro-reclamation* is an in-situ cleanup method based on the electrokinetic phenomena which occur when a direct current is introduced to the soil. Electro-reclamation has been used to remove light metal contaminants from groundwater. In one case, 74% of the initial lead and copper content of contaminated soil was removed by this technique (Lageman et al., 1989). The application of electrokinetic phenomena to the removal of organic wastes from soils is also under investigation (Renaud and Probstein, 1987).

The cost estimates obtained from the given sources for the remediation procedures described above are summarized in Table 2-1. Note that not every technique works for a given waste situation. Variation in cost will be due to factors such as site location, labor costs, and contaminant type.

In cases where direct groundwater treatment is not economically feasible, containment of the contaminated groundwater to prevent leaching into streams and drinking water supply lines is the immediate goal. Two currently-used containment procedures are solidification (also called grouting) and slurry wall construction. In grouting, a solidifying agent such as cement is injected into the aquifer to reduce its permeability and slow contaminant leaching. Costs for gouting can range from $90 to $200 per ton (James and Sanning, 1989). Slurry walls can be constructed to shield an underground contaminant source from moving groundwater (Figure 2-1). The walls are constructed by digging trenches and backfilling them with a material with low permeability, such as cement, soil, bentonite, or a mixture of these. This method is only effective if an adequate seal can be made between the cement and a low permeability layer at the base of the aquifer. Costs of construction vary widely depending on the type and availability of fill material and depth of slurry wall. Approximate costs have

Table 2-1: Cost Comparison of Aquifer Remediation Technologies

Remediation Technique	Cost [$/ton]	Source
Off-site Incineration	250 - 500	(Vervalin, 1989)
Supercritical Water Oxidation	77 - 480 †	(Crawford, 1989)
Bioremediation	40 - 70	(Staps, 1989)
High Pressure Soil Washing	80 - 120 *	(James and Sanning, 1989)
In-situ Thermal Heating	30 - 58	(James and Sanning, 1989)
Off-site Thermal Heating	375	(James and Sanning, 1989)
Electroreclamation	50 - 450	(Lageman et al., 1989)

† Cost per ton of treated groundwater, not aquifer material
* Does not include cost of pre- and post-washing treatment

Note cost values are very site-dependent. Values in table give representative ranges.

Figure 2-1: Slurry Wall Configurations

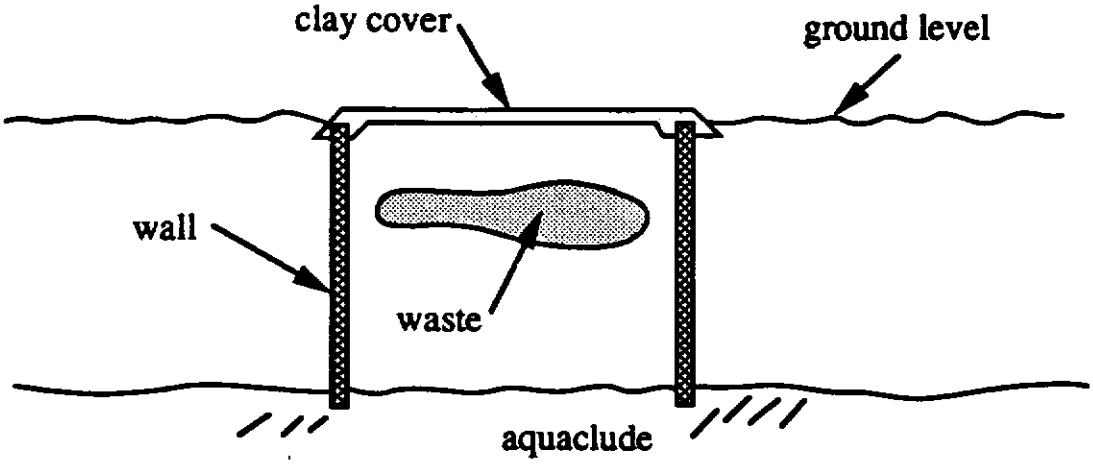

(Ryan, 1980)

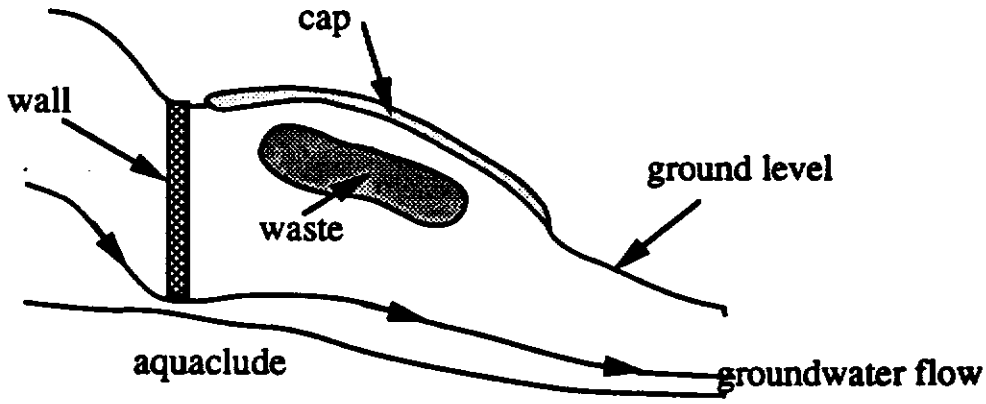

(Tolman et al., 1978)

been reported by Spooner et al., 1982, to range from $2 to 235 (1979 dollars) per square foot of wall.

It would be desirable in PAH-contaminated aquifers to initiate a cleanup procedure that both fulfills the immediate requirement of containment and eventually removes the contaminant from the aquifer. In the cleanup of various organic wastes, the pump-and-treat method has been shown to be inefficient (Mackay and Cherry, 1989) due to organic adsorption onto aquifer material. Containment procedures such as slurry wall construction require permanent monitoring and maintenance. A guarantee of complete containment is difficult, if not impossible, to obtain due largely to the potential for leakage under the base of the wall.

2.2. Proposed Process Description

The proposed system provides immediate containment, and eventual removal of contaminant from groundwater. The system is passive in that groundwater is not pumped, it is filtered of contaminant as it moves naturally through a series of treatment wells. Figure 2-2 is a schematic of the proposed system. It shows a cross-sectional view of a region of contamination in an aquifer. The contaminant plume has been elongated in the direction of groundwater flow. As in many contaminated groundwater situations, it is important, first, to provide *containment* of the plume to prevent contaminant leaching to drinking water or irrigation supplies.

As pictured, the plume is located in the water-saturated region of the aquifer (below the water table) and is assumed organic in nature. In the case of a chemical spill of pure organic liquid (such as gasoline), there is generally a layer of the pure organic floating on the water table. This layer is most easily removed by pumping, but leaching of the organic to the groundwater up to that organic species' solubility in water will have taken place. Even though most organics have low solubility in water (such as PAH's and pesticides), many remain toxic at even lower levels. For example, the organic pesticides endrine, lindane, and toxaphene have water solubilities 0.2, 7, and 3 mg/L, respectively; but they are hazardous at much lower concentrations -- 0.0002, 0.004, and 0.005 mg/L, respectively (Freeze and Cherry, 1979). Other examples include volatile organic components of gasoline. For instance, the amount of benzene and toluene in gasoline is generally 2-5% and 6-7% by volume, respectively (Cline et al., 1991); these are significantly high levels. The U.S. Environmental Protection Agency primary drinking water regulations set maximum permissible levels of benzene

Figure 2-2: Proposed Barrier Concept

Cross-Sectional View

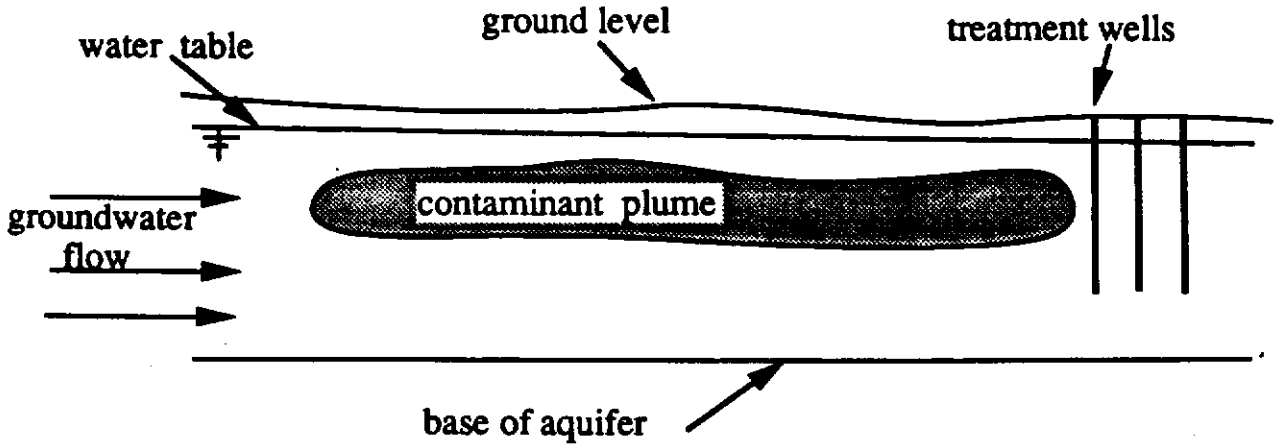

Overhead View

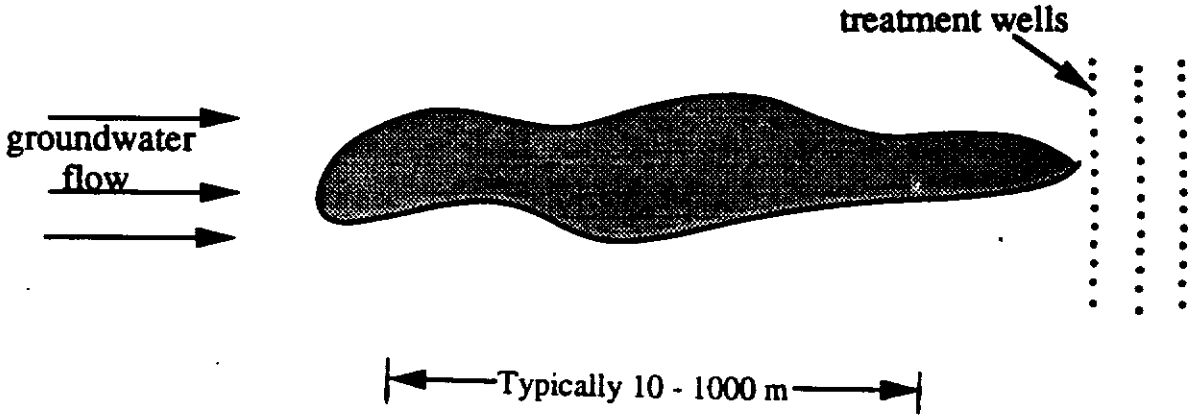

and toluene at 0.005 and 2 mg/L, respectively (Cotruvo and Vogt, 1990). However, the solubility of benzene and toluene in water is much higher – 1790 and 627 mg/L, respectively (May et al., 1978). Thus, a relatively small spill of gasoline can result in contamination of a large amount of water above legal concentration limits.

The treatment wells in Figure 2-2 are cylindrical monitoring-type wells from 5 to 15 cm in diameter. These wells are arranged in lines perpendicular to the direction of groundwater flow. In the case of non-unidirectional groundwater flow, the wells would be arranged in such a way as to intercept all of the passing contaminant. A variation of the system replaces the cylindrical wells with a long, rectangular well extending perpendicularly to the direction of groundwater flow.

Figure 2-3 shows a cross-section of one of the treatment wells from Figure 2-2. Inside each well is placed a bundle of hollow fiber membrane tubes (each approximately 1 mm in diameter) filled with an aqueous, macromolecular copolymer solution. Contaminant travels through the membrane wall via molecular diffusion and adsorbs to hydrophobic sites of the copolymer. The copolymer is chosen to greatly enhance the solubilization of the organic species in aqueous solution. The copolymer solution may be recirculated intermittently when it becomes sufficiently loaded with contaminant for copolymer regeneration or waste incineration. The pore size of the membrane is chosen large enough to allow passage of contaminant into the copolymer solution, but small enough to prevent passage of copolymer out of the membrane interior. Contaminant removal takes place passively as the plume slowly moves through

Figure 2-3: Proposed Process -- Single Well Cross-Section

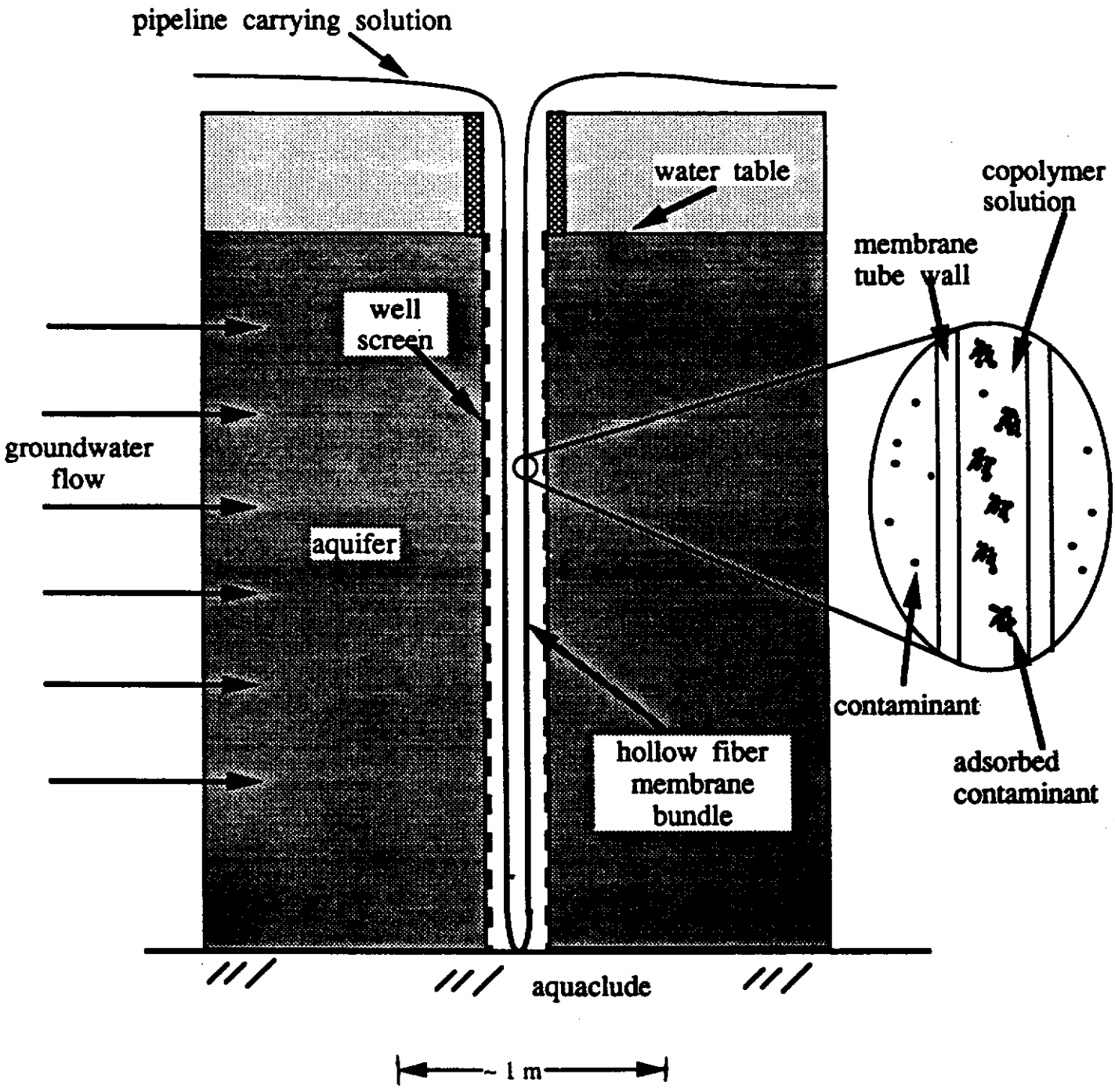

the cleanup area. In this way, immediate containment of the contaminant plume is achieved as is eventual removal of the contaminant. Intermittent replacement (i.e. monthly to yearly) of the copolymer solution is the only required operational procedure following installation.

Operating specifications to be determined for such a system include copolymer and membrane type, membrane average pore size, copolymer concentration, well spacing and configuration, and membrane configuration in each individual well. Factors affecting the optimum choices for the above specifications include groundwater flowrate and flow direction (governed by aquifer properties such as conductivity and hydraulic gradient), contaminant type and properties (solubility, molecular diffusion coefficient in water, molecular weight), and remediation requirements. These factors and operating specifications will be discussed in this work.

The membranes used in this work are Supelco's polysulfone ultrafiltration membranes, described in more detail in Chapter 5. The membranes used are anisotropic and have nominal molecular weight cutoffs of 2000 and 50,000 g/mol. Membranes best suited to the groundwater remediation system are those that are sufficiently resistant to microbial attack, chemical degradation, and fouling. Work is currently being done to develop coatings which make industrial ultrafiltration membranes more resistant to fouling (Brink and Romijn, 1990, and Nystrom, 1989). This is a topic of concern in ultrafiltration technologies as well, where harsh environments are often encountered.

The copolymer used in this experiment is N-vinylpyrrolidone/styrene, discussed in detail in Chapter 4. It is nontoxic and has both hydrophobic and

hydrophilic properties. Thus, it is an effective organic solubilizer, and it forms a stable suspension in water. The key features of the copolymer chosen for the system are its hydrophobicity (organic-solubilization capacity) and its molecular weight. The latter attribute is important since membrane pore size must be considerably less than the size of the copolymer molecule to prevent leakage.

2.3. Previous Investigations of Enhanced Solubilization of Aromatic Compounds in Aqueous Solution

One important aspect in the design of the proposed groundwater remediation system is the ability of the filtrate (copolymer solution) to accumulate contaminant. In many contaminated aquifers, pure organic liquid contaminates groundwater up to its saturation limit, which for many organic compounds is very low (< 1 ppm). But as mentioned before, many of the contaminants are harmful at even lower levels. The copolymer chosen for the system in effect enhances the solubility of contaminant in aqueous solution, and thus enables its concentration, quite analogous to the phase partitioning that occurs with carbon adsorption and solvent extraction, discussed in Section 2.1.

Recently, the use of surfactants whose molecules form micellar structures has been investigated for the enhanced solubilization of hydrophobic organic compounds in water (Valsaraj and Thibodeaux, 1989, Edwards et al., 1991, and Hurter and Hatton, 1992). In light of new membrane separation techniques (Hurter and Hatton, 1992), the use of easily separable, high molecular weight surfactants provides an alternative to carbon adsorption and solvent extraction. The molecular weight of the surfactants used in the above studies range from a few hundred to 13,000 g/mol. The copolymer used in this paper, N-vinylpyrrolidone/styrene (NVPS), is of approximate molecular weight 3.4 million g/mol.

The general method for quantifying the ability of a surfactant to concentrate a contaminant in aqueous solution is by means of a partition

coefficient. A surfactant-water partition coefficient, K_{sw}, is determined for a given surfactant-water-solute system, as defined by the following:

$$K_{sw} \equiv \frac{\text{g solute in surfactant pseudophase / g surfactant}}{\text{g solute in aqueous pseudophase / g water}} \qquad (2\text{-}1)$$

The surfactant solution is thought of as a combination of two interspersed "pseudophases" – a surfactant pseudophase and a water pseudophase – between which the solute (contaminant) molecules partition. How well a surfactant works depends on how large its partition coefficient is, and hence, how much the solute favors being in the surfactant rather than the water. The partition coefficient is generally modeled as a constant over a wide range of solute concentrations.

Values of partition coefficients of solutes (model contaminants) used in this work in a variety of surfactants are shown in Table 2-2. The values listed are logarithms of sufactant-water partition coefficient and are based on solubility measurements where the aqueous pseudophase was saturated with solute. A goal for this study was to choose a copolymer whose *polymer*-water partition coefficients are as high as the values in Table 2-2 for the solutes chosen. The polymer-water partition coefficient, K_{pw}, is completely analogous to surfactant-water partition coefficient, K_{sw}, (Equation 2-1) and is defined as follows:

$$K_{pw} \equiv \frac{\text{g solute in polymer pseudophase / g polymer}}{\text{g solute in aqueous pseudophase / g water}} \qquad (2\text{-}2)$$

Table 2-2: Partition Coefficients of Naphthalene and Phenanthrene in a Variety of Surfactants at 25°C

Solute	Water Solubility Csat, (mg/L)	Log K_{ow} (conc. ratio)	Log K_{sw} (P103)	Log K_{sw} (Brij 30)	Log K_{sw} (Igepal CA-720)	Log K_{sw} (Tergitol NP-10)	Log K_{sw} (Triton X-1000)
Naphthalene	31.2	3.37	3.31	3.29	3.02	2.99	3.10
Phenanthrene	1.29	4.46	4.60	4.27	4.07	4.14	4.16
Sources	(Bohon and C., 1951) (May et al., 1978)	(Hansch and L., 1979)	(Hurter and H., 1992)	(Edwards et al., 1991)	(Edwards et al., 1991)	(Edwards et al., 1991)	(Edwards et al., 1991)

2.4. Previous Investigations of Transmembrane Transport of Organic Compounds in Aqueous Solution

An important part of this project is the study of molecular diffusive transfer through anisotropic membranes. Most transmembrane diffusion studies deal with membranes of well-characterized geometries, such as track-etched membranes whose pores are of uniform diameter. The membranes used in this work are asymmetric, anisotropic membranes whose geometries are not easily characterized. Only average effective pore size and membrane thicknesses are known. However, these asymmetric membranes are important in the application of the proposed system, since they are easier to produce and are generally less expensive than track-etched membranes. The asymmetric membranes have been used in industrial ultrafiltration processes for years.

Some of the studies of transmembrane molecular diffusion using track-etched membranes are discussed here. Deen et al. (1981), studied solute diffusion through microporous membranes. The pore sizes used in this study were large compared to the solute sizes. Other diffusion studies using large pore to solute size ratios (above 2.0) include those by Beck and Schultz (1972), and Bohrer et al. (1984). Baltus and Anderson (1983) studied asphaltene diffusion in mica membranes. Studies of more hindered transmembrane diffusion of solute include Malone and Anderson (1978) and Wong and Quinn (1976).

Robertson and Zydney (1990) studied hindered molecular diffusion of bovine serum albumin (size 39Å x 139Å) through *anisotropic* ultrafiltration membranes of average pore diameters between 55Å and 1000Å. Resistances were measured in a well-stirred diffusion cell apparatus. An ultrafiltration

membrane sheet of approximately 3-cm^2 surface area divided the cell. An aqueous solution of the albumin was initially introduced on one side of the cell, and was allowed to diffuse through the membrane to the other side for 12 to 24 hours. The concentration of each cell after this time period was then recorded and resistances calculated. Membrane resistances could only be determined to within about an order of magnitude for most of their experiments.

There were two important differences between the experimental procedure used in this thesis and the procedure in the Robertson and Zydney (1990) study in an effort to obtain more replicable results. First, a higher membrane surface area was used in this study (600 cm^2 versus 3 cm^2) since membrane variability was cited by Robertson and Zydney as being a possible source of error. Secondly, in this study concentration was monitored continuously via on-line UV-VIS spectrophotometry. In the Roberson and Zydney procedure, only one data point could be obtained per run. The diffusion experiments and modeling techniques used in this study are discussed in detail in Chapter 5 of this work.

3. Thesis Objectives and Approach

The objectives of this thesis are threefold. The first two objectives involve the experimental and theoretical study of fundamental phenomena -- solubility and diffusive transport -- important to the membrane/copolymer remediation system proposed in Section 2.2. The third objective concerns a lab-scale demonstration of the proposed system. Information from the first two objectives were used in modeling the lab-scale demonstration of objective three.

The first objective of this work was to quantify the enhanced solubilization of three model aromatic contaminants – toluene, naphthalene, and phenanthrene -- in aqueous amphipathic copolymer solution. The copolymer used was N-vinylpyrrolidone/styrene, a high molecular weight (3.4 million g/mol) random-structured copolymer. Solubility experiments were conducted and a thermodynamic analysis was completed. This work is discussed in Chapter 4, and the results tell how well contaminant may be concentrated in copolymer solutions used in the proposed process.

The second objective of this thesis was to quantify the rate of molecular diffusive transport of the aromatic solutes from the contaminated aqueous phase through anisotropic hollow fiber membranes used to contain the aqueous copolymer solution. Diffusive transport experiments were conducted and analysis completed, both discussed in detail in Chapter 5. The results tell how quickly the contaminant diffuses through the membrane and into the copolymer solution used in the proposed process. A comparison of experimental and modeled results gives insight into what factors are most important in decreasing

mass transfer resistance, thus increasing the effectiveness of the proposed system.

The third objective is the demonstration of the proposed remediation system on a laboratory scale. The extraction of solute from an aqueous naphthalene plume moving through a soil matrix is demonstrated in two types of model aquifer systems described in Chapter 6. Data from the solubility and transport experiments were used as inputs in the theoretical modeling of the objective three experiments. Finally, a copolymer/membrane remediation system is developed and evaluated for treating a hypothetical contaminated aquifer.

4. Ehanced Solubility of Aromatics in Amphipathic Copolymer Solution

This chapter describes the experiments performed to quantify the enhanced solubility of three aromatic solutes -- toluene, naphthalene, and phenanthrene -- in aqueous solutions of N-vinylpyrrolidone/ styrene copolymer. Thermodynamic analysis was used to develop a methodology for generalizing the results so that the solubilization capacities of NVPS and other copolymers can be estimated for various hydrophobic compounds of interest.

4.1. Materials for Experiments

The copolymer used in this study, N-vinylpyrrolidone/ styrene, was obtained as a 40 weight% copolymer solution in water. The supplier, Scientific Polymer Products, Inc., reported that the copolymer is composed of styrene and N-vinylpyrrolidone monomers in a weight ratio of 60 to 40. The hydrophilic character of the copolymer allows it to form a stable suspension in water, and its hydrophobic nature lends it organic solubilization capacity. NVPS is nontoxic and is generally no more expensive than sodium dodecylsulfate, a commonly used surfactant; research quality NVPS is about $40 per kg of 40wt.% solution (Scientific Polymer Products, Inc., 1991). The average molecular weight was reported as approximately 3.4 million g/mol. NVPS is a random copolymer as shown in Figure 4-1. The hydrophobic model organic compounds used in this study were toluene (99.8% pure), naphthalene (99+% pure), and phenanthrene (98% pure). These were chosen as representative 1-, 2-, and 3-ring aromatic compounds. The toluene was obtained from Aldrich Chemical Company, Inc.,

and the naphthalene and phenanthrene were obtained from Sigma Chemical Company. These chemicals were used without further purification.

Figure 4-1: Structure of Copolymer, N-Vinylpyrrolidone/styrene (NVPS)
A random sequential arrangement of ring structures x and y on the copolymer chain with x to y weight ratio of 60:40 is depicted.

N-vinylpyrrolidone/styrene:

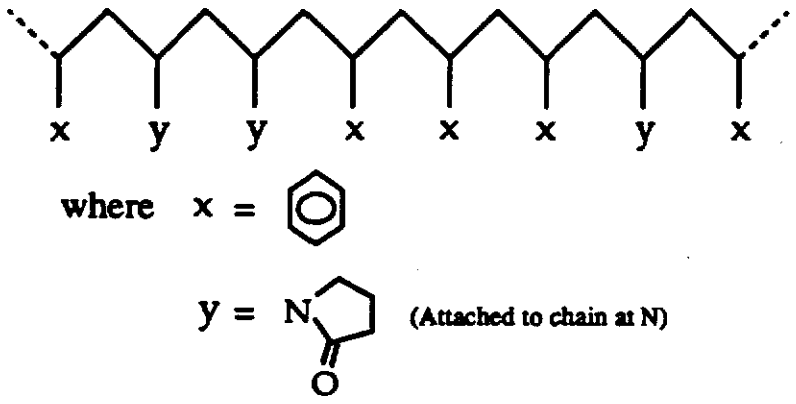

4.2. Experimental Procedures

Since organics tend to adsorb onto solid surfaces such as the sample containers used in concentration measurements, careful handling techniques must be employed. Plastic, polyethylene, and polypropylene bottles are particularly troublesome. To avoid this potential problem, 25-ml glass flasks were filled with aqueous NVPS copolymer solutions of known concentration and about 8 grams of either solid naphthalene or phenanthrene. Other 25-ml glass flasks were filled with aqueous NVPS solution and about 10 ml of liquid toluene. Very low headspace was allowed in the flasks (< 2 ml). The flasks were covered, shaken, and allowed to equilibrate at 23.0 ± 0.1°C in a constant-temperature water bath.

Solution concentrations of naphthalene, phenanthrene, and toluene were determined by absorbance measurements from a Perkin-Elmer Lambda 3B UV/VIS spectrophotometer, using quartz suprasil cells. Measurements were made at maximum absorbance wavelengths for each compound: 276 nm (2760 Å) for naphthalene, 293 nm for phenanthrene, and 261 nm for toluene.

Extinction coefficients for the absorbance of naphthalene and phenanthrene were measured as follows. A saturated aqueous solution of the organic solid was created by circulating water through a generating column filled with organic solid as described in the literature (Hurter and Hatton, 1992). The solution was held at 23.0 ± 0.1°C with a constant temperature bath. A fraction of the circulating solution was diverted to the spectrophotometer through a 1-cm-pathlength flow cell where its absorbance was read on-line.

Constant circulation ensured a saturated solution of solute was maintained, regardless of any solute adsorbed to the tubing or container walls. All tubing was made of Teflon. The Beer's law extinction coefficients were experimentally determined at solute absorbance peaks and agreed to within 2% of published values (Bohon and Claussen, 1951, and Wauchope and Getzen, 1972).

The absorbance of NVPS must be taken into account in sample concentration determination, since aqueous NVPS absorbs light at ultraviolet as well as visible wavelengths. The extinction coefficient of aqueous NVPS was experimentally measured at the solute absorbance peaks – 276, 293, and 261 nm. The extinction coefficient was also measured at 400 nm, a wavelength at which the organic model compounds we selected have zero absorbance. Thus, the total polymer-water-solute solution absorbance at the three lower wavelengths equals that from both NVPS and the organic compound present in solution. The exact NVPS concentration of the sample was measured by solution absorbance at 400 nm. All measurements were made using a 1-cm-pathlength reference cell filled with pure water. The above technique was experimentally justified by direct measurement of naphthalene dissolved into concentrated NVPS solutions of 19 and 23 weight percent, respectively.

Three sets of NVPS solutions were maintained in contact with the model organic compounds to allow equilibration for one day before the initial absorbance measurement. Absorbance measurements of one test sample from each of the naphthalene, phenanthrene, and toluene sample sets were taken daily to determine when equilibrium concentrations had been reached (assumed when absorbance readings changed < 2% from the previous day's reading). An additional three days of equilibration were allowed after it was determined

equilibrium had been reached for a given sample set before all samples were analyzed.

The sampling technique was as follows. Solute-contacted NVPS solution samples were first passed through Schliecher and Schwell brand filter paper to remove any visible solid organic particles. Each solution was then pipetted and diluted so that the absorbance reading, $A = \ln \frac{I_o}{I}$, in a 1-cm-pathlength cell never exceeded 1.5. At least six replicate absorbance readings were taken at each wavelength to insure precision. Before a reading was taken, the withdrawing syringe was contacted repeatedly with solution to allow any adsorptive equilibrium between the solution and the syringe wall. The absorbance was then measured at the wavelength of maximum absorption of the given solute and at 400 nm. The concentrations of both NVPS and the organic were then calculated.

4.3. Experimental Results

The saturated equilibrium concentrations of toluene, naphthalene, and phenanthrene in solutions of NVPS are given in Table 4-1 and are plotted in Figure 4-2 as a function of NVPS to water weight ratio. Each concentration measurement for a solute is given as a multiple of the solute's saturated concentration in pure water at 23.0°C (Table 4-2). For example, a solution with an NVPS to water weight ratio of 0.04 will solubilize about 100 times the naphthalene, or about 2000 times the phenanthrene that an equal amount of pure water will solubilize. Figure 4-2 shows a linear relationship between the solute concentration and the NVPS to water ratio for each of the three solutes. Such linear relationships have been observed for systems of solid solute partitioning between two immiscible liquids (Prausnitz et al., 1986).

A surfactant-water partition coefficient may be derived for each solute-surfactant system, and because the saturation behavior is linear, each partition coefficient will be constant. The overall amount of solute in the solution is divided into solute associated with the water and polymer pseudophases. Here, a pseudophase is defined as one of two separate interspersed phases. The water and polymer pseudophases are interspersed, but remain chemically separate and undissolved in each other. The concentration basis defined as follows is used to express the partitioning of solute between these two pseudophases:

$$\frac{C}{C_{w,sat}} = \frac{C_w + C_p}{C_{w,sat}} = \frac{C_w}{C_{w,sat}} + \frac{C_p}{C_{w,sat}} \qquad (4\text{-}1)$$

Table 4-1: Saturated Concentrations of Solutes in Aqueous NVPS Solutions at 23°C

Toluene		Naphthalene		Phenanthrene	
g NVPS / g water	$C/C_{w,sat}$	g NVPS / g water	$C/C_{w,sat}$	g NVPS / g water	$C/C_{w,sat}$
.0069	19.0	.0051	13.9	.0100	366
.0104	25.1	.0101	25.9	.0211	1020
.0197	46.6	.0152	38.9	.0316	1530
.0234	47.6	.0205	51.1	.0416	2020
.0243	59.0	.0256	62.1	.0531	2710
.0406	89.9	.0309	78.6	.0652	3150
.0793	204.5	.0362	87.9		
		.0416	99.8		
		.0472	110.7		

C = solute concentration in NVPS solution

$C_{w,sat}$ = saturated concentration of solute in pure water
(= constant for each solute at system temperature and pressure, given in Table 1-2)

$C/C_{w,sat}$ = factor of solute concentration "enhancement" provided by the NVPS

Figure 4-2: Enhanced Solubility of Phenanthrene, Naphthalene, and Toluene in Aqueous NVPS Solution as a Function of NVPS:Water Weight Ratio

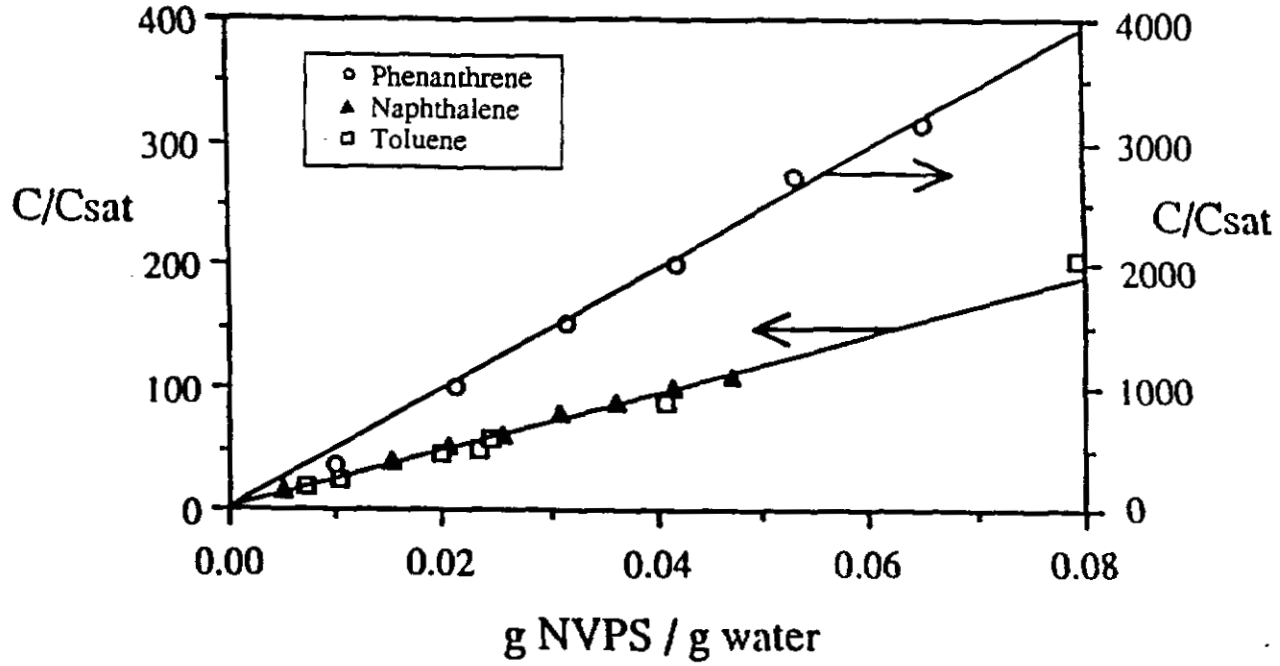

Table 4-2: Comparison of Surfactant Partition Coefficients for Model Solutes

Solute	Water Solubility Csat, (mg/L)	Log K_{ow} (conc. ratio)	Log K_{pw} (NVPS) (this work)	Log K_{sw} (P103)	Log K_{sw} (Brij 30)	Log K_{sw} (Igepal CA-720)	Log K_{sw} (Tergitol NP-10)	Log K_{sw} (Triton X-1000)
Toluene	627	2.73	3.39 ± .04	----	----	----	----	----
Naphthalene	31.2	3.37	3.38 ± .01	3.31	3.29	3.02	2.99	3.10
Phenanthrene	1.29	4.46	4.69 ± .02	4.60	4.27	4.07	4.14	4.16
Sources:	(*a*, *b*)	(*c*)	(*this work*)	(*d*)	(*e*)	(*e*)	(*e*)	(*e*)

(a) Bohon and Claussen, 1951
(b) May et al., 1978
(c) Hansch and Leo, 1979
(d) Hunter and Hasson, 1992
(e) Edwards et al., 1991

where C = g solute per ml solution, C_p = g solute in "polymer" pseudophase per ml solution, C_w = g solute in "water" pseudophase per ml solution, and $C_{w,sat}$ = g solute in pure water at saturation per ml water. K_{pw} and NVPS to water weight ratio are defined as follows:

$$K_{pw} \equiv \frac{\text{g solute in NVPS polymer / g polymer}}{\text{g solute in water / g water}} \tag{4-2}$$

$$M \equiv \frac{\text{g NVPS}}{\text{g water}} \tag{4-3}$$

Then for $C_w \cong C_{w,sat}$, the relationship between measured solute concentration and NVPS to water weight ratio becomes the following:

$$\frac{C}{C_{w,sat}} = 1 + K_{pw} M \tag{4-4}$$

Values of K_{pw} for NVPS-water partitioning for the three solutes are given in Table 4-2 with 95% confidence intervals.

4.4. Thermodynamic Solubility Analysis

Values from the literature of log K_{sw}, surfactant-water partition coefficient, with the same concentration basis as K_{pw} are shown in Table 4-2 for a variety of surfactants with naphthalene and phenanthrene solutes. Table 4-2 also lists values of log K_{ow}, the octanol-water partition coefficient, for the solutes. The similarity and apparent correlation of values of K_{sw} and K_{ow} has been noted by each of the investigators. All the surfactants in Table 4-2 except NVPS are reported to form micelles whose hydrophobic cores attract and concentrate hydrophobic solutes in aqueous solution. However, NVPS, which is too large and unstructured (it is a random, not a block copolymer) to form micelles, displays a very similar K_{pw}- K_{ow} correlation for the naphthalene and phenanthrene data. The values of K_{pw} for NVPS are higher than the K_{sw} values of the other surfactants. This may be due to the high relative hydrophobicity of the aromatic styrene monomer which makes up 60 weight% of the copolymer. The relative hydrophile of NVPS, N-vinylpyrrolidone, exhibits some hydrophobic character as well due to its hydrocarbon ring (Molyneaux, 1984).

Thermodynamic analysis of two-phase equilibrium was used to predict the relationship between K_{pw} and K_{ow} for the solute-water-NVPS systems. Consider a system consisting of a polymer surfactant phase in contact with an aqueous phase. A solid solute is added and allowed to dissolve until both the water and NVPS phases are saturated with solute. At saturation, the liquid phases are in thermodynamic equilibrium, and the solute component fugacities in each phase are equal:

$$\hat{f}_i^w = \hat{f}_i^p \qquad (4\text{-}5)$$

where superscripts w and p denote the aqueous and polymer phases, respectively, and subscript i denotes solute i. The fugacity of the solute in each phase can be expressed as a liquid-phase fugacity. Expressed in terms of activity coefficients, Equation 4-5 becomes the following:

$$\gamma_i^w x_i^w f_i^L = \gamma_i^p x_i^p f_i^L \qquad (4\text{-}6)$$

where, in general, γ_i^α denotes the aqueous-phase activity coefficient of solute i in phase α, x_i^α denotes the mole fraction of solute i in phase α, and f_i^L denotes the reference fugacity of pure solute i in a liquid state at the temperature and pressure of the mixture. Since the reference state is pure solute i, γ_i^α approaches 1.0 as x_i^α goes to 1.0. The value of the polymer phase activity coefficient may be estimated using a conventional Flory-Huggins model for the excess Gibbs free energy (Prausnitz et al., 1986). For polymer solutions of high chain length, it is more convenient to use a weight basis for this calculation (Patterson et al., 1971); therefore, we can rewrite Equation 4-6 noting that the same reference state is selected for solute i:

$$\gamma_i^w x_i^w = \gamma_i^{*p} w_i^p \qquad (4\text{-}7)$$

where γ_i^{*p} is the activity coefficient of solute i in the polymer phase calculated on a weight fraction basis, and w_i^p is the weight fraction of solute i in the polymer phase. We define K_{pw}^*, an alternate form of polymer-water partition coefficient, as follows:

$$K_{pw}^* \equiv \frac{w_i^p}{x_i^w / V_w} \; [=] \; \frac{\text{g solute in polymer/g polymer phase}}{\text{mol solute in aqueous phase/L aqueous phase}} \qquad (4\text{-}8)$$

where v_w is the molar volume of the aqueous phase in units of L/mol, assumed equal to the molar volume of water at system temperature and pressure. The relationship between measured K_{pw} reported in Table 4-2 and K^*_{pw} above is:

$$K^*_{pw} = K_{pw} \frac{MW_{sol}}{1000\ g/L} \cdot R_p \qquad (4\text{-}9)$$

where MW_{sol} is the solute molecular weight [g/mol] and R_p is the ratio of polymer mass to polymer phase mass, the latter term including the mass of the solute partitioned into the polymer pseudophase. Using Equation 4-7, we may substitute activity coefficients for mass and mole fraction into Equation 4-8 to obtain:

$$\frac{w_i^P}{x_i^w} = \frac{\gamma_i^w}{\gamma_i^{*P}} \qquad (4\text{-}10)$$

$$K^*_{pw} = v_w \frac{\gamma_i^w}{\gamma_i^{*P}} \qquad (4\text{-}11)$$

Using Equation 4-9, $\log K_{pw}$ can be expressed as:

$$\log K_{pw} = \log v_w - \log \gamma_i^{*P} + \log \gamma_i^w - \log \frac{MW_{sol}}{1000} - \log R_p \qquad (4\text{-}12)$$

All of the terms on the right side of Equation 4-12 can be calculated and appear in Table 4-3. All logarithms are base 10.

Table 4-3: Activity Coefficients and Other Parameter Inputs: NVPS-Solute-Water Systems

Solute	Log Kow [(a)]	Log γ_i^o	Log γ_i^w	Log γ_i^{*p}	Log $\frac{MWsol}{1000}$	Log P	Log K_{pw} (Equ. 4-12)	Log K_{pw} (Equ. 4-26)	Log K_{pw} (measured)
Toluene	2.73	0.34 [(b)]	3.99	0.17	-1.04	-0.41	3.53	3.55	3.39
Naphthalene	3.37	0.53 [(c)]	4.93	0.41	-0.89	-0.03	3.70	3.61	3.38
Phenanthrene	4.46	0.82 [(c)]	6.43	0.41	-0.75	-0.03	5.06	4.85	4.69

Constants: $\log_{10} v_o = -0.80$

$\log_{10} v_w = -1.74$

v_i [=] L/mol

(a) Values taken from Hansch and Leo, 1979.
(b) Value taken from Thomas et al., 1982.
(c) Values estimated using UNIFAC/UNIQUAC method (Lyman et al., 1990).

All logarithms are base 10.

Values of log γ_i^{*p} were calculated using the following modified Flory-Huggins equation (Patterson et al., 1971):

$$\ln_e a_i = \ln_e(\gamma_i^{*p}\ w_i^p) = \ln_e \phi_i + (1 - \frac{1}{r})\,\phi_p + \chi \phi_p^{\,2} \qquad (4\text{-}13)$$

where subscript i represents the solute, subscript p represents the copolymer, a_i is the solute activity, ϕ_i and ϕ_p are volume fractions of the solute and polymer respectively, r is the ratio of average copolymer molar volume to solute molar volume, and χ is the so-called Flory parameter that is typically fit to data. χ reflects the intermolecular forces between solute and polymer. For solutes with molecular structure similar to the copolymer monomers, χ approaches zero and the solution becomes athermal indicating near ideal solution behavior (Prausnitz

et al., 1986). Lacking data, we set $\chi = 0$. Calculation of γ_i^{*P} requires an estimate of ϕ_i, which we obtained from the solute-NVPS solubility data. Values of γ_i^{*P} do not vary considerably from 1.0 as expected from the molecular similarity between the solutes and copolymer monomers. A conservative error estimate for values of γ_i^{*P} in Table 4-3 is 50%.

Values of γ_i^w for the three solutes were obtained as follows. Consider first the binary system of liquid toluene and water at thermodynamic equilibrium at T = 23.0 °C and P = 1 atm. The fugacities of toluene in the toluene-rich phase and the water-rich phase can be equated to yield:

$$\gamma^w_{toluene}\, x^w_{toluene}\, f^L_{toluene} = \gamma^{tol}_{toluene}\, x^{tol}_{toluene}\, f^L_{toluene} \qquad (4\text{-}14)$$

where superscript tol represents the toluene-rich liquid phase and $f^L_{toluene}$ is the reference fugacity of pure toluene in its liquid state of aggregation at system temperature and pressure. Assuming the solubility of water in the toluene phase is negligible, $\gamma^{tol}_{toluene} \cong 1.0$, $x^{tol}_{toluene} \cong 1.0$, and Equation 4-14 reduces to the following:

$$\gamma^w_{toluene} = \frac{1}{x^w_{toluene}} \qquad (4\text{-}15)$$

where $x^w_{toluene}$ is the solubility of toluene in water (expressed as a mole fraction) at system temperature and pressure (T = 23 °C, P = 1 atm), as listed in Table 4-2.

Since naphthalene and phenanthrene are solids at the system temperature and pressure, we must modify the above approach somewhat to determine γ_i^w

for naphthalene and toluene solutes. Equate and express fugacities of the solute in the solid and liquid phases of the solute-water binary as follows:

$$\hat{f}_i^L = f_i^s \tag{4-16}$$

$$\hat{f}_i^L = \gamma_i^w x_i^w f_{i,ref}^L \tag{4-17}$$

$$f_i^s = \nu_i(T, P_{vp,i}^s)\, P_{vp,i}^s \exp\left(\int_{P_{vp,i}^s}^{P} \frac{v_i^s}{RT}\, dP\right) \tag{4-18}$$

where $f_{i,ref}^L$ denotes the reference fugacity of pure solute i in a liquid state at system temperature and pressure, $\nu_i(T, P_{vp,i}^s)$ is the fugacity coefficient of pure i vapor at system temperature and vapor pressure of the solid $P_{vp,i}^s$, and v_i^s is the molar volume of solute i in the solid phase. The fugacity f_i^s does not have an overbar ($\hat{}$) because the solid phase is assumed to be pure. The exponential term in Equation 4-18 is the Poynting correction factor as described in the literature (Modell and Reid, 1983) and accounts for expressing f_i^s at system pressure (1 atm) in terms of f_i^s at the vapor pressure of solute i. For pressures around atmospheric and temperatures below the solute's critical point, as is the case with our system, the Poynting correction factor is very near 1.0 (Modell and Reid, 1983). Assume the vapor of solute i is an ideal gas such that pure component fugacity coefficient $\nu_i(T, P_{vp,i}^s) = 1.0$. Then, Equations 4-16 to 4-18 yield the following:

$$\gamma_i^w = \frac{P_{vp,i}^s}{x_i^w f_{i,ref}^L} \tag{4-19}$$

The reference liquid phase fugacity of solute i, $f_{i,ref}^{L}$, may be expressed as follows:

$$f_{i,ref}^{L} = P_{vp,i}^{l} \exp\left(\int_{P_{vp,i}^{l}}^{P} \frac{v_i^{l}}{RT} dP\right) \qquad (4\text{-}20)$$

where $P_{vp,i}^{l}$ denotes the vapor pressure of pure subcooled liquid i at system temperature, and the exponential term is the Poynting correction factor, again assumed approximately equal to 1.0. Note the subcooled liquid reference state may not be practically accessible in that the system may enter an unstable region. By substituting Equation 4-20, Equation 4-19 becomes:

$$\gamma_i^{w} = \frac{P_{vp,i}^{s}}{x_i^{w} P_{vp,i}^{l}} \qquad (4\text{-}21)$$

Values of $P_{vp,i}^{s}$ at T = 23.0 °C were obtained for naphthalene and phenanthrene using an Antoine equation curve fit for pure solid solute over a temperature range that includes 23.0 °C (Stephenson and Malanowski, 1987). Values of $P_{vp,i}^{l}$ were obtained by extrapolating the liquid phase Antoine equation curves to the subcooled temperature, 23.0 °C (Stephenson and Malanowski, 1987) (Figure 4-3 qualitatively shows how this was done). Solubilities of naphthalene and phenanthrene in water at system temperature and pressure were obtained from the literature (May et al., 1978). The resulting values of γ_i^{w} calculated from Equation 4-21 are shown in Table 4-3.

Figure 4-3: Qualitative Phase Diagram for Pure Solute i Demonstrating Extrapolation Below the Triple Point to Obtain $P^{l}_{vp,i}$

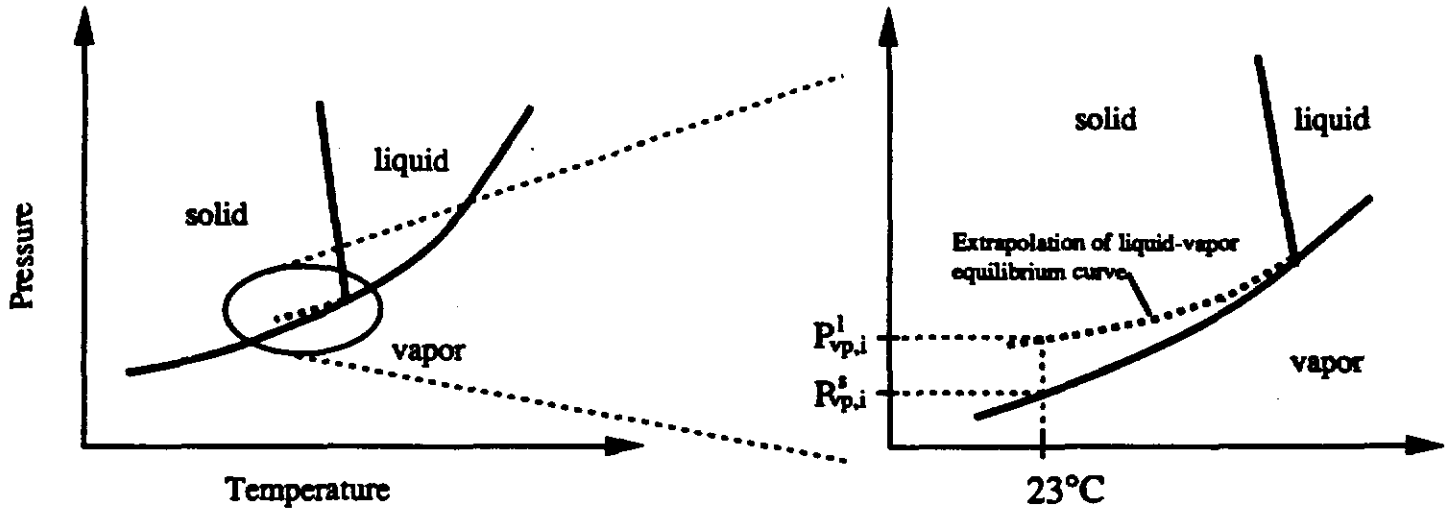

We can now bring octanol-water partition coefficient K_{ow} into the correlation. Assume a solute is introduced into a liquid-liquid two-phase system of octanol and water until both phases are saturated with solute i and the system is in equilibrium. If we assume both phases are immiscible -- that is, there is a negligible concentration of octanol in the water-rich phase (and vice-versa) -- we may define K_{ow} as follows:

$$K_{ow} \equiv \frac{C_i^o}{C_i^w} [=] \frac{\text{g solute i in octanol-rich phase / mL octanol}}{\text{g solute i in water-rich phase / mL water}} \qquad (4\text{-}22)$$

Assuming negligible volume changes upon mixing, K_{ow} can be written as follows:

$$K_{ow} = \frac{x_i^o / v_o}{x_i^w / v_w} \qquad (4\text{-}23)$$

where superscripts o and w denote the octanol and aqueous phases, respectively, and v_o and v_w are the molar volumes of pure octanol and water, respectively, at system temperature and pressure in units of L/mol. Equating liquid-phase fugacities or activities as in Equation 4-6:

$$\gamma_i^w x_i^w = \gamma_i^o x_i^o \qquad (4\text{-}24)$$

Combining Equations 4-23 and 4-24 yields the following expression for water-phase solute activity coefficient:

$$\log \gamma_i^w = \log K_{ow} + \log \gamma_i^o - \log \frac{v_w}{v_o} \qquad (4\text{-}25)$$

Since the aqueous phases in both the polymer-water and octanol-water solute systems are modeled as binary mixtures of water saturated with solute (we assumed no solubility of the polymer or octanol in the water-rich phase), the aqueous-phase solute activity coefficient γ_i^w is the same for both systems. By substituting Equation 4-25 into Equation 4-12 we obtain a linear relationship between log K_{pw} and log K_{ow}:

$$\log K_{pw} = \log K_{ow} + \log \gamma_i^o + \log v_o - \log \gamma_i^{*p} - \log \left(\frac{MW_{sol}}{1000}\right) - \log R_p \qquad (4\text{-}26)$$

Values of all the terms on the right of Equation 4-26 are shown in Table 4-3 for the solutes toluene, naphthalene, and phenanthrene and the NVPS copolymer.

Values of log K_{ow} in Table 4-3 are the medians of experimental values at T = 25°C and P = 1 bar (Hansch and Leo, 1979). Standard deviations of these experimental K_{ow} values are 14% and 29% for toluene and naphthalene, respectively. Only one value of K_{ow} for phenanthrene was listed.

The value of γ_i^o for toluene is an experimental value at infinite dilution of toluene and standard temperature and pressure (Thomas et al., 1982). This value of γ_i^o is relatively close to 1.0, and will not change considerably at higher toluene mole fraction; therefore, estimated error of γ_i^o for the toluene system considered here is below 25%. Values of γ_i^o for naphthalene and phenanthrene at system temperature and pressure and saturated solute mole fraction were obtained using the UNIFAC/UNIQUAC activity coefficient estimation method (Lyman et al., 1990). The source quotes an average 25% error estimate for this method.

All estimates from Equations 4-12 and 4-26 are within about a factor of two of the experimental K_{pw} values -- a good agreement considering estimated errors in required parameters. Equations 4-12 and 4-26 give very similar K_{pw} predictions. All parameters in Table 4-3 were calculated independently of the experimental NVPS solubility data with the exception of log γ_i^{*P} and log R_P which required an estimate of solute mole fraction in the polymer phase. These two terms account for about 15% of the total log K_{pw} estimate.

Within a given class of solutes, a clear linear relationship is generally observed between surfactant-water solute partition coefficients, K_{sw}'s, and octanol-water solute partition coefficients, K_{ow}'s (Edwards et al., 1991). A linear K_{sw}-K_{ow} empirical relationship does not clearly exist for all three NVPS-solute systems investigated here, since the experimental K_{pw} for toluene is too high for such a relationship to be valid. However, toluene is a substituted benzene and does not strictly fall in the class of unsubstituted polycyclic aromatic hydrocarbons as do naphthalene and phenanthrene. A more accurate relationship between K_{pw} and K_{ow} (for example, Equation 4-12 or 4-26) would account for variations of the solute activity coefficients in the octanol and polymer (or surfactant) phases. The traditional linear K_{sw}-K_{ow} relationship assumes both the solute-octanol and solute-surfactant activity coefficients (γ_i^o and γ_i^s) are the same for compared solutes. This assumption, however, may be valid for chemically similar solutes within a given class. For example, the difference between the log K_{pw}'s of naphthalene and phenanthrene (both non-substituted polyaromatics) in NVPS is similar to the difference between their log K_{ow}'s (1.31 versus 1.01, respectively).

We can estimate values of χ, the Flory-Huggins parameter from Equation 4-13, using the differences between experimental log K_{pw}'s and log K_{pw}'s calculated from Equation 4-26. We must use the error estimates of Equation 4-26 inputs listed in this section to obtain ranges of χ for the three solute systems. We obtain $\chi = 2.4 \pm 1.5$, 0.61 ± 0.26, and 0.42 ± 0.26 for the toluene, naphthalene, and phenanthrene solute-NVPS systems, respectively. The χ values for naphthalene and phenanthrene in NVPS solution are somewhat similar to χ's calculated for n-decane/polyethylene and n-dodecane/polyethylene systems (Patterson et al.,

1971); these are 0.32 ± 0.005 and 0.27 ± 0.01, respectively. The χ found for the toluene/NVPS system is somewhat higher.

5. Transmembrane Diffusion of Organic Solute in Aqueous Solution

5.1. Transmembrane Mass Transfer Modeling

There are two fundamental pieces of information that must be quantitatively known to determine how well the proposed membrane/ copolymer barrier system will work in a given application. First, how concentrated the contaminant can become in the copolymer solution must be known. This requires equilibrium solubilization measurements and theory, discussed in Chapter 4. Secondly, how quickly the contaminant can diffuse through the microporous membrane and into the copolymer solution must be quantified. The modeling of this transport phenomena is the topic of this section. Models are developed here to show what information can be obtained from experiments, and how that information can be extended to more generalized cases.

As proposed in Chapter 2, the barrier process consists of membrane tubes filled with copolymer solution placed in either a cylindrical or rectangular well. The solution can be pumped out and replaced when it becomes sufficiently concentrated with contaminant. In this application of the system, there is negligible convection of contaminant into the copolymer since there is negligible convective flux of contaminant-containing water into or out of the membrane tubes. The primary means of transport of the contaminant through the microporous membrane and into the copolymer solution is molecular diffusion. The goal, then, of the transport experiments is to measure the rate of aqueous-phase molecular diffuson of a given species of organic contaminant through an asymmetric, microporous membrane into a given copolymer solution.

In most experimental measurements of diffusivity, there will be some convective flux of diffusing species caused by a finite pressure gradient existing between the two compartments through which transport occurs. The goal in these experiments is to minimize the convective flux contribution by minimizing the transmembrane pressure gradient. Also, if aqueous phase molecular diffusion is slow enough, transport may occur by solid-phase surface diffusion (Bitter, 1991). In summary these three modes of solute transport may occur simultaneously to a greater or lesser degree in these experiments. They can be defined in terms of unidirectional fluxes across the membrane in the x direction as follows:

Aqueous phase molecular diffusion:

$$F_{md} = -D_{md,AB}\frac{\partial C}{\partial x} \qquad (5\text{-}1)$$

Convection:

$$F_{conv} = -\frac{k}{\mu}\frac{\partial P}{\partial x}C \qquad (5\text{-}2)$$

Surface molecular diffusion:

$$F_{sd} = -D_{sd,AB}\frac{\partial q}{\partial x} \qquad (5\text{-}3)$$

where F_{md}, F_{conv}, and F_{sd} are the solute flux contributions by molecular diffusion, convection, and surface diffusion, respectively [g/cm^2 s]; $D_{md,AB}$ is the aqueous-phase molecular diffusion coefficient of solute A through solvent B [cm^2/s]; $D_{sd,AB}$ is the surface diffusion coefficient [cm^2/s]; k is the membrane permeability [cm^2]; μ is the solution viscosity [g/cm s], P is the solution pressure [g/cm s^2]; $\partial P/\partial x$ is the transmembrane pressure gradient; q is the adsorbed concentration of solute A in the membrane [g/cm^3]; and C is the liquid-phase

concentration of solute A [g/cm^3]. Expressions 5-1 and 5-3 assume a Fickian model of diffusion in which the diffusive solute flux is directly proportional to the solute concentration gradient, the constant of proportionality being the diffusion coefficient (Treybal, 1987).

Section 5.3 of this chapter discusses the justification of neglecting convection and surface molecular diffusion (Equations 5-2 and 5-3) as sources of solute flux in the experiments. The models in this section assume solute transport occurs solely by aqueous-phase molecular diffusion following Equation 5-1 such that:

$$F_{tot} \approx F_{md} \tag{5-4}$$

where F_{tot} is the total measured solute flux [g/cm^2 s].

Film theory is used to describe aqueous-phase transport of solute molecules from the outside of the membrane tube to the inside of the tube. Figure 5-1 shows a cross-section of a membrane tube wall with a hypothetical aqueous-phase concentration profile of the diffusing species. As assumed in Equation 5-1, diffusion of solute from the outer to the inner aqueous solution is driven by a concentration gradient. Resistance to this diffusive transport is posed both by the fluid and the membrane wall through which the solute diffuses. Film theory suggests that each of these layers of resistance can be characterized by an effective thickness, δ_i, through which the solute diffuses. The thicknesses of the fluid layers δ_1 and δ_4 are assumed to be functions of the flow characteristics of the bulk fluid away from the membrane wall. Estimates of these thicknesses can be obtained from correlations in the literature (Kakac, 1985

Figure 5-1: Concentration Profile -- Membrane Tube Cross-Section

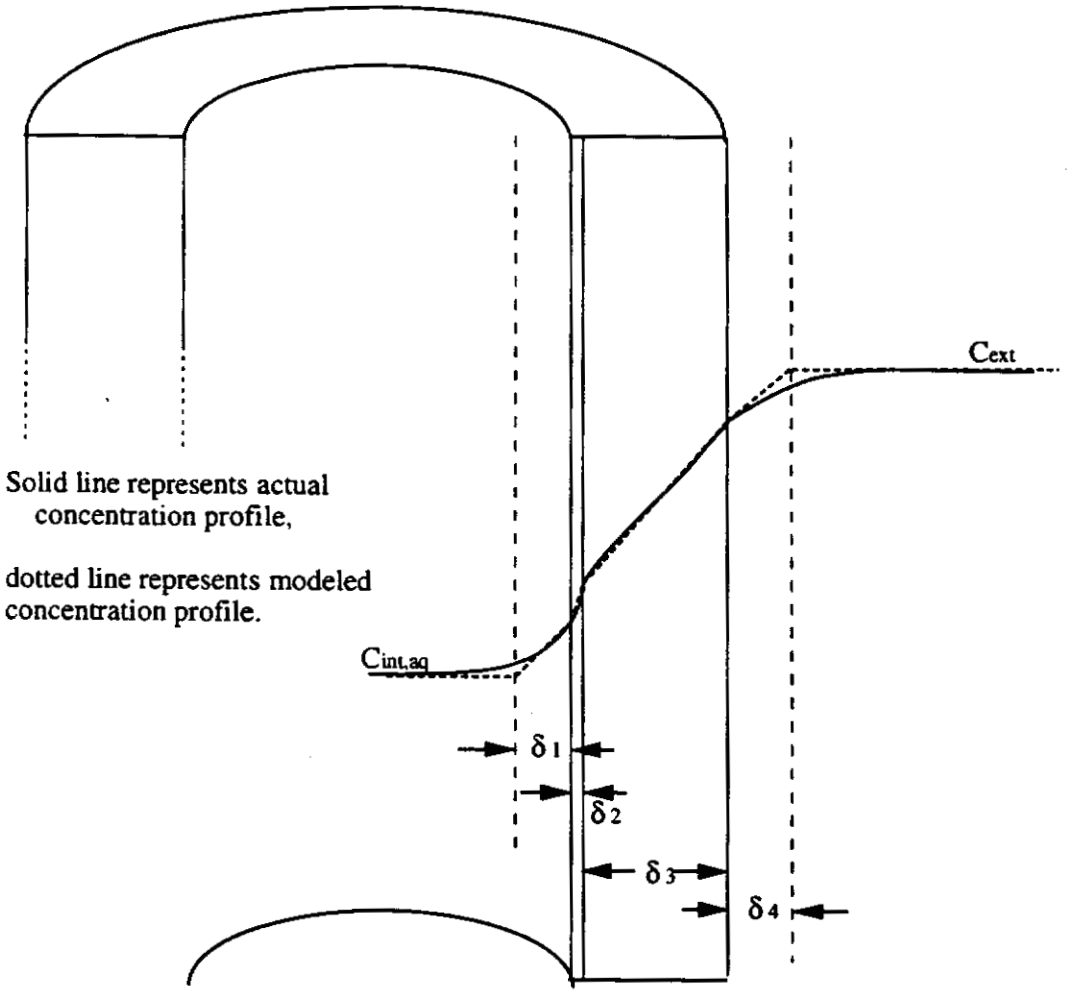

δ_1 = interior fluid boundary layer

δ_2 = membrane skin thickness

δ_3 = membrane support layer thickness

δ_4 = exterior fluid boundary layer

Note: Boundary layers not drawn to scale.

and Treybal, 1987). The resistance to diffusive transport of solute A of each of the film layers can be defined as follows:

$$R_i \equiv \frac{\delta_i}{D_{AB}} \tag{5-5}$$

where R_i is the resistance of film layer i [s/cm]; δ_i is the effective film thickness of layer i [cm]; and D_{AB} is the diffusion coefficient of solute A through solvent B [cm^2/s]. From Figure 5-1, the diffusive transport resistances appear in series, so the overall resistance equals the sum of the individual film layer resistances:

$$R_{tot} = \sum_{i=1}^{4} \frac{\delta_i}{D_{AB}} \tag{5-6}$$

where R_{tot} is the total diffusive transport resistance [s/cm]. With $\partial C/\partial x$ approximated as $\Delta C/\delta$, the overall flux can then be described by the following:

$$F_{tot} = \frac{(C_{ext} - C_{int,aq})}{R_{tot}} \tag{5-7}$$

where F_{tot} is the total flux of solute A from the membrane exterior to the interior [g/cm^2 s]; C_{ext} is the concentration of solute A in the exterior bulk solution [g/cm^3] and $C_{int,aq}$ is the aqueous phase concentration of solute A in the interior bulk solution [g/cm^3].

The goal of the diffusion experiments is to obtain values of R_{tot} for given systems and compare those values to predicted values from literature correlations. One such experiment is diagrammed schematically in Figure 5-2.

Figure 5-2: Schematic Diagram of Transmembrane Transport Experiment -- Solute Transport into Aqueous Solution

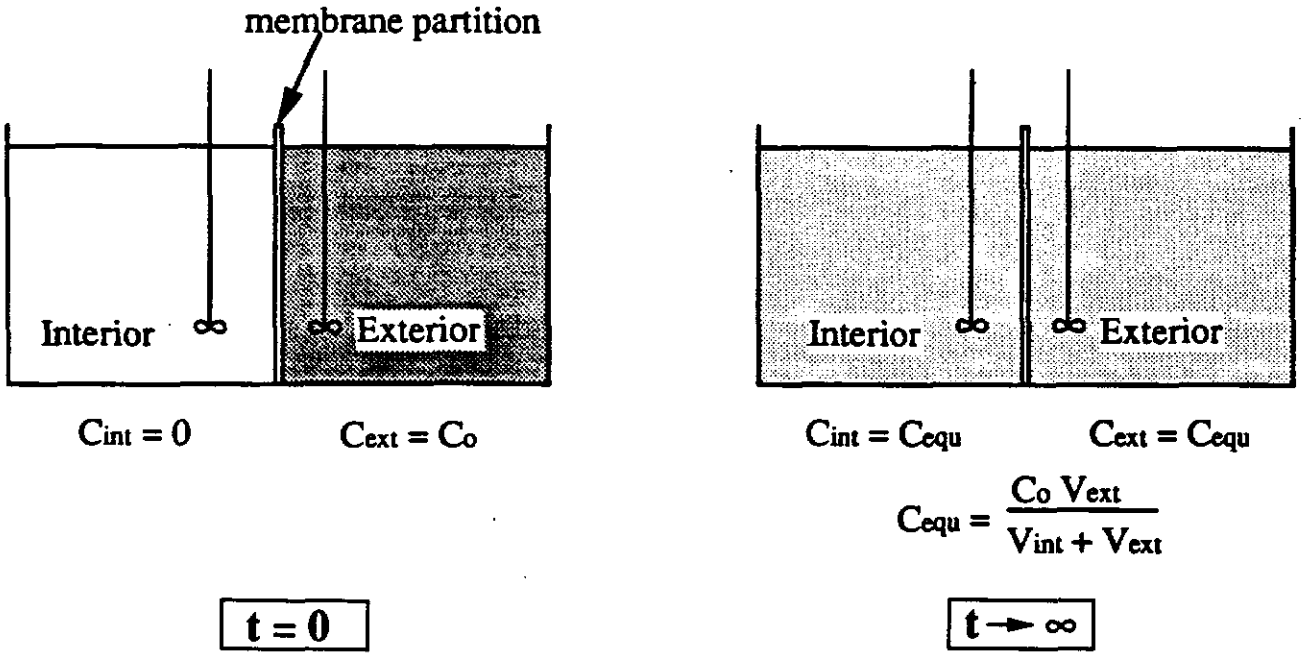

Solute A is introduced to a well-mixed aqueous phase of volume V_{ext}, exterior to a membrane partition, at concentration C_o. The aqueous solution interior to the membrane partition initially has no solute A present. The solute is allowed to diffuse from the exterior to the interior by means of a concentration gradient driving force. Eventually, that driving force ceases to exist (represented in Figure 5-2 by $t \rightarrow \infty$) when the concentration of solute A in the interior and exterior solutions become equal. Experiments involving transmembrane transport of solute from an exterior aqueous solution of initial concentration C_o to an interior aqueous solution of inital zero solute concentration have the following governing equations and initial conditions:

Governing Equations: Interior Solution

$$V_{int} \frac{dC_{int}}{dt} = \frac{A_{tot}}{R_{tot}}(C_{ext} - C_{int}) \qquad (5\text{-}8)$$

Exterior Solution

$$V_{ext} \frac{dC_{ext}}{dt} = -\frac{A_{tot}}{R_{tot}}(C_{ext} - C_{int}) \qquad (5\text{-}9)$$

Initial Conditions:

$$C_{int}\,(t=0) = 0 \qquad (5\text{-}10)$$

$$C_{ext}\,(t=0) = C_o \qquad (5\text{-}11)$$

where V_{int} is the interior solution volume [cm^3]; V_{ext} is the exterior solution volume [cm^3]; A_{tot} is the overall surface area of membrane [cm^2]; and R_{tot} is the total diffusive transport resistance [s/cm]. Concentrations are functions of time only, since the exterior and interior solutions are assumed well-mixed. Equations 5-8 and 5-9 are simple mass conservation expressions; the left-hand terms are net accumulations of solute into the given solution and the right-hand terms are the net fluxes into the given solution. Solving the coupled equations with respect to the initial conditions, the following expressions for interior solutions solute concentration is obtained:

$$C_{int} = C_o\left(\frac{V_{ext}}{V_{ext} + V_{int}}\right)\left[1 - \exp\left(-\frac{A_{tot}}{R_{tot}}\left(\frac{1}{V_{int}} + \frac{1}{V_{ext}}\right) t\right)\right] \qquad (5\text{-}12)$$

This can be expressed as follows:

$$\Omega_1(t) = \frac{1}{R_{tot}}\, t \qquad (5\text{-}13)$$

$$\text{where } \Omega_1(t) = -\frac{1}{A_{tot}\left(\frac{1}{V_{int}} + \frac{1}{V_{ext}}\right)} \ln\left[1 - \frac{C_{int}}{C_o}\left(\frac{V_{ext} + V_{int}}{V_{ext}}\right)\right]$$

Thus, for a given experiment, values of $\Omega_1(t)$ can be graphed with time t to obtain R_{tot}, the overall diffusive transport resistance for the experimental system. These experimental values can then be compared to values predicted from literature correlations.

The interior aqueous phase concentration, $C_{int,aq}$, cannot exceed C_{ext} for net solute transport into the membrane to occur. In the proposed membrane/copolymer barrier system, the interior phase contains both water and amphipathic copolymer. As described in Chapter 4, the aqueous copolymer solution comprising the interior solution is modeled as a mixture of two separate, yet interspersed pseudophases -- an aqueous pseudophase and a copolymer pseudophase. The solute concentration pertinent to transmembrane transport is the aqueous pseudophase concentration; it is the concentration that is "seen" by the exterior solution solute molecules. Transport from the exterior solution to the interior aqueous pseudophase will occur until their solute concentrations are equal.

As described in Chapter 4, an equilibrium is assumed to exist at all times between the solute concentration of the interior aqueous pseudophase and the interior polymer pseudophase. This equilibrium is characterized by the polymer-water partition coefficient, K_{pw}, of the polymer-water-solute system. Therefore, a "reaction" term can be derived which describes the transport of solute out of the aqueous pseudophase and into the polymer pseudophase. Let L be the mass of

solute in the polymer per mass of polymer and M be the polymer to water mass ratio. Then the product M • L is the mass of solute in polymer per mass of water. The partition coefficient, K_{pw}, was shown to be a constant for the polymer-water-solute systems under investigation here, and the following relation holds:

$$K_{pw} = \frac{L}{C_{int,aq}} \tag{5-13}$$

where $C_{int,aq}$ is the interior aqueous pseudophase concentration of solute A [g/cm^3]. It is assumed equilibrium between the aqueous and polymer pseudophases is maintained at all times. The transfer of solute from the interior aqueous pseudophase to the interior polymer pseudophase can be expressed by the following "reaction" term, which is simply the time rate of change of solute mass in polymer per unit volume of water:

$$r = -\frac{d}{dt}(M \cdot L) = -M\frac{dL}{dt} \tag{5-14}$$

where r is the rate at which solute is transferred from the aqueous pseudophase to the polymer pseudophase [g/cm^3 s]. Substituting Equation 5-13 into Equation 5-14 above, we get

$$r = M K_{pw}\frac{dC_{int,aq}}{dt} \tag{5-15}$$

In this way, the model states the solute passes through the membrane and enters the interior aqueous pseudophase, then immediately comes to equilibrium with the interior polymer pseudophase. The maintenance of this equilibrium condtion behaves as a "reaction" of or disappearance of solute from the interior aqueous pseudophase. In this way, the concentration of solute in the interior solution

which is many times its normal saturated aqueous phase concentration can be properly modeled. This enhancement of solubility is characterized by the polymer-water partition coefficient, K_{pw}.

An implicit assumption in the use of this "reaction" term is that the transfer of solute form the interior aqueous pseudophase to the interior polymer pseudophase occurs on a faster time scale than transfer of solute from the exterior phase solution to the interior aqueous pseudophase. This can be justified by noting the respective diffusion lengths in the two cases. Diffusion from the exterior to the interior of the membrane occurs over a length of about 0.275 mm for all experiments described in this chapter. Diffusion from the aqueous pseudophase to the interspersed polymer pseudophase occurs over a much smaller, molecular length scale (i.e. 1 nanometer). Therefore, the transmembrane diffusion would easily be the rate limiting process of the two.

Figure 5-3 shows a schematic diagram of a transmembrane transport experiment involving transfer of solute from an exterior aqueous solution to an interior aqueous, copolymer solution. This more closely demonstrates the proposed groundwater contaminant barrier system, since solute diffuses into a copolymer solution. Initially, an aqueous copolymer solution is introduced to the interior of a membrane tube of volume V_t at zero solute concentration. The exterior solution is maintained at a constant, saturated solute concentration. Molecular diffusive transport from the exterior to the interior is allowed until the copolymer solution has an aqueous pseudophase concentration equal to the exterior phase concentration. The governing equation and initial conditions for this experiment are as follows:

Figure 5-3: Schematic Diagram of Transmembrane Transport Experiment -- Solute Transport Into Copolymer Solution

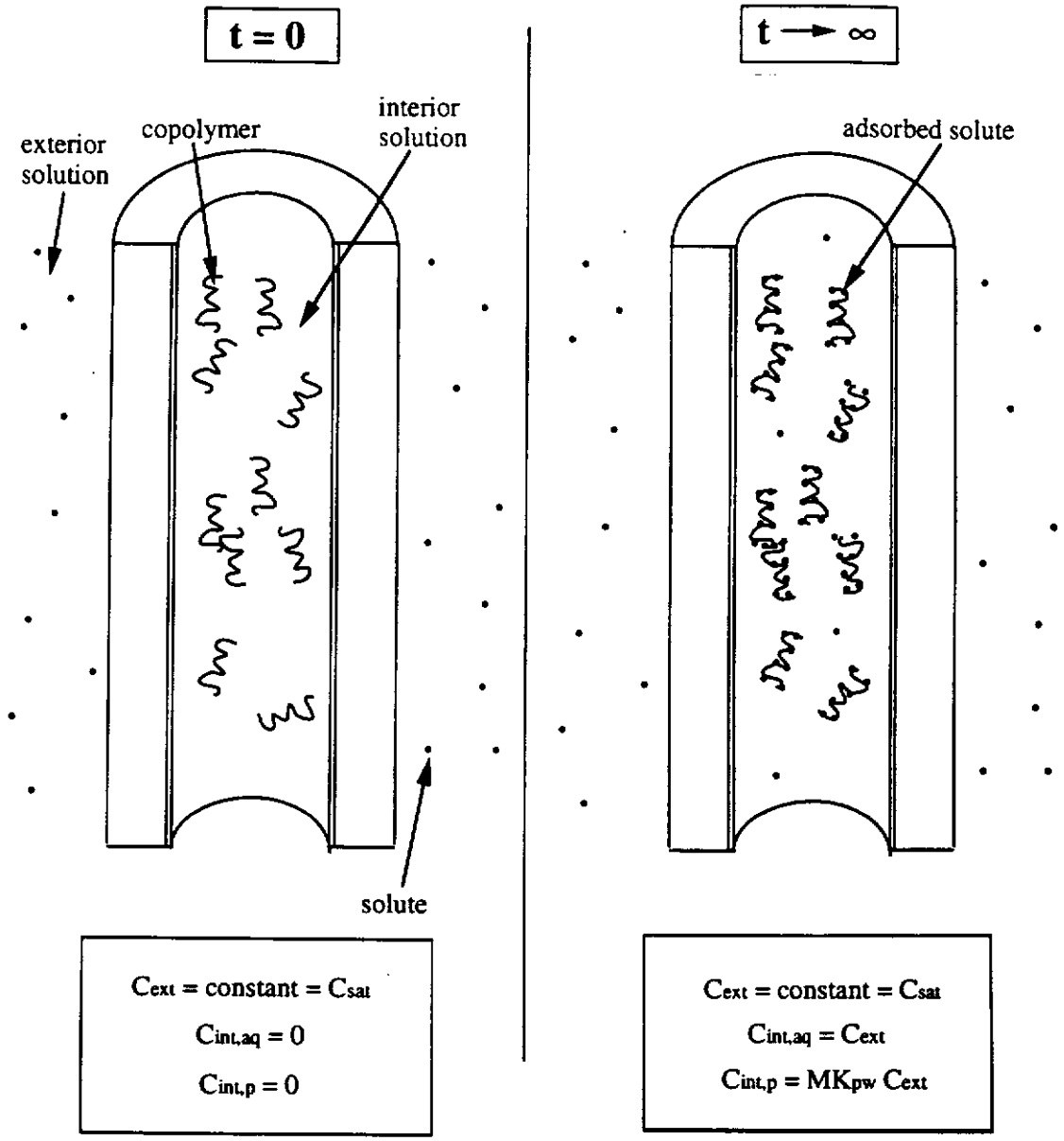

Note: Not to scale.

Governing Equation:

$$V_t \frac{dC_{int,aq}}{dt} = -\frac{A_t}{R_{tot}}(C_{ext} - C_{int,aq}) - MK_{pw}V_t\frac{dC_{int,aq}}{dt} \qquad (5\text{-}16)$$

Initial Conditions:

$$C_{int,aq}(t=0) = 0 \qquad (5\text{-}17)$$

$$C_{ext} = C_{sat} \text{ at all time t} \qquad (5\text{-}18)$$

where V_t is the membrane tube interior volume [cm^3]; $C_{int,aq}$ is the interior aqueous pseudophase solute concentration [g/cm^3]; C_{ext} is the exterior solution solute concentration [g/cm^3]; C_{sat} is the saturated concentration of solute in water [g/cm^3]; A_t is the membrane tube surface area [cm^2], R_{tot} is the overall membrane tube resistance [s/cm]; M is the ratio of polymer to water mass in the interior copolymer solution [g/cm^3], and K_{pw} is the polymer-water partition coefficient of the solute [dimensionless]. The governing equation follows from a mass balance on the interior *aqueous pseudophase.* The term on the left-hand side is the accumulation of solute in this phase, the first term on the right-hand side is the net transport of solute into this phase, and the second term on the right-hand side is the "reaction" term from Equation 5-15, describing the transfer of solute out of the interior aqueous pseudophase and into the interior polymer pseudophase. The measured interior phase solute concentration is the sum of the solute's concentration in the two pseudophases:

$$C_{int} = C_{int,aq} + C_{int,p} \qquad (5\text{-}19)$$

where C_{int} is the measured interior concentration [g/cm^3 solution]; $C_{int,aq}$ is the solute concentration in the aqueous pseudophase [g/cm^3 solution]; and $C_{int,p}$ is

the solute concentration in the polymer pseudophase [g/cm^3 solution]. It is assumed equilibrium exists between the pseudophases such that:

$$\frac{C_{int,p}}{C_{int,aq}} = M K_{pw} \tag{5-20}$$

Using this relationship along with Equation 5-19, we may solve Equation 5-16 for measured interior solution concentration, C_{int}, as follows:

$$\frac{C_{int}}{C_{sat}} = (1 - e^{-Bt})(1 + M K_{pw}) \tag{5-21}$$

$$\text{where } B = \frac{A_t}{V_t R_{tot}(1 + M K_{pw})}.$$

As with Equation 5-12, the above equation can be expressed as follows:

$$\Omega_2(t) = \frac{1}{R_{tot}} t \tag{5-22}$$

$$\text{where } \Omega_2(t) = -\ln\left[1 - \frac{C_{int}/C_{ext}}{(1 + M K_{pw})}\right] / b \,,$$

$$b = \frac{A_t}{V_t(1 + M K_{pw})}$$

Similarly, values of $\Omega_2(t)$ can be graphed with time t to obtain R_{tot} for a given system. As in the previous case, the experimental R_{tot} values can then be compared to values predicted from literature correlations.

Experiments will show that the effect of solute adsorption onto membrane material does not appreciably affect R_{tot} determination, and that the assumption

of fast assimilation of solute into the copolymer pseudophase with respect to transmembrane transport holds true.

5.2. Materials for Experiments

The copolyer used in this study, N-vinylpyrrolidone/styrene (NVPS), was obtained as a 40 weight% copolymer solution in water. The supplier, Scientific Polymer Products, Inc., reported that the copolymer is composed of styrene and N-vinylpyrrolidone monomers in a weight ratio of 60 to 40. NVPS is a random copolymer as shown in Figure 4-1. As explained in Chapter 4, the hydrophilic character of the copolymer allows it to form a stable suspension in water, and its hydrophobic nature lends it organic solubilization capacity. In the diffusion experiments of this chapter, aqueous solutions of less than 3 wt.% NVPS were used. The average molecular weight of NVPS was reported as approximately 3.4 million g/mol, and its radius of gyration approximately 940 Å. By contrast, naphthalene, one of the model organics used in this study, is approximately 5 Å in length and 3 Å in width and depth (Fessenden and Fessenden, 1986). Thus, a membrane can readily be chosen whose average pore diamter is less than copolymer molecular size, but greater than solute size.

The hydrophobic model organic compounds used in the diffusion experiments were naphthalene (99+% pure) and phenanthrene (98% pure), obtained from Sigma Chemical Company. These chemicals were used without further purification.

The membranes used in the diffusion experiments were Supelco, Inc.'s polysulfone ultrafiltration hollow fiber membranes. The membranes were furnished in 8-inch-long cartridges each containing 308 individual hollow fiber tubes of 0.5mm internal diameter. The bulk of the membrane thickness,

0.275 mm, is made up of a support structure for the microporous membrane layer. This microporous layer, reported as between 0.1 and 0.2 micrometer in thickness, is called the "skin" layer and gives the membrane its molecular sieving properties. The reported effective surface area of each membrane tube is 2.06 cm^2. The membranes have a porosity of 86% as determined from water displacement experiments. The cartridge of membranes has ends potted in epoxy such that flow through the interior of the tubes can be separated from flow exterior to the membrane tubes. The cartridge itself is made of the same material as the membrane tubes -- polysulfone. Membrane cartridges of two different nominal molecular weight cutoffs were used -- 2000 and 50,000 g/mol. These correspond to membranes of approximate average "skin" layer pore diameters of 10 Å and 50 Å, respectively. These sizes were chosen to allow the passage of model organic contaminant (naphthalene or phenanthrene) from the exterior to the interior of the tubes while preventing the leakage of NVPS copolymer from the interior to the exterior of the tubes. Two sizes were chosen so that the effect of different "skin" layer pore diameters might be observed during measurements of the total membrane tube resistance, R_{tot}.

All pumps used in the diffusion experiments were teflon-lined piston-diaphragm pumps supplied by Cole Parmer Company. The teflon lining was required to minimize adsorption of organic solute onto the pump surfaces. All tubing used in the diffusion experiments was 1/4"- and 1/8"- internal-diameter teflon tubing. Swagelok stainless steel and brass fittings were used for all connections.

Solution concentrations of naphthalene and phenanthrene were determined by absorbance measurements from a Perkin-Elmer Lambda 3B

UV/VIS spectrophotometer, using quartz Suprasil flow-through cells. Measurements were made at maximum absorbance wavelengths for each compound: 276 nm for naphthalene and 293 nm for phenanthrene.

Extinction coefficients for the absorbance of naphthalene and phenanthrene were measured as follows. A saturated aqueous solution of the organic solid was created by circulating water through a generating column filled with organic solid as described in the literature (Hurter and Hatton, 1992). The solution was held at 23.0 ± 0.1 °C with a constant temperature bath. A fraction of the circulating solution was diverted to the spectrophotometer through a 1-cm-pathlength flow cell where its absorbance was read on-line. Constant circulation insured a saturated solution of solute was maintained, regardless of any solute adsorbed to the tubing or container walls. The Beer's law extinction coefficients were experimentally determined from absorbance measurements of organic-solute-saturated solutions at solute absorbance peaks using a 1-cm-pathlength cell and agreed to within 2% of published values (Bohon and Claussen, 1951 and Wauchope and Getzen, 1972). Higher concentrations of organic can be accurately measured by using flow cells of lower pathlength (0.02 cm and 0.001 cm pathlength cells were also used in this work). Beer's law states:

$$A_s = \varepsilon_b \cdot C \cdot L_c \qquad (5\text{-}23)$$

where A_s is the spectrophotometer absorbance reading [dimensionless]; ε_b is the Beer's law extinction coefficient [cm^2/g]; C is the concentration of solute in solution [g/cm^3]; and L_c is the spectrophotometer cell pathlength [cm].

The extinction coefficients of aqueous NVPS were also experimentally measured at the solute absorbance peaks -- 276 and 293 nm -- as well as at 400 nm, a wavelength at which the organic model compounds have zero absorbance. Plots of NVPS concentration versus absorbance used in determining its extinction coefficients at the above wavelengths are shown in Figure 5-4. Thus, the total absorbance of a polymer-water-solute solution at the two lower wavelengths equals that from both NVPS and the organic compound present in solution. The exact NVPS concentration of the sample was then measured by solution absorbance at 400 nm, and organic solute (naphthalene or phenanthrene) absorbance and concentration was then computed. This technique was experimentally justified by direct measurement of naphthalene dissolved into concentrated NVPS solutions of 19 and 23 wt.%.

Figure 5-4: Absorbance Versus NVPS Concentration

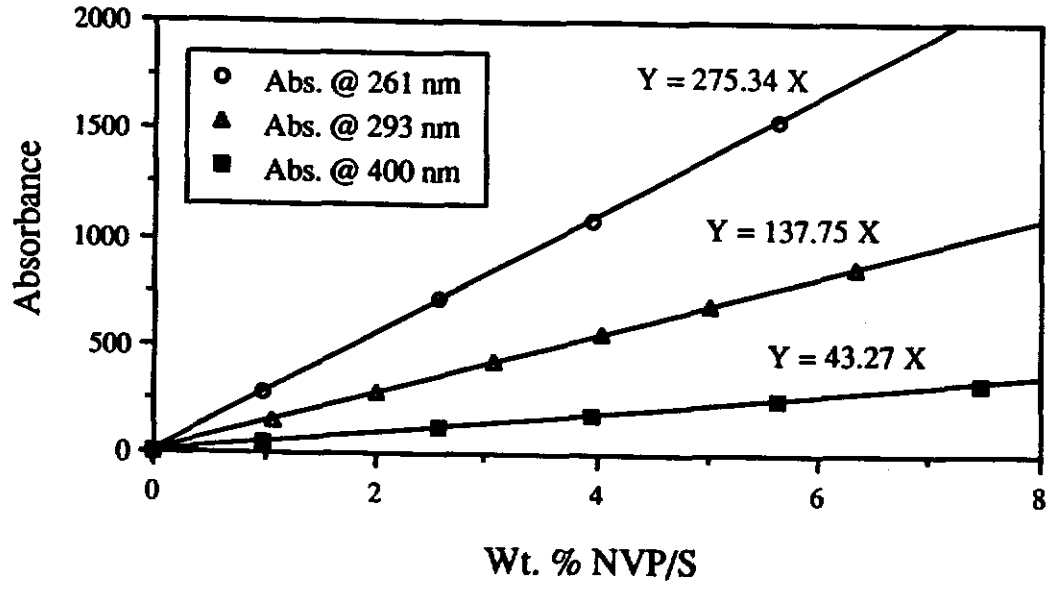

5.3. Transmembrane Pressure Gradient Measurement

The experimental set-up for all diffusion experiments in this work is shown in Figure 5-5. The system consists of a membrane tube cartridge through which solution is pumped both interior and exterior to the hollow membrane fibers, teflon-lined piston-diaphragm pumps which are used to transport the fluid, and a PAH column through which the exterior-side solution is passed to keep the solution saturated with organic solute. When a given parcel of solution is not in transit through the membrane or PAH column, it resides in the interior or exterior soluton reservoir. The solutions in these glass flasks are sealed from the surrounding air and are well-mixed by magnetic stirrers. Side-streams from both the interior and exterior solution lines are sent through quartz flow cells in the UV/VIS spectrophotometer for on-line concentration measurement. Then the solutions are returned to their respective solution reservoirs.

As discussed in Section 5.1, three modes of solute transport (aqueous phase molecular diffusion, convection, and surface molecular diffusion) from the exterior solution to the interior solution are possible. These are aqueous phase molecular diffusion, convection, and surface molecular diffusion. This section describes under what exterior and interior solution flowrates transport via convection is much less than transport via molecular diffusion. In order to use Equation 5-2 for transmembrane convective flux, we must know the transmembrane pressure gradient as a function of co-current exterior and interior solution flowrate. The gradient term in Equation 5-2 is approximated as follows:

$$\frac{\partial P}{\partial x} \approx \frac{\Delta P_{tm}}{\delta_{mem}} \qquad (5\text{-}24)$$

Figure 5-5: Diffusion Experiment Set-Up

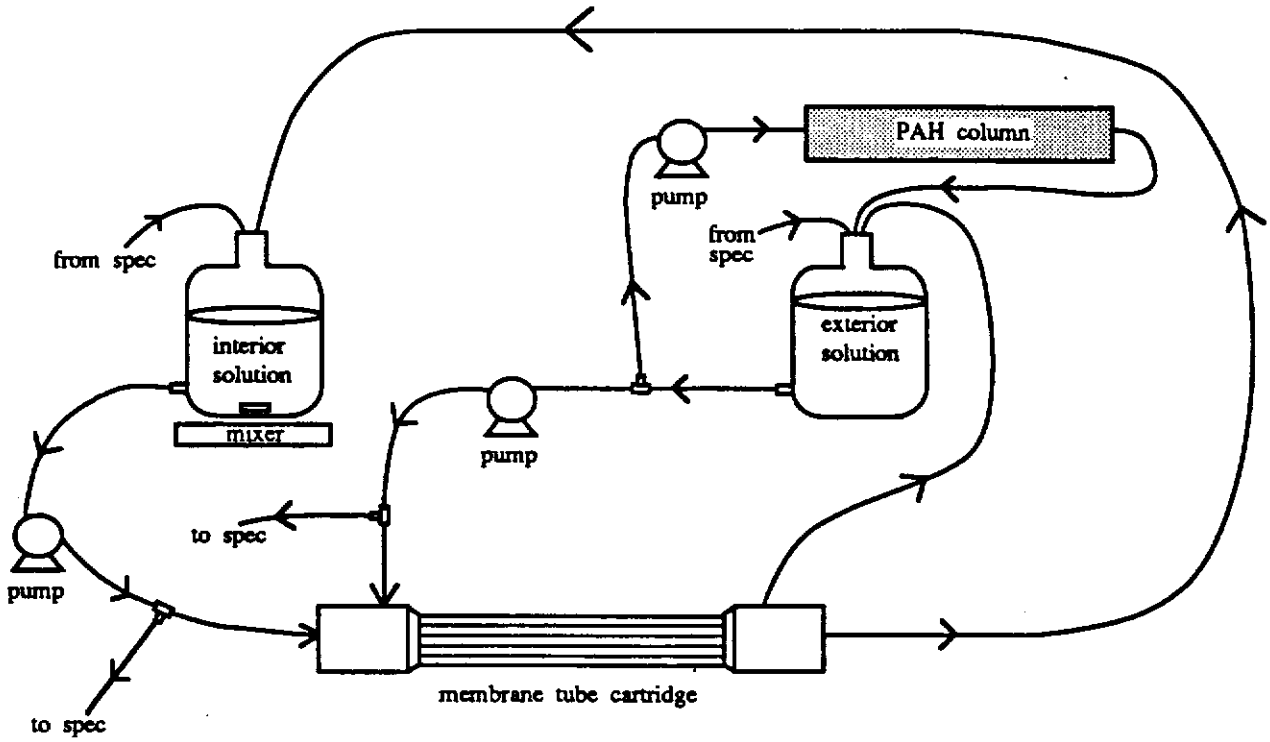

where ΔP_{tm} is the transmembrane pressure difference (difference between fluid pressure in the interior and exterior of the membrane at a particular point along the length of the membrane) [inches water]; and δ_{mem} is the thickness of the membrane [cm]. The transmembrane pressure gradient changes along the length of the membrane.

Figure 5-6 shows the pressure drop from the entrance to the exit of the *interior* side of the membrane plotted as a function of interior side flowrate. The difference in the pressures, ΔP, was measured using a water manometer. The straight line represents ΔP predictions using the Hagen-Poiseuille equation for pressure drop under laminar flow conditions as a function of flow velocity through a cylinder of length L and diameter D (Bird et al., 1968):

$$\Delta P = \frac{32 \mu L_t V}{D^2} \qquad (5\text{-}25)$$

where L_t is the tube length [cm]; V is the velocity of fluid flowing through the tube [cm/s]; and D is the tube diameter [cm]. Reynolds number ranged from 0 to 41.3, well below 2100 where turbulent flow would occur. The measured pressure drops agree to within the accuracy of the parameters used in the Hagen-Poiseuille equation as shown by the dotted lines in Figure 5-6. The figure shows the method of pressure difference measurement is accurate and can be used to measure *transmembrane* pressure difference as a function of exterior and interior flowrate. For simplicity, the exterior and interior flowrates are kept equal to each other in these tests.

Figure 5-6: Membrane Interior Pressure Drop as a Function of Flowrate Q -- Measurements and Model Predictions

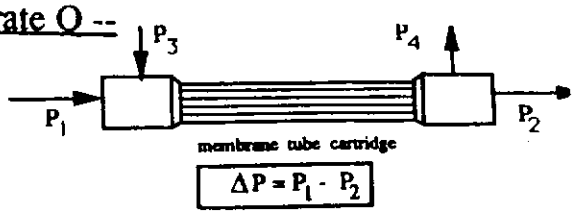

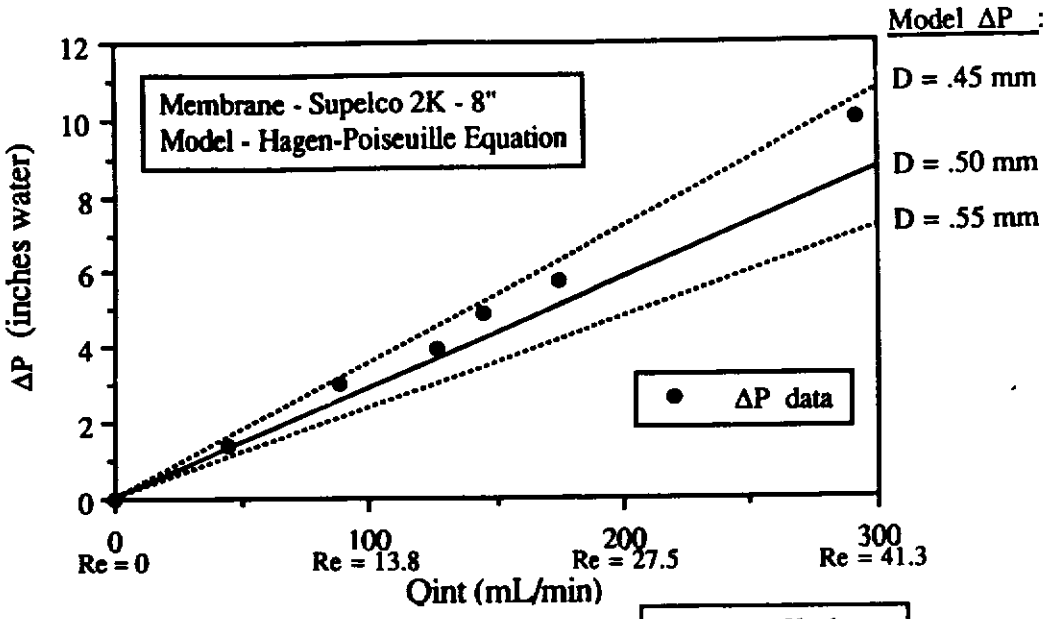

Hagen-Poiseuille Equation:

$$\Delta P = \frac{32 \mu L V}{D^2}$$

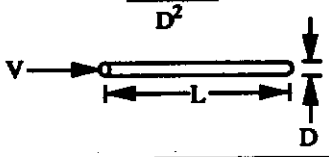

Parameters Used:

$\frac{\mu}{\rho} = 1 \times 10^{-6} m^2/s$

L = 8 inches

D = 0.5 mm (± 10%)

A = 0.6047 cm^2

V = Q/A

$Re = \frac{DV\rho}{\mu}$

$Re = \frac{Q(mL/min)}{7.26}$

Figure 5-7 shows measured transmembrane pressure difference as a function of exterior and interior solution flowrate. Meausrement of ΔP_{tm} was made at both the entrance and exit of the membrane tube cartridge. These are shown as solid and open circles on the graph. These data were correlated to express transmembrane pressure gradient at the entrance and exit of the membrane cartridge as empirical functions of flowrate. Because the Hagen-Poiseuille equation predicts a linear pressure profile along the length of a tube, it was assumed that the average transmembrane pressure difference along the tube equals the arithmetic average of the pressure differences at the entrance and the exit of the cartridge. Thus, an experimentally-determined empirical expression for average transmembrane pressure gradient is given as a function of flowrate:

$$\Delta P_{tm,avg}(\text{in. water}) = 0.00749\ Q\ (\text{mL/min}) + 6.05 \times 10^{-5}\ Q^2\ (\text{mL/min}) \qquad (5\text{-}26)$$

where $\Delta P_{tm,avg}$ is the average transmembrane pressure difference [inches water]; and Q is the interior solution flowrate (set equal to the exterior solution flowrate) [mL/min]. Note that for all flowrates and at all positions along the membrane the interior pressure is greater than the corresponding exterior pressure.

Now, the ratio of molecular diffusive flux to convective flux can be determined as a function of flowrate, Q, and overall membrane diffusion resistance, R_{tot}. All diffusion is assumed to be aqueous-phase molecular diffusion (this assumption is justified later), whose flux is given by Equation 5-1. The concentration gradient is approximated as follows:

$$\frac{\partial C}{\partial x} = \frac{dC}{dx} \approx \frac{\Delta C}{\Delta x} = \frac{C_o - 0}{\delta_{mem}} \qquad (5\text{-}27)$$

Figure 5-7: Measured Transmembrane Pressure Gradients

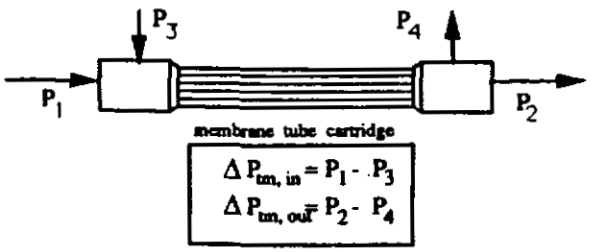

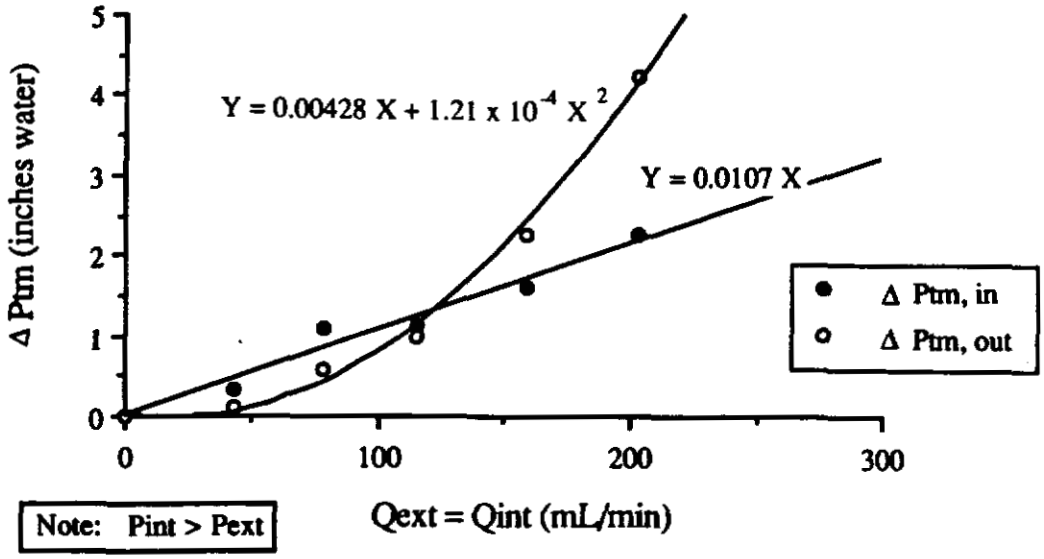

Note: Pint > Pext

Average ΔP_{tm} (inches water) = 0.00749 Q (mL/min) + 6.05 x 10^{-5} Q^2 (mL/min)

where C_o is the concentration of exterior solution [g/cm^3]; the concentration of the interior solution is 0; and δ_{mem} is the membrane thickness [cm]. Then equation 5-1 becomes:

$$F_{md} = D_{md,AB}\frac{C_o}{\delta_{mem}} \tag{5-28}$$

where F_{md} is the molecular diffusive flux of solute through the membrane [g/cm^2 s]; and $D_{md,AB}$ is the diffusion coefficient of solute A through water. As shown in equations 5-5 to 5-7, the above flux may be written as follows:

$$F_{md} = \frac{C_o}{R_{tot}} \tag{5-29}$$

Using Equations 5-2 and 5-24, the following expression for convective flux is obtained:

$$F_{conv} = \frac{k}{\mu}\frac{\Delta P_{tm}}{\delta_{mem}} C_o \tag{5-30}$$

The ratio of convective to diffusive flux can be written as follows:

$$\frac{F_{conv}}{F_{md}} = \frac{k}{\mu}\frac{\Delta P_{tm}}{\delta_{mem}} R_{tot} \tag{5-31}$$

The manufacturer's values for permeability and membrane thickness are as follows:

$$\frac{k}{\mu}\text{(water @ 25°C)} = 2.35 \times 10^{-5}\ \text{cm}^2/\text{psi}\cdot\text{s} \tag{5-32}$$

$$\delta_{mem} = 0.275 \text{ mm} \tag{5-33}$$

The value of μ in Equation 5-32 is from Streeter and Wylie (1985). Substituting Equations 5-32, 5-33, and 5-28 into Equation 5-31, we obtain a practical expression for our system of the ratio of convective to diffusive flux as a function of flowrate and overall membrane diffusive resistance:

$$\frac{F_{conv}}{F_{md}} = 0.00094 \cdot (1.26 \times 10^{-5} Q + 1.24 \times 10^{-6} Q^2) R_{tot} \tag{5-34}$$

where Q is the flowrate in units of [mL/min]; and R_{tot} is the total diffusive resistance in units of [s/cm]. Curves of this flux ratio are plotted as functions of Q in Figure 5-8 for various overall membrane diffusive resistances. From the figure, it is clear that convective flux is negligible to diffusive flux as long as flowrate is below 40 mL/min and membrane tube diffusive resistance, R_{tot}, is below 10,000 s/cm. From later data, it will be shown that R_{tot} is indeed below 10,000 s/cm for all diffusion experiments in this study. Also, interior and exterior solution flowrate is kept below 40 mL/min for all experiments. Note that convective flux can be calculated directly by Equation 5-30 and in all experiments is negligible to diffusive flux. Convective flux is less than 1% of total measured flux for all experiments.

We have assumed that all diffusion is due to aqueous phase molecular diffusion and have neglected the possibility of solid phase surface diffusion. In general, surface diffusion is important in solute transport through membranes only when the average pore size of the membrane is much less than the size of

Figure 5-8: Ratio of Convective to Diffusive Flux as a Function of Flowrate Q and Resistance R_{tot}

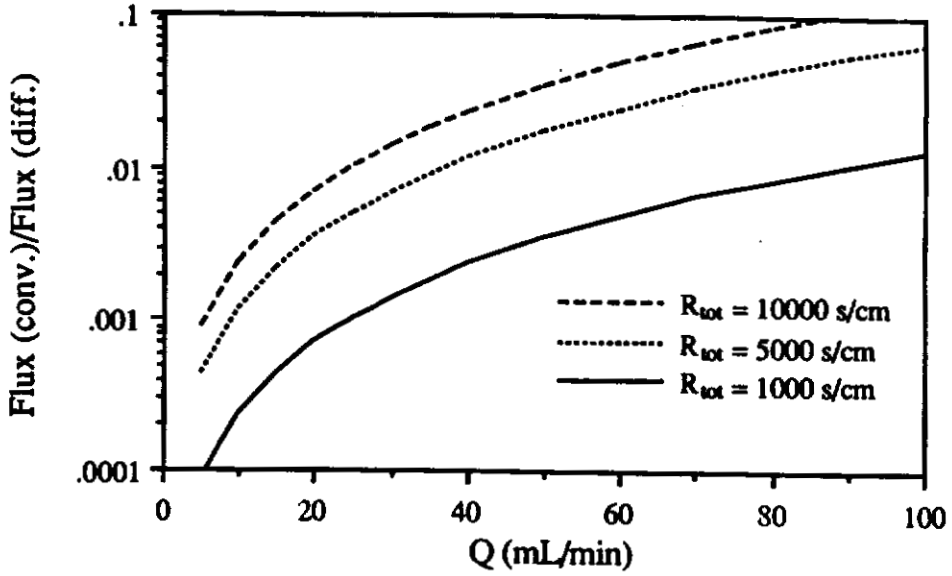

$$\frac{F_{conv}}{F_{md}} = 0.00094\,(1.26 \times 10^{-5} Q + 1.24 \times 10^{-6} Q^2)\, R_{tot}$$

Q in [mL/min]
R_{tot} in [s/cm]

the solute molecule (Bitter, 1991). However, the solutes used in this study are all smaller than the average pore sizes of the membranes used. Also, solute surface diffusion coefficients are generally around 1×10^{-8} cm^2/s (Treybal, 1987), about 3 orders of magnitude lower than aqueous phase molecular diffusion coefficients of the solutes used in this study. Thus, it is expected aqueous phase molecular diffusion will dominate and surface diffusion effects can be safely neglected.

5.4. NVPS Leakage Test

Tests were conducted to determine any detectable transport of NVPS copolymer from the interior side of the membrane to the exterior using each of the 2000 and the 50,000 molecular weight cutoff membranes.. Very little or no leakage was expected since the radius of gyration of the NVPS molecule is so much larger than the average pore sizes of the skin layers of the membranes used (940 Å versus 10 to 50 Å). The experimental set-up used is pictured in Figure 5-5.

First, a solution of approximately 2 wt.% NVPS in water was placed in the exterior solution reservoir, and circulation through the membrane tube cartridge was begun. There was no flow through the PAH column pictured in Figure 5-5. At the same time, circulation of distilled water was begun through the *interior* side of the cartridge. The flowrate for both solutions was 40 mL/min. A side-stream from the interior solution flowed through a 1-cm-pathlength flow cell in the UV spectrophotometer which measured absorbance at 400 nm wavelength. Flow was continued for about four hours.

No absorbance of the interior solution was detected at 400 nm at any time during either experiment. Therefore, according to the accuracy of the spectrophotometer measurement (±0.001 absorbance unit) and the extinction coefficient of NVPS at 400 nm, the maximum leakage of NVPS that could have occurred was 0.002% of the charged NVPS in the exterior solution. This is a negligible amount, thus the assumption of no NVPS leakage is satisfactory.

5.5. Naphthalene Diffusion into Copolymer Solution

The experimental set-up for the naphthalene diffusion experiments is shown schematically in Figure 5-5. The purpose of these experiments is to obtain a measure of R_{tot}, the total membrane resistance to aqueous phase molecular diffusive transport of naphthalene from the exterior to the interior solutions. The experimental technique minimizes the problem of naphthalene adsorption onto solid apparatus surfaces by maintaining a constant exterior naphthalene concentration and by allowing transport into a copolymer interior solution, not a pure water interior solution. The copolymer solution provides more attractive (hydrophobic) and more available "adsorption" sites to naphthalene molecules than do solid apparatus surfaces; thus there is a negligible loss of naphthalene from the interior solution to the solid surfaces. The experiment also employs a large surface area membrane (over 600 cm^2), which reduces irregularity errors reported in small surface area stirred-cell experiments (Robertson and Zydney, 1990).

5.5.1. Experimental Procedure

The exterior solution reservoir shown in Figure 5-5 was filled with a known volume of water (approximately 200 mL). The PAH column was filled with solid naphthalene crystals and flow of the exterior solution through the column was maintained at a minimum of 150 mL/min. The exterior-side naphthalene solution was pumped through the membrane cartridge at 40 mL/min. A side-stream of the exterior solution was sent on-line to a quartz flow cell in the UV spectrophotometer for naphthalene concentration

measurement at 276 nm wavelength. The concentration was monitored until the exterior solution became saturated with naphthalene – allowing for any adsorption onto the solid surfaces of the apparatus. Adsorption was not a problem since the exterior solution was maintained at saturated naphthalene concentration throughout the experiment, in adsorptive equilibrium with all apparatus solid surfaces. The fast flowrate of exterior solution through the naphthalene column provided sufficient mixing such that all exterior solution concentration readings were stable to within the precision of the spectrophotometer. The magnetic stirrer in the interior solution reservoir was turned on to provide well-mixed conditions. Throughout the experiment, flowrates of the exterior and interior solutions through the membrane cartridge were fixed at 40 mL/min each.

Distilled water was flushed through the membrane tube interior for 30 minutes (while exterior solution was held at saturated concetration) in an effort to allow the naphthalene concentration profile in the membrane to become linear before the experiment was begun (Figure 5-9). It was later found that since the residence time of a diffusing solute molecule in the membrane was less than two minutes, this step was unnecessary and had negligible effect on the experimental results.

After the flushing step, the interior solution was allowed to recirculate and a known amount of NVPS copolymer was added into the interior solution reservoir. A side-stream of the interior solution was continuously sent on-line to a quartz flow cell in the UV spectrophotometer for naphthalene and NVPS concentration measurement at 276 nm and 400 nm wavelengths. As discussed

previously, NVPS absorbs light at both 276 nm and 400 nm, while naphthalene only absorbs at the 276 nm wavelength; therefore, using the solute extinction coefficients, the concentrations of naphthalene and NVPS of the interior solution were determined as a functions of time. The NVPS concentration did not change during the experiment (as determined to the precision limit of the spectrophotometer). The naphthalene concentration increased in the interior solution as it diffused through the membrane. The naphthalene concentration increased to many times the saturated naphthalene concentration in water, about 31 mg/L (May et al., 1978).

After the experiment, the exterior solution concentration and temperature were measured and were unchanged from their values before the introduction of NVPS to the interior solution.

Figure 5-9: Concentration Profile Along Cross-Section of Membrane Wall

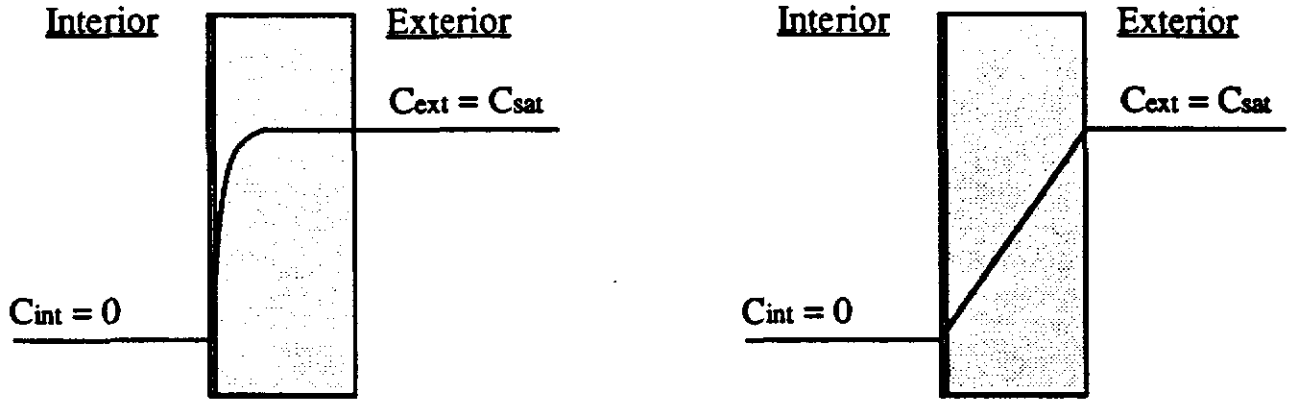

Before Flushing Interior Solution

After Flushing Interior Solution

5.5.2. Experimental Results

The data for all naphthalene diffusion runs conducted with the 2000 and 50,000 nominal molecular weight cutoff membranes are listed in Appendix A. A sample run using the 2000 MW cutoff membrane is shown in Figure 5-10. The naphthalene concentrations of the interior solution (shown as multiples of the saturated concentration of naphthalene in pure water -- 31 mg/L) are plotted versus time. For example, after 100 minutes, the naphthalene concentration of the interior copolymer solution was about 10 times naphthalene's saturated concentration in water. The interior solution's copolymer concentration in this particular experiment was 2.66 wt.%. The exterior solution concentration is given by the dotted line at $C/C_{sat} = 1$, constant for the entire experiment.

Figure 5-10: Naphthalene Diffusion Through 2000 MW Cutoff Membrane Into NVPS Copolymer Solution

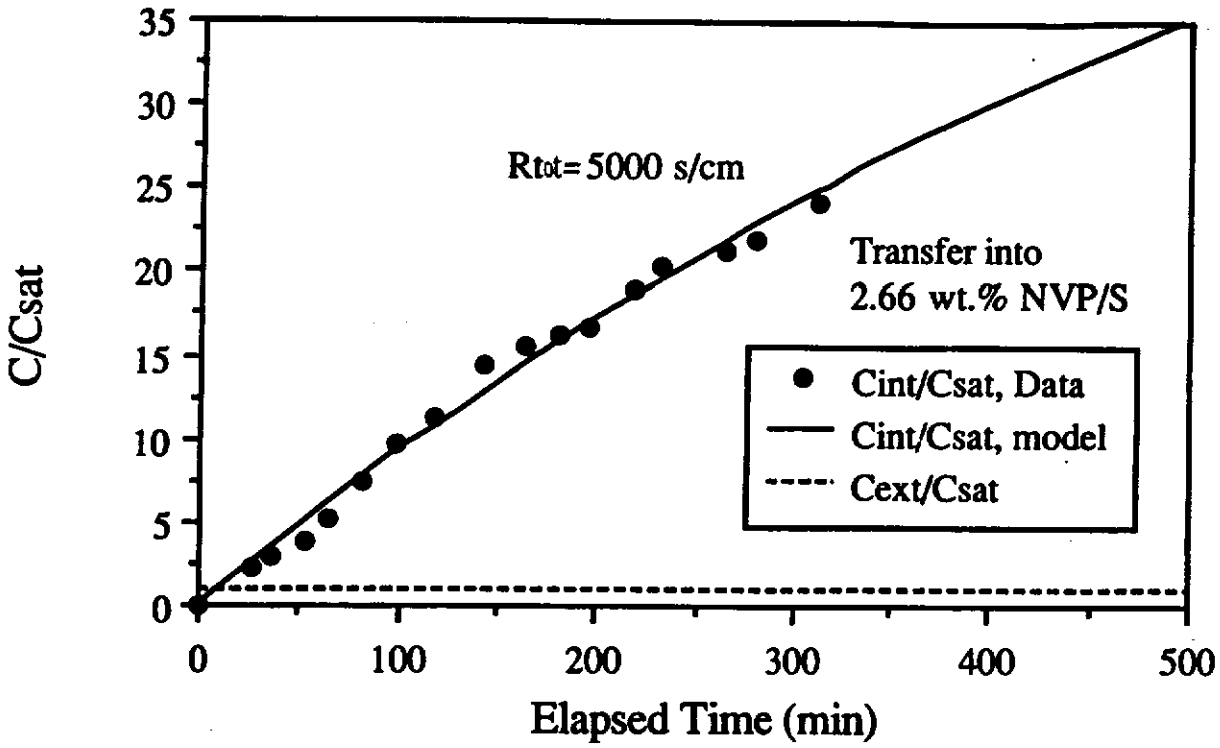

We now wish to determine R_{tot}, the total resistance to molecular diffusive transport of naphthalene from the exterior to the interior solution for this experiment. This can be determined by using Equation 5-22:

$$\Omega(t) = \frac{1}{R_{tot}} t \qquad (5\text{-}22)$$

$$\text{where } \Omega(t) = -\ln\left(1 - \frac{C_{int}(t)/C_{sat}}{(1 + M\,K_{pw})}\right) / b$$

$$b = \frac{A_t}{V_t\,(1 + M\,K_{pw})}$$

A plot of normalized concentration, $\Omega(t)$, versus time is shown in Figure 5-11 for this experiment. This curve is clearly linear and was fitted using a least-squares regression. The inverse of the slope is 5000 s/cm, which is the value of R_{tot} for this experiment.

The experiment was repeated twice using the 2000 MW cutoff membrane and NVPS copolymer interior solution concentrations of below 3 wt.%. The experiment was also conducted twice using the 50,000 MW cutoff membrane and NVPS concentrations of below 3 wt.%. The normalized data from these experiments are shown in the $\Omega(t)$ versus time plot of Figure 5-12. It is clear that the slopes for the 2000 and 50,000 MW membrane data are very close. Linear regressions of the data yield slopes shown in Table 5-1. The slope corresponds to a total resistance, R_{tot}, of between 4880 and 5030 s/cm (95% confidence interval).

Figure 5-11: Naphthalene Diffusion Through 2000 MW Cutoff Membrane Into NVPS Copolymer Solution -- Normalized Data

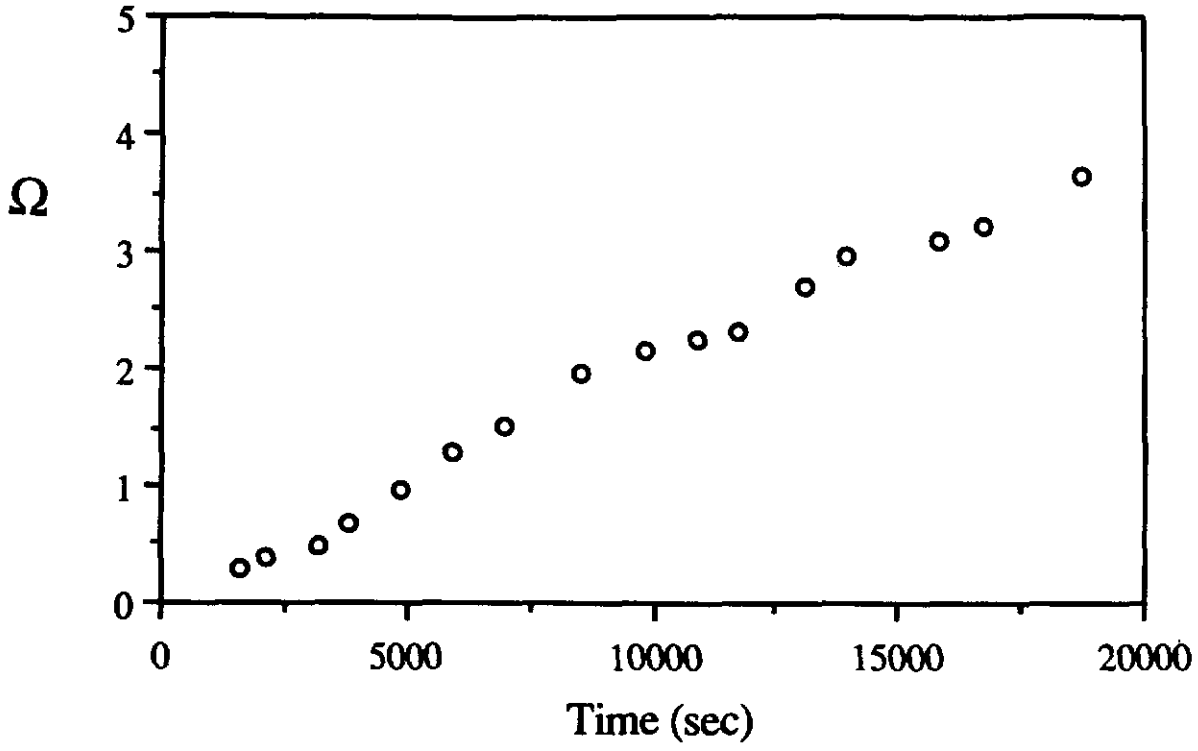

Figure 5-12: Naphthalene Diffusion Through 2K and 50K MW Cutoff Membranes Into NVPS Copolymer Solution -- Normalized Data

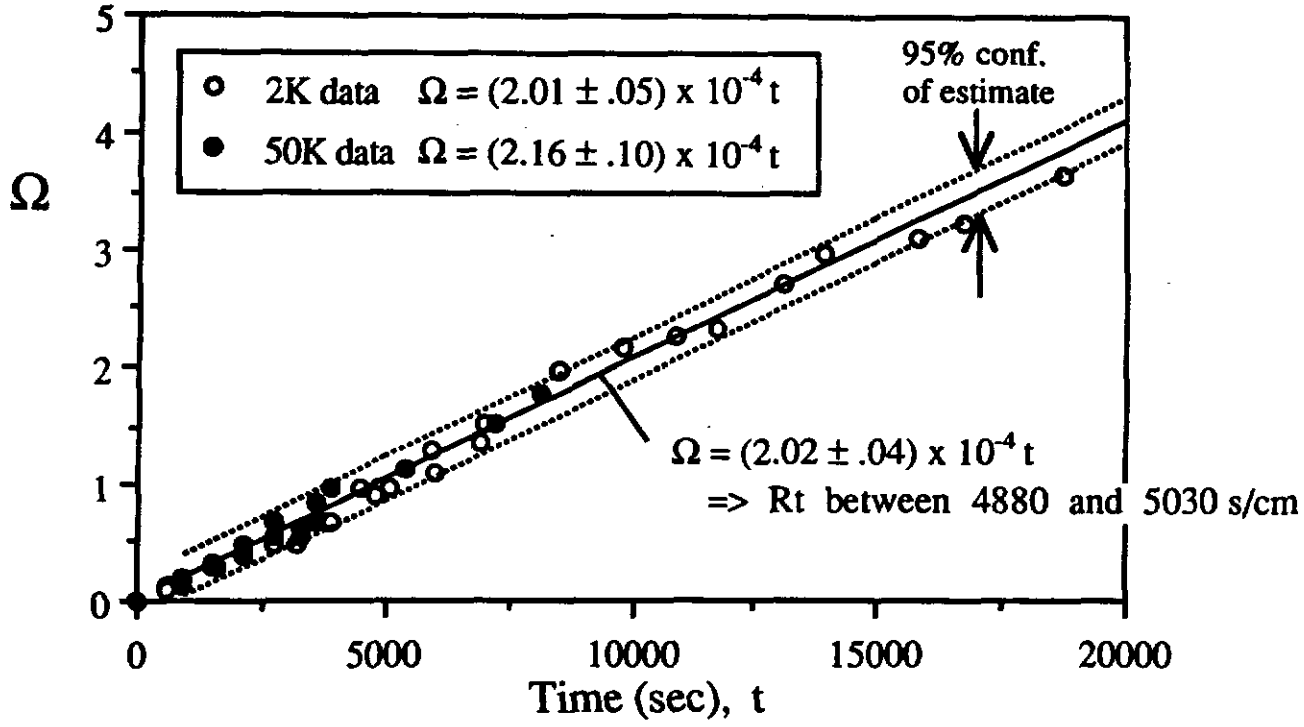

$$\Omega = -\ln\left(1 - \frac{C_{int}/C_{sat}}{1 + M K_{pw}}\right) / b = \frac{t}{R_{tot}}$$

Table 5-1: Slopes of Normalized Concentration Versus Time Plots

Solute	Membrane MW Cutoff	Slope of Ω vs. t	R_{tot} (s/cm)
Naphthalene	2000	(2.01±0.05) x 10^{-4} cm/s	4980 ± 120
Naphthalene	50,000	(2.16±0.10) x 10^{-4} cm/s	4630 ± 210
Naphthalene	Pooled Data	(2.02±0.04) x 10^{-4} cm/s	4950 ± 100

All variations in $d\Omega/dt$ and R_{tot} cited to 95% confidence.

A pooled variance of estimate t-test on data from the 2000 and 50,000 MW membrane runs was conducted (Volk, 1958). From the test it was determined that the statistical chance the slopes determined from the two data sets are the same is 22%. This means that the existence of any real difference between the true 2000 and 50,000 MW membrane run slopes is uncertain. The only difference between the two types of membranes was the average pore size of the thin, 0.1-0.2-μm skin layer. The support structures of the membranes were identical. It will be shown in Section 5.7 that the membrane support structure is the expected primary contributor to R_{tot} according to diffusion models, since it is much thicker than the microporous skin layer. The data in Figure 5-12 supports this statement, since the membrane support structures of the membranes used in the two data sets were identical, and approximately the same R_{tot}'s were determined for both membranes.

5.6. Phenanthrene Diffusion into Copolymer Solution

5.6.1. Experimental Procedure

The experimental procedure followed for the phenanthrene diffusion experiments was identical to the naphthalene diffusion experimental procedure described earlier in Section 5.5.1. with the following exceptions. The PAH column was filled with solid phenanthrene-coated glass beads instead of solid naphthalene. Also, measurement of NVPS and phenanthrene concentration was determined by UV spectrophotometer absorbance readings at 293 and 400 nm wavelengths, not 276 nm.

The phenanthrene concentrations of the interior solution were measured on-line as a function of time. These concentrations rose according to the Equation 5-22 model as phenanthrene diffused from the constant-concentration exterior solution, through the membrane, and into the interior NVPS copolymer solution.

5.6.2. Experimental Results

The data for all phenanthrene diffusion runs conducted using the 2000 and 50,000 nominal molecular weight cutoff membranes are shown in Appendix B. A plot of normalized concentration, $\Omega(t)$, versus time is shown in Figure 5-13 for all phenanthrene diffusion experiments. The curve is clearly linear and was fitted using a least-squares regression. Slopes using only 2000 and 50,000

Figure 5-13: Phenanthrene Diffusion Through 2K and 50K MW Cutoff Membranes Into NVPS Copolymer Solution -- Normalized Data

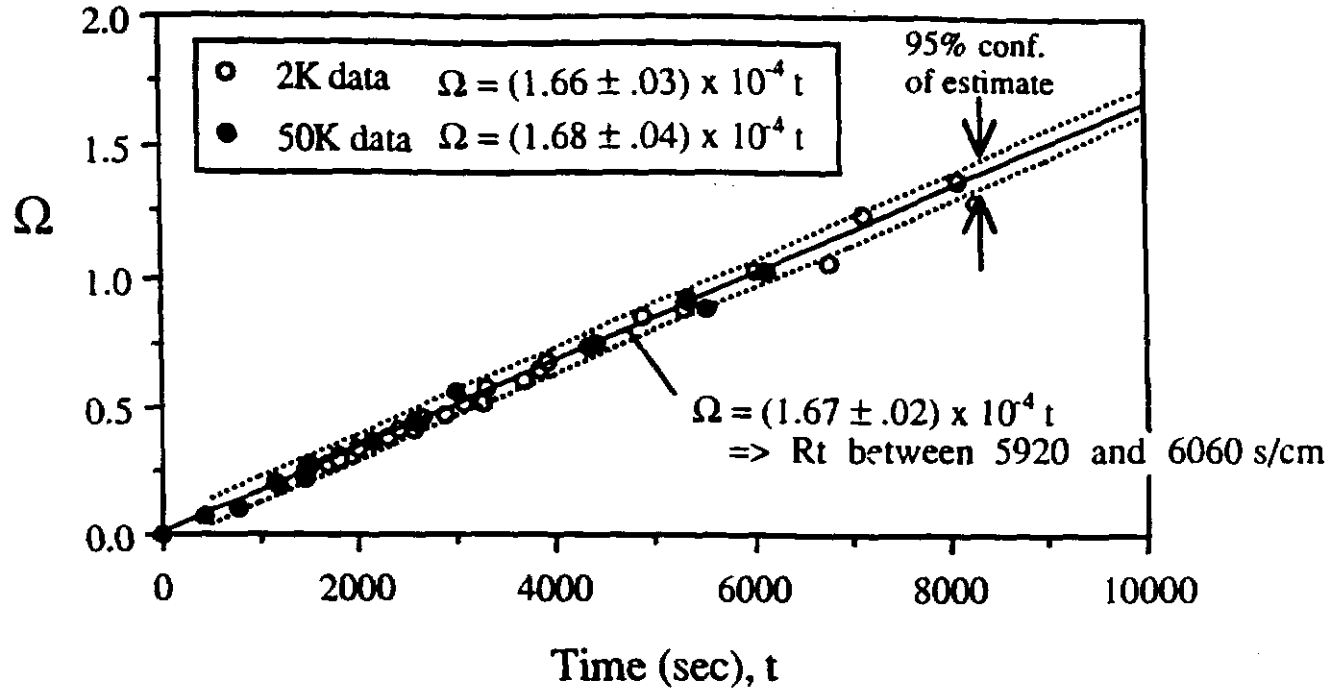

Table 5-2: Slopes of Normalized Concentration Versus Time Plots

Solute	Membrane MW Cutoff	Slope of Ω vs. t	R_{tot} (s/cm)
Phenanthrene	2000	(1.66±0.03) x 10^{-4} cm/s	6020 ± 100
Phenanthrene	50,000	(1.68±0.04) x 10^{-4} cm/s	5950 ± 140
Phenanthrene	Pooled Data	(1.67±0.02) x 10^{-4} cm/s	5990 ± 70

All variations in dΩ/dt and R_{tot} cited to 95% confidence.

membrane run data were also determined using least-squares linear regression. The slopes are listed in Table 5-2. The pooled slope corresponds to a total resistance, R_{tot}, of between 5920 and 6020 s/cm (95% confidence interval) for phenanthrene diffusive transport from exterior to interior solutions.

A pooled variance of estimate t-test on the 2000 and 50,000 membrane run data slopes was conducted for the phenanthrene diffusion experiments. From the test, it was determined that the statistical chance the slopes determined from the two data sets are the same is 68%. Therefore, the existence of any real difference between the true 2000 and 50,000 membrane run experimental slopes is unlikely. As with the naphthalene diffusion tests, this result was not surprising, since the expected primary contributor to diffusive resistance, the membrane support layer, was identical in both the 2000 and 50,000 membrane tests.

5.7. Comparison of Experimental Results with Model Predictions

R_{tot}, the total resistance to aqueous phase molecular diffusion of solute from the exterior to the interior solution, can be divided into the following four sources in series:

1. Membrane support layer
2. Membrane skin layer
3. Interior fluid boundary layer
4. Exterior fluid boundary layer

These are depicted in Figure 5-1. In this section, the contribution of each layer to Rtot will be predicted from literature models and will be compared to the experimental R_{tot}'s from Figures 5-12 and 5-13.

Since the pore sizes of the membrane support layers for all experiments are orders of magnitude larger than the solute molecular sizes, there is no size-exclusion factor for the molecular diffusive resistance of the membrane support layer. Thus, the resistance through the layer is equal to the mass transfer resistance of the average water-filled pore length determined as follows:

$$R_1 = \frac{\delta_{sup}\,\tau_{sup}}{D_{AB}\,\varepsilon_{sup}} \qquad (5\text{-}35)$$

where R_1 is the mass transfer resistance of the membrane support layer [cm/s]; D_{AB} is the molecular diffusion coefficient of solute A in water [cm^2/s]; δ_{sup} is

the support layer thickness [cm]; τ_{sup} is the support layer tortuosity [dimensionless]; and ε_{sup} is the support layer porosity [dimensionless].

The membrane skin layers, on the other hand, have average pore sizes comparable to the solute sizes. An approach for approximating the diffusive resistance of such an anisotropic membrane layer is given by Roberts and Zydney, 1990, as:

$$R_2 = \frac{\delta_{skin}\,\tau_{skin}}{\phi\, D_{AB}\, \varepsilon_{skin}} \qquad (5\text{-}36)$$

where R_2 is the mass transfer resistance of the membrane skin layer [cm/s]; and ϕ is the ratio of pore solute concentration to bulk phase concentration [dimensionless]. Values of ϕ can be approximated for various solute-membrane systems using a technique developed by Bungay and Brenner, 1973, for anisotropic membranes. The technique involves modeling the membranes as intersecting matrices of random planes. The diffusion coefficients of solutes in water used in this study were determined using the Hayduk and Laudie method as described in Lyman, 1990. The method has a reported 5.8% average absolute error and is generally used to estimate diffusion coefficients of organic compounds in water.

The remaining two boundary layers are fluid boundary layers interior and exterior to the membrane wall. In the diffusion experiments, the interior and exterior solutions flowed along the length of the membrane wall. The thicknesses of the fluid layers are assumed to be functions of the flow characteristics of the bulk fluid away from the membrane wall. For determining

interior boundary layer resistance, we use the Graetz-Nusselt solution for laminar flow through a thermally-developing tube with specified wall temperature (Kakac, 1985). A relationship for the Nusselt number is given as follows:

$$Nu = 3.66 + \frac{0.0668}{x^{*\,1/3}(0.04 + x^{*2/3})} \tag{5-37}$$

where Nu is the Nusselt number [dimensionless]; x^* is nondimensional tube length (= $x/D_h\,Pe$); x is the tube length [cm]; D_h is the hydraulic diameter of the tube [cm]; Pe is the Peclet number (= $D_h\,V/\alpha$); V is the mean fluid velocity through the tube [cm/s]; and α is the thermal diffusivity [cm^2/s]. This relation is converted from a heat transfer to a mass transfer correlation using the analogous mass transfer nondimensional terms (Treybal, 1987). Note that the solution is now good for laminar flow through a *concentrationally*-developing tube with specified wall *concentration*. By mass transfer analogy, Equation 5-37 becomes:

$$Sh = \frac{k_L' D_h}{D_{AB}} = 3.66 + \frac{0.0668}{x^{*\,1/3}(0.04 + x^{*2/3})} \tag{5-38}$$

where Sh is the Sherwood number [dimensionless]; x^* is nondimensional pipe length (= $x/D_h\,Pe_m$); Pe_m is the mass transfer Peclet number (= $D_h\,V/D_{AB}$); D_{AB} is the diffusion coefficient of solute A in water; and k_L' is the mass transfer coefficient { = $1/R_3(1 + K_{pw})$} [cm/s]. Solving Equation 5-38 for resistance, R_3, (inverse of mass transfer coefficient):

$$R_3 = \frac{D_h}{Sh\ D_{AB}(1 + K_{pw}M)} \tag{5-39}$$

where R_3 is the mass transfer resistance of the interior fluid boundary layer [s/cm]; K_{pw} is the polymer-water partition coefficient [dimensionless]; and M is the polymer to water weight ratio [dimensionless]. The polymer-water partition coefficient is required in the calculation of R_3 since the interior solution is an aqueous copolymer solution. The K_{pw} term is required to scale the mass transfer coefficient of the interior solution to aqueous phase concentrations from which R_{tot} is defined. For example, in the interior solution, flux through a fluid boundary layer can be written as:

$$F_{fbl} = k' \Delta C_{int} \tag{5-40}$$

where F_{fbl} is the flux of solute through the fluid boundary layer [g/cm^2 s]; ΔC_{int} is the overall interior solution concentration difference between the ends of the boundary layer [g/cm^3]; and k' is the mass transfer coefficient [cm/s]. However, we have defined overall flux from the exterior solution to the interior solution in terms of $C_{int,aq}$, the *aqueous* phase solute concentration. The following holds true for our systems:

$$\frac{C_{int,p}}{C_{int,aq}} = M K_{pw} \tag{5-41}$$

$$C_{int} = C_{int,aq} + C_{int,p} \tag{5-42}$$

where $C_{int,aq}$ is the aqueous pseudophase solute concentration of the interior solution [g/cm^3 solution]; $C_{int,p}$ is the polymer pseudophase solute concentration of the interior solution [g/cm^3 solution]; and C_{int} is the overall

interior solution solute concentration [g/cm^3 solution]. C_{int} can be related to the aqueous phase concentration, $C_{int,aq}$, as follows:

$$C_{int} = C_{int,aq}(1 + M\ K_{pw}) \tag{5-43}$$

Substituting this into Equation 5-40:

$$F_{fbl} = k' \Delta C_{int,aq}\ (1 + M\ K_{pw}) \tag{5-44}$$

Thus, the true mass transfer resistance of the interior solution fluid boundary layer is the inverse of the coefficient of $\Delta C_{int,aq}$ in Equation 5-44, or in other words:

$$R_3 = \frac{1}{k'(1 + M\ K_{pw})} \tag{5-45}$$

where k' is defined by Equation 5-38.

A Nusselt number correlation from Kakac, 1985, is used in determining the resistance of the exterior fluid layer. The correlation was developed for heat transfer in the case of flow exterior to staggered tube bundles (>16 tubes), good for Reynolds numbers, Re, between 1 and 500:

$$Nu = 1.04\ Re^{0.4}\ Pr^{0.36} \tag{5-46}$$

where Re is the Reynolds number (= $d_c\ G'/\mu$); d_c is the cylinder outer diameter [cm]; G' is the average fluid mass flux [g/cm^2 s]; μ is the fluid viscosity [g/cm s]; and Pr is the Prandtl number. By mass transfer analogy,

$$Sh = \frac{k_L' d_c}{D_{AB}} = 1.04\, Re^{0.4} Sc^{0.36} \qquad (5\text{-}47)$$

where Sc is the Schmidt number (= $\mu/\rho\, D_{AB}$); and ρ is the fluid density [g/cm^3]. Solving Equation 5-47 for resistance:

$$R_4 = \frac{d_c}{Sh\, D_{AB}} \qquad (5\text{-}48)$$

where R_4 is the mass transfer resistance of the exterior fluid boundary layer [s/cm].

Values of boundary layer resistance as given by Equations 5-35, 5-36, 5-39, and 5-48 are given in Table 5-3 for the solute-copolymer systems studied here, under experimental conditions. The modeled resistance approximates the measured overall resistance for both the naphthalene and phenanthrene diffusive transfer experiments with less than 10% error. This is within the collective error of model inputs for these experiments. The dominant modeled source of resistance is the membrane support layer. The experimental data reflect the fact that phenanthrene has a slightly lower diffusivity in water than naphthalene, since D_{AB}(phen.) < D_{AB}(naph.); thus, the overall resistance for phenanthrene transport is greater than for naphthalene transport. The model also shows that the resistance of the membrane skin layer is negligible compared to overall resistance. This explains the negligible difference between the experimentally-measured resistances using the 2000 and 50,000 MW membranes. The membranes were identical except for their skin layers.

Table 5-3: Mass Transfer Resistances – Modeled Versus Measured

Resistance Type (i)	Modeled Resistance R_i (s/cm)			
	Naphthalene Transport		Phenanthrene Transport	
	2K mem.	50K mem.	2K mem.	50K mem.
1. Membrane Support Layer (Equation 5-35)	4100	4100	4900	4900
2. Membrane Skin Layer (Equation 5-36)	90	0	200	50
3. Interior Fluid Boundary Layer (Equation 5-39)	100	100	10	10
4. Exterior Fluid Boundary Layer (Equation 5-48)	400	400	500	500
R^*_{tot} = Total Modeled Resistance:	4700	4600	5600	5500
R_{tot} = Total Measured Resistance: (from Figures 5-12 and 5-13)	4980 ± 120	4630 ± 210	6020 ± 100	5950 ± 140

6. Aquifer Simulation Experiments

6.1. Mass Transfer of Organic Solute in an Aquifer

One of the major goals of this thesis was to demonstrate the effective use of the proposed barrier system on a laboratory scale. Related specific objectives were to model the lab-scale system mathematically and to discuss applicability of models to larger scale systems with different contaminants, soil types, and treatment well configurations. All of these require an understanding of organic solute mass transfer in an aquifer. This section develops a general framework for the evaluation of contaminant transport in an aquifer. Properties of the aquifer and contaminant that are important to transport are discussed as are several means of quantifying them. This overview is written with relevance to the proposed contaminant barrier system in mind.

Conservation and Constitutive Equations

A convection-dispersion model is generally used to describe contaminant transport in an aquifer. The model follows from a mass balance on a volume of contaminated fluid, V, shown in Figure 6-1 with surface S, normal vector **n**, and concentration C(x,y,z,t) expressed, for example, in rectangular coordinates. The mass balance follows:

$$\frac{d}{dt}\int_V C\,dV = -\int_S \mathbf{F}\cdot\mathbf{n}\,dS + \int_V R_V\,dV \qquad (6\text{-}1)$$

where R_v is the volumetric rate of formation of contaminant [g/cm^3 s]; and **F** is the net flux of contaminant into volume V [g/cm^2 s]. Quantities in **bold**

represent vector quantities. Equation 6-1 states that the rate of accumulation of contaminant in volume V (left hand term) equals the net rate at which contaminant passes into the surface of the volume (first term on right-hand side) plus the rate at which contaminant is formed within the volume. Equation 6-1 may be simplified by using the Gauss-Ostrogradskii Divergence Theorem (Bird et al., 1960) which states the following:

$$\int_S \mathbf{F} \cdot \mathbf{n}\, dS = \int_V \nabla \cdot \mathbf{F}\, dV \qquad (6\text{-}2)$$

Equation 6-2 becomes the following:

$$\int_V \left(\frac{\partial C}{\partial t} + \nabla \cdot \mathbf{F} - R_v\right) dV = 0 \qquad (6\text{-}3)$$

Figure 6-1: Volume of Contaminated Fluid in a Rectangular Coordinate System

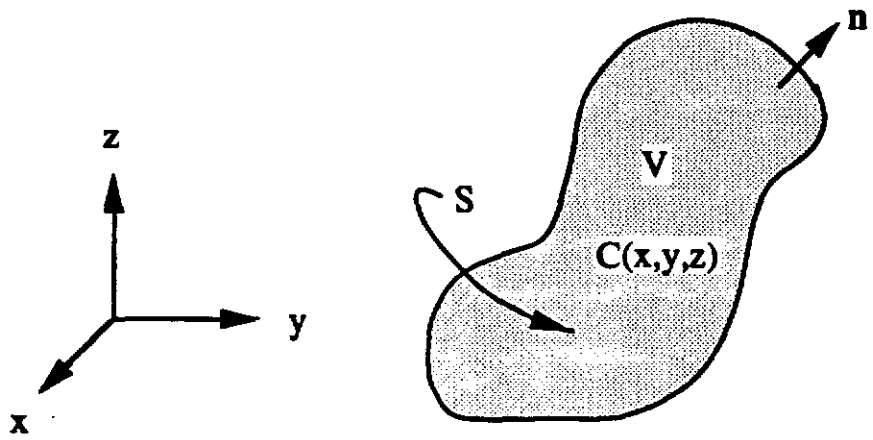

By allowing the volume to become differentially small, we obtain:

$$\frac{\partial C}{\partial t} = -\nabla \cdot \mathbf{F} + R_v \qquad (6\text{-}4)$$

The flux is generally expressed as follows:

$$\mathbf{F} = C\mathbf{u} - D\nabla C \qquad (6\text{-}5)$$

where **u** is velocity vector [cm/s]; and D, a function of position, is the dispersion coefficient to be discussed in more detail later. Equation 6-5 assumes that the conductive (C**u**) and dispersive (D∇C) parts of the flux can be separated.

At this point, it is convenient to assume that density is constant throughout the volume. Most organic contaminants have low solubility (ppm or less) in water, although the concentrations may be toxic at these low levels (i.e. endrine, lindane, and toxaphene) (Freeze and Cherry, 1979). Thus, the density of the contaminated water is generally very close to the density of pure water, and the assumption of constant density throughout the volume is valid. Cases where this assumption is invalid include multiphase contaminated aquifer systems and cases where temperature gradient is significant. The focus of this thesis is modeling contaminant transport in a single aqueous phase through the porous network of an isothermal aquifer, so the assumption of constant density is valid. We can thus apply the equation of continuity for an incompressible fluid of constant density:

$$\nabla \cdot \mathbf{u} = 0 \qquad (6\text{-}6)$$

Substituting equation 6-5 into 6-4, we obtain:

$$\frac{\partial C}{\partial t} = -\nabla \cdot (C\mathbf{u} - D\nabla C) + R_v \qquad (6\text{-}7)$$

Simplifying using Equation 6-6:

$$\frac{\partial C}{\partial t} = -\mathbf{u} \cdot \nabla C + \nabla \cdot D\nabla C + R_v \qquad (6\text{-}8)$$

In all aquifer simulation experiments in this work, there is no variation in the z-direction; therefore, we may neglect the z-terms in Equation 6-8. Expressing Equation 6-8 for a 2-D rectangular coordinate system, we obtain:

$$\frac{\partial C}{\partial t} + u_x\frac{\partial C}{\partial x} + u_y\frac{\partial C}{\partial y} = \frac{\partial}{\partial x}\left(D_x\frac{\partial C}{\partial x}\right) + \frac{\partial}{\partial y}\left(D_y\frac{\partial C}{\partial y}\right) + R_v \qquad (6\text{-}9)$$

where D_x is the dispersion coefficient in the x-direction [cm^2/s]; D_y is the dispersion coefficient in the y-direction [cm^2/s]; u_x is the groundwater seepage velocity in the x-direction [cm/s]; and u_y is the groundwater seepage velocity in the y-direction. All of the dispersion coefficient and velocity terms can be functions of position in the x- and y-directions as used in this equation. Variation of any parameter in the z-direction is not accounted for in Equation 6-9. In aquifers made up of layers of varying permeability, the simplification of the problem from three to two spatial dimensions may not be justified. In many instances, Equation 6-9 may be simplified by assuming that D_x and D_y are constants throughout the domain being modeled. Using this assumption we obtain the 2-D dispersion-convection equation for the continuous aqueous phase:

$$\frac{\partial C}{\partial t} + u_x\frac{\partial C}{\partial x} + u_y\frac{\partial C}{\partial y} = D_x\frac{\partial^2 C}{\partial x^2} + D_y\frac{\partial^2 C}{\partial y^2} + R_v \qquad (6\text{-}10)$$

Retardation Term

The reaction term R_v in Equation 6-10 may be used to account for disappearance of contaminant from the aqueous phase by reaction to form another species, or it may be used to account for the transfer of contaminant out of the aqueous phase and *onto* the solid phase of the aquifer. For most contaminated aquifers of interest, the latter use of R_v is more important. This transfer of organic contaminant from the aqueous to the solid phase is called adsorption. Adsorption can be characterized by using a linear equilibrium adsorption isotherm for the partitioning of the contaminant between the aqueous phase and the solid material of the aquifer (Ball and Roberts, 1991). First, assume an equilibrium exists such that the following relation holds (Carberry, 1976):

$$K_d = \frac{S}{C} = \text{constant} \qquad (6\text{-}11)$$

where K_d is the solid-liquid contaminant partition coefficient [cm^3/g]; S is the mass of contaminant adsorbed to aquifer solids per mass of aquifer solids [g/g]; and C is the mass of contaminant in the aqueous phase per unit volume of the aquifer aqueous phase [g/cm^3]. The aquifer properties bulk density, ρ_b, and porosity, n, are defined as follows:

$$\rho_b \equiv \frac{\text{mass of aquifer solids}}{\text{bulk volume of aquifer}} \qquad (6\text{-}12)$$

$$n \equiv \frac{\text{volume of aquifer pores}}{\text{bulk volume of aquifer}} \tag{6-13}$$

Therefore, we can write:

$$S\frac{\rho_b}{n} = \frac{\text{mass of solute adsorbed}}{\text{volume of solution}} \tag{6-14}$$

We wish to define R_v, the term in Equation 6-10, as the rate at which mass leaves the aqueous phase and enters the solid phase by adsorption per volume of aquifer solution. In terms of our variables:

$$R_v = -\frac{\partial}{\partial t}(S\frac{\rho_b}{n}) = -\frac{\rho_b}{n}\frac{\partial S}{\partial t} \tag{6-15}$$

Bulk density and porosity are assumed constant with time. Using Equation 6-11 to write solid-phase-based concentration S in terms of aqueous-phase-based concentration C, the following is obtained:

$$R_v = -\frac{\rho_b}{n}K_d\frac{\partial C}{\partial t} \tag{6-16}$$

Substituting this expression into Equation 6-10 for R_v:

$$(1 + \frac{\rho_b}{n}K_d)\frac{\partial C}{\partial t} + u_x\frac{\partial C}{\partial x} + u_y\frac{\partial C}{\partial y} = D_x\frac{\partial^2 C}{\partial x^2} + D_y\frac{\partial^2 C}{\partial y^2} \tag{6-17}$$

The retardation coefficient, R_d, may be defined as follows:

$$R_d \equiv 1 + \frac{\rho_b}{n}K_d \tag{6-18}$$

In using this term in Equation 6-17, it has been assumed that the equilibrium of contaminant between the aqueous and solid phases is maintained at all times, and that this equilibrium may be expressed in terms of a constant solid-liquid partition coefficient as given in Equation 6-11 over the complete range of concentrations encountered in the aquifer domain. This assumption becomes increasingly good for aquifers with slower groundwater flow, since more time is available for an adsorptive equilibrium to be reached.

Solid-Liquid Partition Coefficient

There is work in the literature which describes methods of estimating values of K_d for contaminants of interest given various aquifer soil properties (Lion et al., 1990). However, due to the complexity of some soil compositions, the most reliable determination of K_d for a particular soil-solute system is by experimental measurement. It is important, too, to note that values of K_d may vary spatially in a real aquifer due to nonhomogeneity of the soil material (Bakr et al., 1978).

It is well-known that hydrophobic organic contaminants in aquifers partition preferentially onto the organic (as opposed to the inorganic) portions of the solid material in contact with the solution (Freeze and Cherry, 1979). More specifically, for aquifer materials whose organic matter fraction, f_{om}, is greater than 0.002, it is generally assumed partitioning of nonpolar organic solutes occurs primarily on the organic portion of the soil (Karickoff et al., 1984 and Schwarzenbach and Westal, 1981). Empirical relationships have been developed to describe solute partitioning between soil and aqueous solutions in terms of the solute's preference for dissolving in nonpolar organic solvents rather than in

water. This preference is reflected in the solute's octanol-water partition coefficient, K_{ow}. Values of K_{ow} have been determined for many organic solutes. The relationship between K_d and K_{ow} for a given class of solutes often takes the following form:

$$\log K_d = \log f_{om} + a \log K_{ow} + b \qquad (6\text{-}19)$$

where $K_{ow} \equiv \frac{\text{mass solute in octanol / volume octanol}}{\text{mass solute in water / volume water}}$; a and b are empirically-determined constants; and f_{om} is the fraction organic matter of the aquifer.

Dispersion Coefficients

Much work has been done to derive useful expressions for the determination of aquifer dispersion coefficients (i.e. Hatton and Lightfoot, 1982; Freeze and Cherry, 1979; Bear, 1972; and Houghton and Hatton, 1989). Dispersion coefficients for solute transport in porous media are commonly expressed as empirical functions of velocity as follows:

$$D_l = \alpha_l u_l + D^* \qquad (6\text{-}20)$$

$$D_t = \alpha_t u_l + D^* \qquad (6\text{-}21)$$

where D_l and D_t are longitudinal and transverse dispersion coefficients, respectively [cm^2/s]; α_l and α_t are longitudinal and transverse dispersivities, respectively [cm]; u_l is unidirectional groundwater velocity [cm/s]; and D^* is solute molecular diffusion coefficient [cm^2/s]. For most groundwater velocities, the velocity-dependent terms on the right of Equations 6-20 and 6-21 dominate

the molecular diffusion coefficient. Thus, charaterization of the dispersivity parameters, α_l and α_t, above becomes primary to the determination of the dispersion coefficient.

The dispersivity is a function of pore and particle size scales, orientation, and the type of geological material in an aquifer. The value for dispersivity may vary up to five orders of magnitude depending on the scale upon which the measurement is based. However, care must be taken in using the large so-called "macrodispersivities" as they often do not represent true mechanical dispersion. On a lab-scale, small values of dispersivity are obtained -- in general, on the order of 0.1 to 1cm (Freeze and Cherry, 1979). Measured values of dispersivity in the tank experiments of this thesis fall in this range. Even in full-scale application, the dispersivities on a well-diameter scale should be used in modeling -- and these values should be near lab-scale values. On a scale representative of field dispersivity measurements (test wells from 4 to 100 meters apart), dispersivities from a few centimeters to hundreds of meters may be obtained (Anderson, 1979). Inadequate sampling techniques for dispersivity measurement in stratified aquifers may yield exaggerated dispersivity values (Hatton and Lightfoot, 1984). For example, if the variation of groundwater velocity with aquifer depth is not considered, well tests which average solute concentration along the depth of the well would wrongly attribute convection variations to longitudinal dispersion. This exaggerated "dispersion" effect has been demonstrated for stratified aquifers (Gelhar et al., 1979).

Transverse dispersivity is smaller in magnitude than longitudinal dispersivity, and the difference between their values increases with increasing groundwater seepage velocity. Lab-scale values for α_t as functions of seepage

velocity through porous media are given in the literature (Grane and Gardner, 1961). These can be used to estimate α_t given a measured α_l for a particular lab-scale aquifer system.

Porosity

Porosity, n, is a dimensionless property defined as the ratio of the void space volume to the bulk volume of the porous medium. It gives a measurement of the relative volumes occupied by the solid and aqueous phases of the aquifer. There are direct and indirect methods of measuring porosity, including the mercury injection and gas expansion methods. Depending on the matrix material, values for porosity generally vary from 10 to 80% (Bear, 1972).

Seepage Velocity

Groundwater seepage velocity, u_x [cm/s], can be expressed as a function of the hydraulic conductivity, hydraulic gradient, and effective porosity of an aquifer. The values of seepage velocity are site-dependent and may vary from centimeters per day to meters per day (Codell et al., 1982).

6.2. Materials for Experiments

The experiments described in this chapter make use of a lab-scale aquifer simulator shown in Figure 6-2. The simulator consists of a glass tank separated into sections by glass partitions and stainless steel mesh and filled with Ottawa sand and water. Liquid flow through the tank is caused by a height difference in the glass partitions at either end of the tank. A section-by-section description of the apparatus follows.

Figure 6-2: Groundwater Flow Simulator

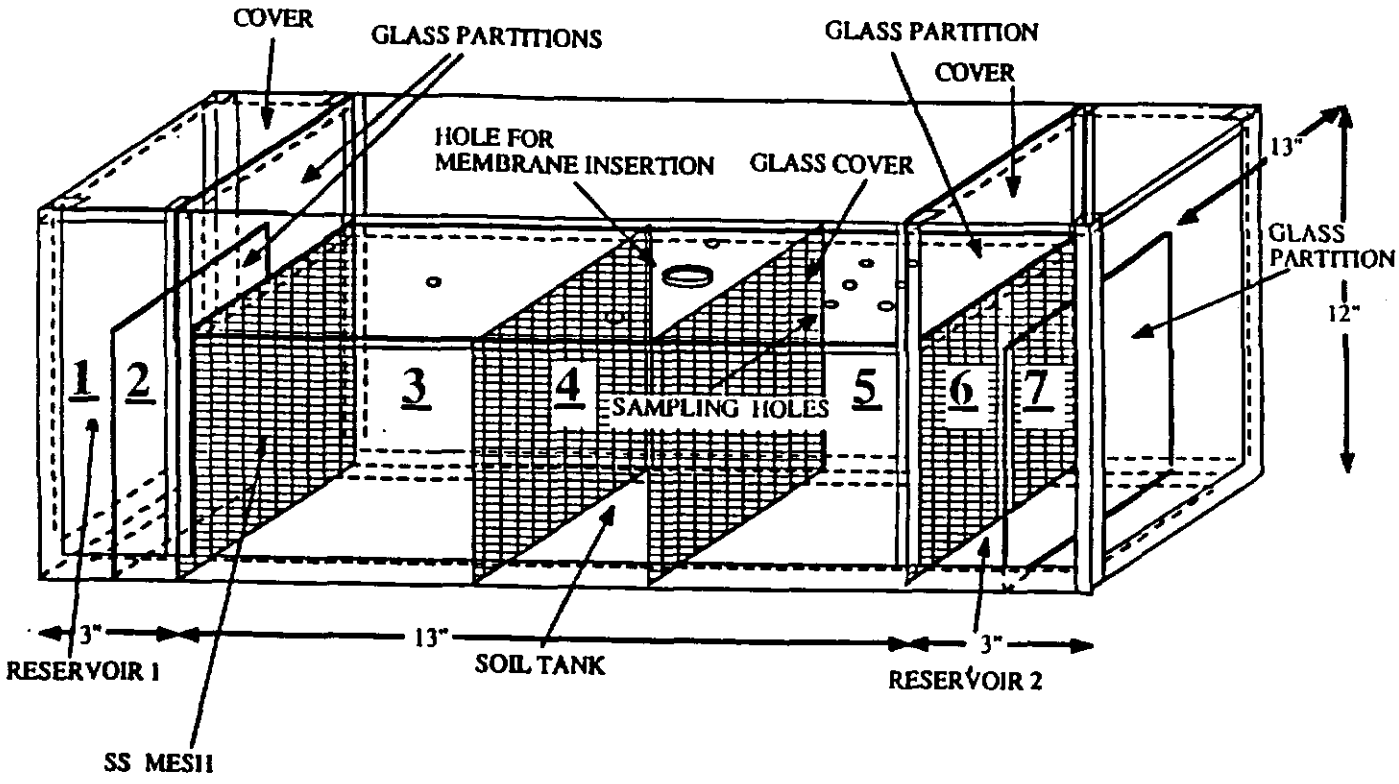

CONST. TEMP. BATH SURROUNDING TANK NOT SHOWN

Liquid solutions are introduced to the tank in section 2 of Figure 6-2. Overflow from this section spills over the glass partition into section 1, where it is continuously siphoned out. In this way, a constant liquid level is maintained in section 2. Section 3 is filled with Ottawa sand, supplied by Gilson Company. The sand has low organic carbon fraction ($f_{oc} = 0.00003 \pm 0.00002$ as determined by Galbraith Laboratories, Inc., from Leco dry combusion and gas purge of acidified suspensions). The Ottawa sand has size distribution such that 100% passes a 2-mm sieve and below 3% passes a 0.25-mm sieve. Thus, Ottawa sand is good for these experiments since it has very low organic carbon fraction (causing less solute retardation) and is well characterized. The sand is saturated with liquid and is separated from section 2 by a wall of size 80 mesh stainless steel (eighty 0.0055-inch wires per inch) with stitching tight enough to prevent flow of sand through it. The glass partitions were sealed to the sides of the tank using silicone sealant. The stainless-steel mesh was sandwiched between thin strips of glass sealed to the sides of the tank using silicone sealant. Section 4 is the so-called "well" area where the membrane/copolymer system can be inserted. As pictured in Figure 6-2, this well area is rectangular and is separated from adjacent sections by stainless-steel mesh. For the 2-D experiment described in Section 6.4., the well area is cylindrical. Section 5 of the tank is filled with Ottawa sand and is separated from adjacent sections again with stainless-steel mesh. Sections 6 and 7 do not contain sand; a constant liquid level is maintained in section 6 by means of the glass partition separating it from section 7. Overflow liquid from section 6 spills into section 7, where it is siphoned out of the tank.

Flow through the tank is driven by a difference in the glass partition levels at the front and the end of the tank. Figure 6-3 shows a schematic diagram of the

tank where the level in section 2 is represented by h_1, and the level in section 6 by h_2, both of which remain constant with time.

Figure 6-3: Cross-Section of Groundwater Flow Simulator

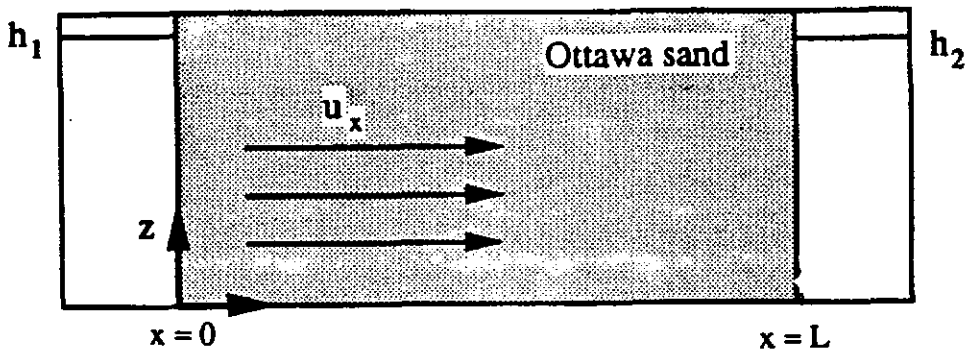

$h_1 > h_2$

Since $h_1 \approx h_2$ (the difference is about 1mm in experiments), there is negligible flow in the z-direction (up or down). Darcy's law for unidirectional fluid flow through a porous matrix assumed to apply to this low Reynolds number ($Re = \frac{\rho u D_p}{\mu} < 0.001$) laminar flow is as follows:

$$u_x = -\frac{k}{\mu}\frac{\partial P}{\partial x} \qquad (6\text{-}22)$$

where u_x is the x-direction longitudinal fluid velocity [cm/s]; k is the porous matrix permeability [cm^2]; μ is the fluid viscosity [g/cm s]; P is the fluid pressure [$g/cm\ s^2$]; and x is the position on the x-axis [cm]. The boundary conditions for pressure as a function of y at both x=0 and x=L are as follows:

$$P(x=0) = \rho g(h_1 - y) + P_{atm} \tag{6-23}$$

$$P(x=L) = \rho g(h_2 - y) + P_{atm} \tag{6-24}$$

where ρ is the fluid density [g/cm^3]; g is acceleration due to gravity [cm/s^2]; P_{atm} is atmospheric air pressure [$g/cm\ s^2$]; h_1 is the water level at x=0 [cm]; h_2 is the water level at x=L [cm]; and L is the length of the tank [cm]. The velocity in Equation 6-22 may be solved for given the pressure profile along the tank (from x=0 to x=L). The conservation equation for flow of an incompressible, Newtonian fluid is as follows:

$$\nabla \cdot \mathbf{u} = 0 \tag{6-25}$$

where **u** is the fluid velocity vector [cm/s]. This simplifies to the following since it has been assumed that there is negligible fluid velocity along tank depth or width ($u_z = 0,\ u_y = 0$):

$$\frac{\partial u_x}{\partial x} = 0 \tag{6-26}$$

Substituting the Darcy's law expression (Equation 6-22) for velocity u_x into Equation 6-26, it follows that:

$$\frac{\partial^2 P}{\partial x^2} = 0 \tag{6-27}$$

Integrating Equation 6-27 using conditions 6-23 and 6-24:

$$\frac{\partial P}{\partial x} = \text{constant} = -\frac{\rho g}{L}(h_1 - h_2) \qquad (6\text{-}28)$$

Substituting into Equation 6-22:

$$u_x = \frac{k}{\mu}\left(\frac{\rho g}{L}\right)(h_1 - h_2) \qquad (6\text{-}29)$$

Thus, liquid flow through the tank should be constant and unidirectional as long as the soil matrix is appropriately isotropic (i.e. negligible spatial variation of soil permeability). In the case of the rectangular well experiment, the flow will also be unidirectional and constant as prescribed by Equation 6-29; however, the effective permeability, k, will be greater since the amount of soil in the tank between x=0 and x=L is less. In the cylindrical well experiment, there will be perturbation of flow near the well. The exact flow field solution for this case is derived in Section 6.4.

The aquifer simulator must be kept nearly isothermal since naphthalene solubility in water varies with temperature and because we want to have a constant density system with no temperature gradients. This is done using a constant temperature bath around the tank. The tank in Figure 6-2 is placed in a larger tank which is filled with water and surrounded by 2"-thick fiberglass insulation. The water in the larger tank is kept at a constant temperature by means of copper coiling placed around the sides of the large tank through which water circulates. The circulating water is maintained at a constant temperature by running it through a circulating bath supplied by Neslab Corporation. In this manner, temperature variations in the soil tank can be kept low. Figure 6-4

Figure 6-4: Aquifer Simulator Temperature Profile

20°C

tank section	depth (in)	width (in)	temp°C time0	temp°C 1hr	temp°C 3hrs	temp°C 6hrs
outer shell end	2	mid	23.60	21.20	20.50	20.20
	6	mid	23.20	20.90		20.20
	10	mid	22.80	20.70	20.40	20.20
outer shell side	2	mid	23.20	21.05	20.70	20.30
	6	mid	23.20	20.95		20.30
	10	mid	22.90	20.75	20.45	20.25
section 2	2	1	23.90	22.80	21.60	20.60
	2	5	23.90			
	2	9	23.90	22.80	21.50	20.70
	6	1	23.90	22.55		
	6	5	23.90			
	6	9	23.90	22.55		
	10	1	23.80	21.95	20.95	20.45
	10	5	23.80			
	10	9	23.80	21.95	20.95	20.45
section 3	2	1				
	2	5				20.60
	2	9				
	6	1				
	6	5				20.65
	6	9				
	10	1				
	10	5				20.65
	10	9				
section 4	2	1	23.85	22.85	21.75	20.70
	2	5	23.90	22.85	21.75	20.60
	2	9	23.85	22.75	21.75	20.60
	6	1	23.75	22.60		
	6	5	23.75	22.45		
	6	9	23.75	22.60		
	10	1	23.65	22.05	21.10	20.40
	10	5	23.65	22.05	21.15	20.60
	10	9	23.65	22.15	21.15	20.55
section 5	2	1				20.70
	2	5				20.70
	2	9				20.60
	6	1				
	6	5				
	6	9				
	10	1				20.60
	10	5				20.65
	10	9				20.55
section 6	2	1	23.65	22.30	21.20	20.50
	2	5	23.60	22.30	21.25	20.50
	2	9	23.60	22.35	21.30	20.50
	6	1				
	6	5				
	6	9				
	10	1	23.45	21.60	20.70	20.40
	10	5	23.40	21.70	21.00	20.45
	10	9	23.40	21.70	21.20	20.45
con temp bath			20.00			
ambient water			22.90			22.60
temperature variance						0.40
temperature range						20.40 - 20.80

30°C

tank section	depth (in)	width (in)	temp°C time0	temp°C 1hr	temp°C 3hrs	temp°C 6hrs	temp°C 12hrs
outer shell end	2	mid	23.90	26.40	29.30	29.70	29.80
	6	mid	22.90	27.80		29.60	29.80
	10	mid	22.10	26.20	28.30	29.20	29.60
outer shell side	2	mid	24.80	26.70	29.40	29.70	29.90
	6	mid	24.00	26.10	28.90	29.60	29.80
	10	mid	22.30	26.40	27.90	29.20	29.70
section 2	2	1	22.10	25.70	26.00	29.10	29.55
	2	5		25.80			
	2	9	22.00	25.50	26.00	29.10	29.575
	6	1					
	6	5					
	6	9					
	10	1	22.20	24.00	27.30	28.85	29.55
	10	5		24.00			29.55
	10	9	22.00	24.00	27.20	28.80	29.55
section 3	2	1					
	2	5	21.85		27.50	28.85	29.40
	2	9					
	6	1					
	6	5					29.50
	6	9					
	10	1					
	10	5	21.85		26.70	28.75	29.50
	10	9					
section 4	2	1	22.20	25.70	27.70	28.80	29.30
	2	5	22.20	25.60	27.70	28.80	29.30
	2	9	22.40	25.40	27.60	28.90	29.30
	6	1					
	6	5					
	6	9					
	10	1	21.80	23.30	26.60	28.65	29.30
	10	5	21.85	23.40	26.70	28.85	29.35
	10	9	21.90	23.40	26.60	28.85	29.35
section 5	2	1			27.50	28.70	29.15
	2	5	21.80	24.20	27.00	28.35	29.10
	2	9			27.55	28.70	29.30
	6	1					
	6	5					
	6	9					
	10	1			27.00	28.70	29.35
	10	5	21.85	23.30	26.50	28.60	29.30
	10	9			27.10	28.75	29.40
section 6	2	1	22.30	25.40	27.50	28.60	29.00
	2	5		25.40		28.60	29.00
	2	9	22.60	25.40	27.50	28.60	29.00
	6	1					
	6	5					
	6	9					
	10	1	22.10	24.60	27.30	28.60	29.00
	10	5		24.60		28.60	29.00
	10	9	22.20	24.55	27.40	28.70	29.00
con temp bath			30.00				
ambient water			22.60			22.70	23.10
temperature variance						0.75	0.58
temperature range						28.35 - 29.10	29.00 - 29.58

shows the temperature at various times and locations in the tank when the temperature of the water circulating through the copper tubing is set at 20°C and 30°C. After six hours, the temperatures in the soil tank vary no more than 0.4°C using the 20°C circulating water. Using the 30°C circulating water, the temperature variation is about 0.6°C after six hours. The room temperature in both cases was about 23°C. The temperature used for all aquifer simulator experiments was 23.0°C, and at least 24 hours constant-temperature-water circulation was allowed before experimentation. Thus, no more than a 0.5°C temperature variation is expected throughout the soil tank.

The tank in Figure 6-2 was covered with plastic wrap, then covered with a glass sheet with sampling holes drilled in it. There was also a large hole drilled in the glass cover to allow for the insertion of the membrane/copolymer system into section 4 of the tank. Liquid samples were drawn from sections 3 and 5 of the tank and analyzed by off-line UV-VIS spectrophotometry.

Fluid from section 2 was saturated with naphthalene by pumping through a plastic generation column filled with solid naphthalene and capped with a glass frit. Naphthalene (99+% pure) was supplied by Sigma Chemical Company. The pumps used in the experiments were teflon-lined piston-diaphragm pumps supplied by Cole Parmer Company. All tubing was made of teflon, and tubing connections were constructed using brass and stainless-steel Swagelok fittings.

Fluid from the "well" area, section 4 of Figure 6-2, was circulated through the membrane/copolymer system and naphthalene concentration analyzed by on-line UV-VIS spectrophotometry (as discussed in Sections 6.3.1. and 6.4.1. of

this paper). Both section 2 and section 4 were kept well-mixed either by high circulation rates or external mixing via a teflon-coated mechanical stirrer.

The membrane/copolymer system used in the tank experiments is exactly as described in Chapter 5. Polysulfone ultrafiltration membranes are filled with a circulating aqueous solution of N-vinylpyrrolidone/styrene copolymer. As in Chapter 5, the membranes were potted in a cartridge to enable the separate flow of well-mixed fluid both interior and exterior to the membrane tubes. Both interior and exterior solutions were well-mixed to simplify mass transfer analysis. Solution flowrates were kept below 40 mL/min through the cartridge so that the convective transmembrane flux of solute remained negligible to diffusive flux as determined by Section 5.3. of this work. Both the interior and exterior solutions were analyzed for naphthalene concentration via on-line UV-VIS spectrophotometry.

The basic purpose of the aquifer simulator experiments was to demonstrate the removal of naphthalene from water flowing through a lab-scale soil matrix by means of the proposed membrane/copolymer system. The rectangular well experiment demonstrates the removal of naphthalene from a pre-contaminated aquifer. The cylindrical well experiment demonstrates the interception of naphthalene from a plume moving through a previously-uncontaminated soil matrix.

6.3. Well-mixed Rectangular Well Experiment

6.3.1. Experimental Procedure

The goal of the well-mixed rectangular well experiment was to demonstrate and model the removal of naphthalene from a pre-contaminated lab-scale aquifer with a constant contaminant source using the proposed membrane/copolymer system. Figure 6-2 shows the soil tank set-up used in the rectangular well experiment. The entire tank was filled with distilled water and flow was initiated through the tank by maintaining constant water levels in sections 2 and 6 such that the level in section 2 was slightly above (by about 0.1 cm) the level of section 6. The overall flowrate through the tank was 0.419 cm^3/s, and remained constant throughout the experiment. This was the lowest flowrate practically obtainable from the given tank system. The seepage velocity of the water through the soil corresponding to this volumetric flowrate was 4.0 cm/hr. This is fast for a groundwater flowrate (about 1 m/day) – most seepage flowrates vary from a few centimeters per day up to several meters per day (Codell et al., 1982). Thus, system efficiency should be higher in actual aquifers, where the groundwater flowrates may be much less than this experimental flowrate.

The tank was kept at 23.0°C by means of the insulated constant temperature bath described in Section 6.2. The temperature bath was allowed to operate 12 hours before the experiment to allow for temperature equilibration. The liquid in section 2 was continuously saturated with naphthalene by pumping through a column filled with solid naphthalene. The naphthalene concentration of the section 2 fluid was determined by on-line UV-VIS spectrophotometry

absorbance readings at 276-nm wavelength. The concentration in section 2 was monitored, and remained at a constant saturated level after about thirty minutes of initial pumpthrough. The plume of naphthalene moved essentially unidirectionally through the simulated aquifer. The concentration of the well section, section 4 of Figure 6-2, was then monitored via on-line absorbance readings. The well concentration increased to saturation as the naphthalene plume reached the well. The membrane/copolymer system was placed in the well prior to the naphthalene saturation of the well, but copolymer solution had not been circulated through the interior of the membrane tubes. This allowed for the naphthalene to adsorb to all materials in the well area before the experimental run began. Any measured decrease, then, in the measured well concentration after the interior copolymer solution began circulating through the membrane would be due to naphthalene transport through the membrane into the copolymer solution, not adsorption onto a surface newly-introduced to the well fluid. Figure 6-5 shows the naphthalene concentration of the well solution as a function of time *before* copolymer solution was introduced to the membrane interior.

Figure 6-6 is a schematic diagram of the membrane/copolymer apparatus placed in section 4 of the tank. Fluid from the mixed well was circulated exterior to the membrane tubes by flowing up through a hole in the end cap which extended down into the rectangular well. Circulation of NVPS copolymer solution through the interior of the tubes was begun after the exterior solution (from the well) had become sufficiently saturated with naphthalene and its concentration was stable. The interior solution was circulated to and from a 200-mL reservoir beaker. The concentration of the well solution was monitored as a

Figure 6-5: Naphthalene Concentration of Well Before Copolymer Introduction

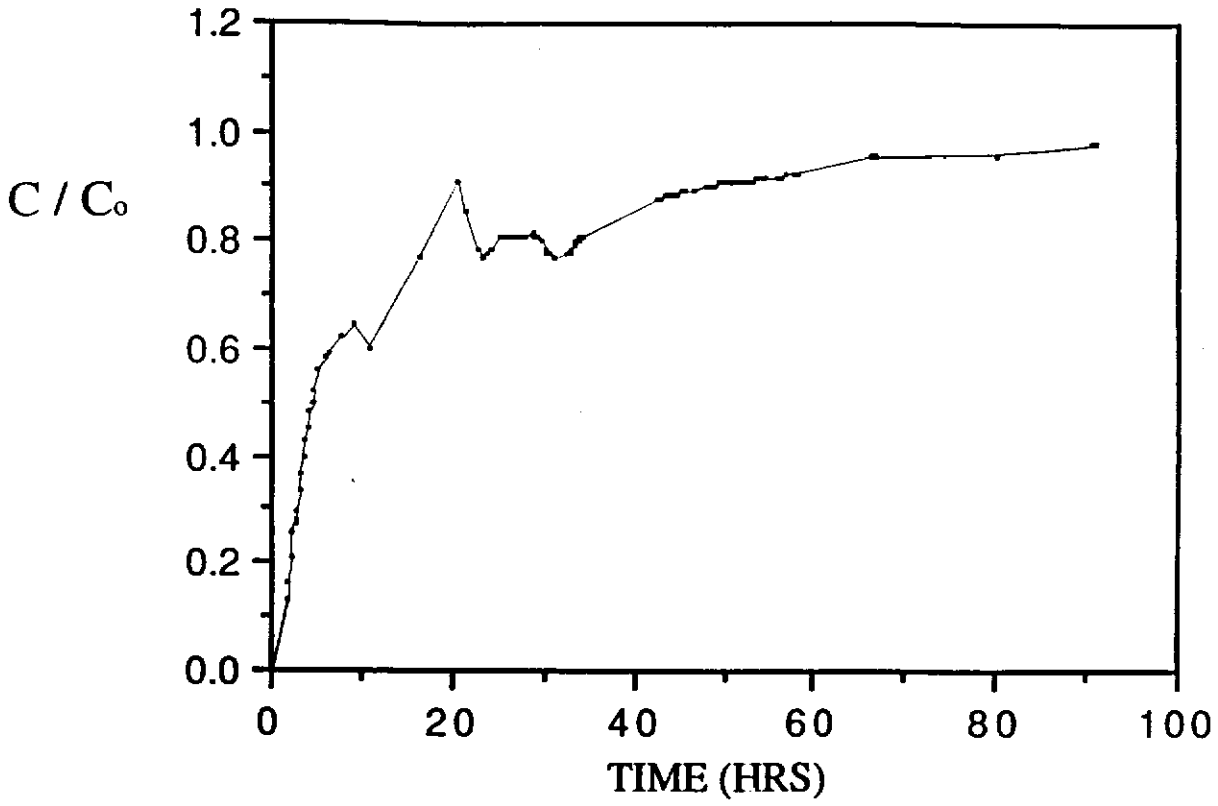

Figure 6-6: Membrane / Copolymer Apparatus Used in Rectangular Well Experiment

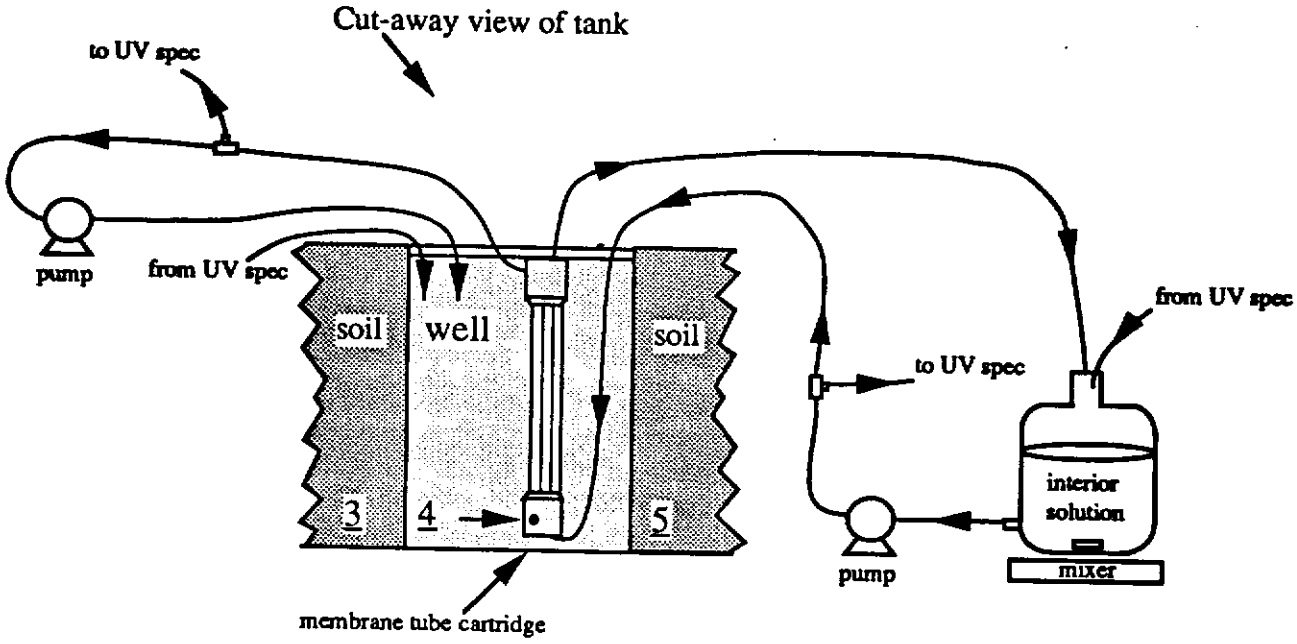

function of time, where time zero was defined as the time that the copolymer solution was introduced to the membrane interior. The decrease in well concentration demonstrates the transport of naphthalene out of the exterior solution and into the interior solution, and hence, the concept of passive remediation using the membrane copolymer system for this application. These data are shown and analyzed in Section 6.3.3. We now wish to model the decrease in well concentration so that the analysis of the experimental results can be extended to other aquifer remediation situations with more realistic (i.e. lower) groundwater flowrates.

6.3.2. Model Development

This section describes a theoretical model for the concentration of the well (section 4 of Figure 6-2) as a function of time in the rectangular well experiment. Time zero for the experiment is defined as the time at which circulation of the NVPS copolymer solution is begun through the interior of the membrane tubes. Prior to this time the entire tank was saturated with naphthalene such that all aqueous samples had a constant measured naphthalene concentration of 31 mg/L, the saturated naphthalene concentration maintained in section 2 of the tank. Any decrease in naphthalene concentration of the well fluid is due to transport of naphthalene into the copolymer solution. Both the well solution and the interior copolymer solution are well-mixed (justified by agreement within 1% of absorbance measurements of solution samples taken from different locations throughout the well). Therefore, the concentrations being modeled will be functions of time only. Transmembrane transport is assumed to be aqueous-phase Fickian molecular diffusion as concluded from the Chapter 5 experiments.

The governing equations for naphthalene concentration in the well region consist of two mass balances -- one on the membrane interior solution and one on the well solution itself:

Membrane Tube Interior Mass Balance:

$$V_t \frac{dC_{int,aq}}{dt} = \frac{A_t}{R_{tot}} (C_{well} - C_{int,aq}) - MK_{pw}V_t \frac{dC_{int,aq}}{dt} \qquad (6\text{-}30)$$

Well Mass Balance:

$$V_w \frac{dC_{well}}{dt} = Q (C_o - C_{int,aq}) - \frac{NA_t}{R_{tot}} (C_{well} - C_{int,aq}) \qquad (6\text{-}31)$$

where V_t is the membrane tube interior volume [cm^3]; V_w is the well volume [cm^3]; A_t is the membrane tube surface area [cm^2]; R_{tot} is the overall membrane tube resistance [s/cm]; M is the polymer to water mass ratio (in copolymer solution) [g/g]; K_{pw} is the polymer-water partition coefficient of solute [dimensionless]; Q is the fluid flow rate into the well [cm^3/s]; N is the number of membrane tubes; C_o is the solute concentration of fluid entering the well [g/cm^3]; $C_{int,aq}$ is the interior aqueous pseudophase solute concentration [g/cm^3]; and C_{well} is the solute concentration of the well fluid [g/cm^3]. The initial conditions are as follows:

Initial Conditions:

$$C_{well}(t=0) = C_o \qquad (6\text{-}32)$$

$$C_{int,aq}(t=0) = 0 \qquad (6\text{-}33)$$

Equation 6-30 states that the net accumulation of solute in the aqueous pseudophase of the interior copolymer solution is equal to the net transport into the tube from the well fluid (via transmembrane diffusion) minus the transport of solute into the copolymer pseudophase of the interior copolymer solution. This latter transport term, derived in Chapter 5, accounts for the equilibrium of solute between the aqueous and copolymer pseudophases of the interior solution. Equation 6-31 states that the net accumulation of solute in the well equals the net flux of solute into the well minus the flux of solute into the membrane tubes. The solution flowing into the well is at constant, saturated solute concentration, C_{sat}. Initially, the well is saturated with solute up to its solubility limit, C_{sat}. Also, the solution interior to the membrane is initially free of solute. The solution using Equations 6-30 to 6-33 is as follows:

$$\frac{C_{well}}{C_{sat}} = \frac{\alpha}{a_1 - a_2}\left(e^{-a_1\tau} - e^{-a_2\tau}\right) + 1 \qquad (6\text{-}34)$$

where $\alpha = \frac{NA_t}{QR_{tot}}$; $\beta = \frac{A_t V_w}{QR_{tot} V_t (1 + MK_{pw})}$;

$$a_1 = \frac{a - \sqrt{a^2 - 4\beta}}{2}; \quad a_2 = \frac{a + \sqrt{a^2 - 4\beta}}{2};$$

$$a = 1 + \alpha + \beta; \quad \tau = \frac{t}{V_w/Q}.$$

A plot of Equation 6-34 versus time using hypothetical inputs permits a better understanding of the model solution. Figure 6-7 shows plots of solute concentration for a hypothetical treatment well with the given parameter inputs (note logarithmic time scale). The solution flowing into the well is at the solute's saturated concentration C_{sat}, and the well concentration is initially also equal to C_{sat}. As solute transport procedes into the copolymer solution, the solute

Figure 6-7: Well Solute Concentration -- Model of Hypothetical Case

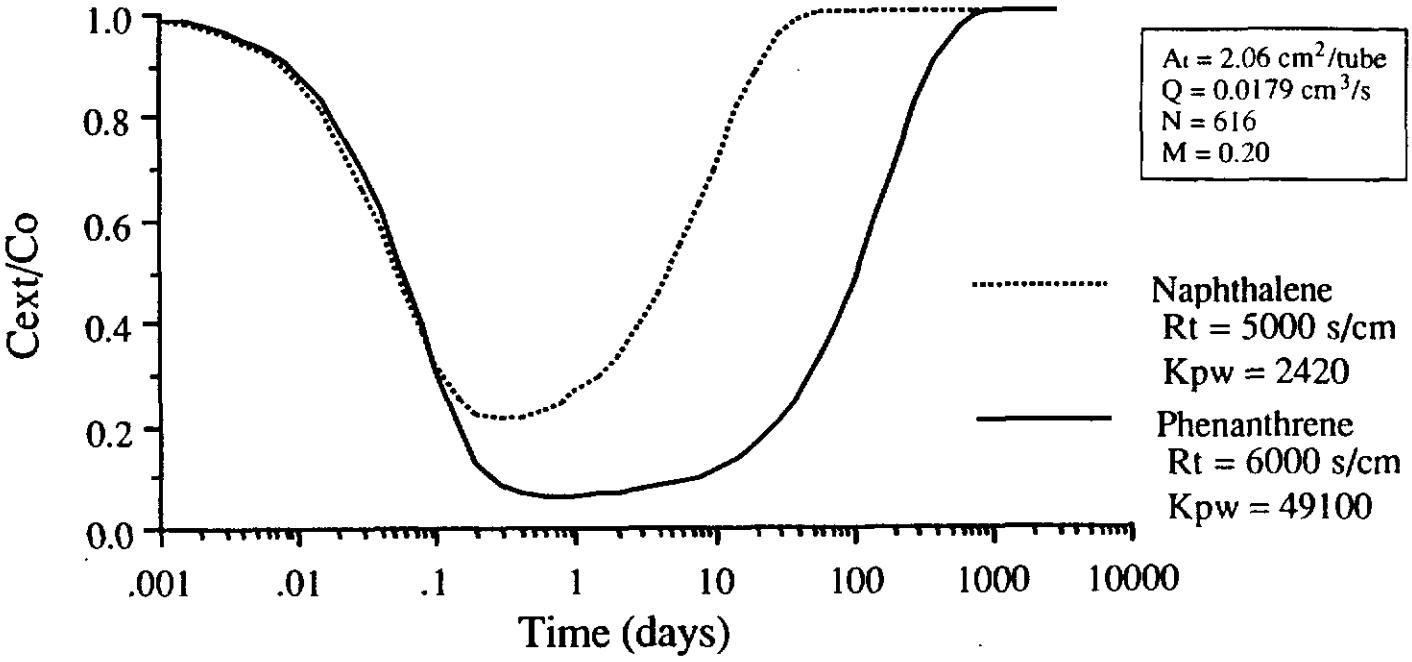

concentration of the well decreases. The initial modeled decrease in well concentration (seen in Figure 6-7) depends on the magnitude of the resistance to solute mass transfer posed by the membrane. The eventual increase in well concentration back up to the solute concentration of incoming solution is caused by the loading of solute in the copolymer pseudophase of the interior solution. The aqueous pseudophase solute concentration increases, and so the driving force for transport into the membrane, the quantity (C_{well} - $C_{int,aq}$), diminishes eventually to zero. Figure 6-7 shows the well concentration of two solutes -- naphthalene and phenanthrene. Data from Chapters 4 and 5 of this work was used as input; namely the solute-NVPS partition coefficients and the overall membrane tube resistances to solute molecular diffusion. In the naphthalene

contamination case, the rate of solute concentration decrease in the well is slightly greater than in the phenanthrene contamination case. This is due to the slightly higher diffusivity (lower R_{tot}) of naphthalene through the membrane pores. The increasing part of the curve in Figure 6-7 is primarily governed by the solute-copolymer coefficient, K_{pw}. The partition coefficient of the copolymer, NVPS, is much higher for phenanthrene than naphthalene solute, so the low interior solution solute concentration, and hence the transmembrane diffusion driving force, lasts longer.

The flowrate through the well used in Figure 6-7 would correspond to a seepage velocity of 5 cm/day through a rectangular well 8-inches long in an aquifer of 50% porosity. The membrane/copolymer system used in this well is modeled as a 1-inch diameter bundle of polysulfone membrane tubes, each of 1-mm diameter. The copolymer solution in the tubes is modeled as having an NVPS to water weight ratio of 0.20. The resistance to molecular diffusive mass transfer is as determined from the Chapter 5 experiments with naphthalene and phenanthrene, and the polymer-water partition coefficients used are as determined in Chapter 4 of this work. Figure 6-7 shows that the system would effectively reduce the solute concentration of the well solution to about 6% of the incoming concentration given the above inputs. The copolymer solution would have to be replaced approximately every 20 to 30 days for the case of phenanthrene contamination to provide sustained decrease in solute concentration. However, a higher R_{tot} may be realized in actual system application using these membranes if the copolymer solution and well solution are not circulated; thus, the decrease in well concentration may not be as pronounced as modeled. More pronounced decreases may be realized by increasing the amount of membrane tubes in the well, or by reducing the

diffusive resistance of the membrane tubes. This could be done by using tubes with thinner support structure layers.

6.3.3. Comparison of Experimental Results with Model Simulations

Figure 6-8 shows the experimental results of the well-mixed rectangular well experiment. The naphthalene concentration of the well solution is plotted as a function of time elapsed from the introduction of copolymer solution to the membrane tube interior. The well concentration decreases as naphthalene diffuses into the copolymer solution. As described earlier, no other cause for the disappearance of naphthalene from the well solution was possible in this experimental set-up. The decrease in well solution concentration is not as great as in the hypothetical model of Figure 6-7. This is due to the much higher flowrate used in the experimental run (Figure 6-8).

Figure 6-8 shows predicted well concentrations using Equation 6-34 and given experimental inputs. Using the experimentally-determined membrane diffusive resistance from Chapter 5, R_{tot} = 5000 s/cm, the model predicts a bigger concentration decrease than was seen experimentally. The data are more closely predicted using an R_{tot} between 15,000 and 20,000 s/cm in the Equation 6-34 model. This is probably due to the transient desorption of naphthalene adsorbed to the solid surfaces in the well. The well was saturated with naphthalene for about 100 hours before introduction of the copolymer solution to the membrane interior. The well solution concentration had stabilized, and had come to adsorptive equilibrium with all surfaces in contact with it. As the well concentation decreased after copolymer solution was introduced, some of the

adsorbed naphthalene desorbed back into the solution, thus dampening the expected decrease in the well solution's naphthalene concentration. This desorption effect is not a factor in the 2-D cylindrical well experiment since the tank is initially uncontaminated when copolymer solution is introduced at time zero.

Figure 6-8: Rectangular Well Experiment -- Naphthalene Concentration of Well Fluid

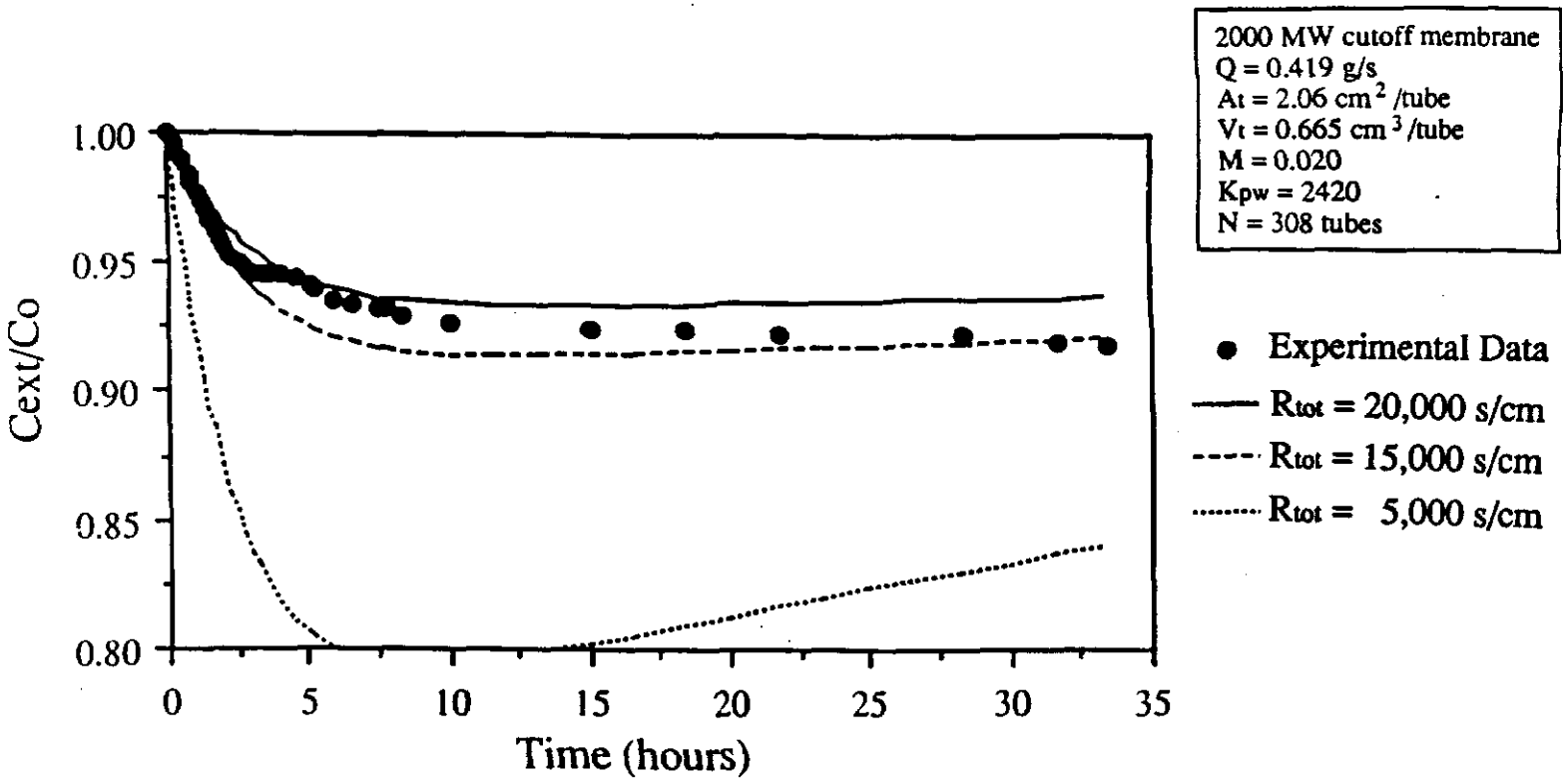

6.4. Well-mixed Cylindrical Well 2-D Experiment

6.4.1. Experimental Procedure

The 2-D cylindrical well experiment was designed to demonstrate the ability of the system to intercept an encroaching plume of naphthalene solute from a cylindrical well. The experiment differs from the rectangular well experiment in that the plume leaving the well is a function of position in two dimensions -- length and width. Another difference is that initially, the tank is free of naphthalene in the 2-D experiment. The same copolymer/membrane system is used in the two experiments, as are the naphthalene saturation column and naphthalene concentration measurement systems.

Figure 6-9 is a schematic diagram of the proposed experiment. The tank shown in Figure 6-2 is used in the 2-D experiment; however, the rectangular well (section 4) has been replaced with a cylindrical well 2-inches in diameter. Figure 6-9 depicts overhead views of the tank at various stages of the experiment. The tank is filled with clean Ottawa sand of the same size distribution described in Section 6.3. Initially, the concentration of naphthalene is zero throughout the tank. A constant flow of saturated naphthalene solution begins travelling toward the well. This solution comes from section 2 of the tank (Figure 6-2) and is kept at naphthalene's saturated concentration in water, C_{sat}, by means of circulation through a column filled with solid naphthalene.

At time $t=t_2$ (Figure 6-9), the naphthalene solution reaches the mixed well, and naphthalene begins to be filtered by the membrane/copolymer system. Note the streamlines in Figure 6-9 are bent inward toward the well. This is due

Figure 6-9: 2-D Cylindrical Well Run -- Experimental Schematic With Overhead Views of Soil-Filled Tank

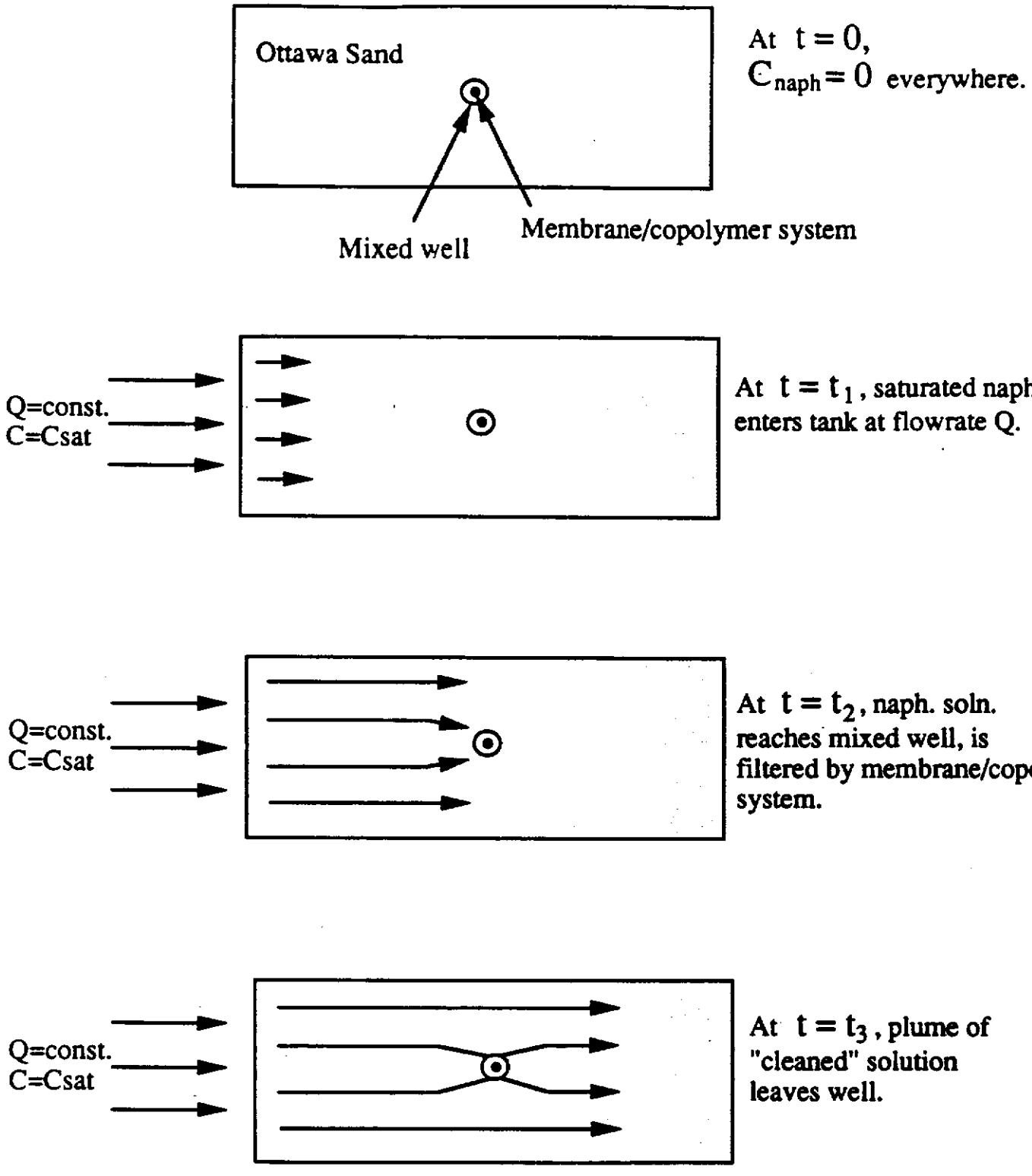

to the lower permeability of the well region with respect to the surrounding soil. An exact solution for this flow field is derived in the next section.

At time $t=t_3$ (Figure 6-9), a plume of partially filtered naphthalene solution leaves the well area. On either side of this plume is solution of higher naphthalene concentration which has not passed directly through the treatment well. The shape of this 2-D concentration plume will depend on system parameters, such as membrane resistance and copolymer-water partition coefficient, as well as soil matrix properties such as dispersion coefficient and seepage velocity.

The 2-D run was conducted under the following experimental conditions:

1. Well volume, $V_w = 573.4\ cm^3$
2. Interior solution volume per tube, $V_t = 0.67\ cm^3$
3. Seepage velocity, $u_x = 0.001038\ cm/s$
4. Overall volumetric flowrate through the tank, $Q = 0.333\ cm^3/s$
5. Soil porosity, $n = 0.38$
6. Interior solution polymer to water mass ratio, $M = 0.00362$
7. Napthalene's NVPS-water partition coefficient, $K_{pw} = 2420$
8. Surface area per tube, $A_t = 2.06\ cm^2$
9. Number of tubes, N=308

Both the aqueous solution in the well and the interior copolymer solution were assumed to be well-mixed, justified by absorbance measurements of solution at various locations. Note that the well volume in this experiment was considerably less than the well volume in the rectangular well experiment, while the

membrane system remained identical; so there are bigger concentration decreases of the well solution in the 2-D experiment.

6.4.2. Model Development

The goals of the 2-D cylindrical well experiment were to experimentally demonstrate the decreased concentration plume of solute leaving a membrane/copolymer system treatment well, to model the well's naphthalene concentration as a function of time, and to model the plume profile as a function of length, width, and time. The models can then be extended to predict system performance with real-scale contaminated aquifers.

Modeling conditions and parameters are shown in Figure 6-10. The modeling scheme is divided into two parts. First, the well concentration, $C_{well}(t)$, is modeled analytically as a function of time given an experimentally-determined functional form for incoming fluid concentration $C_o(t)$. Secondly, the naphthalene concentration of the region behind the well is solved for numerically using $C_{well}(t)$ and $C_o(t)$ as boundary conditions.

The concentration of the solution outside the well at x=0, $C_o(t)$, is obtained by off-line absorbance measurements taken at various times. This concentration increases from zero and asymptotically approaches C_{sat}, the saturated concentration of naphthalene in water, as the concentration front moves past x=0. The rate at which this increase occurs depends upon both the mechanical dispersion of solute in the x-direction and the retardation of solute by adsorption onto the soil surfaces. An empirical expression for the increase in $C_o(t)$ with time

Figure 6-10: 2-D Cylindrical Well Run -- Modeling Conditions and Parameters Shown in an Overhead View of Soil-Filled Tank

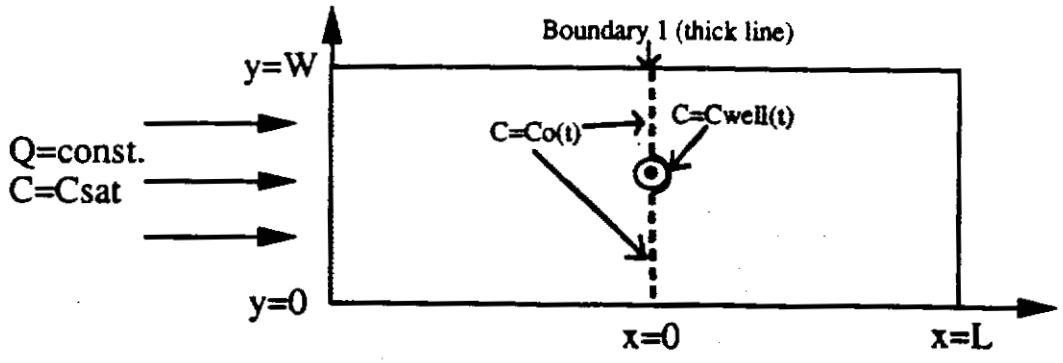

Figure 6-11: $C_o(t)$ Curve Fit -- 2-D Cylindrical Well Experiment
(t=0 when naphthalene reaches the well)

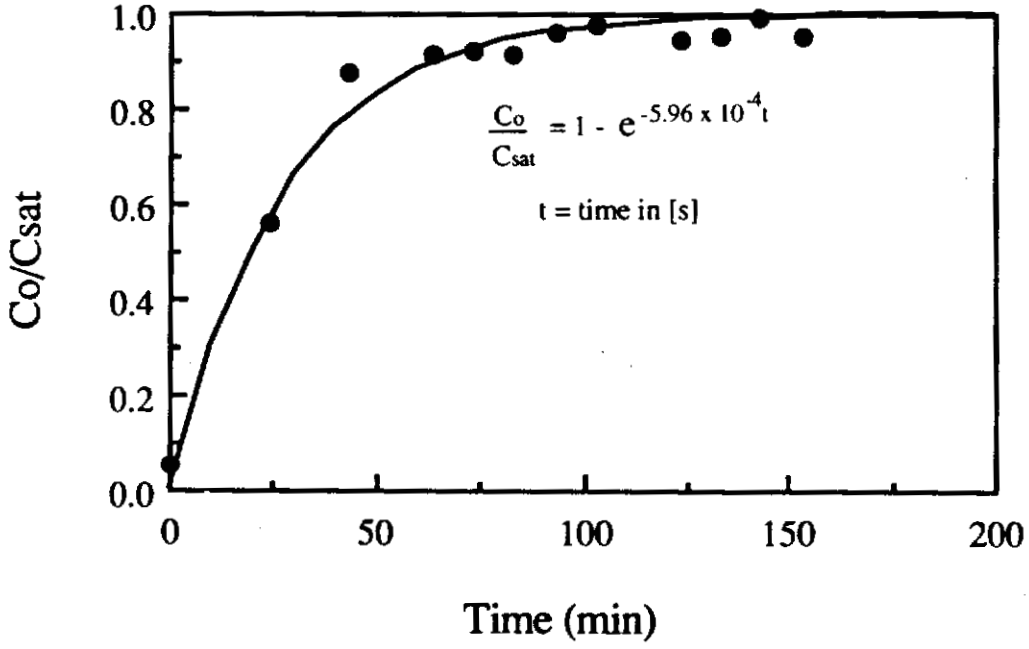

is determined by a fit of the experimental data. This is shown in Figure 6-11. The concentration profile of the plume before it reaches the well is a function of length only, not width. Such a profile was used to determine the x-direction dispersion coefficient, D_x, and retardation coefficient, R_d, for the lab-scale aquifer as will be discussed later.

There are two assumptions that are made implicitly by using $C_o(t)$ as a function of time only, and not a function of position along the width of the tank. One is that the soil matrix is sufficiently isotropic such that flow is unidirectional and retardation effects are the same along the width of the tank. The second assumption is that there is no back-mixing of the fluid from the treatment well. Both assumptions are justified experimentally, and their implications on a scale analysis of the problem are explained further in the next section.

Next, the empirical functional form of $C_o(t)$ is used as an input in determining the concentration of the well-mixed cylindrical well. The mixed well solute concentration model is similar to the model defined in Equations 6-30 to 6-33 for the rectangular well experiment, but with important differences. One of the differences is that here, the naphthalene concentration of fluid entering the well, $C_o(t)$, is a function of time. $C_o(t)$ increases from zero up to C_{sat}; it does not begin and stay at C_{sat} as in the rectangular well experiment. Another difference is that the initial concentration of the well and membrane interior solutions are zero. Time zero in the model below is defined as the time at which naphthalene just reaches the well at x=0. The governing equations and initial conditions for the 2-D experiment are as follows:

Membrane Tube Interior Mass Balance:

$$V_t \frac{dC_{int,aq}}{dt} = \frac{A_t}{R_{tot}} (C_{well} - C_{int,aq}) - MK_{pw}V_t \frac{dC_{int,aq}}{dt} \qquad (6\text{-}35)$$

Well Mass Balance:

$$V_w \frac{dC_{well}}{dt} = Q (C_o(t) - C_{well}) - \frac{NA_t}{R_{tot}} (C_{well} - C_{int,aq}) \qquad (6\text{-}36)$$

Initial Conditions:

$$C_{well}(t=0) = 0 \qquad (6\text{-}37)$$

$$C_{int,aq}(t=0) = 0 \qquad (6\text{-}38)$$

where V_t is the membrane tube interior volume [cm^3]; V_w is the well volume [cm^3]; A_t = membrane tube surface area [cm^2]; R_{tot} is the overall membrane tube resistance [s/cm]; M is the polymer to water mass ratio (of the copolymer solution) [g/g]; K_{pw} is the polymer-water partition coefficient of the solute [dimensionless]; Q is the fluid flow rate into the well [cm^3/s]; N is the number of membrane tubes; $C_o(t)$ is the solute concentration of fluid entering the well [g/cm^3]; $C_{int,aq}$ is the interior aqueous-pseudophase solute concentration [g/cm^3]; and C_{well} is the well fluid solute concentration [g/cm^3]. The solution defined by Equations 6-35 to 6-38 is shown below:

$$\frac{C_{well}}{C_{sat}} = Ae^{-d_1\tau} + Be^{-d_2\tau} + g_1e^{-b_2\tau} + 1 \qquad (6\text{-}39)$$

where the parameters are defined as follows:

$$A = \frac{g_1(b_2 - d_2) - d_2}{d_2 - d_1};\quad B = \frac{g_1(b_2 - d_1) - d_1}{d_1 - d_2};\quad g_1 = \frac{b_2 a_1 - a_3}{b_2^2 a_1 - b_2 a_2 + a_3};$$

$$d_1 = \frac{\frac{a_2}{a_1} + \sqrt{\left(\frac{a_2}{a_1}\right)^2 - 4\frac{a_3}{a_1}}}{2};\quad d_2 = \frac{\frac{a_2}{a_1} - \sqrt{\left(\frac{a_2}{a_1}\right)^2 - 4\frac{a_3}{a_1}}}{2};\quad b_2 = \frac{V_w}{Q} b_1;$$

$$b_1 = 5.96 \times 10^{-4};\quad a_1 = \frac{V_t Q R_{tot}}{N A_t}(1 + M K_{pw});$$

$$a_2 = V_t\left(1 + \frac{Q R_{tot}}{N A_t}\right)(1 + M K_{pw}) + \frac{V_w}{N};\quad a_3 = \frac{V_w}{N};\quad \tau = \frac{t}{V_w/Q}$$

So the naphthalene concentration in the well eventually increases to the saturated concentration of naphthalene in water. How fast this occurs is a function of rate of naphthalene transport into the well, rate of transport into the copolymer solution, and the naphthalene loading capacity on the NVPS copolymer. Initially, the well naphthalene concentration is zero.

Now we have an analytical expression for well-mixed well concentration as a function of time given the incoming fluid concentration $C_o(t)$ and experimental input parameters. The expressions for $C_o(t)$ and $C_{well}(t)$ are used as boundary conditions in the governing equation for naphthalene concentration in the tank beyond the well at x=0. The governing equation has as its domain the area defined by the following, shown in Figure 6-10:

$$0 \le x \le L$$

$$0 \le y \le W \qquad (6\text{-}40)$$

The governing equation for solute transport through this assumed isotropic domain is as follows:

$$\frac{\partial C}{\partial t} + u_x(x,y)\frac{\partial C}{\partial x} + u_y(x,y)\frac{\partial C}{\partial y} = D_x\frac{\partial^2 C}{\partial x^2} + D_y\frac{\partial^2 C}{\partial y^2} - \frac{\rho_b}{n}K_d\frac{\partial C}{\partial t} \qquad (6\text{-}41)$$

where $u_i(x,y)$ is the i component of velocity [cm/s]; D_i is the dispersion coefficient in the i direction [cm^2/s]; K_d is the solute soil-water partition coefficient [(g/g)/(g/mL)]; ρ_b is the soil bulk density [g/cm^3]; n is the aquifer porosity [dimensionless]; and C is solute concentration of aqueous solution in the domain, a function of x, y, and t [g/cm^3]. Equation 6-41 was derived in Section 6.1. The boundary and initial conditions that apply for the problem are as follows:

$$\frac{\partial C}{\partial y} = 0 \quad \text{at } y=W \qquad (6\text{-}42)$$

$$\frac{\partial C}{\partial y} = 0 \quad \text{at } y=0 \qquad (6\text{-}43)$$

$$\frac{\partial C}{\partial x} = 0 \quad \text{at } x=L \qquad (6\text{-}44)$$

$$C(t) \text{ is known along } x=0 \qquad (6\text{-}45)$$

$$C(x,y) = 0 \text{ at } t=0 \text{ for all } x, y \qquad (6\text{-}46)$$

The first two conditions dictate no flux across the tank walls. Condition 6-44 is the Danckwerts boundary condition (Danckwerts, 1953) for flow out of a porous medium. Condition 6-45 is the real driving force for solute entrance into the

domain of the problem. Solute concentration is $C_o(t)$ along the dotted boundary in Figure 6-10 and $C_{well}(t)$ along the edge of the well. $C_o(t)$ was determined in functional form from direct measurement, and $C_{well}(t)$ was solved for analytically from Equation 6-39. Condition 6-46 is the initial condition for all points throughout the soil matrix domain.

Since the solute concentrations at all domain points and times in the experiment are low (below 31 ppm), the aqueous density throughout the experiment is approximately constant. Therefore, the flow field can be solved for separately from the concentration problem shown above. The x- and y-components of velocity obtained from the flow field solution are used in the solution to Equation 6-41. The well-known solution for fluid flow through a non-pumped well under natural hydraulic head can be derived as follows. Figure 6-12 shows an overhead view of a well in a surrounding soil matrix. It is assumed Darcy's law applies both in the well (Domain I) and outside the well (Domain II) such that:

$$\mathbf{q}_I = - T_I \nabla h \tag{6-47}$$

$$\mathbf{q}_{II} = - T_{II} \nabla h \tag{6-48}$$

where $\mathbf{q}_I$ is the velocity field outside the well [cm/s]; $\mathbf{q}_{II}$ is the velocity field in the well [cm/s]; T_I and T_{II} are the transmissivities of domains I and II, respectively [cm^2/s]; and ∇h is the gradient of hydraulic head (equal for both domains [cm^{-1}]. The conservation of mass states:

$$\frac{\partial \rho}{\partial t} + \nabla \cdot (\rho n \mathbf{q}) = 0 \tag{6-49}$$

Figure 6-12: Streamlines for Flow Field About a Cylindrical Well

Velocity Field

$$\mathbf{q}_f = [\, q_x(1 + \frac{R^2}{r^2}) \cos\phi \,]\, \mathbf{e}_r - [\, q_x(1 - \frac{R^2}{r^2}) \sin\phi \,]\, \mathbf{e}_\phi$$

Streamfunction

$$\psi = q_x \left(r + \frac{R^2}{r} \right) \sin\phi$$

Graph of Streamlines

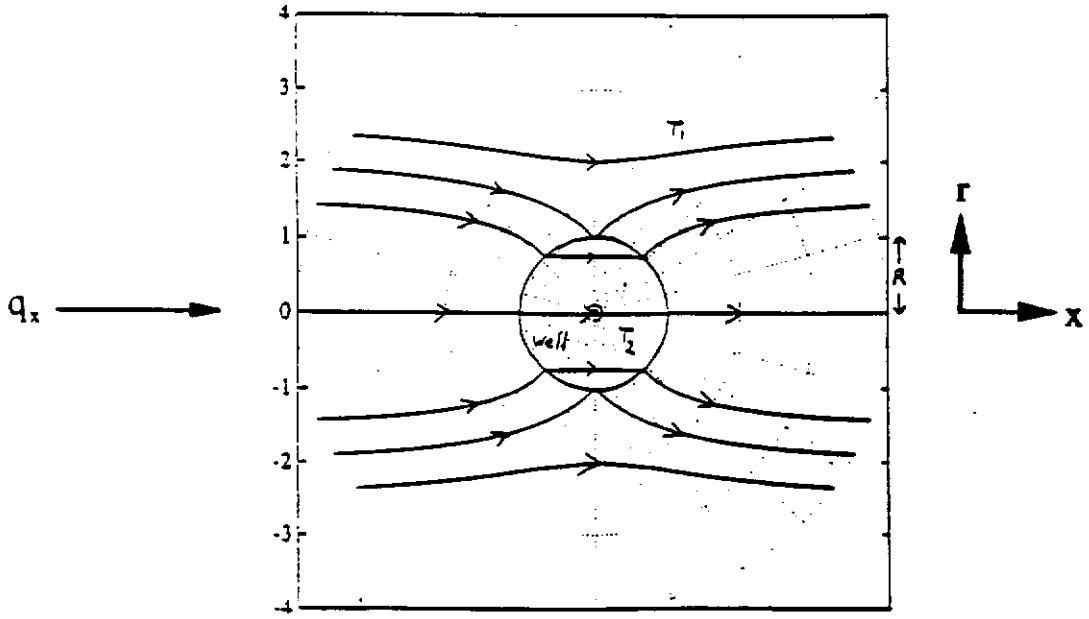

which applies for both $\mathbf{q}_I$ and $\mathbf{q}_{II}$. Since density, ρ, and porosity, n, are constant, Equation 6-49 reduces to the following:

$$\nabla \cdot \mathbf{q} = 0 \tag{6-50}$$

Substituting equations 6-47 and 6-48 into Equation 6-50 yields Laplace's equation for hydraulic head:

$$\nabla^2 h = 0 \tag{6-51}$$

This is solved here using a cylindrical coordinate system (r, ϕ). Boundary conditions for both Domains I and II are finiteness of hydraulic head at $r = 0$ and as $r \rightarrow \infty$. Also, the flowrate is known far from the well (constant and unidirectional as shown in Figure 6-13). Equation 6-51 is solved using these boundary conditions for each of the two domains. The following assumption is made in the solution:

$$T_{II} >> T_I \tag{6-52}$$

This states the transmissivity of the well area of Domain II (where there is no soil-posed resistance) is much greater than the transmissivity of the soil are of Domain I (where soil-posed resistance is substantial). The resulting solution for velocity field outside the well is as follows:

$$\mathbf{q}_{II} = [q_x(1 + \frac{R^2}{r^2})\cos\phi]\, \mathbf{e}_r + [q_x(1 - \frac{R^2}{r^2})\sin\phi]\, \mathbf{e}_\phi \tag{6-53}$$

where R is the radius of the well [cm]; q_x is the unidirectional velocity far from the well; and $\mathbf{e}_r$ and $\mathbf{e}_\phi$ are unit vectors in a cylindrical coordinate system. The streamfunction for this flow field is as follows:

$$\psi = - q_x(r + \frac{R^2}{r}) \sin\phi \tag{6-54}$$

Streamlines obtained from Equation 6-54 are shown in Figure 6-12. It is clear from the figure that all streamlines up to a distance of twice well radius from the center of the well pass through the well. In other words, a region of width twice the diameter of the well is intercepted by the well. Values of u_x and u_y can be obtained from Equation 6-54 by converting to a rectangular coordinate system:

$$u_x = q_x\left(1 + \frac{(x^2 + y^2)\,R^2 - 2\,y^2R^2}{(x^2 + y^2)^2}\right) \tag{6-55}$$

$$u_y = q_x\left(\frac{2\,R^2x\,y}{(x^2 + y^2)^2}\right) \tag{6-56}$$

Note that this is valid for a rectangular coordinate system whose origin is at the *center of the well.*

It is important to note that the simulator tank walls have negligible effect on the flow field solution in this experiment. Equation 6-54 yields the distortion length (maximum distance a streamline bends toward the well) of a streamline at a distance r directly beneath or above the well, given by the following:

$$l_d = \frac{R^2}{r} \tag{6-57}$$

where l_d is the distortion length [cm]. Thus, for the tank of half-width 6" and well radius 1", the distortion length at the tank wall is less than 1/6".

At this point, we are ready to solve Equation 6-41 numerically over the domain shown in Figure 6-10. An explicit finite difference procedure was used for the solution. First, a mesh is designed for the 2-D domain. The mesh sizing and time step interval are chosen such that a stable, convergent solution is achieved. The partial derivatives in Equation 6-41 are approximated by the centered and forward difference equations below:

$$\frac{\partial^2 C_i(m)}{\partial x^2} = \frac{C_E(m) - 2C_i(m) + C_W(m)}{k^2} + O(k^2) \tag{6-58}$$

$$\frac{\partial^2 C_i(m)}{\partial y^2} = \frac{C_N(m) - 2C_i(m) + C_S(m)}{l^2} + O(l^2) \tag{6-59}$$

$$\frac{\partial C_i(m)}{\partial x} = \frac{C_E(m) - C_W(m)}{2k} + O(k) \tag{6-60}$$

$$\frac{\partial C_i(m)}{\partial y} = \frac{C_N(m) - C_W(m)}{2l} + O(l) \tag{6-61}$$

$$\frac{\partial C_i(m)}{\partial t} = \frac{C_i(m+1) - C_i(m)}{h} + O(h) \tag{6-62}$$

where $C_i(m)$ is the solute concentration at node i and time step m [g/cm^3]; $C_{N,S,E,W}(m)$ is the solute concentration at nodes directly north, south, east, and west of position i [g/cm^3]; h is the time interval Δt [s]; k is the x-direction spatial

interval Δx [cm]; and l is the y-direction spatial interval Δy [cm]. Substitution of Equations 6-58 to 6-62 into Equation 6-41 yields the following explicit finite difference equation for concentration at node i:

$$C_i(m+1) = C_i(m)\left(1 - \frac{2hD_x}{R_d k^2} - \frac{2hD_y}{R_d l^2}\right) + C_E(m)\left(\frac{hD_x}{R_d k^2} - \frac{hD_y}{2kR_d}\right) + \qquad (6\text{-}63)$$

$$C_W(m)\left(\frac{hD_x}{R_d k^2} + \frac{hu_x}{2kR_d}\right) + C_N(m)\left(\frac{hD_y}{R_d l^2} - \frac{hu_y}{2lR_d}\right) + C_S(m)\left(\frac{hD_y}{R_d l^2} + \frac{hu_y}{2lR_d}\right)$$

where retardation coefficient $R_d = 1 + \frac{\rho_b}{n} K_d$ [dimensionless]; D_x and D_y are assumed constants throughout the solution domain, and v_x and v_y are evaluated at each node i. The approximation error of Equation 6-63 tends to zero in the limit as time and space intervals -- h, k, and l -- go to zero. The time discretization must be chosen with regard to the spatial discretization to prevent an unstable solution. The time interval is chosen such that:

$$h \leq \frac{R_d}{2\left(\frac{D_x}{k^2} + \frac{D_y}{l^2}\right)} \qquad (6\text{-}64)$$

for the solution to be numerically stable. The *grid* Peclet number gives the maximum allowable choice of spatial inteval size for a diffusion-convection problem (Price et al., 1965). For an evenly-spaced 2-D grid, this condition is as follows:

$$\frac{1}{2} Pe_g k^* < 1 \qquad (6\text{-}65)$$

where $Pe_g = \frac{Lu_x}{D_x}$; $k^* = \frac{k}{L}$;

and L is the domain length [cm].

Conditions 6-64 and 6-65 are met by the discretizations used in the Equation 6-63 numerical solution. Time interval convergence tests for modeling the 2-D experiment were performed and are detailed in Section 6.4.4. They show that time intervals chosen for all model outputs yield stable, convergent solutions. Decreasing the spatial node points in the half-domain from 12,553 to just over 7000 nodes resulted only in a 0.2% average change in the solution using base case inputs (see Section 6.4.4.), so it was concluded spatial discretizaton is small enough to represent a convergent solution for all modeled cases. The code for the finite difference solution is listed in Appendix C.

6.4.3. Scale Analysis

Before discussing simulations using the 2-D model, it is helpful to see what a scale analysis of the experimental problem tells about the expected solutions. First of all, Peclet numbers are defined for the problem as follows:

$$Pe_x = \frac{Lu_x}{D_x} \qquad (6\text{-}66)$$

$$Pe_y = \frac{Lu_x}{D_y} \qquad (6\text{-}67)$$

where L is the characteristic length for the problem (here, the diameter of the well -- 2 inches) [cm]; u_x is the unidirectional seepage velocity far from the well [cm/s]; D_x is the dispersion coefficient in the x-direction [cm^2/s]; and D_y is the dispersion coefficient in the y-direction [cm^2/s].

Values of D_x and D_y for the experiment model were estimated as follows. The profile of naphthalene concentration as a function of position along the x-axis *before* the naphthalene reached the well area is shown in Figure 6-13. The elapsed time is 102 minutes and the position x given indicates distance from the start of the soil matrix. Concentration measurements were made using off-line UV-VIS spectrophotometry and the accuracy of the measurements are indicated by the error bars. Samples could not be taken any closer together because of possible mixing, as a full milliliter of extracted fluid was needed for each concentration measurement. All samples were taken at equivalent depths.

Figure 6-13: Naphthalene Concentration Front Profile to Derive Dispersivity D_x

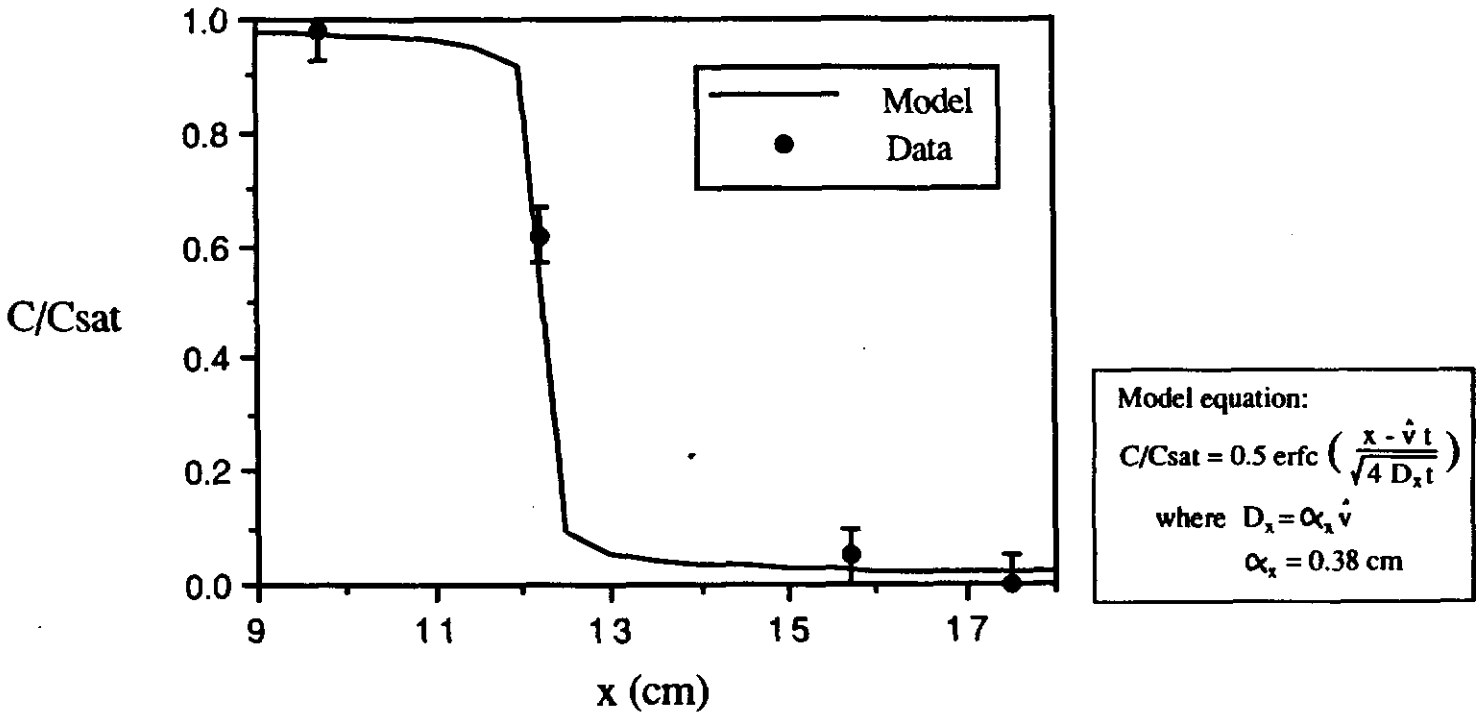

The well-known solution for a concentration front moving through a porous medium is as follows (Freeze and Cherry, 1979):

$$\frac{C}{C_{sat}} = 0.5 \text{ erf} \left(\frac{x - \hat{u}t}{\sqrt{4D_x t}}\right) \qquad (6\text{-}68)$$

where $\hat{u}$ is the effective solute seepage velocity ($=\frac{u_x}{R_d}$) [cm/s]; u_x is the unidirectional fluid seepage velocity [cm/s]; R_d is the retardation coefficient [dimensionless]; x is the distance from solute entrance [cm]; and t is the time from introduction of constant concentration front to the porous medium at x=0 [s]. This equation is fitted to the data in Figure 6-13. An accurate value for retardation coefficient was determined by dividing actual seepage velocity by the apparent solute velocity,$\hat{u}$, which is equal to the position x where C/C_{sat} equals 0.5 divided by the elapsed time at which the profile was measured. For this experiment, R_d=1.4. Using the model for the x-direction dispersion coefficient derived in Section 6.1., D_x is defined by the following:

$$D_x = \alpha_x u_x + D^* \qquad (6\text{-}20)$$

where D^* is the *molecular diffusion* coefficient for solute in water [cm^2/s]; α_x is the dispersivity in the x-direction [cm]; and u_x is the unidirectional seepage velocity. If this form for D_x (constant in this experiment) is adopted, the dispersivity determined by the curve fit in Figure 6-13 is α_x = 0.38 cm. The molecular *diffusion* coefficient is negligible to the first right-hand-side term in Equation 6-20. The value of dispersivity is in the normal range for this kind of sand (Freeze and Cherry,1979, report a range of α_x from 1 to 10mm). The accuracy of the fit in Figure 6-13 is somewhat limited by the number and accuracy of data points used.

It will be shown, however, that the exact value of the x-direction dispersivity is not critical to the solution of Equation 6-41.

The value of D_y in this experiment was approximated using a correlation between D_x and D_y for soil of various porosities as a function of seepage velocity u_x (Grane and Gardner, 1961). For a medium of porosity 41% (0.25mm glass beads) at $u_x = 0.001$ cm/s, the following relationship was obtained:

$$D_y \cong 0.5D_x \tag{6-68}$$

For a medium of porosity 21.7% (Berea sandstone) at $u_x = 0.001$ cm/s, the following relationship held:

$$D_y \cong 0.11D_x \tag{6-69}$$

Both Equations 6-68 and 6-69 were used in the model for Equation 6-41, with very similar results, as will be shown. Since the soil used in the 2-D cylindrical well experiment has 38% porosity, Equation 6-68 will be used as an approximation for D_y in the remainder of this section.

From Equations 6-66 and 6-67, the Peclet numbers for the 2-D experiment can be estimated:

$$Pe_x = 13 \tag{6-70}$$

$$Pe_y = 25 \tag{6-71}$$

The Peclet number gives information about the nature of the dispersion-convection problem. Most importantly, for the condition of our experiment,

convection of solute in the x-direction is a much more dominant transport mechanism that dispersion in either the x-direction or y-direction. Thus, the solution of Equation 6-41 will not be particularly sensitive to values of dispersivity in either the x- or y-direction. The solution of Equation 6-41 will, however, be sensitive to the flow field solution given by Equations 6-55 and 6-56. Thus, we can expect the width of fluid affected by the treatment well to be about twice the diameter of the well. This is supported by the 2-D model results in the next section.

The assumption that there is no backmixing of the fluid from the treatment well to the region behind the well is related to the Peclet number analysis above. Experimental measurements of the concentrations just behind the well agreed with the concentrations along x=0 away from the well (Figure 6-10) within 5%, which is below the error estimate of off-line measurements (about 8%). This could be predicted from Equation 6-70; for this experiment, convective flux dominates dispersive flux in the porous medium, so backmixing of well fluid does not occur.

6.4.4. Comparison of Results with Model

The steps followed thus far to model the 2-D cylindrical well are summarized here. First, $C_o(t)$ was determined by experimental measurement and was fitted by an empirical function (Figure 6-11). The naphthalene concentration of the well-mixed well was measured as a function of time and is plotted in Figure 6-14. The analytical model for well concentration given by

Figure 6-14: $C_o(t)$ and $C_{well}(t)$ -- 2-D Cylindrical Well Experimental Data and Model

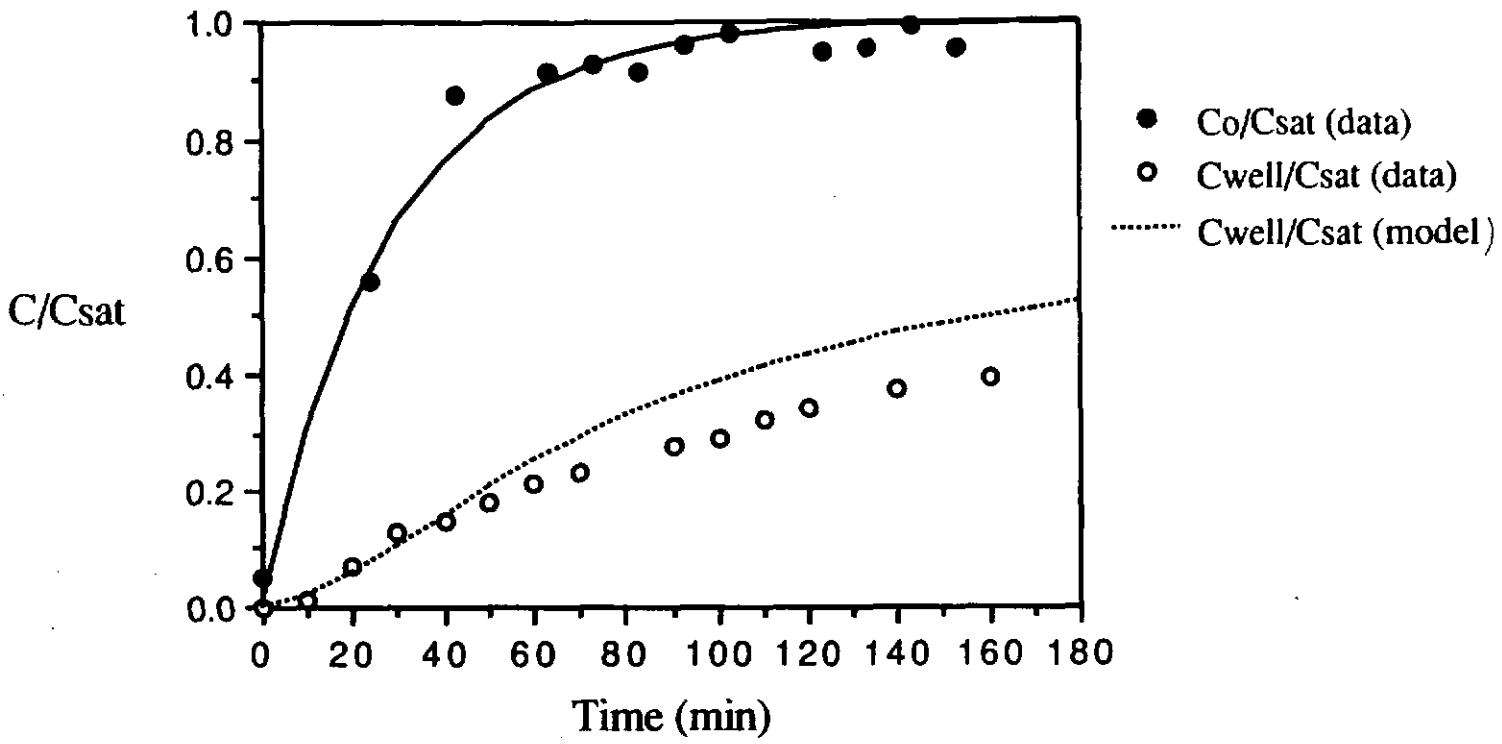

Equation 6-39 using experimental inputs (Figure 6-16) is also shown in Figure 6-14. The model predicts the experimental well concentration within about $0.1C_{sat}$.

A sensitivity analysis was conducted on the inputs used in the model, Equation 6-39. Curve fits of the data by artificially varying input parameters are shown in Figure 6-15. Figure 6-15 shows how much the input parameters must be changed to obtain a close fit of the experimental data. Membrane resistance R_{tot} would have to be decreased 60%, or membrane surface area NA_t would have to be increased 100%, or well volume V_w would have to be increased 36% for Equation 6-39 to provide a close fit of the experimental data. It is not realistic that any of these input values are in this much error. If the well flow-through rate were decreased 38% in the model, Equation 6-39 would yield a close fit of

Figure 6-15: 2-D Cylindrical Mixed Well Model -- Sensitivity Analysis

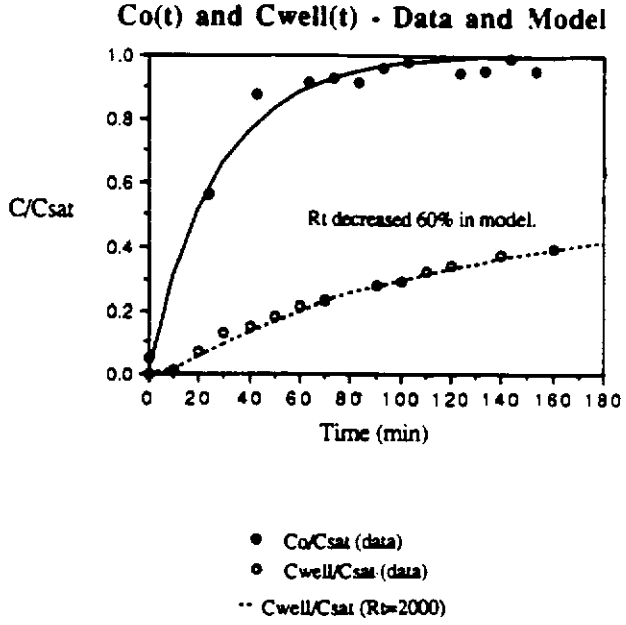

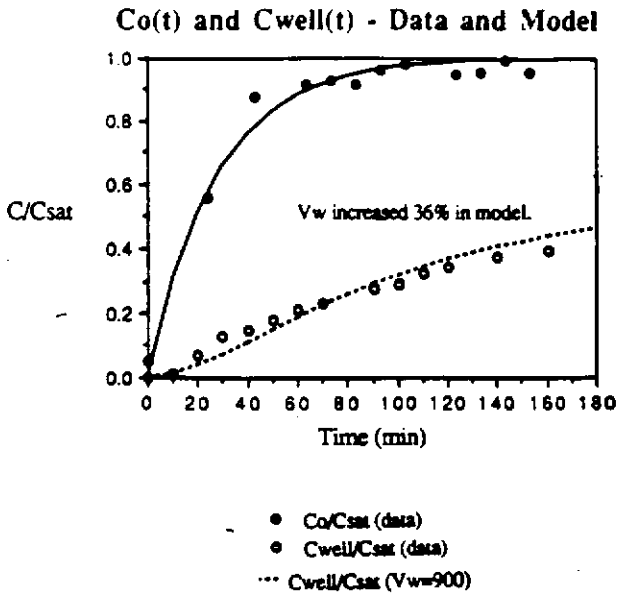

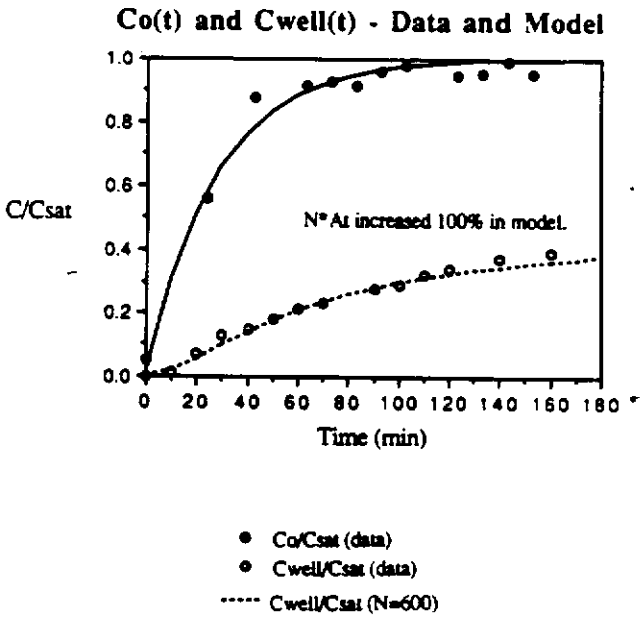

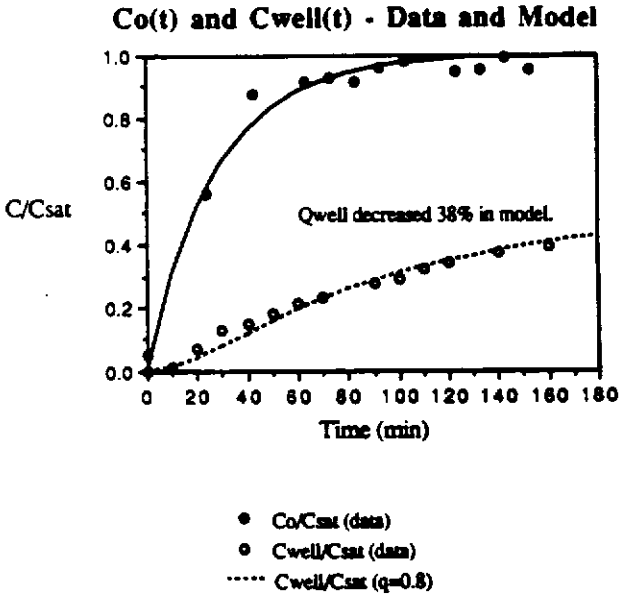

the experimental data. This error is not out of the question, since the well flow-through rate was predicted using both the overall tank flow-through rate measurement and the solution for flow velocity through the cylindrical well (Figure 6-12).

Another possible reason for the disparity between the model predictions and the measured well concentrations is the adsorption of naphthalene to the surfaces in the well. This would cause an additional sink for naphthalene entering the well that is not reflected by the model. A mass balance of naphthalene transferred from the exterior to the interior solution closes within the error of the interior solution naphthalene concentration measurement (about 40%), not accounting for solute adsorption. The uncertainty of this measurement, however, does not permit a conclusive dismissal of the possibility of the aforementioned adsorption effect.

The model of $C_{well}(t)$ and the input function $C_o(t)$ can now be used in the numerical solution of Equation 6-41. A graphical representation of the solution at t = 2 hours using the experimental input parameters is shown in Figure 6-16. The numerical solution was calculated for a half-domain of 12,553 nodes. The concentrations at selected nodes are plotted as heights above an x-y grid, corresponding to the nodal positions. For example, the modeled well concentration after two hours has increased to about 0.42 C_{sat}. This is the level on the vertical axis of the semicircle plotted along x=0. The nearby higher level, about 1.0 C_{sat}, corresponds to the incoming solution not influenced by the presence of the treatment well. A contour plot of the 3-D graph is shown to the right of Figure 6-16. The curves represent aquifer simulator positions of equal solution concentration. Note that the naphthalene plume has proceeded through

Figure 6-16: 2-D Well Experiment Model Output
2-D Concentration Profile at t = 2 hours

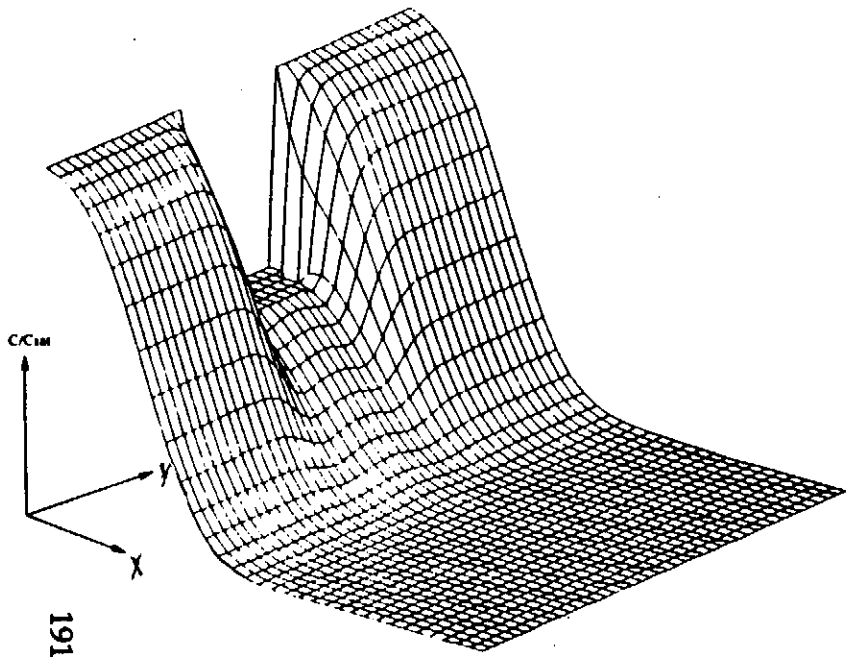

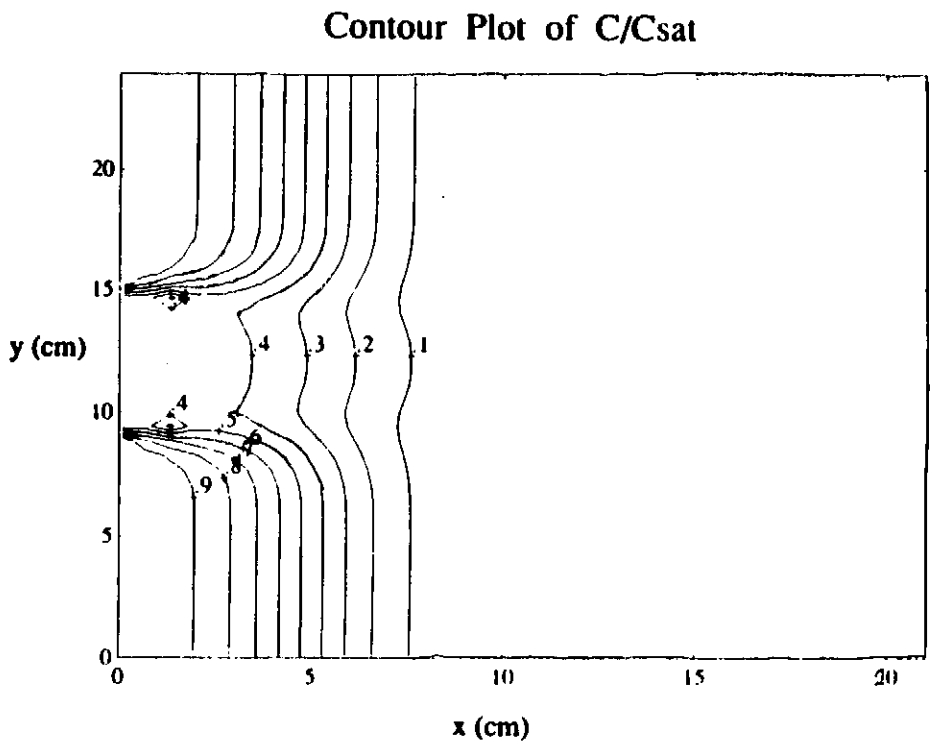

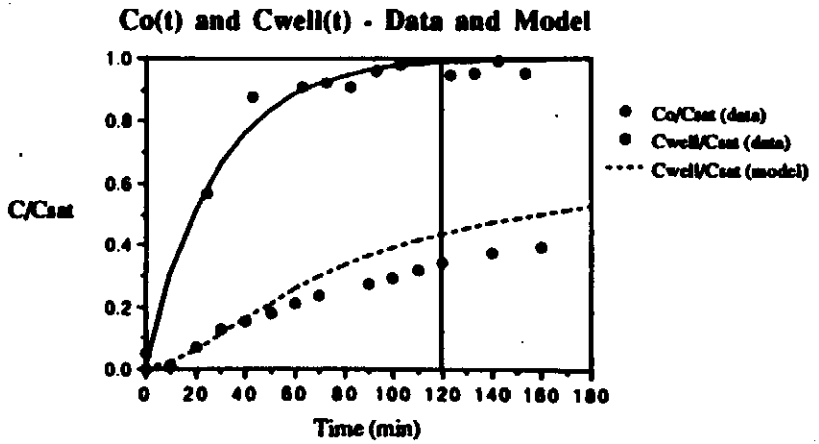

Input Parameters - Base Case

1. Well volume = 573.4 cm^3
2. Tube volume = 0.667 cm^3
3. Seepage velocity = 0.001038 cm/s
4. K_{pw} = 2420
5. M = 0.00362 (mass ratio NVPS:water in interior soln.)
6. R_{tot} = 5000 s/cm
7. Number of tubes = 300
8. Surface area of tube = 2.06 cm^2
9. Domain width = 12.0 cm x 2
10. Domain length = 21.0 cm
11. Retardation coefficient R_d = 1.4
12. Dispersion coef., x-dir., D_x = 0.000394 cm^2/s
13. Dispersion coef., y-dir., $D_y = 0.5\ D_x$
14. Time step length = 10 s
15. Number of time steps taken = 720
16. Porosity = 0.38
17. Well depth = 27.0 cm

only about a third of the length of the tank. The contour plot shows that fluid concentration is diminished by the presence of the treatment well up to a width twice the diameter of the well. The slight "bulge" in solution concentration along the center of the well is due to the flow field solution. The seepage velocity in the x-direction at te middle of the well is faster than the velocity at the far sides of the well; hence, the concentration "dips" on each side of the well.

Figure 6-17 shows the 2-D concentration profile predicted by the model at t = 2 hours using the same input parameters used in Figure 6-16 with the following exception. The time step length is halved and the number of time steps taken is doubled for the solution in Figure 6-17 in order to test for convergence of the numerical solution with time. The solution in Figure 6-17 differs from the Figure 6-16 solution by only 0.1%, so sufficient convergence of the solution with time can be assumed. Decreasing the number of spatial node points in the half-domain from 12,553 to just over 7000 nodes resulted in only a 0.2% average change in the solution; thus, there is sufficient spatial discretization for a convergent solution.

Figure 6-18 shows the effect on the solution at t = 2 hours of decreasing the dispersion coefficient in the y-direction, D_y, from $0.5D_x$ to $0.11D_x$, where D_x is the x-direction dispersion coefficient. All other model inputs remain the same. The only detectable change in the solution is a slight sharpening of the contours in the y-direction. This agrees with the prediction in the scale analysis of Section 6.4.3. that the 2-D solution is insensitive to the x- and y-direction dispersion coefficients due to the high Peclet number calculated for the experiment.

Figure 6-17: 2-D Well Experiment Model Output

2-D Concentration Profile at t = 2 hours -- Test for Convergence

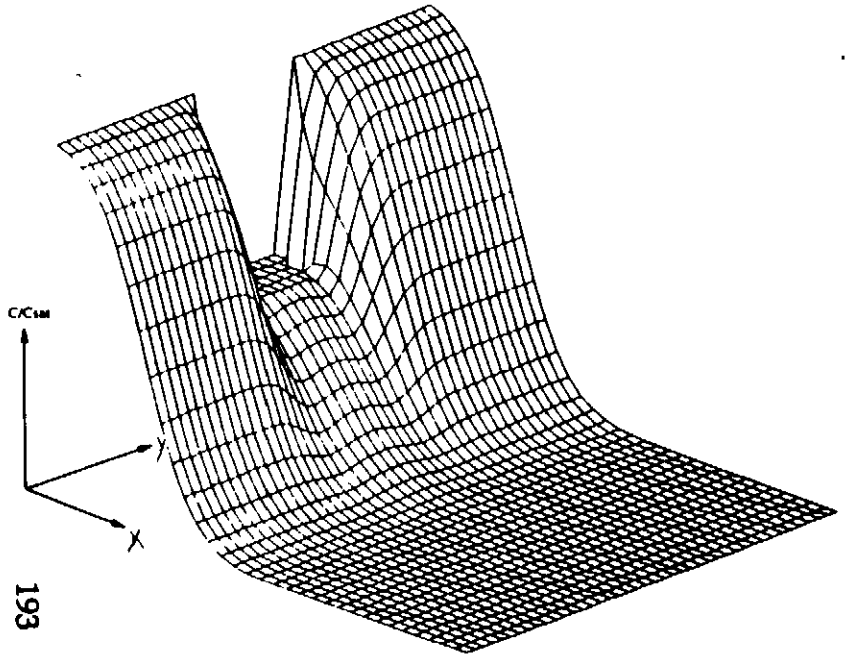

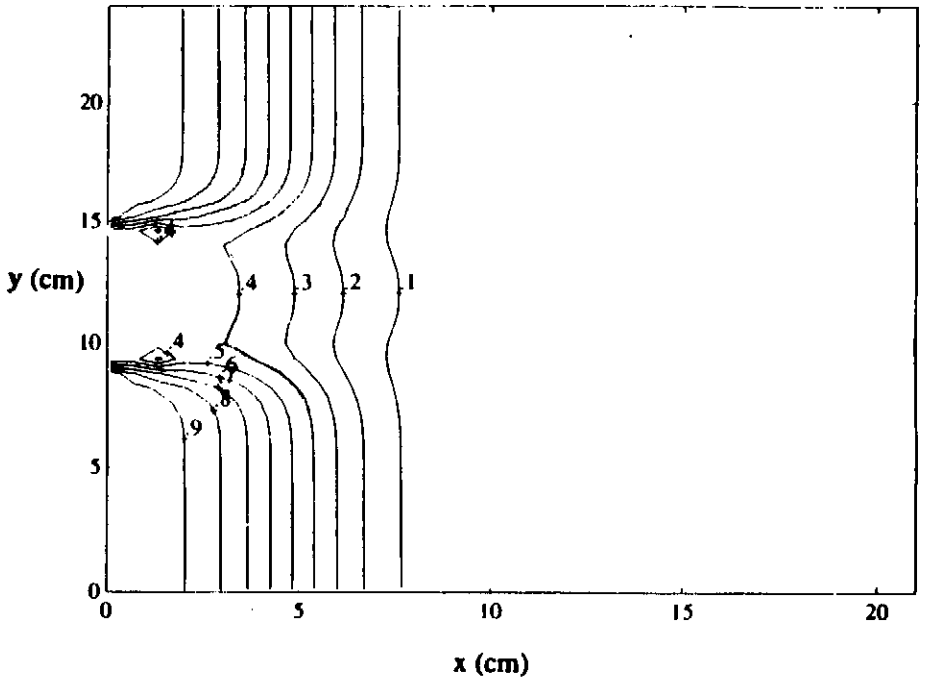

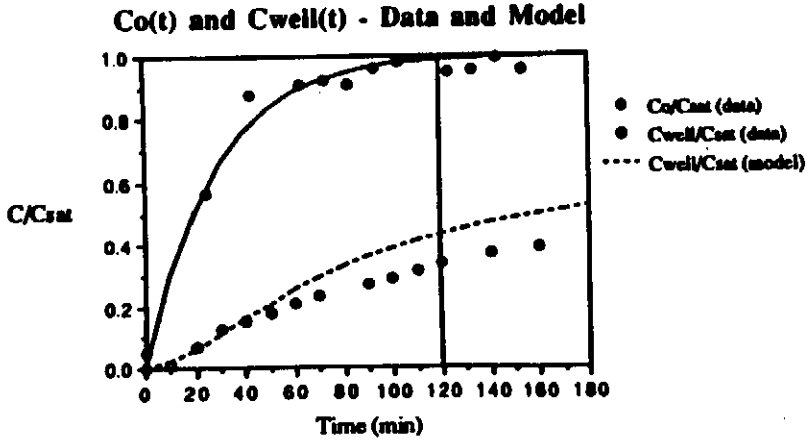

Input Parameters

Base Case with the following changes:

14. Time step length = 5 s
15. Number of time steps taken = 1440

(Time step length halved and number of steps doubled -- test for convergence.)

Figure 6-18: 2-D Well Experiment Model Output
2-D Concentration Profile at t = 2 hours -- Effect of Decreased D_y

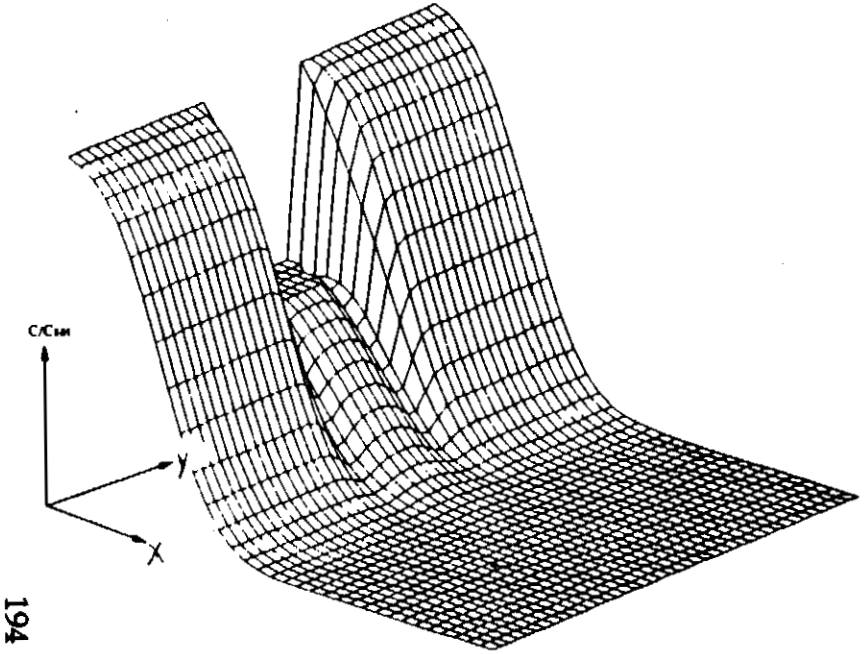

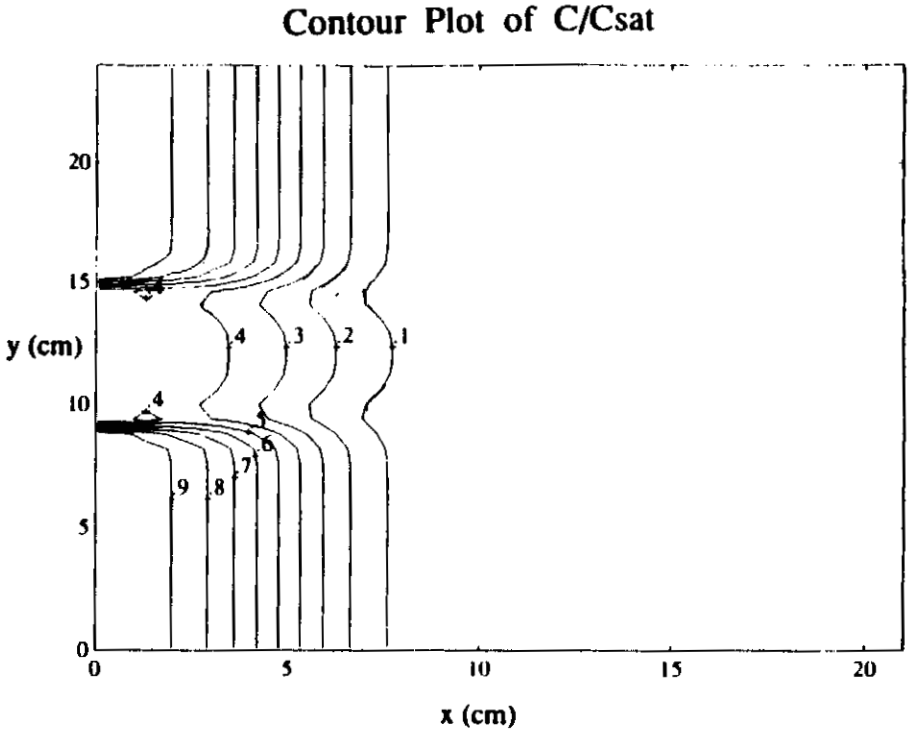

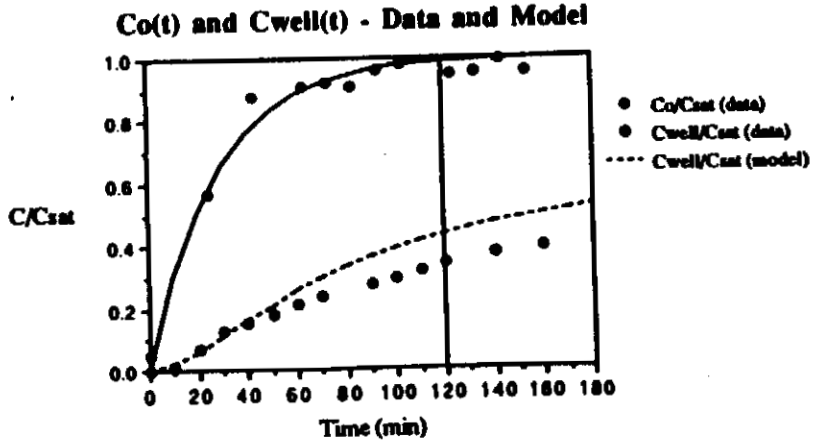

Input Parameters

Base Case with the following change:

13. Dispersion coef., y-dir., $D_y = 0.11\ D_x$

(Dispersion in y-direction decreased by approximately a factor of 5.)

Figure 6-19 shows the model solution using the base case experimental input parameters at a later time, t = 4 hours. At this time, the naphthalene plume has proceeded further along the tank length. Figure 6-20 shows the modeled concentration profile at t = 4 hours using increased polymer concentration and decreased membrane tube resistance inputs. This results in improved extraction performance, demonstrated by the deeper plume cavity in the 3-D graph of Figure 6-20.

The naphthalene concentration of solution samples at various positions in the tank were measured off-line at t = 2 hours. These values are shown superimposed over the modeled concentration profile in Figure 6-21. The data values agree with modeled concentration values within 20% for all points. Note the data plot shows the "bulge" at the center of the well seen previously in the model. The experimental data and the modeling support the conclusions of the scale analysis -- that the decreased concentration plume leaving a cylindrical treatment well has a width about twice the diameter of the well.

Figure 6-19: 2-D Well Experiment Model Output
2-D Concentration Profile at t = 4 hours

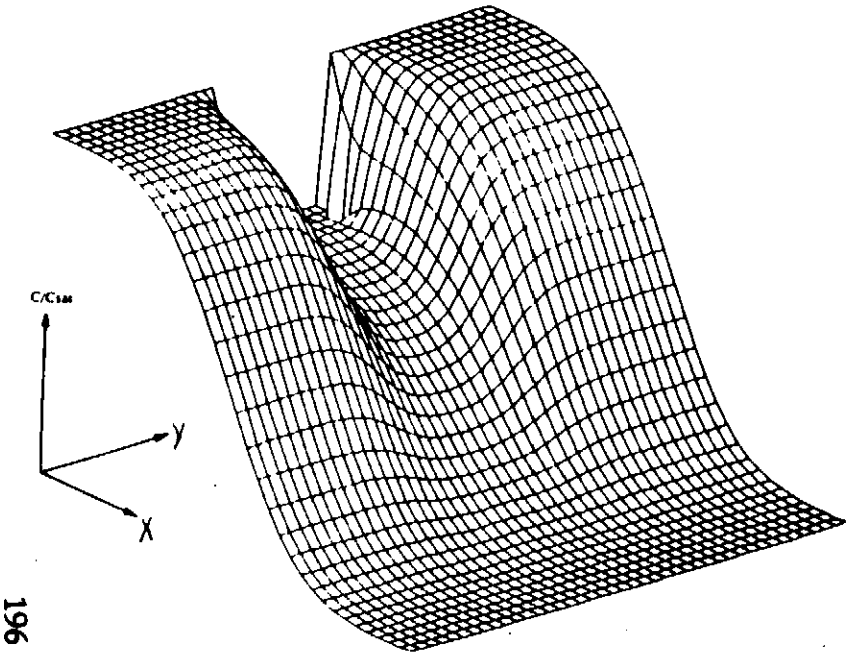

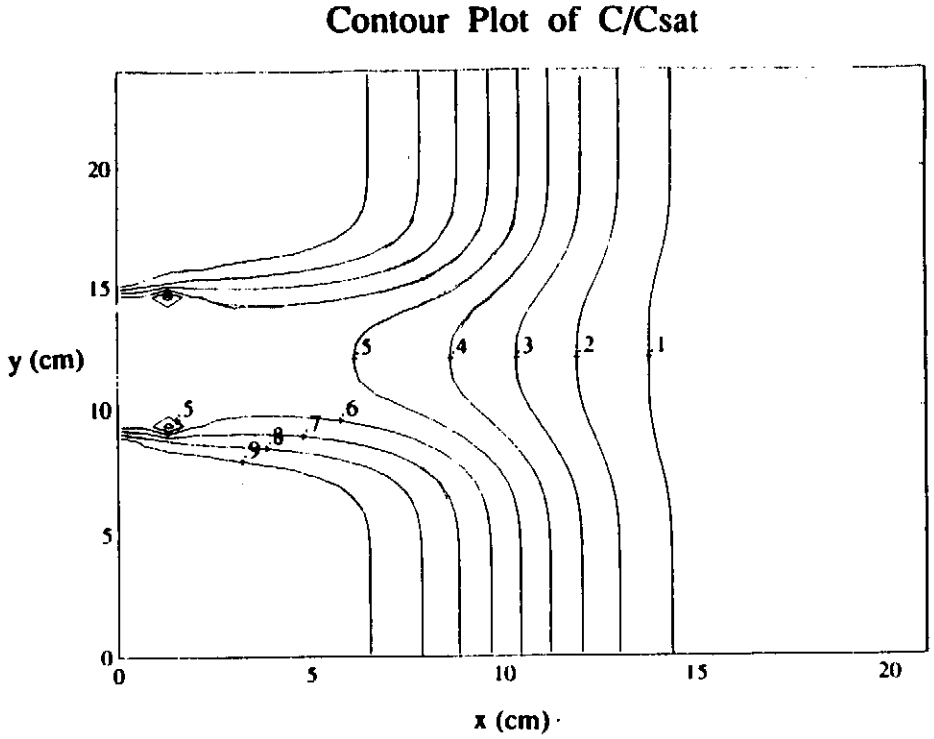

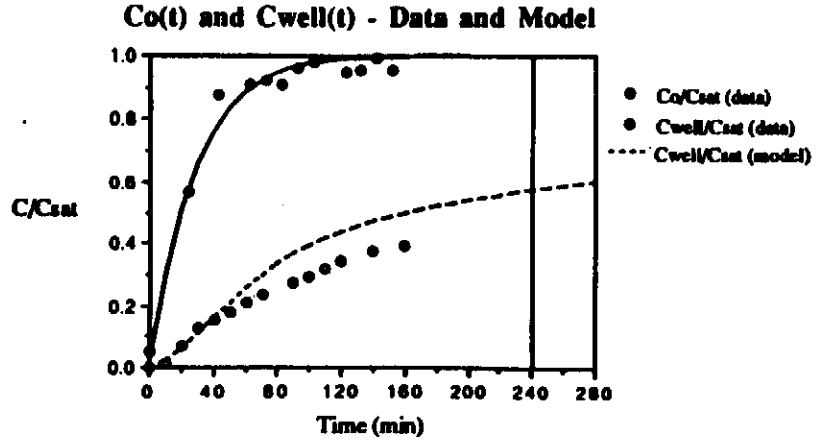

Input Parameters

Base Case with the following change:

15. Number of time steps = 1440

(Doubled time of simulation.)

Figure 6-20: 2-D Well Experiment Model Output

2-D Concentration Profile at t = 4 hours -- Enhanced System Efficiency

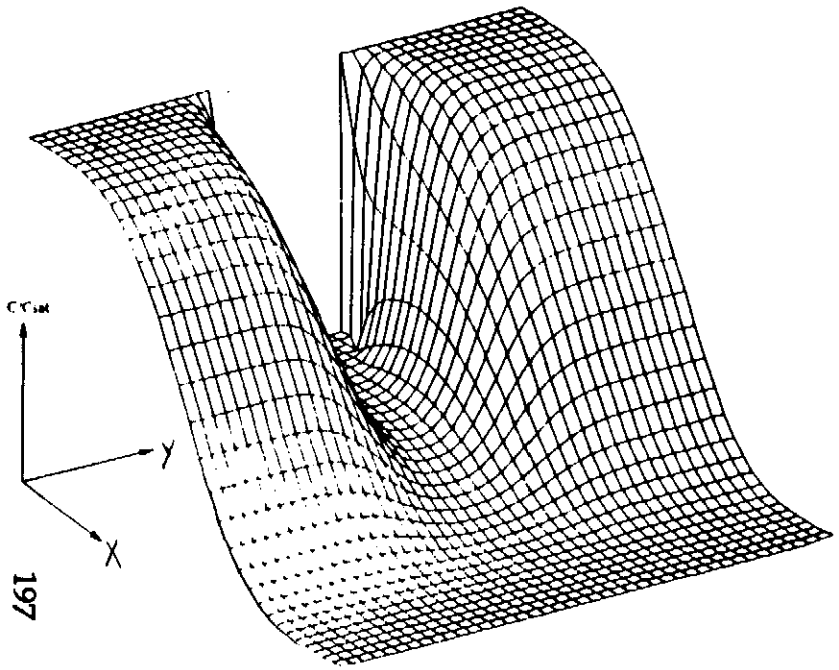

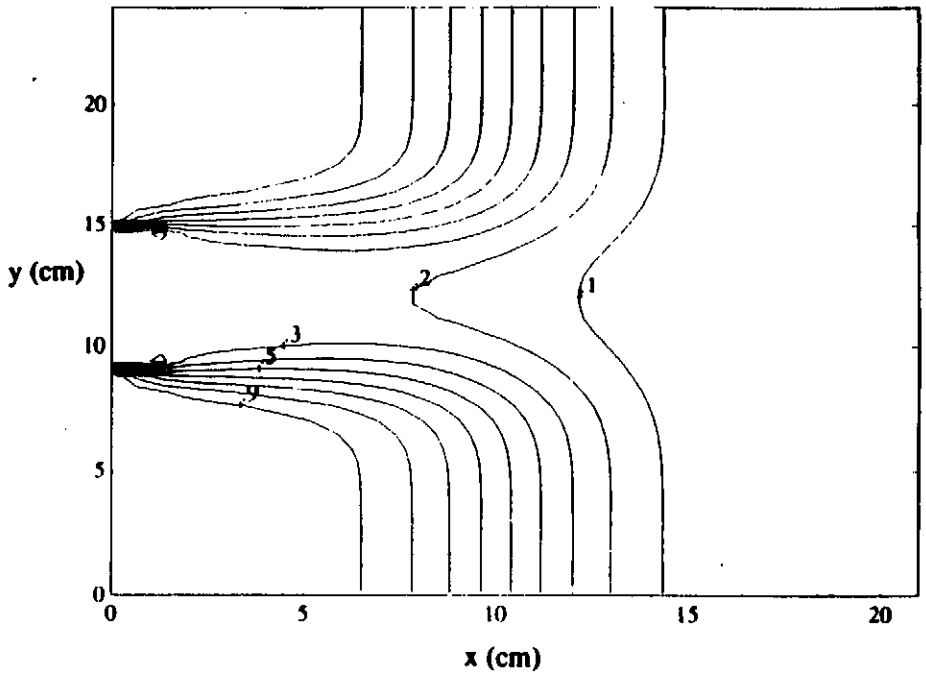

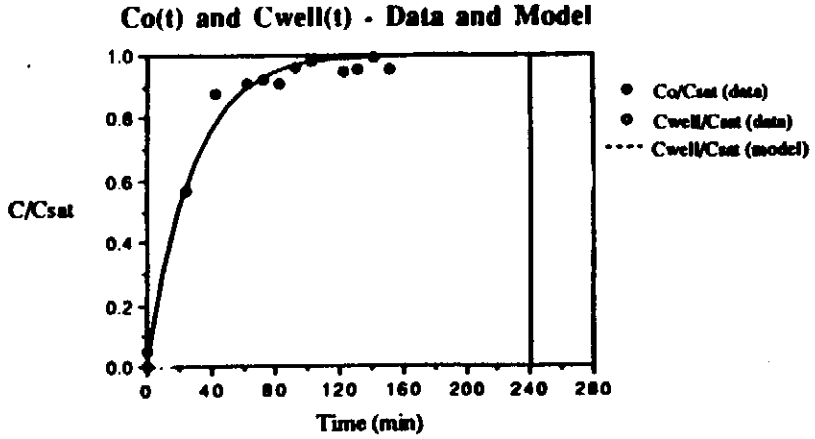

Input Parameters

Base Case with the following changes:

5. M = 0.02
6. R = 1000 s/cm
15. Number of time steps taken = 1440

(Improved extraction performance by increasing polymer concentration and decreasing membrane tube resistance.)

Figure 6-21: 2-D Well Experiment Concentration Data at t= 2 hours -- Data Represents Naphthalene Concentration of Solution at Positions in the Tank Domain Shown in Figure 6-10

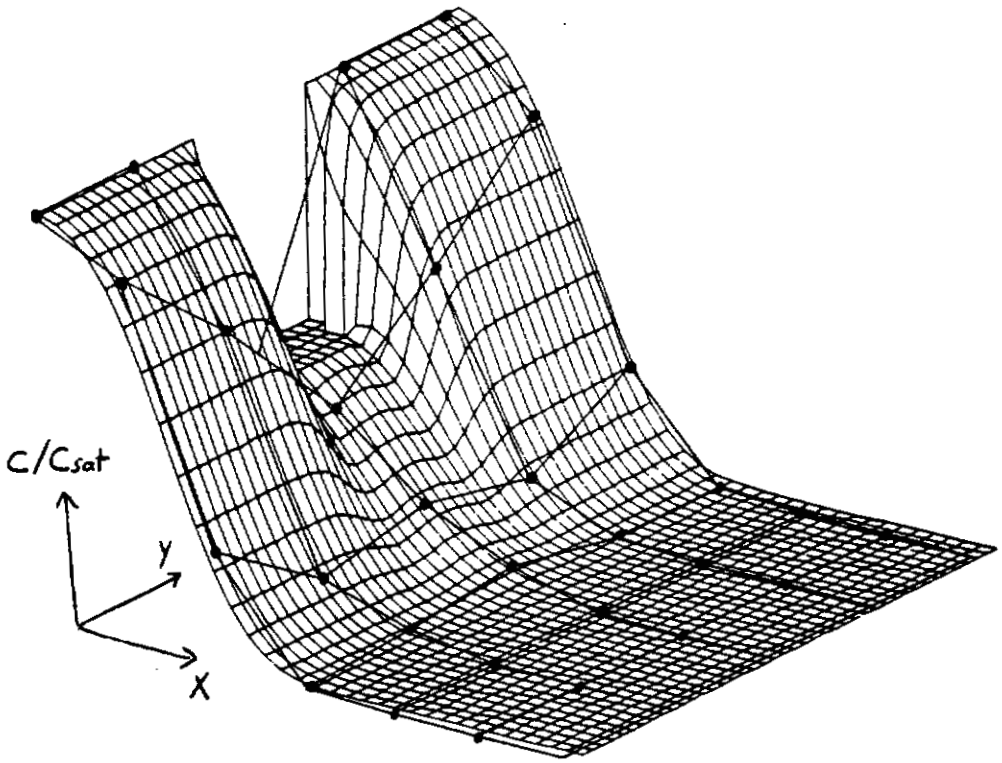

7. Scaling Up to Field Operations

The purpose of this chapter is to model how well the proposed copolymer/membrane groundwater remediation system might work in an actual field application. Questions about which kinds of contaminated aquifers are best suited to cleanup by the proposed system are answered, as well as how to choose cleanup system parameters, such as the number of membrane tubes in a well, for a given contaminated aquifer.

7.1. General Specifications

Before the hypothetical problem is formulated, it must be known which contaminated aquifer properties are important to the problem and how these properties generally vary from site to site. How fast contaminant moves into the treatment well is obviously important -- if the contaminant moves through the well too fast, there will be inadequate time for sufficient contaminant diffusion into the copolymer membranes. As discussed in Chapter 6, the velocity at which contaminant moves into the treatment well can be expressed as a function of groundwater seepage velocity, u_x [cm/s], given by Darcy's law and contaminant retardation factor, R_d [dimensionless], which was defined in Equation 6-18 and is repeated here for a general case:

$$R_d = 1 + \frac{\rho_b}{n} K_d \qquad (7\text{-}1)$$

where ρ_b is aquifer bulk density [g/cm^3], n is aquifer porosity [cm^3/cm^3], and K_d is the solid-liquid contaminant partition coefficient [cm^3/g]. The properties in Equation 7-1 are averaged over the spatial domain of the aquifer. The retardation factor quantifies how much a solute's velocity through the aquifer is retarded due to adsorption onto aquifer solids. Adsorption of solute was shown empirically to be a function of aquifer solid composition (i.e. fraction organic carbon) and solute hydrophobicity as in Equation 6-19. An *effective* solute (contaminant) seepage rate, u_{eff} [cm/s], can be defined as follows using dimensional arguments on the conservation Equation 6-17:

$$u_{eff} = \frac{u_x}{R_d} \tag{7-2}$$

where both velocity of groundwater and adsorption of solute are accounted for. In Chapter 6 it was discussed that groundwater seepage velocity, u_x, typically varies from centimeters per day to meters per day in field applications (Codell et al., 1982). The retardation factor can vary from 1 to 10^3 or higher depending primarily on organic carbon fraction of the aquifer, f_{om}, and solute hydrophobicity (reflected by K_{ow}). Thus, u_{eff} may be as high as meters per day and as low as centimeters per year (nearly immobile). Another factor which may affect the solute transport rate through an aquifer is adsorption of solute onto mobile organic macromolecules (such as humic acids) already present in the groundwater (Magee et al., 1991). Also, since no aquifer is completely isotropic, contaminant seepage rate may vary considerably within a single aquifer. Thus, the speed at which a contaminant moves into the treatment well in a given aquifer is very site-dependent and is a function of average aquifer properties, the degree to which they vary spatially, and the adsorptive characteristics of the contaminant within the porous media.

Another important factor in determining workability of the proposed process is the polymer-water partition coefficient, K_{pw}, of the contaminant in copolymer solution. This factor tells how much the contaminant may be concentrated in the copolymer solution. This factor, like u_{eff} above, may vary orders of magnitude depending on contaminant hydrophobicity and the specific copolymer used. The value of K_{pw} should be at least about 10^3 for a workable system. Equations 4-12 and 4-26 of Chapter 4 describe quantitatively how K_{pw} varies with solute and polymer properties. The contaminant-polymer systems discussed in this chapter will include the naphthalene-NVPS and phenanthrene-NVPS systems.

The overall molecular diffusive resistance of the membrane tubes, R_{tot}, is of importance in the proposed system. Earlier in Chapters 5 and 6, R_{tot} was described primarily as a function of a solute's diffusion coefficient in water and the thickness of the membrane support structure. Other factors which will affect the overall effective resistance to transmembrane solute transport include the degree of mixing in the well and the arrangement of membrane tubes in the well. For the sake of simplicity in this simulation, a bulk concentration model for the well fluid and the interior copolymer fluid will be used (as illustrated in Figure 5-1). This model assumes effective concentrations of both the well fluid and copolymer fluid will vary with time only, not position, and that R_{tot} is a constant.

The critical factor in determining if a proposed system will be effective is the clean-up requirement for a given contaminant/aquifer situation. Requirements are normally set by regulatory groups such as the U.S. Environmental Protection Agency or comparable state or local agencies, which

have determined concentration limits beyond which a contaminant is considered unsafe.

The hypothetical field problem is posed as follows. We wish to know how many membrane tubes per square foot of wall area of the well are needed to maintain a given minimum concentration of contaminant in a treatment well. We also wish to know how long the contaminant concentration in the well can be maintained below a given concentration before the copolymer solution must be replaced for the above systems. Figure 7-1 is a diagram of the proposed application of the membrane/copolymer system, complete with values for well dimensions, copolymer solution properties, and membrane tube properties. The treatment well is rectangular and has a width of 6 inches (15 cm). The membrane tubes used are identical in surface area and volume to the polysulfone tubes used in the experiments described in Chapters 5 and 6; thus, the transmembrane diffusion resistances (R_{tot}) are as listed in Tables 5-1 and 5-2. The rectangular well is initially saturated with contaminant at a concentration C_o [g/cm^3].

The first part of the problem is to determine how many membrane tubes per square foot of wall area are needed to obtain a given minimum contaminant concentration in the well. The required number of tubes is determined as a function of u_{eff} and R_{tot} for the case of *phenanthrene* contamination, where the minimum desired well concentration, $C_{well,min}/C_o$, is 0.1, 0.05, and 0.01. The required number of tubes is also determined for *naphthalene* contamination, where $C_{well,min}/C_o$ is 0.10. The solute's effective velocity is varied from 0.2 cm/day to 20 cm/day and transmembrane diffusive resistance is varied from 1000 to 10,000 s/cm for the above cases.

Figure 7-1: Cross-Section of Hypothetical, Rectangular Treatment Well

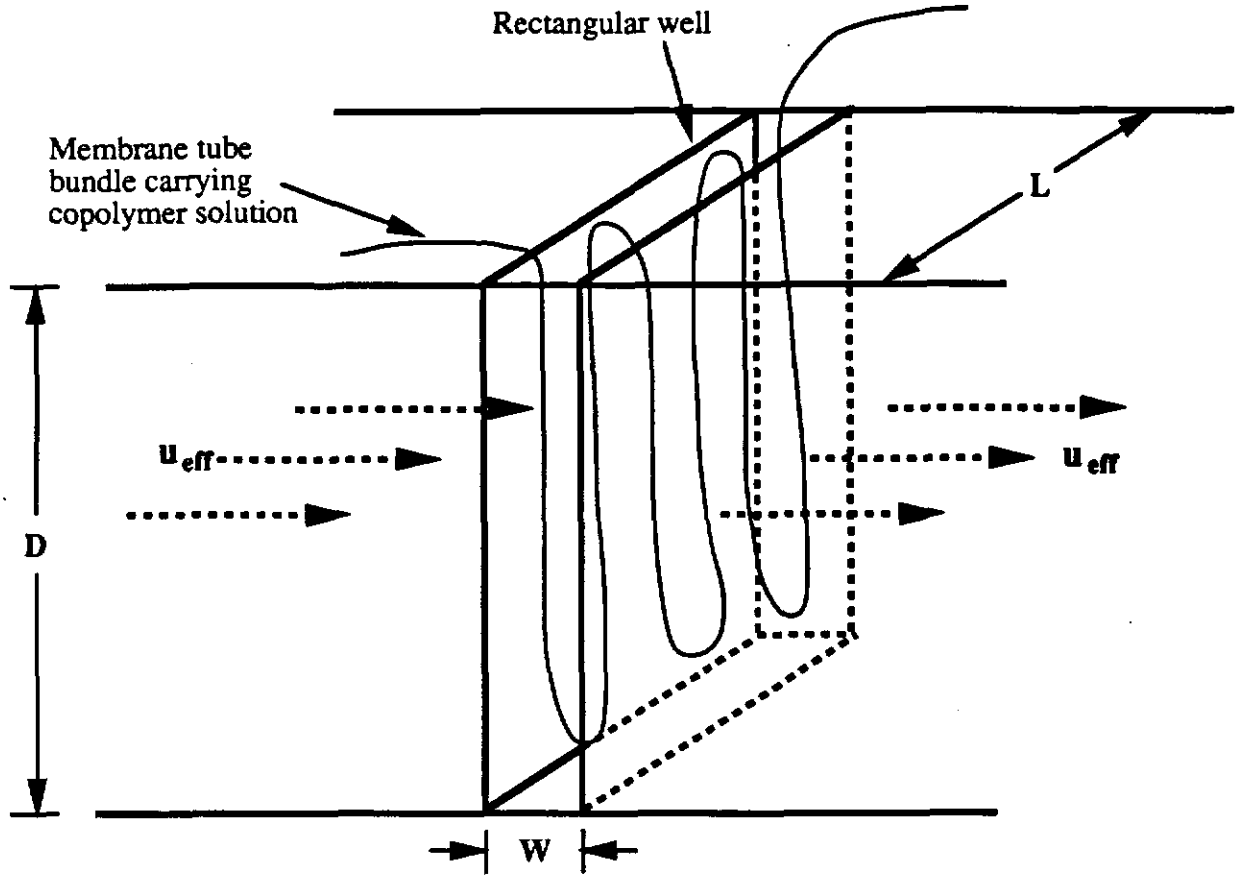

Well Properties

Wall area of the well = D x L
Well width = 6 inches
Well volume = 14,158 cm^3/ ft^2 wall area
Initial contaminant concentration in well = C_o

Membrane Tube Properties

Tube surface area, A = 4.788 cm^2/ ft^2 wall area
Tube volume, V = 0.0598 cm^3 / ft^2 wall area
Nominal MW Cutoff = 50,000 (average pore diameter = 50 Å)
Transmembrane molecular diffusive resistance = R_{tot} [s/cm]

Copolymer Solution Properties

Type copolymer = N-vinylpyrrolidone/styrene
Tube interior soluion polymer:water weight ratio, M = 0.20
Polymer-water partition coefficient K_{pw}(naphthalene) = 2420
Polymer-water partition coefficient K_{pw}(phenanthrene) = 49,100

Aquifer Properties

Porosity, n=0.50
Effective solute transport rate = u_{eff} [cm/s]
Contaminant concentration of fluid entering well = C_o

The second part of the problem is to determine at what interval the copolymer solution must be replaced to keep the well concentration below a given value. The required replacement interval is determined for the phenanthrene remediation systems given in the first part of the problem with maximum allowable concentrations, $C_{well,max}/C_o$, of 0.2, 0.1, and 0.02.

7.2. Governing Equations

The governing equations for the well solution contaminant concentration consist of two mass balances -- one on the membrane interior solution and one on the well solution. The equations and initial conditions which follow are identical to those described in Section 6.3.2. of this paper.

Membrane Tube Interior Mass Balance:

$$V_t \frac{dC_{int,aq}}{dt} = \frac{A_t}{R_{tot}} (C_{well} - C_{int,aq}) - MK_{pw}V_t \frac{dC_{int,aq}}{dt} \qquad (6\text{-}30)$$

Well Mass Balance:

$$V_w \frac{dC_{well}}{dt} = Q (C_o - C_{int,aq}) - \frac{NA_t}{R_{tot}} (C_{well} - C_{int,aq}) \qquad (6\text{-}31)$$

where V_t is the membrane tube interior volume [cm^3]; V_w is the well volume [cm^3]; A_t is the membrane tube surface area [cm^2]; R_{tot} is the overall membrane tube resistance [s/cm]; M is the polymer to water mass ratio (in copolymer solution) [g/g]; K_{pw} is the polymer-water partition coefficient of solute [dimensionless]; Q is the fluid flow rate into the well [cm^3/s]; N is the number of membrane tubes; C_o is the solute concentration of fluid entering the well [g/cm^3]; $C_{int,aq}$ is the interior aqueous pseudophase solute concentration [g/cm^3]; and C_{well} is the solute concentration of the well fluid [g/cm^3]. The initial conditions are as follows:

Initial Conditions:

$$C_{well}(t=0) = C_o \tag{6-32}$$

$$C_{int,aq}(t=0) = 0 \tag{6-33}$$

The solution for contaminant concentration of the well fluid is as follows:

$$\frac{C_{well}}{C_o} = \frac{\alpha}{a_1 - a_2}(e^{-a_1\tau} - e^{-a_2\tau}) + 1 \tag{6-34}$$

where $\alpha = \frac{NA_t}{QR_{tot}}$; $\beta = \frac{A_t V_w}{QR_{tot} V_t (1 + MK_{pw})}$;

$a_1 = \frac{a - \sqrt{a^2 - 4\beta}}{2}$; $a_2 = \frac{a + \sqrt{a^2 - 4\beta}}{2}$;

$a = 1 + \alpha + \beta$; $\tau = \frac{t}{V_w/Q}$.

Figure 7-2 shows the solution of C_{well}/C_o for the case of both naphthalene and phenanthrene contamination of the well in Figure 7-1 with given inputs. The resistance, R_{tot}, and partition coefficient, K_{pw}, for each case is as determined in Chapters 5 and 6 for the lab-scale systems. The effective contaminant velocity into the well, u_{eff}, is chosen as 2 cm/day. The number of membrane tubes in the well is 600 per square-foot of wall area; this corresponds to an approximately 1.4-inch diameter bundle of the 0.5-mm-ID polysulfone membranes per foot of well length.

Note the solution in Figure 7-2 for C_{well}/C_o is independent of the exact incoming contaminant concentration, C_o. This is because the partition

Figure 7-2: C_{well}/C_o Versus Time in a Rectangular Well

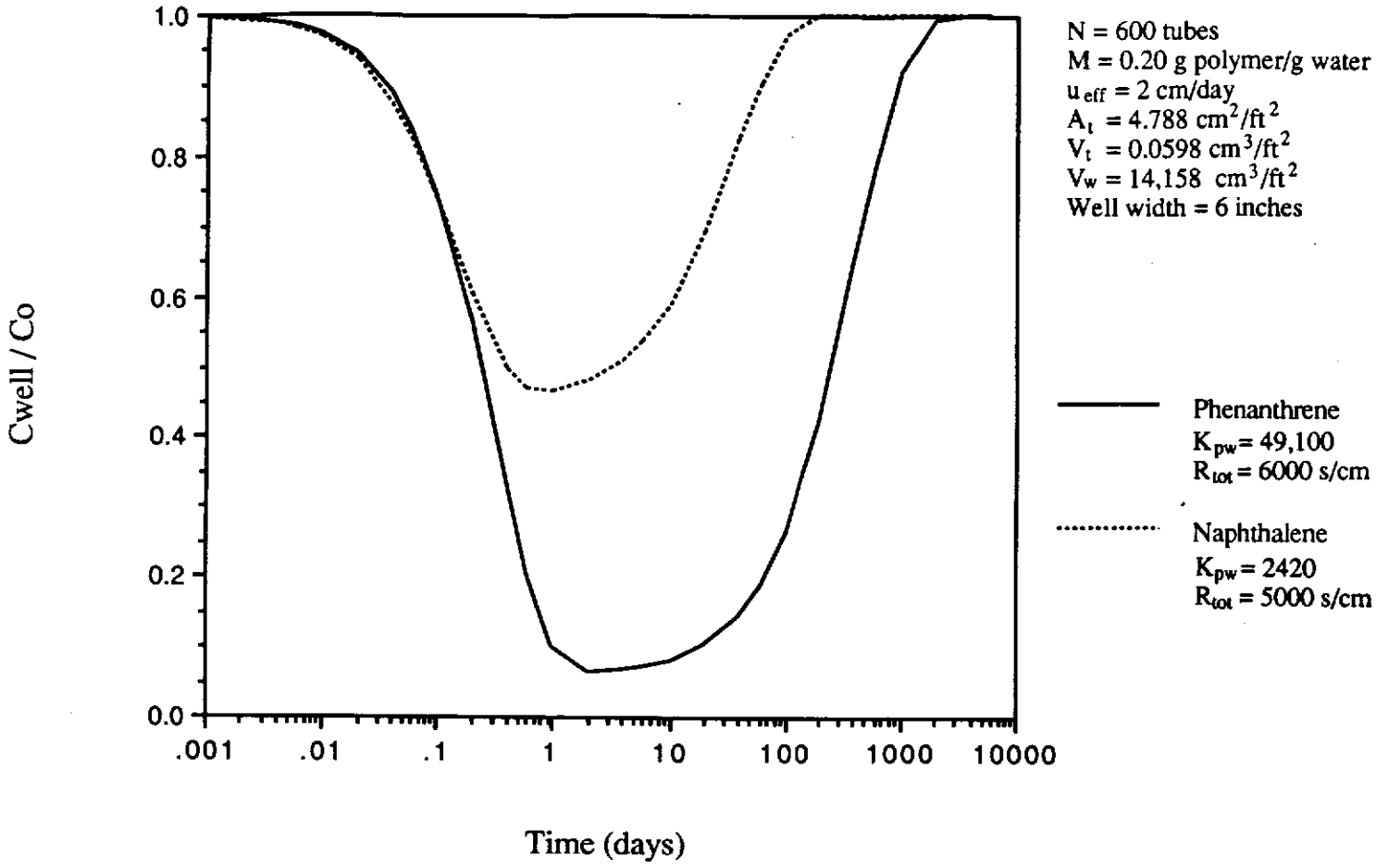

coefficient, K_{pw}, is modeled as a constant. Although a higher loading of contaminant onto copolymer, S, (mass contaminant per mass polymer) is possible at higher aqueous solution concentration, C_{aqu}, this higher loading is not possible at lower aqueous solution concentrations since K_{pw} (which equals S/C_{aqu}) must remain constant as modeled.

In the contamination cases shown in Figure 7-2, the solute concentration in the well initially decreases over a time period of one or two days, the concentration stays low for an interval of 10 to 30 days, then the concentration increases as the copolymer becomes saturated with solute. There are essentially two mechanisms governing the shape of the solution in Figure 7-2. First, the concentration decrease at the beginning of the plot is primarily a function of how fast the solute diffuses through the membrane. Second, the concentration increase at the end of the plot is primarily a function of how quickly the copolymer solution becomes saturated with solute. It is the interplay between these two parts of the solution that determines the important system operability criteria – what minimum solute concentration is obtainable in the well, and how long the low well concentration can be maintained before replacing the copolymer solution becomes necessary.

The hypothetical problem posed in Section 7.1. is somewhat conservative in that better system performance would be achieved in cases where the well is not initially saturated with contaminant. For example, the time allowable before initial replacement of copolymer solution given a maximum allowable well solute concentration is obviously greater if the well is initially free of contaminant.

7.3. Simulation Results

The 3-D graph of Figure 7-3 plots solutions for N as heights corresponding to values of R_{tot} and u_{eff}. The contour graph on the right of Figure 7-3 shows values of constant N (interpolated from the 3-D graph) as a function of R_{tot} and u_{eff}. It can be seen from the graphs that the higher the solute velocity and membrane resistance, the higher the number of tubes required for a minimum well phenanthrene concentration, $C_{well,min}/C_o$, of 0.1. All solutions for N, however, are physically reasonable; the highest plotted contour at N=2000 corresponds to a membrane bundle of approximately 2.5-inches diameter per foot of well length.

Figure 7-3: Required Membrane Tubes, N, for Given $C_{well,min}/C_o$

$$N \text{ required for } \frac{C_{well,min}}{C_o} \text{(phenanthrene)} = 0.10$$

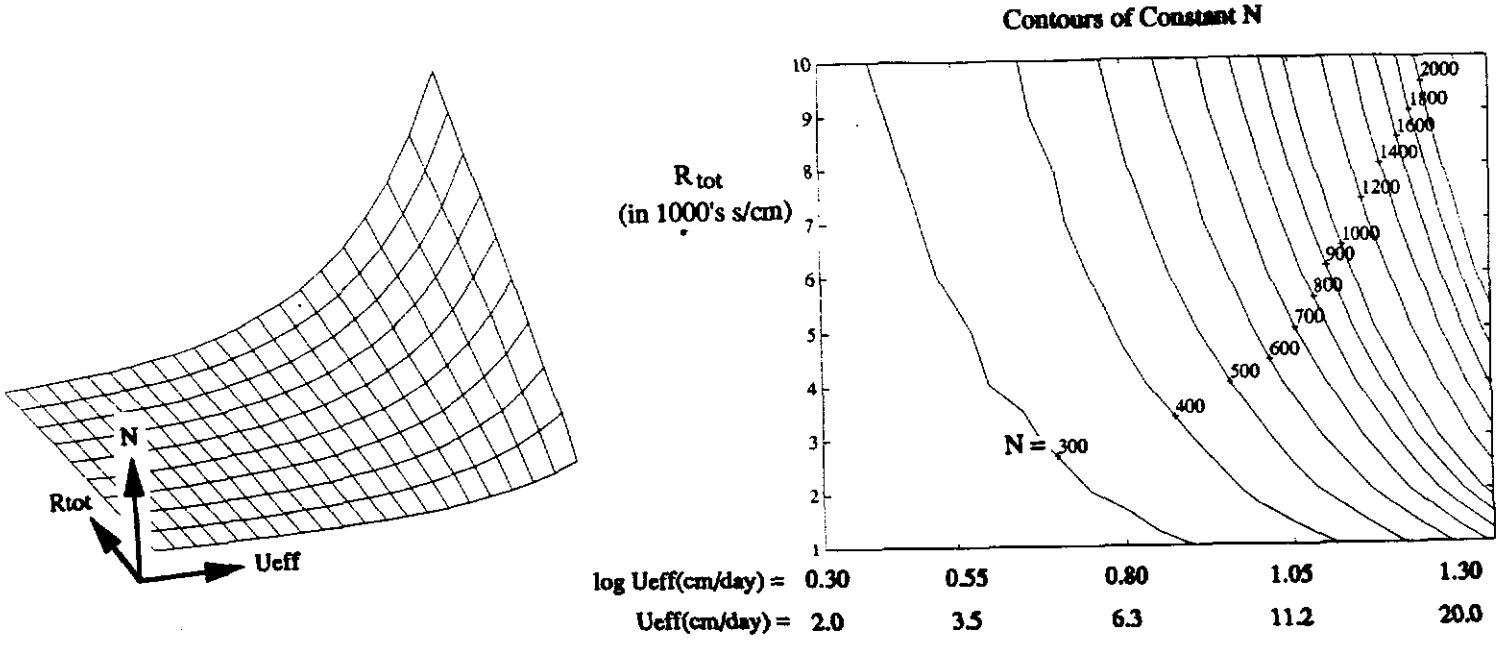

Plots in Figure 7-4 show number of required tubes for different criteria. The first two plots show contours of N tubes required per square-foot of wall area for lower minimum well concentrations of phenanthrene. Only for the case of $C_{well,min}/C_o = 0.01$ at high velocity and high membrane tube resistance do the requirements become physically unreasonable. The six-inch well width will contain up to 15,000 membrane tubes foot of well length, allowing for tube housing and spacing. From the Figure 7-3 and 7-4 (a) and (b) plots, it appears that at a given u_{eff} and R_{tot}, the number of tubes required is approximately proportional to the inverse of the required minimum concentration. For example, about twice as many tubes are required at a given u_{eff} and R_{tot} to achieve $C_{well,min}/C_o = 0.05$ as are required to achieve $C_{well,min}/C_o = 0.10$. Figure 7-4 (c) shows the required number of tubes to achieve a minimum *naphthalene* concentration in the well, $C_{well,min}/C_o$, of 0.10. These values are higher than for the phenanthrene case, and less a function of resistance since the partition coefficient, K_{pw}, for naphthalene in the NVPS copolymer is over an order of magnitude lower than the phenanthrene partition coefficient. Thus, the second part of the curve, governed by K_{pw}, (Figure 7-2) comes into play sooner for the case of naphthalene contamination in determining the minimum concentration obtainable.

The second part of the hypothetical problem was to determine the required copolymer solution replacement time for the above cases given a *maximum* allowable well concentration, $C_{well,max}/C_o$. For example, it can be seen for the case in Figure 7-2 that the copolymer solution should be replaced after about 75 days to keep the well concentration , C_{well}/C_o below 0.20.

Figure 7-4: Required Membrane Tubes, N, for Given $C_{well,min}/C_o$

(a) N required for $\frac{C_{well,min}}{C_o}$ (phenanthrene) = 0.05

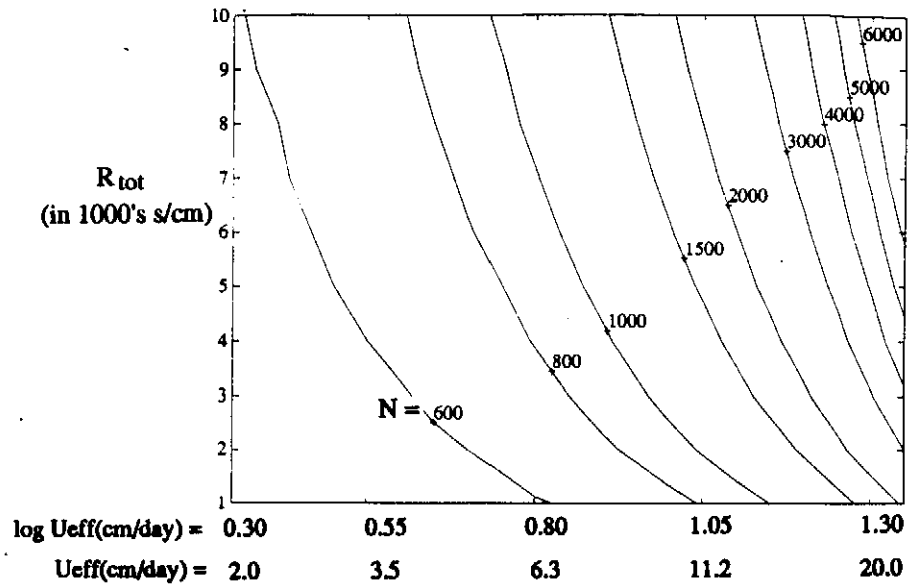

(b) N required for $\frac{C_{well,min}}{C_o}$ (phenanthrene) = 0.01

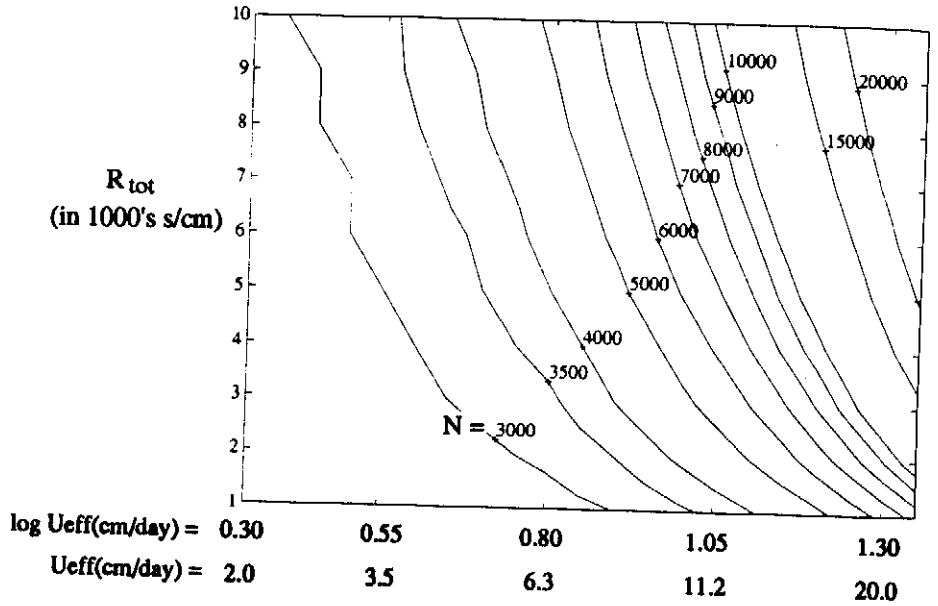

(c) N required for $\frac{C_{well,min}}{C_o}$ (naphthalene) = 0.10

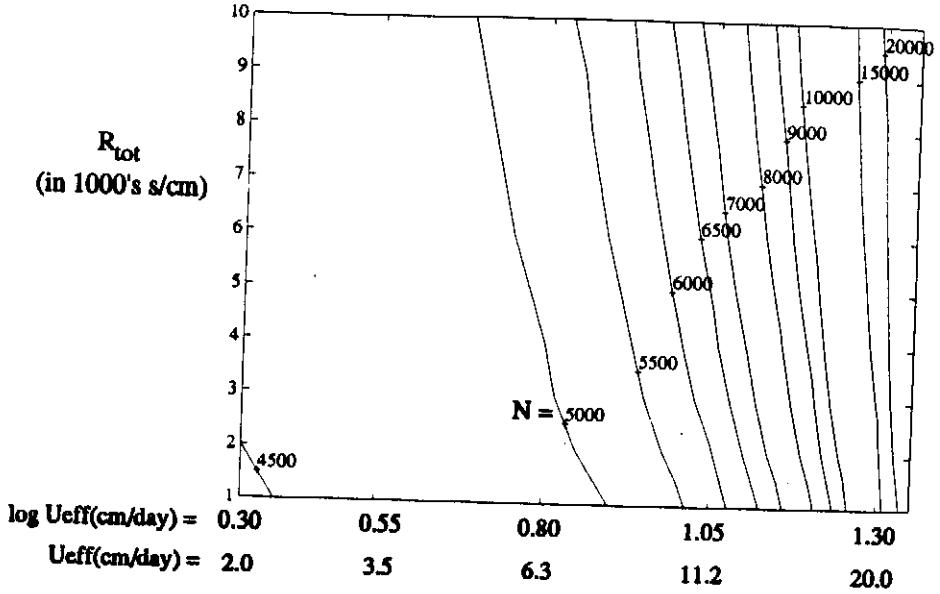

Figure 7-5 (a) shows the required replacement time for the case where the minimum well concentration, $C_{well,min}/C_o$, equals 0.05 and the maximum allowed well concentration, $C_{well,max}/C_o$, equals 0.10. The number of membrane tubes used for points in Figure 7-5 (a) corresponds with the values in Figure 7-4 (a). The required replacement times vary from 20 to 240 days. Required time is a strong function of solute velocity; the higher the velocity, the quicker the copolymer becomes saturated with solute and the sooner the solution must be replaced. Figure 7-5 (b), (c), and (d) shows required replacement times for given $C_{well,min}/C_o$ and $C_{well,max}/C_o$. The number of membrane tubes used in Figure 7-5 (c) and (d) correspond to values shown in Figure 7-4 (b). Longer replacement times are allowable for the cases of lower $C_{well,min}/C_o$ because there is more copolymer solution present (due to higher values of N used); thus, it takes more time to saturate the copolymer.

Conclusions from this hypothetical problem are drawn as follows. The membrane/copolymer system is a more effective contaminant barrier for contaminated aquifers with lower groundwater velocity, higher contaminant hydrophobicity, and higher soil organic carbon fraction (more contaminant adsorption). However, these factors increase the overall remediation time, since it takes longer for the contaminant to travel through the aquifer to the treatment well, where it can be filtered.

The results of this chapter can be extended to the case of cylindrical treatment wells. As shown in Chapter 6, cylindrical wells would have to be spaced about one well-diameter apart in order to intercept all incoming fluid. Average velocity into each well would be twice the observed groundwater velocity due to the sweeping-in effect (Figure 6-13). Using appropriate well

Figure 7-5: Required Interior Solution Replacement Intervals for Given $C_{well,max}/C_o$: Contours of Replacement Time (in Days)

(a) Replacement time given $\frac{C_{well,min}}{C_o}$(phenanthrene) = 0.05 , $\frac{C_{well,max}}{C_o}$(phenanthrene) = 0.10

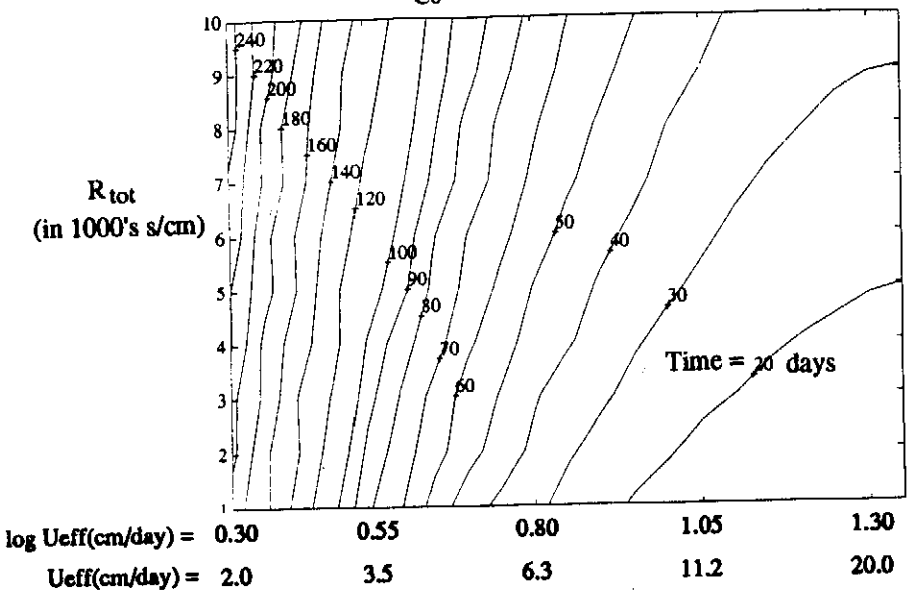

(b) Replacement time given $\frac{C_{well,min}}{C_o}$(phenanthrene) = 0.05 , $\frac{C_{well,max}}{C_o}$(phenanthrene) = 0.20

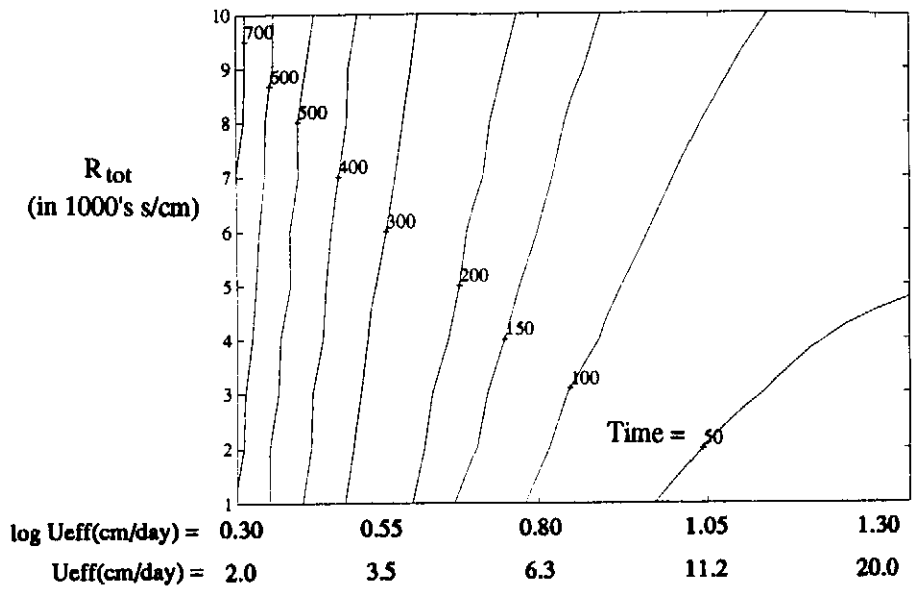

(c) Replacement time given $\frac{C_{well,min}}{C_o}$(phenanthrene) = 0.01 , $\frac{C_{well,max}}{C_o}$(phenanthrene) = 0.10

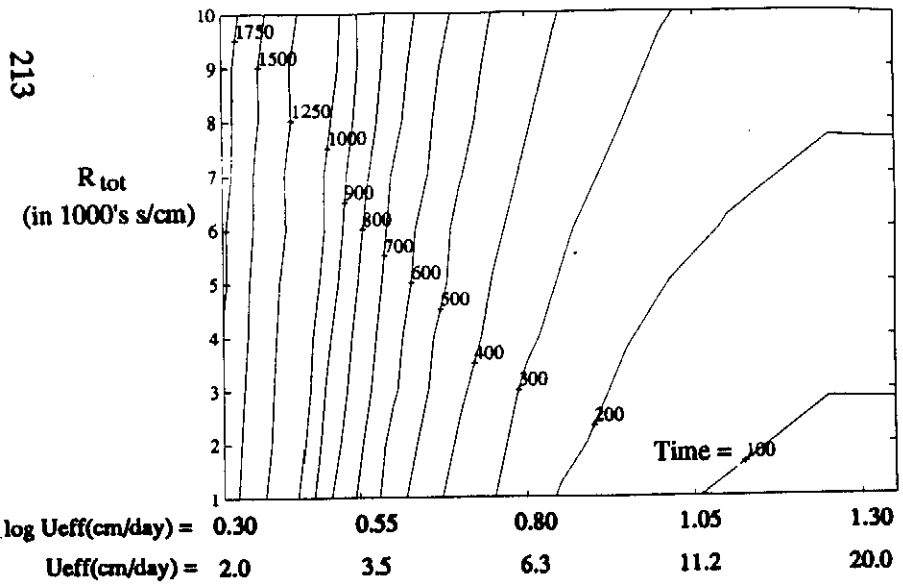

(d) Replacement time given $\frac{C_{well,min}}{C_o}$(phenanthrene) = 0.01 , $\frac{C_{well,max}}{C_o}$(phenanthrene) = 0.02

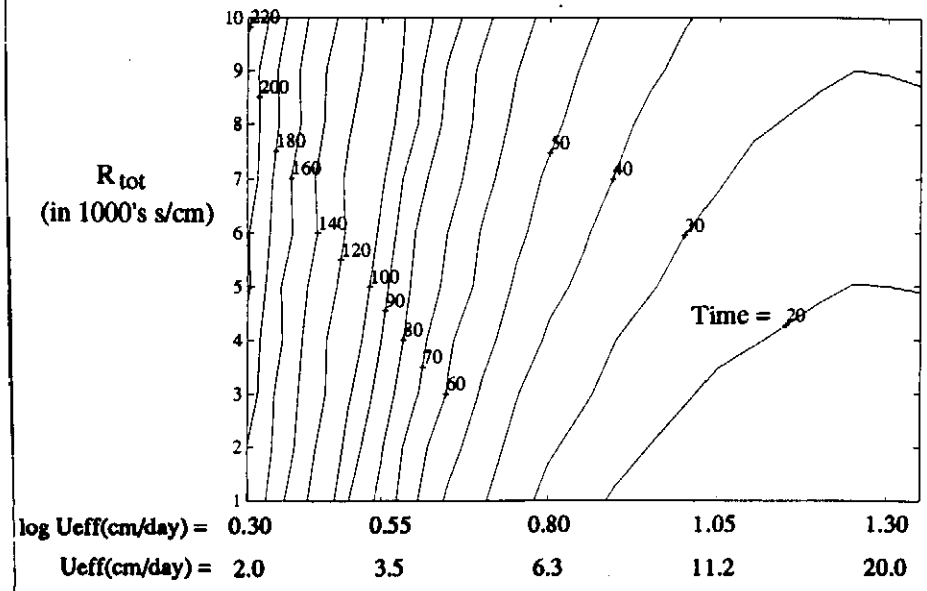

volume and effective solute velocity into the well, Equation 7-7 could be used to solve for solute concentration in the cylindrical well.

Other options for further system improvement include increasing the copolymer concentration of the membrane tube interior solution, M; but this must be balanced with the easy-handling advantage of a lower-viscosity soluion. Also, multiple well barriers may prove effective in certain situations where one rectangular well cannot provide sufficient concentration decrease. It should be emphasized that other factors to be considered in determining system workability include knowledge of groundwater flow direction and aquifer anisotropy. Knowledge of where a contaminated region is and in what direction it is flowing is crucial to any containment or remediation scheme.

8. Conclusions and Recommendations

Basic conclusions of this paper are organized according to the three main thesis objectives. The first objective of this work was to quantify the enhanced solubilization of three aromatic compounds – toluene, naphthalene, and phenanthrene -- in aqueous amphipathic copolymer solution. The copolymer used was N-vinylpyrrolidone/styrene (NVPS), a high molecular weight (3.4 million g/mol) random-structured copolymer. The experiments showed there is evidence of greatly enhanced solubilization of the organics in aqueous NVPS solution. Values of polymer-water partition coefficient, K_{pw}, were determined for the three solutes above in copolymer solution to quantify the ability of the copolymer to concentrate solute. K_{pw} is defined as follows:

$$K_{pw} \equiv \frac{\text{g solute in NVPS polymer / g polymer}}{\text{g solute in water / g water}} \tag{8-1}$$

Constant values of K_{pw} were determined from equilibrium data (Table 4-1) for the three solutes in NVPS solutions, and are as follows:

$$\log_{10} K_{pw} \text{ (toluene)} = 3.39 \pm 0.04 \tag{8-2}$$

$$\log_{10} K_{pw} \text{ (naphthalene)} = 3.38 \pm 0.01 \tag{8-3}$$

$$\log_{10} K_{pw} \text{ (phenanthrene)} = 4.69 \pm 0.02 \tag{8-4}$$

The deviations given correspond to the 95% confidence interval of the data sets. These values of partition coefficient for NVPS systems compare favorably to partition coefficients for other, lower molecular weight surfactant systems (Table 4-2). Two theoretical expressions of K_{pw} for use in prediting K_{pw} for other copolymer-solute systems were derived in Chapter 4 and are repeated here:

$$\log K_{pw} = \log v_w - \log \gamma_i^{*p} + \log \gamma_i^{w} - \log \frac{MW_{sol}}{1000} - \log R_p \qquad (4\text{-}12)$$

$$\log K_{pw} = \log K_{ow} + \log \gamma_i^{o} + \log v_o - \log \gamma_i^{*p} - \log \left(\frac{MW_{sol}}{1000}\right) - \log R_p \qquad (4\text{-}26)$$

where v_o and v_w are the molar volumes of pure octanol and water, respectively, at system temperature and pressure [L/mol]; superscripts p and w refer to the polymer and aqueous pseudophases, respectively; γ_i^{α} denotes the aqueous-phase activity coefficient of solute i in phase α; γ_i^{*p} is the activity coefficient of solute i in the polymer phase calculated on a *weight fraction* basis; MW_{sol} is the molecular weight of the solute [g/mol]; R_p is the ratio of polymer mass to polymer phase mass, the latter term including the mass of the solute partitioned into the polymer pseudophase; and K_{ow} is the octanol-water partition coefficient of the solute i, defined as follows:

$$K_{ow} \equiv \frac{\text{g solute in octanol-rich phase / mL octanol}}{\text{g solute in water-rich phase / mL water}} \qquad (8\text{-}5)$$

Values of K_{ow} are available for a wide variety of solutes (Lyman, 1990). Values of K_{pw} were predicted for the NVPS-solute systems studied here. The predictions compared to within about a factor of two of the experimental data.

It should be emphasized that this solubilization information is important to other organic-contaminated water treatment processes. Since NVPS is a very high molecular weight copolymer, it can be easily filtered from water, allowing concentration and separation of organic solute from an originally dilute aqueous solution.

The second objective of this thesis was to quantify the rate of molecular diffusive transport of the aromatic solutes through anisotropic hollow fiber membranes into an aqueous copolymer solution. Diffusion experiments showed that mass transfer of naphthalene and phenanthrene through anisotropic membrane can be predicted using a Fickian, aqueous-phase molecular diffusion model. Experiments were conducted using a well-mixed solution exterior to the membrane tubes kept at constant solute concentration, C_{sat}. The value of C_{sat} refers to the concentration of solute in pure water at the solute's saturation limit. The solution for solute concentration in the interior copolymer solution, C_{int}, in contact with a constantly solute-saturated exterior solution is as follows:

$$\frac{C_{int}}{C_{sat}} = (1 - e^{-Bt})(1 + M K_{pw}) \qquad (8\text{-}6)$$

$$\text{where } B = \frac{A_t}{V_t R_{tot}(1 + M K_{pw})};$$

M is the polymer to water mass ratio for the interior copolymer solution [g/g]; K_{pw} is the polymer-water partition coefficient for the solute; A_t is membrane tube surface area [cm^2], V_t is membrane tube volume [cm^3]; and R_{tot} is the total resistance to molecular diffusive transport posed by the membrane [s/cm].

Values of R_{tot} were obtained from the diffusion data for the polysulfone membrane tubes used in these experiments (each tube has 0.1-0.2μm-thick skin layer bound to a 0.275mm-thich support structure). These values are as follows:

Table 8-1: Measured Membrane Resistances

Solute	Membrane MW Cutoff	R_{tot} (s/cm)
Naphthalene	2000	4980 ± 120
Naphthalene	50,000	4630 ± 210
Naphthalene	Pooled Data	4950 ± 100
Phenanthrene	2000	6020 ± 100
Phenanthrene	50,000	5950 ± 140
Phenanthrene	Pooled Data	5990 ± 70

The variances shown are 95% confidence intervals determined from the data fits. The experimental values for R_{tot} correspond very closely to the independently-predicted resistances for the experimental systems (to within 15%).

The membrane skin layer resistance to solute transmembrane molecular diffusion was much less than the resistance posed by the thicker membrane support structure for the systems studied here. This statement is supported by both the resistance data and the resistance models. Therefore, using a thinner support structure can significantly decrease the resistance to transmembrane solute diffusion, thus increasing system efficiency.

The third objective of this work was the demonstration of the proposed membrane/copolymer remediation system on a laboratory-scale. The extraction of solute from an aqueous naphthalene plume moving through a soil matrix was demonstrated in two types of system set-ups -- one with a rectangular well, and one with a cylindrical well.

In the rectangular well experiment, the capture of naphthalene from an *initially naphthalene-saturated* lab-scale aquifer was demonstrated experimentally, and well concentration was modeled as a function of time. The match of the well concentration data with the modeled values was affected by desorption of naphthalene from well surfaces.

In the cylindrical well experiment, the capture of naphthalene from an *initially "clean"* lab-scale aquifer was demonstrated experimentally and well concentration was modeled as a function of time. Also, the naphthalene concentration of the plume leaving the cylindrical treatment well was modeled as a function of time and two-dimensional space. Well concentration data agreed well with model predictions (within 20%). The 2-D concentration data also agreed well with model predictions (within 20%). The modeled 2-D concentration profile of the plume leaving the well was more strongly influenced by the velocity field solution than by the soil dispersion coefficients. Thus, for groundwater flow through a cylindrical well of diameter D, the decreased concentration plume has width approximately 2 times the diameter.

Recommended future work related to this thesis includes the development of the proposed system from lab-scale to field-scale. The effects on the proposed remediation system of naturally-occurring humic substances, multicomponent-contaminant systems, and membrane fouling and degradation should be investigated before implementation of the proposed system in the field. The application of the proposed system to cases where contaminated groundwater is actively pumped is another possible area of research.

A study in the improvement of transmembrane diffusion rates and system efficiency should be undertaken; of concern is the minimum required thickness of the membrane support structure for system durability. Membranes with thinner support structures have the potential for improving system efficiency significantly.

Further solubilization studies of systems using NVPS and like copolymers should be undertaken. This study has shown NVPS is a very effective organic solubilizer (compared with currently-used surfactants), and it is available in extremely high molecular weights (over 3 million g/mol). This allows for great flexibility in filtration techniques for solute separation. Thus, the use of NVPS and similar amphipathic copolymers as easily-separable organic filtrants should be investigated for other model organic contaminants not studied in this work. Also, studies of ways to regenerate organic-saturated NVPS -type copolymers would be important in improving the cost efficiency of a proposed organic filtration system. Possible regeneration techniques include solvent extraction for non-volatile solutes and evaporation for volatile organic solutes.

9. Nomenclature

A = Absorbance reading of spectrophotometer [dimensionless]

A_{tot} = overall surface area of membrane [cm^2]

C = aqueous phase solute concentration [g/cm^3]

C_{aqu} = solute concentration in aqueous solution [g/cm^3]

$C_E(m)$ = solute concentration at the node directly east of position i [g/cm^3]

C_{ext} = concentration of solute in exterior bulk solution [g/cm^3]

$C_i(m)$ = solute concentration at node i and time step m [g/cm^3]

C_{int} = aqueous phase concentration of solute in interior bulk solution [g/cm^3]

$C_{int,aq}$ = aqueous phase concentration of solute in interior bulk solution [g/cm^3]

$C_{int,p}$ = polymer pseudophase concentration of solute in interior solution [g/cm^3]

$C_N(m)$ = solute concentration at the node directly north of position i [g/cm^3]

$C_S(m)$ = solute concentration at the node directly south of position i [g/cm^3]

$C_W(m)$ = solute concentration at the node directly west of position i [g/cm^3]

C_{well} = solute concentration in well fluid [g/cm^3]

$C_{well,max}$ = required maximum allowable solute concentration of well fluid [g/cm^3]

$C_{well,min}$ = required minimum solute concentration of well fluid [g/cm^3]

D = membrane tube inner diameter [cm]

D = dispersion coefficient [cm^2/s]

D^* = molecular diffusion coefficient for solute in water [cm^2/s]

D_{AB} = aqueous phase molecular diffusion coefficient of solute A in solvent B [cm^2/s]

D_l = dispersion coefficient in longitudinal direction [cm^2/s]

$D_{md,AB}$ = aqueous phase molecular diffusion coefficient of solute A in solvent B

[cm^2/s]

$D_{sd,AB}$ = solid phase molecular diffusion coefficient of solute A in solid B [cm^2/s]

D_t = dispersion coefficient in transverse direction [cm^2/s]

D_x = dispersion coefficient in the x-direction [cm^2/s]

D_y = dispersion coefficient in the y-direction [cm^2/s]

d_c = membrane tube outer diameter [cm]

Del P = pressure difference from entrance to exit of membrane interior [inches water]

F = net flux of contaminant (flux vector) [$g/cm^2\ s$]

F_{conv} = solute flux via convection [$g/cm^2\ s$]

F_{fbl} = solute flux through fluid boundary layer [$g/cm^2\ s$]

F_{md} = solute flux via molecular diffusion [$g/cm^2\ s$]

F_{sd} = solute flux via solid-phase diffusion [$g/cm^2\ s$]

F_{tot} = total solute flux [$g/cm^2\ s$]

f_{om} = organic matter fraction of aquifer material [dimensionless]

g = acceleration due to gravity [cm/s^2]

G' = average fluid mass flux [$g/cm^2\ s$]

h = hydraulic head [cm/cm]

h = time interval [s]

h = water level in tank [cm]

k = membrane permeability [cm^2]

k = x-direction spatial interval [cm]

K_d = solid-liquid contaminant partition coefficient $\left[\frac{g/g}{g/cm^3}\right]$

K_{ow} = octanol-water partition coefficient $\left[\frac{g/cm^3}{g/cm^3}\right]$

K_{pw} = polymer-water partition coefficient $\left[\frac{g/g}{g/g}\right]$

K_{sw} = surfactant-water partition coefficient $\left[\frac{g/g}{g/g}\right]$

l = pathlength of spectrophotometer cell [cm]

l = y-direction spatial interval [cm]

L = length of tank [cm]

L = concentration (loading) of solute in polymer [g /g]

l_d = fluid flow distortion length [cm]

L_t = membrane tube length [cm]

M = weight ratio of polymer to water [g/g]

n = porosity of aquifer [dimensionless]

P = fluid pressure [g/cm s^2]

P_{atm} = atmospheric air pressure [g/cm s^2]

Pe = heat transfer Peclet number [dimensionless]

Pe_g = grid Peclet number $= \frac{Lu_x}{D_x}$ [dimensionless]

Pe_x = Peclet number calculated for the x-direction = $\frac{Lu_x}{D_x}$ [dimensionless]

Pe_y = Peclet number claculated for the y-direction $= \frac{Lu_x}{D_y}$ [dimensionless]

Pr = Prandtl number [dimensionless]

P_s = solution pressure [g/cm s^2]

Q = volumetric flowrate [mL/min]

q = velocity field solved in cylindrical coordinate system [cm/s]

q = membrane-adsorbed solute concentration [g/cm^3]

R = well radius [cm]

r = rate of solute transfer from aqueous to polymer pseudophase [g/cm^3 s]

R_d = retardation coefficient [dimensionless]

Re = Reynolds number [dimensionless]

R_i = resistance of film layer i [s/cm]

R_t = total diffusive transport resistance [s/cm]

R_{tot} = total diffusive transport resistance [s/cm]

R_v = volumetric rate of formation of contaminant [g/cm^3 s]

R_1 = mass transfer resistance of membrane support layer [cm/s]

R_2 = mass transfer resistance of membrane skin layer [cm/s]

R_3 = mass transfer resistance of interior fluid boundary layer [cm/s]

R_4 = mass transfer resistance of exterior fluid boundary layer [cm/s]

S = mass of contaminant adsorbed to aquifer solids per mass of aquifer solids [g/g]

Sh = Sherwood number [dimensionless]

T_I = transmissivity of domain I [cm^2/s]

T_{II} = transmissivity of domain II [cm^2/s]

$\mathbf{u}$ = velocity vector [cm/s]

$\hat{u}$ = effective solute velocity through soil matrix = $\frac{u_x}{R_d}$ [cm/s]

u_{eff} = effective solute velocity through soil matrix = $\frac{u_x}{R_d}$ [cm/s]

u_l = unidirectional groundwater velocity [cm/s]

u_x = x-component of velocity vector [cm/s]

u_y = y-component of velocity vector [cm/s]

V = average velocity of fluid through tubing [cm/s]

V_{ext} = volume of solution exterior to membrane [cm^3]

V_{int} = volume of solution interior to membrane [cm^3]

V_t = volume of solution interior to membrane [cm^3]

W = width of tank [cm]

x = position along x-axis [cm]

x = membrane tube length [cm]

α = thermal diffusivity [cm^2/s]

α_l = longitudinal dispersivity [cm]

α_t = transverse dispersivity [cm]

δ_i = *effective film thickness [cm]*

δ_{mem} = overall thickness of membrane tube [cm]

δ_1 = membrane support layer thickness [cm]

δ_2 = membrane skin layer thickness [cm]

ΔP_{tm} = transmembrane pressure difference [inches water]

ε = membrane support layer porosity [dimensionless]

ε_b = Beer's law extinction coefficient [cm^2/g]

ε_2 = membrane skin layer poroisty [dimensionless]

μ = solution viscosity [g/cm s]

ϕ = ratio of pure solute concentration to bulk phase concentration [d'less]

ρ = fluid density [g/cm^3]

ρ_b = bulk density of aquifer [g/cm^3]

ρ_w = density of water [g/cm^3]

τ = membrane tortuosity [dimensionless]

τ_2 = membrane skin layer tortuosity [dimensionless]

Ω = normalized interior solution concentration [cm]

10. Appendices

Appendix A – Data from Naphthalene Diffusion Experiments

Data from each of the naphthalene transmembrane diffusion runs described in Chapter 5 are listed here in Tables A-1 to A-5. Graphs of the C_{int}/C_{sat} data versus time are in Figures A-1 to A-5 (figure numbers correspond to the table numbers). Curve fits of the data using Equation 5-21 are shown for each run. In all cases, the value of C_{ext}/C_{sat} was maintained at 1.0 throughout the run. Tables include all constants used in determining the normalized concentration, Ω, and the expression of Ω for each run.

Table A-1: May 19, 1992 Run – Naphthalene Diffusion Through 2000 MW Cutoff Membrane

Time (sec)	C/C_{sat}	$\Omega = -\ln\left[1 - \frac{C/C_{sat}}{13.430}\right] / 0.62$
0	0	0
600	0.765	0.095
900	1.148	0.144
1500	2.295	0.302
2100	3.060	0.417
2700	3.443	0.478
3300	3.826	0.541
3900	4.591	0.675
4500	6.121	0.981
5100	6.121	0.981
6900	7.651	1.360
8700	8.416	1.589

Constants:

$A_t = 2.06\ cm^2/tube$

$V_t = 0.247\ cm^3/tube$

$M = 0.00514$

$K_{pw} = 2420$

$N = 308\ tubes$

Figure A-1: May 19, 1992 Run -- Naphthalene Diffusion Through 2000 MW Cutoff Membrane

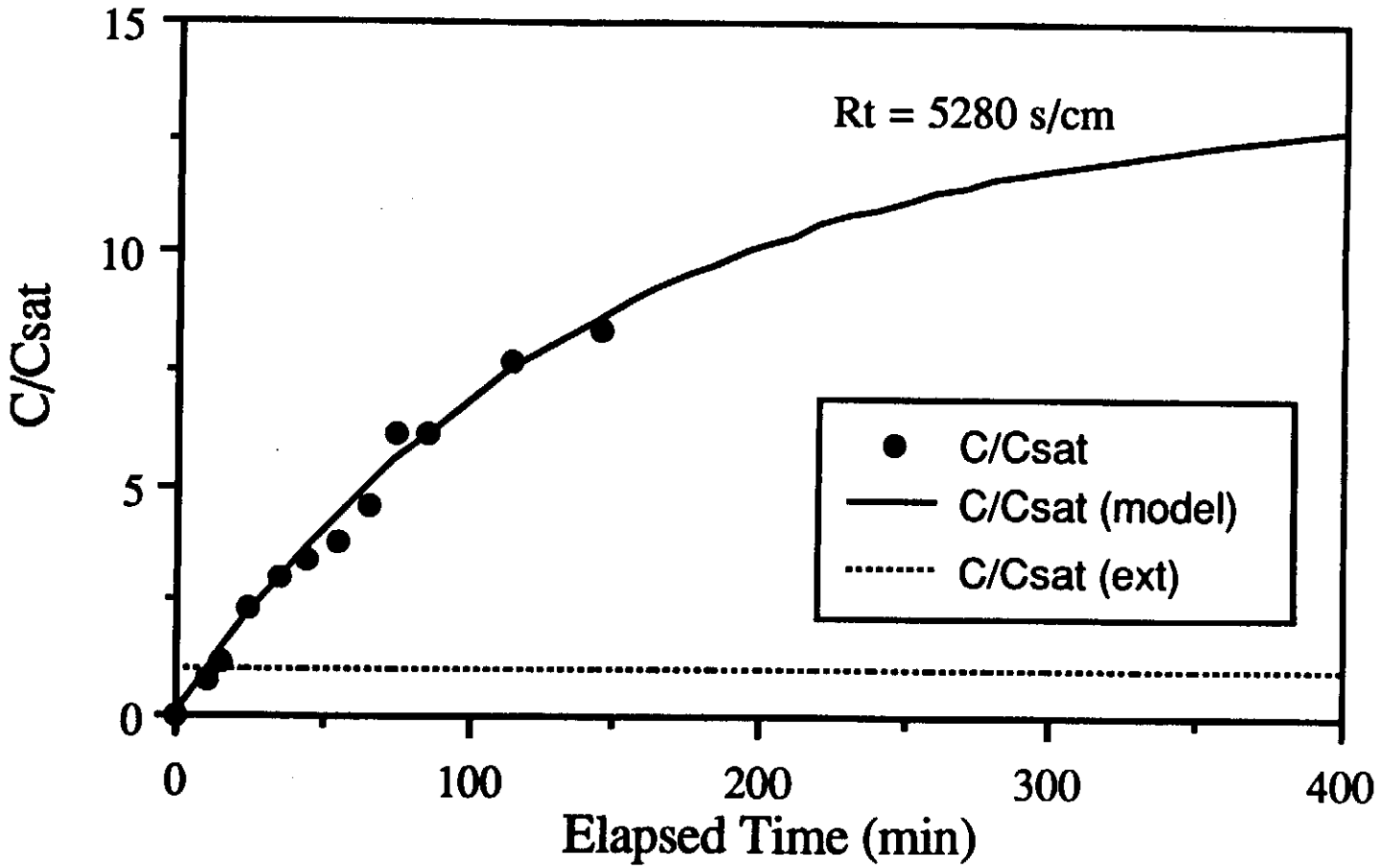

Table A-2: May 25, 1992 Run – Naphthalene Diffusion Through 2000 MW Cutoff Membrane

Time (sec)	C/C_{sat}	$\Omega = -\ln\left[1 - \frac{C/C_{sat}}{11.684}\right] / 0.56$
0	0	0
600	0.769	0.121
900	1.154	0.185
2100	2.308	0.392
2700	3.077	0.545
4800	4.615	0.896
6000	5.385	1.102

Constants:

$A_t = 2.06\ cm^2/tube$

$V_t = 0.315\ cm^3/tube$

$M = 0.00441$

$K_{pw} = 2420$

$N = 308$ tubes

Figure A-2: May 25, 1992 Run -- Naphthalene Diffusion Through 2000 MW Cutoff Membrane

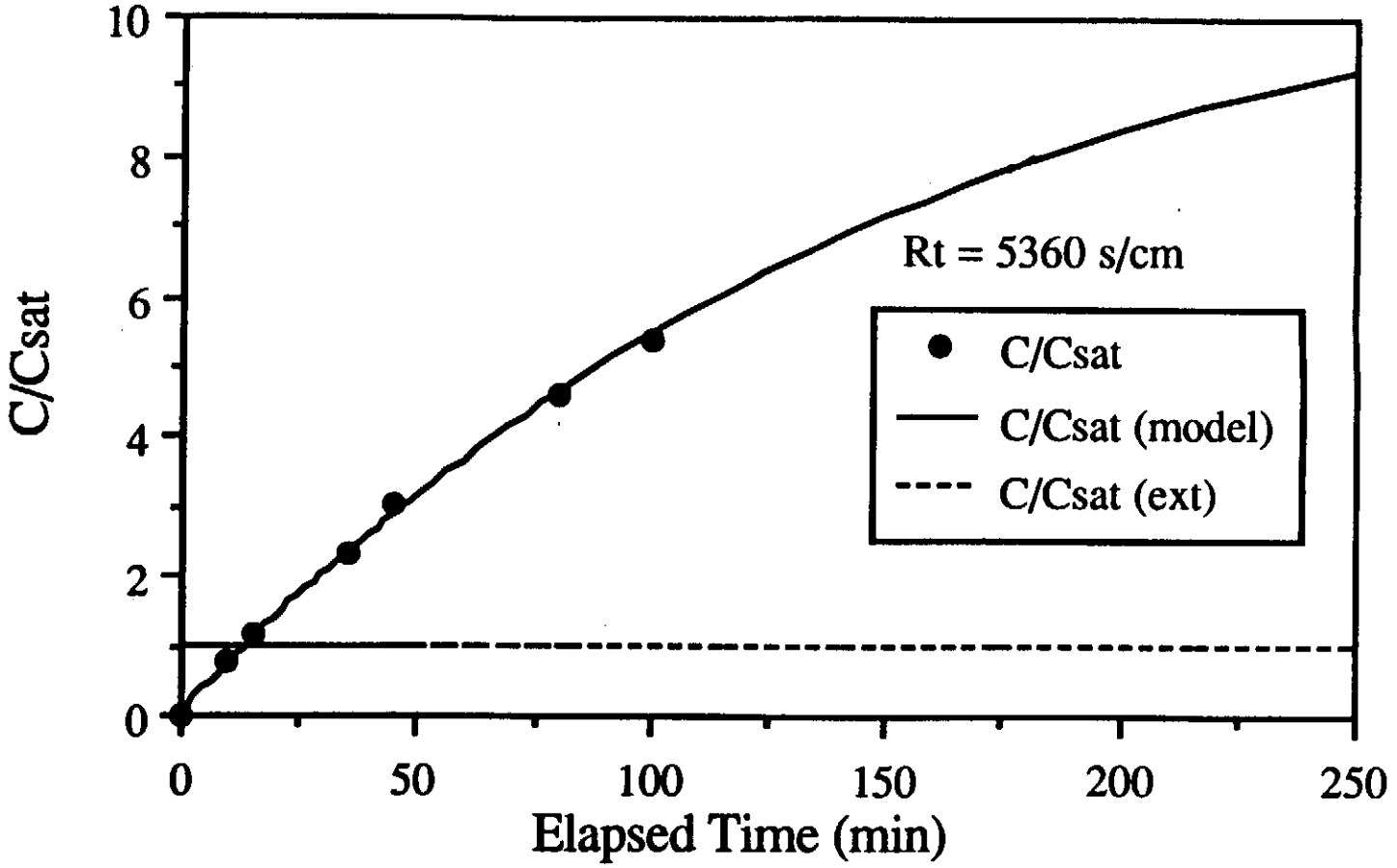

Table A-3: June 29, 1992 Run – Naphthalene Diffusion Through 2000 MW Cutoff Membrane

Time (sec)	C/C_{sat}	$\Omega = -\ln [1 - \frac{C/C_{sat}}{67.131}] / 0.122$
0	0	0
1560	2.266	0.282
2160	3.021	0.378
3180	3.776	0.475
3840	5.287	0.673
4860	7.553	0.979
5940	9.819	1.296
7020	11.329	1.515
8520	14.350	1.972
9840	15.483	2.150
10860	16.239	2.271
11700	16.616	2.332
13080	18.882	2.708
13920	20.393	2.969
15840	21.148	3.102
16740	21.903	3.238
18720	24.169	3.659

Constants:

$A_t = 2.06\ cm^2/tube$

$V_t = 0.252\ cm^3/tube$

$M = 0.0273$

$K_{pw} = 2420$

$N = 308\ tubes$

Figure A-3: June 29, 1992 Run -- Naphthalene Diffusion Through 2000 MW Cutoff Membrane

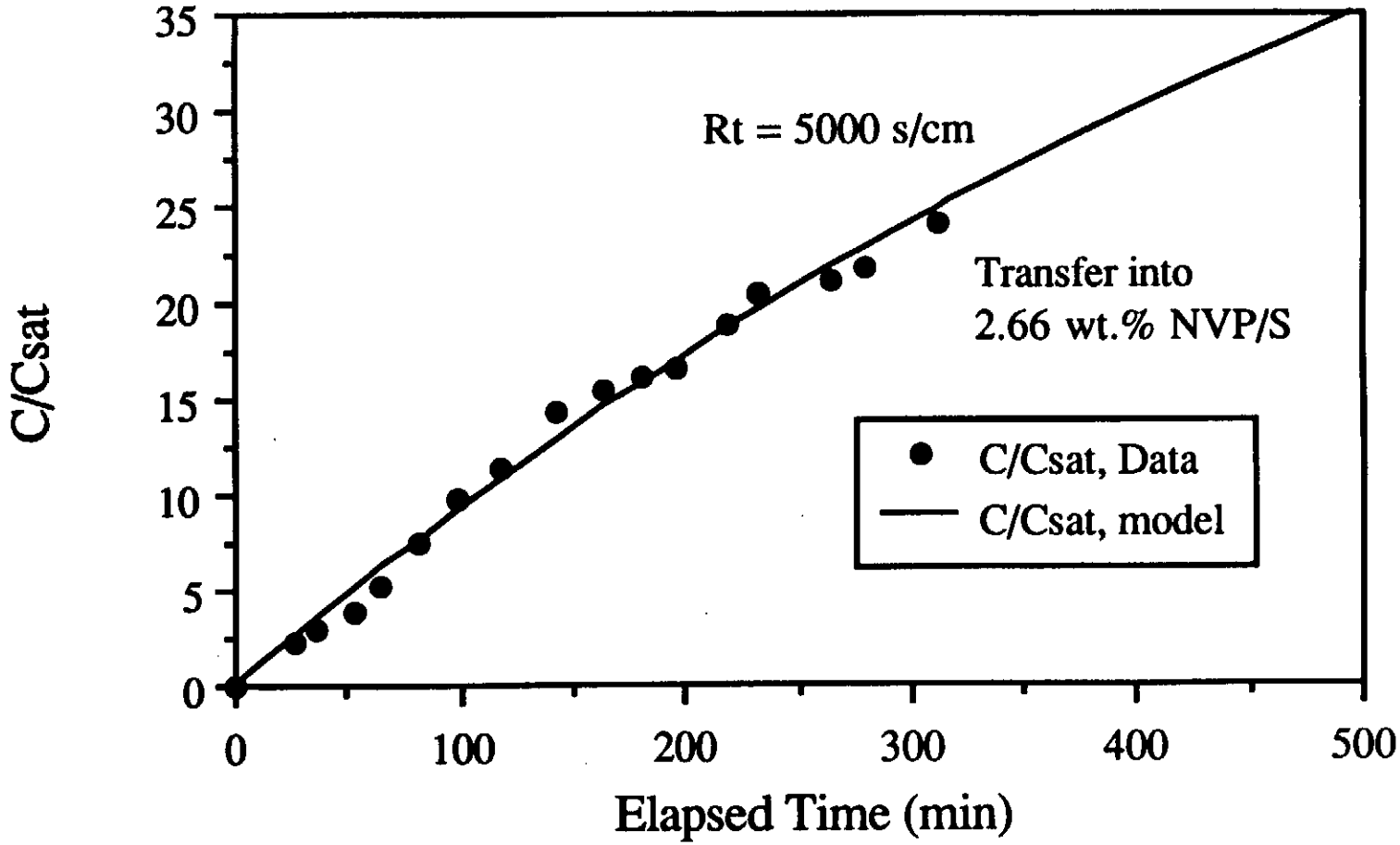

Table A-4: June 23, 1992 Run -- Naphthalene Diffusion Through 50,000 MW Cutoff Membrane

Time (sec)	C/Csat	$\Omega = -\ln\left[1 - \frac{C/C_{sat}}{15.975}\right] / 0.473$
0	0	0
900	1.100	0.151
1500	2.206	0.314
2100	2.941	0.430
2700	3.676	0.553
3300	4.044	0.617
3600	4.412	0.683

Constants:

$A_t = 2.06\ cm^2/tube$

$V_t = 0.273\ cm^3/tube$

$M = 0.00619$

$K_{pw} = 2420$

$N = 308$ tubes

Figure A-4: June 23, 1992 Run -- Naphthalene Diffusion Through 50,000 MW Cutoff Membrane

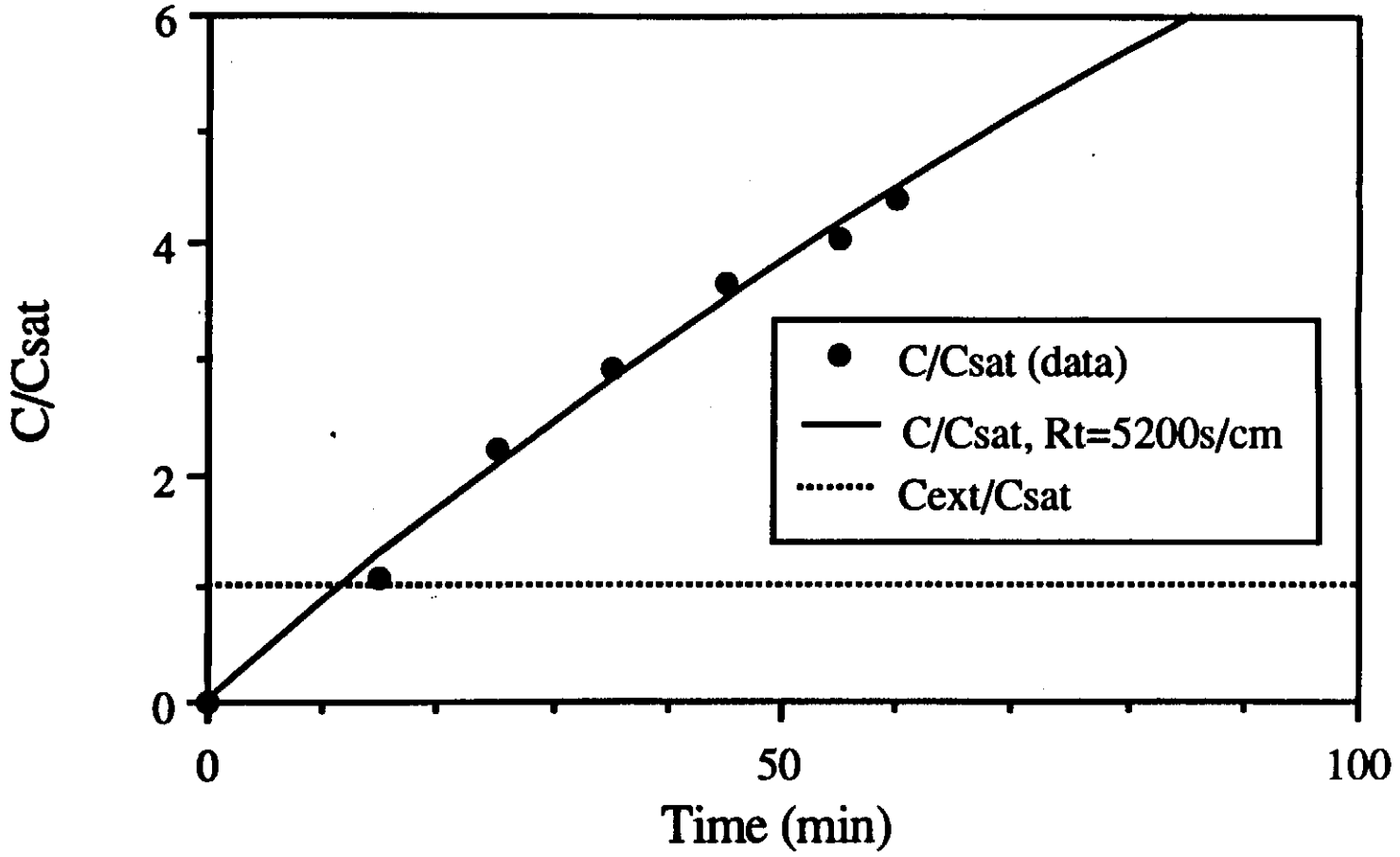

Table A-5: June 18, 1992 Run -- Naphthalene Diffusion Through 2000 MW Cutoff Membrane

Time (sec)	C/C_{sat}	$\Omega = -\ln\left[1 - \frac{C/C_{sat}}{16.625}\right] / 0.455$
0	0	0
1500	2.250	0.319
2100	3.371	0.498
2700	4.496	0.693
3600	5.245	0.833
3900	5.995	0.983
5400	6.746	1.144
7200	8.334	1.529
8100	9.168	1.762

Constants:

$A_t = 2.06\ cm^2/tube$

$V_t = 0.272\ cm^3/tube$

$M = 0.00646$

$K_{pw} = 2420$

$N = 308\ tubes$

Figure A-5: June 18, 1992 Run -- Naphthalene Diffusion Through 50,000 MW Cutoff Membrane

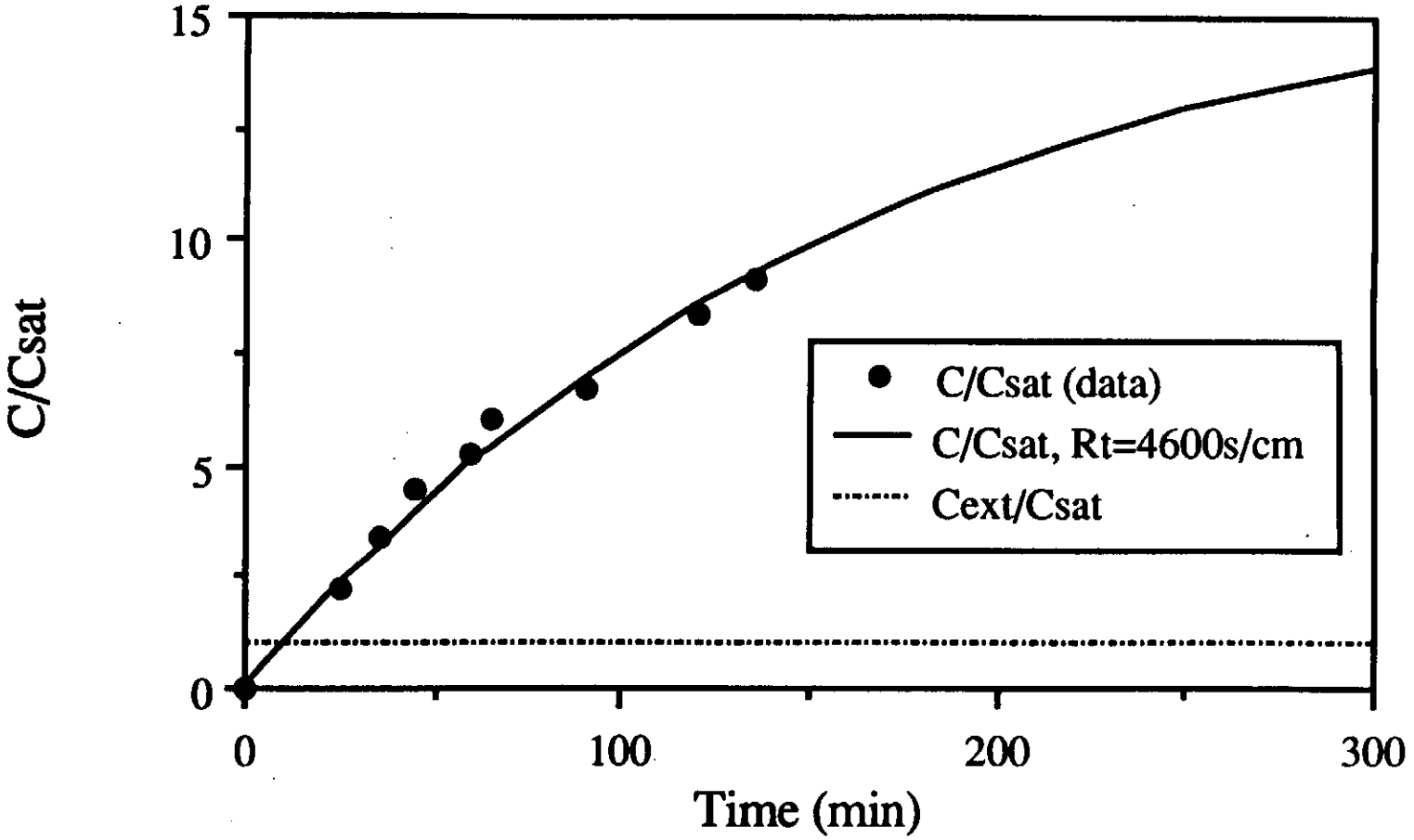

Appendix B -- Data from Phenanthrene Diffusion Experiments

Data from each of the phenanthrene transmembrane diffusion runs described in Chapter 5 are listed here in Tables B-1 to B-5. Graphs of the C_{int}/C_{sat} data versus time are in Figures B-1 to B-5 (figure numbers correspond to the table numbers). Curve fits of the data using Equation 5-21 are shown for each run. In all cases, the value of C_{ext}/C_{sat} was maintained at 1.0 throughout the run. Tables include all constants used in determining the normalized concentration, Ω, and the expression of Ω for each run.

Table B-1: July 17, 1992 Run -- Phenanthrene Diffusion Through 2000 MW Cutoff Membrane

Time (sec)	C/C_{sat}	$\Omega = -\ln\left[1 - \frac{C/C_{sat}}{203.3}\right] / 0.03689$
0	0	0
1140	1.50	0.201
1500	2.00	0.268
1800	2.25	0.302
2400	3.00	0.403
2880	3.50	0.471
3300	4.25	0.573
3900	5.00	0.675
5300	6.50	0.881
6000	7.50	1.019
8100	10.00	1.367

Constants:

$A_t = 2.06\ cm^2/tube$

$V_t = 0.275\ cm^3/tube$

$M = 0.00412$

$K_{pw} = 49{,}100$

$N = 308\ tubes$

Table B-2: July 23, 1992 Run -- Phenanthrene Diffusion Through 2000 MW Cutoff Membrane

Time (sec)	C/C_{sat}	$\Omega = -\ln\left[1 - \frac{C/C_{sat}}{289.2}\right] / 0.03083$
0	0	0
1680	2.50	0.282
1980	3.00	0.339
2280	3.375	0.382
2580	3.625	0.410
3060	4.50	0.510
3660	5.25	0.596
5280	7.75	0.884
6780	9.25	1.058
8280	11.25	1.291

Constants:

$A_t = 2.06\ cm^2/tube$

$V_t = 0.231\ cm^3/tube$

$M = 0.00587$

$K_{pw} = 49{,}100$

$N = 308\ tubes$

Figure B-2: July 23, 1992 Run -- Phenanthrene Diffusion Through 2000 MW Cutoff Membrane

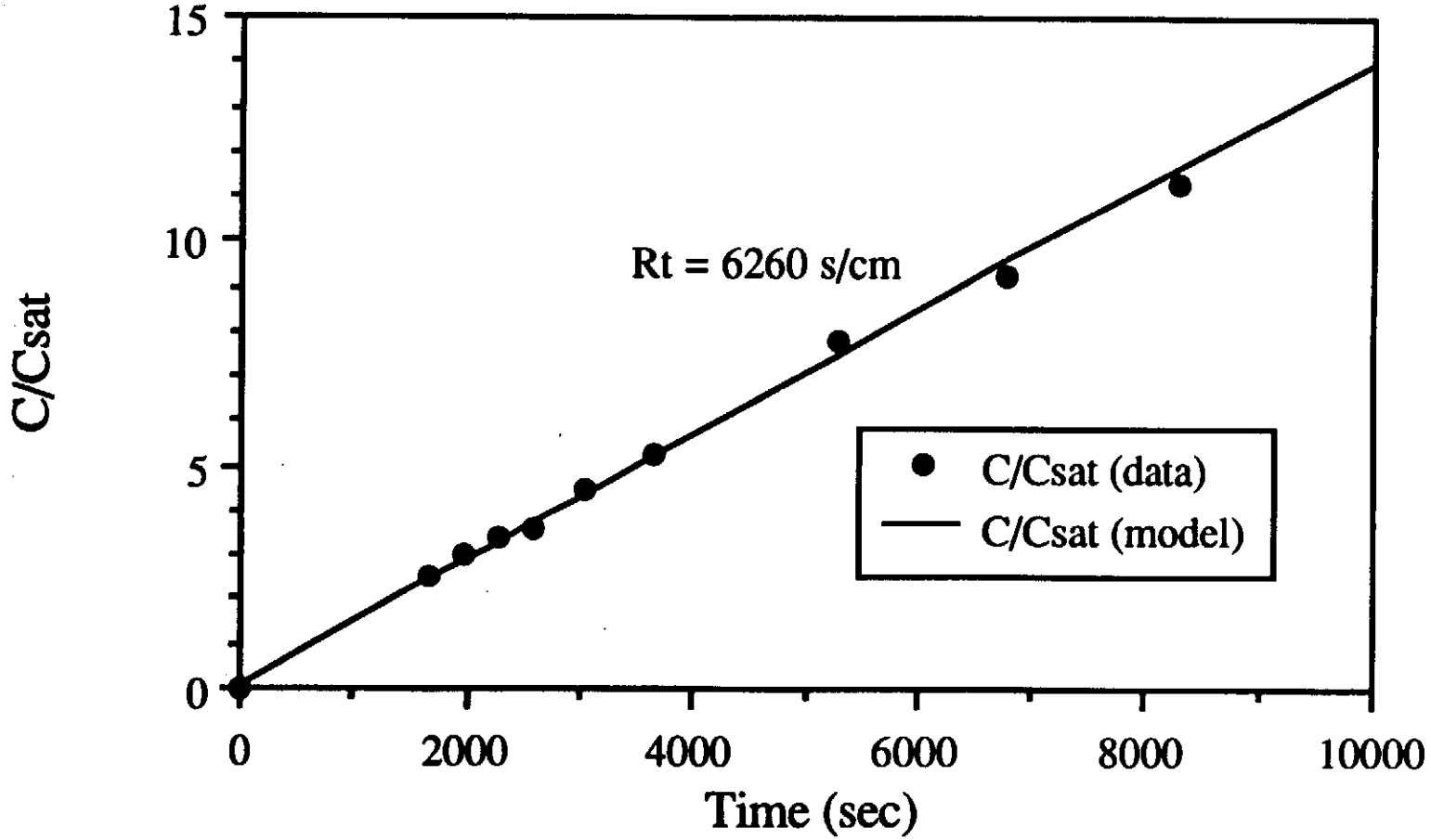

Table B-3: July 24, 1992 Run -- Phenanthrene Diffusion Through 2000 MW Cutoff Membrane

Time (sec)	C/C_{sat}	$\Omega = -\ln [1 - \frac{C/C_{sat}}{204.0}] / 0.03838$
0	0	0
1440	1.75	0.224
1800	2.25	0.289
2640	3.50	0.451
3240	4.00	0.516
3840	5.00	0.647
4860	6.50	0.844
5340	7.00	0.910
7140	9.50	1.243

Constants:

$A_t = 2.06\ cm^2/tube$

$V_t = 0.263\ cm^3/tube$

$M = 0.00413$

$K_{pw} = 49{,}100$

$N = 308$ tubes

Figure B-3: July 24, 1992 Run -- Phenanthrene Diffusion Through 2000 MW Cutoff Membrane

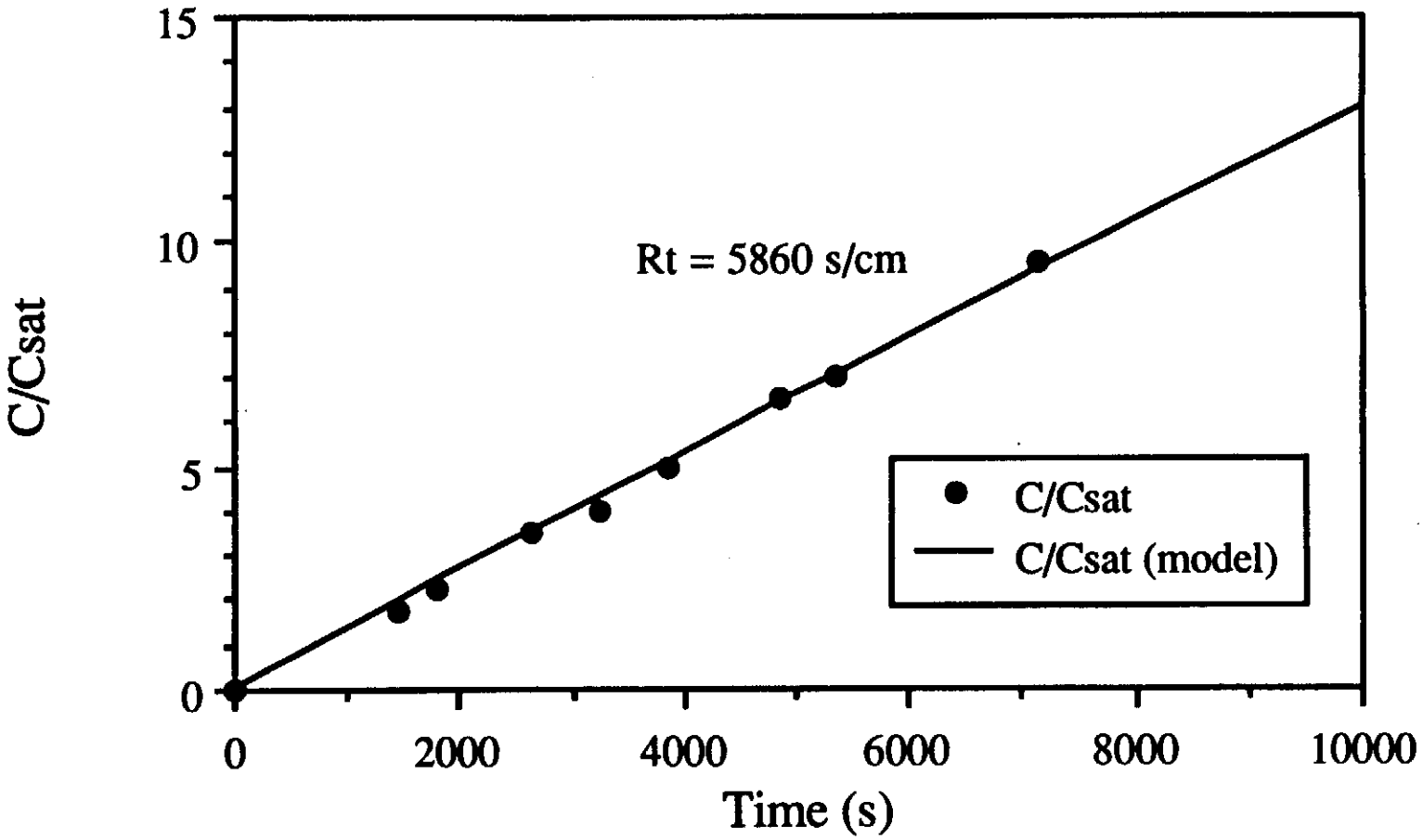

Table B-4: July 30, 1992 Run -- Phenanthrene Diffusion Through 50,000 MW Cutoff Membrane

Time (sec)	C/C_{sat}	$\Omega = -\ln\left[1 - \frac{C/C_{sat}}{218.7}\right] / 0.03682$
0	0.	0
420	0.578	0.072
780	0.867	0.108
1440	2.023	0.252
2160	2.890	0.361
2580	3.468	0.434
4320	5.780	0.727
5520	6.936	0.875
6120	8.092	1.024

Constants:

$A_t = 2.06\ cm^2/tube$

$V_t = 0.256\ cm^3/tube$

$M = 0.00443$

$K_{pw} = 49{,}100$

$N = 308$ tubes

Figure B-4: July 30, 1992 Run -- Phenanthrene Diffusion Through 50,000 MW Cutoff Membrane

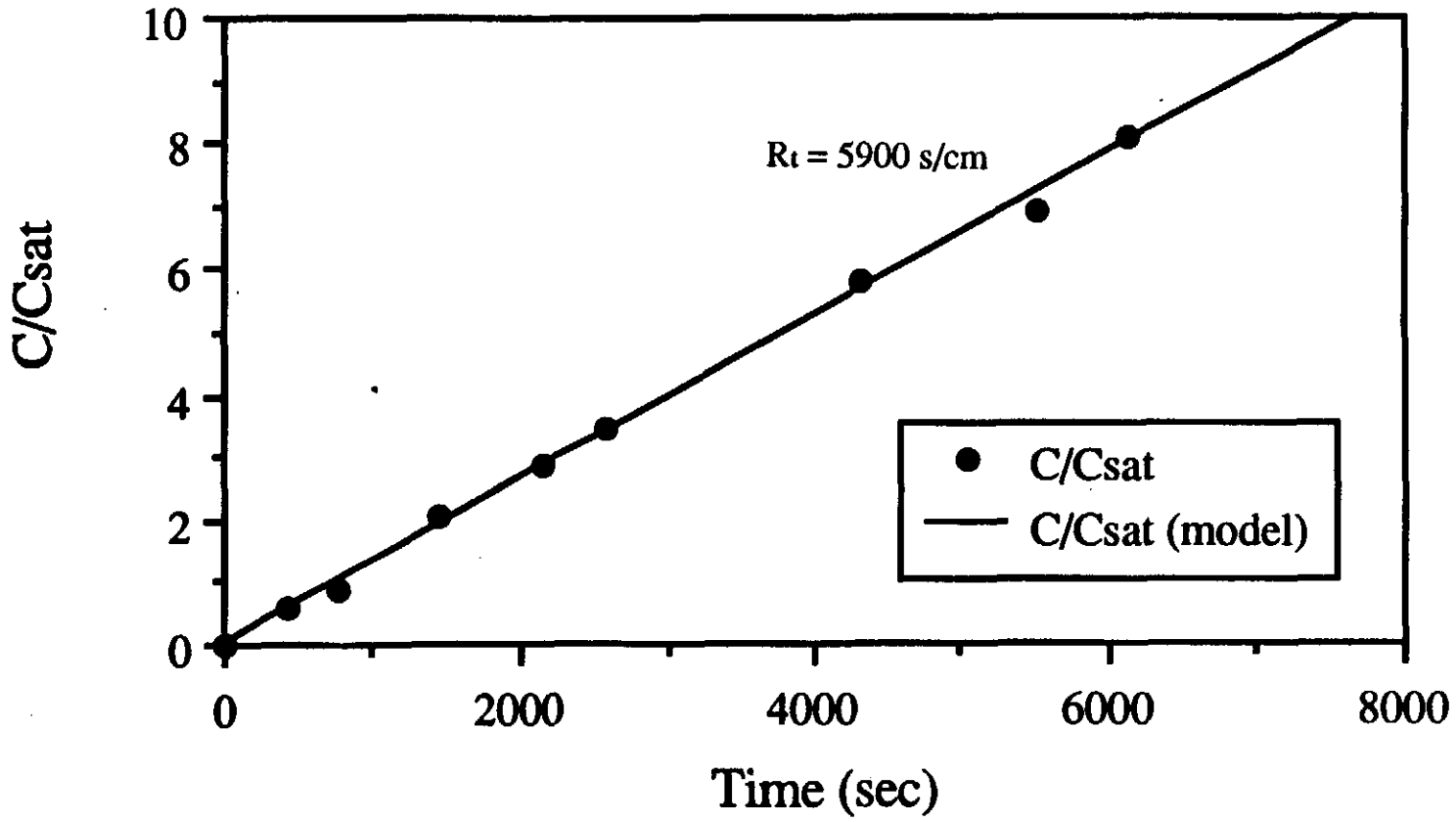

Table B-5: July 31, 1992 Run -- Phenanthrene Diffusion Through 50,000 MW Cutoff Membrane

Time (sec)	C/C_{sat}	$\Omega = -\ln\left[1 - \frac{C/C_{sat}}{218.7}\right] / 0.03682$
0	0.	0
1200	1.25	0.183
1500	1.875	0.274
3000	3.75	0.552
4410	5.00	0.738
5340	6.25	0.926

Constants:

$A_t = 2.06\ cm^2/tube$

$V_t = 0.300\ cm^3/tube$

$M = 0.00367$

$K_{pw} = 49{,}100$

$N = 308$ tubes

Figure B-5: July 31, 1992 Run -- Phenanthrene Diffusion Through 50,000 MW Cutoff Membrane

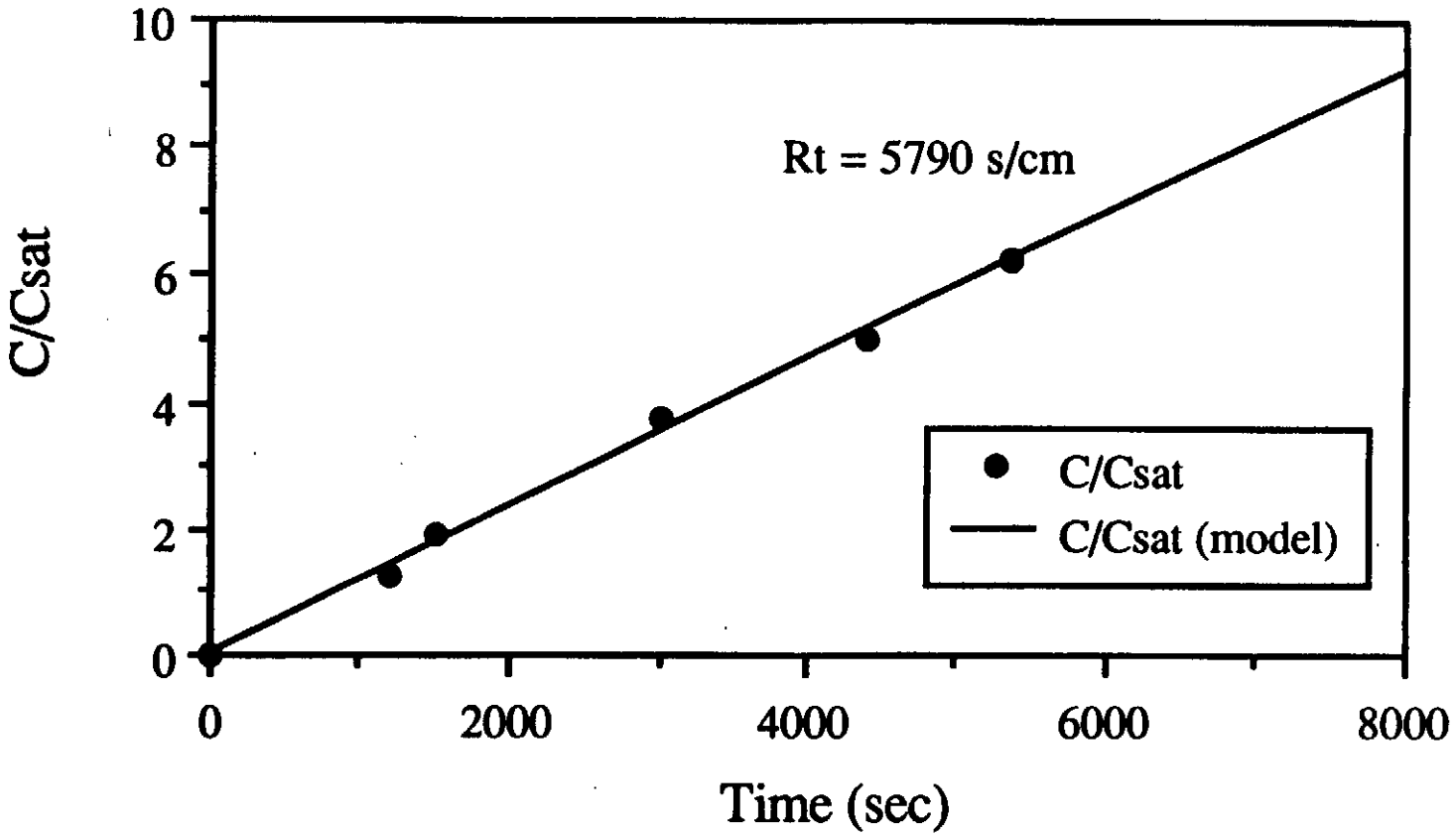

Appendix C -- Computer Code for Numerical Solution of 2-D Concentration Profile

Attached is the fortran computer code for the numerical solution of the two-dimensional concentration profile in Chapter 6. The concentration is solved at 12,553 nodes and at a given number of time steps. The numbering of the nodes in the problem domain is illustrated in Figure C-1. The solution was assumed symmetric about the y=0 axis in order to reduce the required number of nodal equations to be solved.

Figure C-1: Nodal arrangement for 2-D Numerical Solution

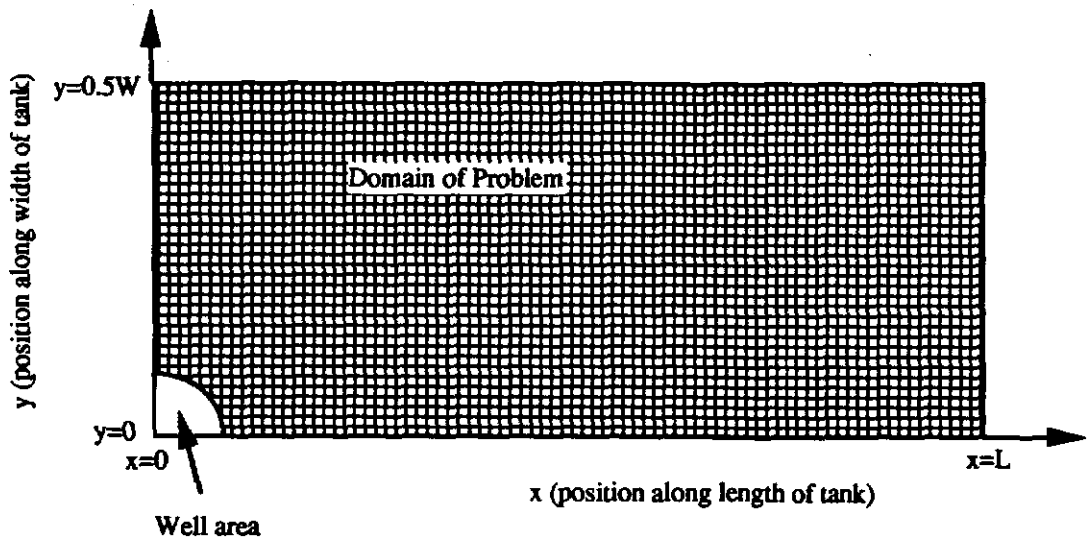

There are 106 nodes along the x-direction,
and 120 nodes along the y-direction.
There are 12,553 nodes in all.

Nodes are numbered from the lower left-hand corner
from left to right, then up to the next row.

The interval lengths are changeable.

Nodes are numbered around the well area as shown below.

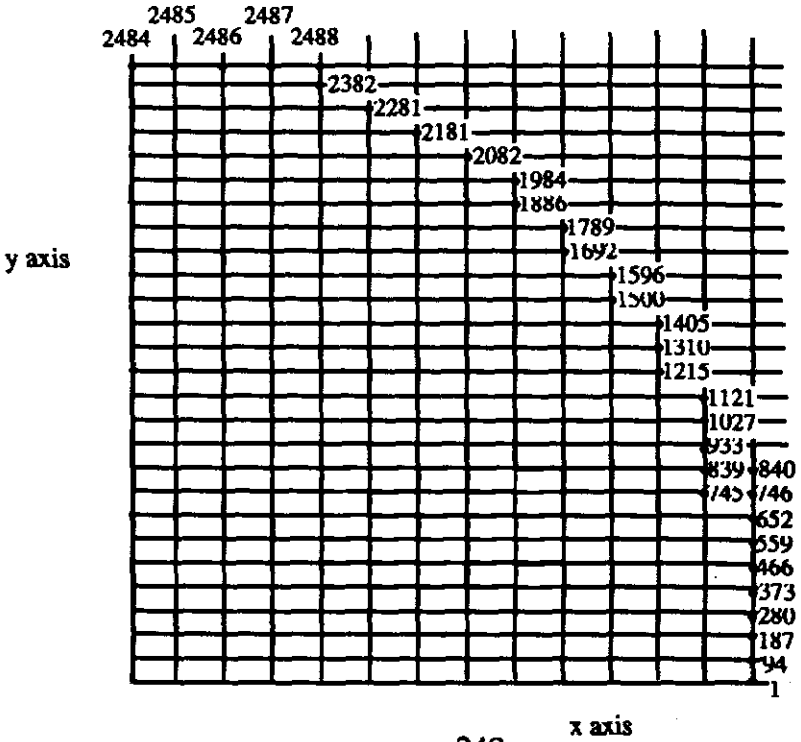

```
c Fortran Program "2D.F"
c by Bill Haulbrook
c February 1993

c This program outputs c/csat at various locations within and on the
c 2-D boundary used in the 2-D tank exeriment in January 1993.  The
c leading edge boundary introduces contaminant to the 2-D field from the
c non-well-influenced fluid (co/csat) and the well fluid (cwell/csat).
c Values of co/csat as a function of time are given in the program by a
c previously-determined curve fit.  Values of cwell/csat(t) are calculated
c by an analytical solution given various inputs.  The velocity is
c determined by evaluating a given analytical function at nodal positions.
c Output of c/csat is only given for specified nodes.  There are 12,553
c nodes used in the following finite difference scheme.
c
c
c Section I:  Define input variables.
c
      implicit real*8(A-H, O-Z)
      real*8 c(12553),a2(12553),a3(12553),a4(12553),a5(12553)
      real*8 vy(12553),x(12553),y(12553),cold(12553),vx1(12553)
      real*8 vx(12553),xx(34),yy(21),cc(34,21)
      write(*,10)
      write(*,11)
 10   format(/,1x,'Enter the following values',/,'1. Well volume, vw, [cm3]',
     * / '2. Single membrane tube volume, vt, [cm2]', / ,'3. Average
     * seepage flowrate, qx, [cm/s]', / ,'4. Polymer-water partition
     * coefficient, pw, [d'less]',/,'5. Weight ratio polymer:water,
     * pl, [d'less]')
 11   format('6. Overall tube resistance, rt, [s/cm]',/,'7. Number of
     * membrane tubes, p2, [d'less]',/,'8. Single tube surface area, at,
     * [cm2]',/,'9. Domain width, domw, [cm]',/,'10. Domain length, doml,
     * [cm]',/,'11. Retardation coefficient, rd, [d'less]',/,
     * '12. Dispersion coefficient, x-direction, disx, [cm2/s]',/,
     * '13. Dispersion coefficient, y-direction, disy, [cm2/s]',/,
     * '14. Time step interval, tint, [s]',/,'15. Number of time steps,
     * instep, [d'less]',/,'16. Soil porosity, por, [d'less]',/,
     * '17. Well depth, dep, [cm]')
      read(*,*) vw,vt,qx,pw,pl,rt,p2,at,domw,doml,rd,disx,disy
      read(*,*) tint,instep,por,dep
c
c Section II:  Define x and y for each of the nodes and calculate vx, vy,
c              and nodal equation coefficients for each node.
c
      do 20 i1=1,93
      y(i1)=0.0
 20   continue
      do 22 i1=94,186
      y(i1)=1.0
 22   continue
      do 24 i1=187,279
      y(i1)=2.0
 24   continue
      do 26 i1=280,372
      y(i1)=3.0
 26   continue
      do 28 i1=373,465
      y(i1)=4.0
 28   continue
      do 30 i1=466,558
      y(i1)=5.0
 30   continue
      do 32 i1=559,651
      y(i1)=6.0
 32   continue
      do 34 i1=652,744
```

```
      y(i1)=7.0
34    continue
      do 36 i1=745,838
      y(i1)=8.0
36    continue
      do 38 i1=839,932
      y(i1)=9.0
38    continue
      do 40 i1=933,1026
      y(i1)=10.0
40    continue
      do 42 i1=1027,1120
      y(i1)=11.0
42    continue
      do 44 i1=1121,1214
      y(i1)=12.0
44    continue
      do 46 i1=1215,1309
      y(i1)=13.0
46    continue
      do 48 i1=1310,1404
      y(i1)=14.0
48    continue
      do 50 i1=1405,1499
      y(i1)=15.0
50    continue
      do 52 i1=1500,1595
      y(i1)=16.0
52    continue
      do 54 i1=1596,1691
      y(i1)=17.0
54    continue
      do 56 i1=1692,1788
      y(i1)=18.0
56    continue
      do 58 i1=1789,1885
      y(i1)=19.0
58    continue
      do 60 i1=1886,1983
      y(i1)=20.0
60    continue
      do 62 i1=1984,2081
      y(i1)=21.0
62    continue
      do 64 i1=2082,2180
      y(i1)=22.0
64    continue
      do 66 i1=2181,2280
      y(i1)=23.0
66    continue
      do 68 i1=2281,2381
      y(i1)=24.0
68    continue
      do 70 i1=2382,2483
      y(i1)=25.0
70    continue
      do 72 i1=2484,2589
      y(i1)=26.0
72    continue
      do 74 i1=2590,2695
      y(i1)=27.0
74    continue
      do 110 iy=28,120
      i1=2696 + (iy-28)*106
      i2=2801 + (iy-28)*106
      do 100 i3=i1,i2
```

```
      y(i3)=1.0*iy
  100 continue
  110 continue
c
c
      do 120 i1=0,94
      i2=2484+106*i1
      x(i2)=0.0
  120 continue
      do 122 i1=0,94
      i2=2485+106*i1
      x(i2)=2.0
  122 continue
      do 124 i1=0,94
      i2=2486+106*i1
      x(i2)=4.0
  124 continue
      do 126 i1=0,94
      i2=2487+106*i1
      x(i2)=6.0
  126 continue
      do 128 i1=0,94
      i2=2488+106*i1
      x(i2)=8.0
  128 continue
      do 130 i1=0,94
      i2=2489+106*i1
      x(i2)=10.0
  130 continue
      do 132 i1=0,94
      i2=2490+106*i1
      x(i2)=12.0
  132 continue
      do 134 i1=0,94
      i2=2491+106*i1
      x(i2)=14.0
  134 continue
      do 136 i1=0,94
      i2=2492+106*i1
      x(i2)=16.0
  136 continue
      do 138 i1=0,94
      i2=2493+106*i1
      x(i2)=18.0
  138 continue
      do 140 i1=0,94
      i2=2494+106*i1
      x(i2)=20.0
  140 continue
      do 142 i1=0,94
      i2=2495+106*i1
      x(i2)=22.0
  142 continue
      do 144 i1=0,94
      i2=2496+106*i1
      x(i2)=24.0
  144 continue
      do 146 i1=0,94
      i2=2497+106*i1
      x(i2)=26.0
  146 continue
      x(2382)=8.0
      x(2281)=10.0
      x(2383)=10.0
      x(2181)=12.0
      x(2282)=12.0
```

x(2384)=12.0
x(2082)=14.0
x(2182)=14.0
x(2283)=14.0
x(2385)=14.0
x(1886)=16.0
x(1985)=16.0
x(2083)=16.0
x(2183)=16.0
x(2284)=16.0
x(2386)=16.0
x(1692)=18.0
x(1789)=18.0
x(1887)=18.0
x(1986)=18.0
x(2084)=18.0
x(2184)=18.0
x(2285)=18.0
x(2387)=18.0
x(1500)=20.0
x(1596)=20.0
x(1693)=20.0
x(1790)=20.0
x(1888)=20.0
x(1987)=20.0
x(2085)=20.0
x(2185)=20.0
x(2286)=20.0
x(2388)=20.0
x(1215)=22.0
x(1310)=22.0
x(1405)=22.0
x(1501)=22.0
x(1597)=22.0
x(1694)=22.0
x(1791)=22.0
x(1889)=22.0
x(1988)=22.0
x(2086)=22.0
x(2186)=22.0
x(2287)=22.0
x(2389)=22.0
x(745)=24.0
x(839)=24.0
x(933)=24.0
x(1027)=24.0
x(1121)=24.0
x(1216)=24.0
x(1311)=24.0
x(1406)=24.0
x(1502)=24.0
x(1598)=24.0
x(1695)=24.0
x(1792)=24.0
x(1890)=24.0
x(1989)=24.0
x(2087)=24.0
x(2187)=24.0
x(2288)=24.0
x(2390)=24.0
x(1)=26.0
x(94)=26.0
x(187)=26.0
x(280)=26.0
x(373)=26.0
x(466)=26.0

```
      x(559)=26.0
      x(652)=26.0
      x(746)=26.0
      x(840)=26.0
      x(934)=26.0
      x(1028)=26.0
      x(1122)=26.0
      x(1217)=26.0
      x(1312)=26.0
      x(1407)=26.0
      x(1503)=26.0
      x(1599)=26.0
      x(1696)=26.0
      x(1793)=26.0
      x(1891)=26.0
      x(1990)=26.0
      x(2088)=26.0
      x(2188)=26.0
      x(2289)=26.0
      x(2391)=26.0
      do 220 ix=14,105
      do 202 i1=0,7
      i2=ix-12+i1*93
      x(i2)=2.0*ix
  202 continue
      do 204 i1=1,5
      i2=ix-13+652+i1*94
      x(i2)=2.0*ix
  204 continue
      do 206 i1=1,3
      i2=ix-13+1122+i1*95
      x(i2)=2.0*ix
  206 continue
      do 208 i1=1,2
      i2=ix-13+1407+i1*96
      x(i2)=2.0*ix
  208 continue
      do 210 i1=1,2
      i2=ix-13+1599+i1*97
      x(i2)=2.0*ix
  210 continue
      do 212 i=1,2
      i2=ix-13+1793+i1*98
      x(i2)=2.0*ix
  212 continue
      i2=ix-13+2088
      x(i2)=2.0*ix
      i2=ix-13+2188
      x(i2)=2.0*ix
      i2=ix-13+2289
      x(i2)=2.0*ix
      i2=ix-13+2391
      x(i2)=2.0*ix
      do 214 i=0,94
      i2=ix-13+2497+i1*106
      x(i2)=2.0*ix
  214 continue
  220 continue
c
c
c Calculate well radius, wr, [cm], x-direction interval, y-dir. interval
c
      wr=(2.6/12.0)*domw
      wr2=wr*wr
      xint=doml/105.0
      yint=domw/120.0
```

```
c
c Calc. vx(i) and vy(i), [cm/s]:
c
      do 250 i=1,12553
      vx1(i)=(x(i)*x(i)+y(i)*y(i))*wr2-2.0*y(i)*y(i)*wr2
      vx(i)=qx*(1+vx1(i)/(x(i)*x(i)+y(i)*y(i))**2.0)
      vy(i)=qx*(2.0*wr2*x(i)*y(i))/(x(i)*x(i)+y(i)*y(i))**2.0
c
c Calc. nodal equation coefficients:
c
      a2(i)=tint*disx/(rd*xint*xint)-tint*vx(i)/(rd*2.0*xint)
      a3(i)=tint*disx/(rd*xint*xint)+tint*vx(i)/(rd*2.0*xint)
      a4(i)=tint*disy/(rd*yint*yint)-tint*vy(i)/(rd*2.0*yint)
      a5(i)=tint*disy/(rd*yint*yint)+tint*vy(i)/(rd*2.0*yint)
 250  continue
      a1=1.0-2.0*tint*disx/(rd*xint*xint)-2.0*tint*disy/(rd*yint*yint)
c
c  Section III:  Nodal equations, time loop.  At each time step cwell and co
c  are calculated (these appear in boundary D1 equations).  Before time
c  stepping, set cold(i)=0.0 for each node (initial condition).
c
      do 260 i=1,12553
      cold(i)=0.0
 260  continue
      qwell=qx*por*dep*4.0*wr
c
c Time stepping:
c
      do 5000 itstep=1,instep
c
c Define time, t, [s], and nondimensional time, tau
c
      t = tint*itstep
      tau = t*qwell/vw
c
c Calculate well concentration at time t.  Also calculate Co(t) concentration
c (conc. at x=0 boundary away from well) at time t.
c
      a11=vt*qwell*rt*(1.0+p1*pw)/(p2*at)
      a22=vt*(1.0+p1*pw)*(1.0+rt*qwell/(p2*at))+vw/p2
      a33=vw/p2
      b22=0.000596*vw/qwell
      d11=((-1.0*a22/a11)+((a22/a11)**2.0-4.0*(a33/a11))**0.5)/2.0
      d22=((-1.0*a22/a11)-((a22/a11)**2.0-4.0*(a33/a11))**0.5)/2.0
      g11=(b22*a11-a33)/(b22*b22*a11-a22*b22+a33)
      a44=(g11*(b22+d22)+d22)/(d11-d22)
      a55=(g11*(b22+d11)+d11)/(d22-d11)
      term1=a44*exp(d11*tau)
      term2=a55*exp(d22*tau)
      term3=g11*exp(-1.0*b22*tau)
      cwell=term1+term2+term3+1.0
      co=1.0 - exp(-0.000596*t)
c
c Nodal equations.
c
c Governing equations for points IN boundary.
c
      do 310 i=95,185
      c1=a1*cold(i)+a2(i+1)*cold(i+1)+a3(i-1)*cold(i-1)
      c2=a4(i+93)*cold(i+93) +a5(i-93)*cold(i-93)
      c(i)=c1+c2
 310  continue
      do 312 i=188,278
      c1=a1*cold(i)+a2(i+1)*cold(i+1)+a3(i-1)*cold(i-1)
      c2=a4(i+93)*cold(i+93) +a5(i-93)*cold(i-93)
      c(i)=c1+c2
```

```
312  continue
     do 314 i=281,371
     c1=a1*cold(i)+a2(i+1)*cold(i+1)+a3(i-1)*cold(i-1)
     c2=a4(i+93)*cold(i+93) +a5(i-93)*cold(i-93)
     c(i)=c1+c2
314  continue
     do 316 i=374,464
      c1=a1*cold(i)+a2(i+1)*cold(i+1)+a3(i-1)*cold(i-1)
      c2=a4(i+93)*cold(i+93) +a5(i-93)*cold(i-93)
      c(i)=c1+c2
316  continue
     do 318 i=467,557
      c1=a1*cold(i)+a2(i+1)*cold(i+1)+a3(i-1)*cold(i-1)
      c2=a4(i+93)*cold(i+93) +a5(i-93)*cold(i-93)
      c(i)=c1+c2
318  continue
     do 319 i=560,650
     c1=a1*cold(i)+a2(i+1)*cold(i+1)+a3(i-1)*cold(i-1)
     c2=a4(i+93)*cold(i+93) +a5(i-93)*cold(i-93)
      c(i)=c1+c2
319  continue
     do 320 i=653,743
     c1=a1*cold(i)+a2(i+1)*cold(i+1)+a3(i-1)*cold(i-1)
     c2=a4(i+94)*cold(i+94) +a5(i-93)*cold(i-93)
      c(i)=c1+c2
320  continue
     do 330 i=746,837
     c1=a1*cold(i)+a2(i+1)*cold(i+1)+a3(i-1)*cold(i-1)
     c2=a4(i+94)*cold(i+94) +a5(i-94)*cold(i-94)
      c(i)=c1+c2
330  continue
     do 332 i=840,931
     c1=a1*cold(i)+a2(i+1)*cold(i+1)+a3(i-1)*cold(i-1)
     c2=a4(i+94)*cold(i+94) +a5(i-94)*cold(i-94)
      c(i)=c1+c2
332  continue
     do 334 i=934,1025
     c1=a1*cold(i)+a2(i+1)*cold(i+1)+a3(i-1)*cold(i-1)
     c2=a4(i+94)*cold(i+94) +a5(i-94)*cold(i-94)
      c(i)=c1+c2
334  continue
     do 336 i=1028,1119
     c1=a1*cold(i)+a2(i+1)*cold(i+1)+a3(i-1)*cold(i-1)
     c2=a4(i+94)*cold(i+94) +a5(i-94)*cold(i-94)
      c(i)=c1+c2
336  continue
     do 340 i=1122,1213
     c1=a1*cold(i)+a2(i+1)*cold(i+1)+a3(i-1)*cold(i-1)
     c2=a4(i+95)*cold(i+95) +a5(i-94)*cold(i-94)
      c(i)=c1+c2
340  continue
     do 350 i=1216,1308
     c1=a1*cold(i)+a2(i+1)*cold(i+1)+a3(i-1)*cold(i-1)
     c2=a4(i+95)*cold(i+95) +a5(i-95)*cold(i-95)
      c(i)=c1+c2
350  continue
     do 352 i=1311,1403
     c1=a1*cold(i)+a2(i+1)*cold(i+1)+a3(i-1)*cold(i-1)
     c2=a4(i+95)*cold(i+95) +a5(i-95)*cold(i-95)
      c(i)=c1+c2
352  continue
     do 354 i=1406,1498
     c1=a1*cold(i)+a2(i+1)*cold(i+1)+a3(i-1)*cold(i-1)
     c2=a4(i+96)*cold(i+96) +a5(i-95)*cold(i-95)
      c(i)=c1+c2
354  continue
```

```
      do 370 i=1501,1594
      c1=a1*cold(i)+a2(i+1)*cold(i+1)+a3(i-1)*cold(i-1)
      c2=a4(i+96)*cold(i+96) +a5(i-96)*cold(i-96)
       c(i)=c1+c2
370   continue
      do 380 i=1597,1690
      c1=a1*cold(i)+a2(i+1)*cold(i+1)+a3(i-1)*cold(i-1)
      c2=a4(i+97)*cold(i+97) +a5(i-96)*cold(i-96)
       c(i)=c1+c2
380   continue
      do 390 i=1693,1787
      c1=a1*cold(i)+a2(i+1)*cold(i+1)+a3(i-1)*cold(i-1)
      c2=a4(i+97)*cold(i+97) +a5(i-97)*cold(i-97)
       c(i)=c1+c2
390   continue
      do 400 i=1790,1884
      c1=a1*cold(i)+a2(i+1)*cold(i+1)+a3(i-1)*cold(i-1)
      c2=a4(i+98)*cold(i+98) +a5(i-97)*cold(i-97)
       c(i)=c1+c2
400   continue
      do 410 i=1887,1982
      c1=a1*cold(i)+a2(i+1)*cold(i+1)+a3(i-1)*cold(i-1)
      c2=a4(i+98)*cold(i+98) +a5(i-98)*cold(i-98)
       c(i)=c1+c2
410   continue
      do 420 i=1985,2080
      c1=a1*cold(i)+a2(i+1)*cold(i+1)+a3(i-1)*cold(i-1)
      c2=a4(i+99)*cold(i+99) +a5(i-98)*cold(i-98)
       c(i)=c1+c2
420   continue
      do 430 i=2083,2179
      c1=a1*cold(i)+a2(i+1)*cold(i+1)+a3(i-1)*cold(i-1)
      c2=a4(i+100)*cold(i+100) +a5(i-99)*cold(i-99)
       c(i)=c1+c2
430   continue
      do 440 i=2182,2279
      c1=a1*cold(i)+a2(i+1)*cold(i+1)+a3(i-1)*cold(i-1)
      c2=a4(i+101)*cold(i+101) +a5(i-100)*cold(i-100)
       c(i)=c1+c2
440   continue
      do 450 i=2282,2380
      c1=a1*cold(i)+a2(i+1)*cold(i+1)+a3(i-1)*cold(i-1)
      c2=a4(i+102)*cold(i+102) +a5(i-101)*cold(i-101)
       c(i)=c1+c2
450   continue
      do 460 i=2383,2482
      c1=a1*cold(i)+a2(i+1)*cold(i+1)+a3(i-1)*cold(i-1)
      c2=a4(i+106)*cold(i+106) +a5(i-102)*cold(i-102)
       c(i)=c1+c2
460   continue
      do 470 i=2488,2588
      c1=a1*cold(i)+a2(i+1)*cold(i+1)+a3(i-1)*cold(i-1)
      c2=a4(i+106)*cold(i+106) +a5(i-106)*cold(i-106)
      c(i)=c1+c2
470   continue
      do 480 i=2591,2694
      c1=a1*cold(i)+a2(i+1)*cold(i+1)+a3(i-1)*cold(i-1)
      c2=a4(i+106)*cold(i+106) +a5(i-106)*cold(i-106)
       c(i)=c1+c2
480   continue
      do 510 j=1,92
      j1=2591+106*j
      j2=2694+106*j
      do 500 i=j1,j2
      c1=a1*cold(i)+a2(i+1)*cold(i+1)+a3(i-1)*cold(i-1)
      c2=a4(i+106)*cold(i+106) +a5(i-106)*cold(i-106)
```

```
      c(i)=c1+c2
  500 continue
  510 continue


c
c Governing equs. for points ON boundary:
c
      c(1)=cwell
      c(94)=cwell
      c(187)=cwell
      c(280)=cwell
      c(373)=cwell
      c(466)=cwell
      c(559)=cwell
      c(652)=cwell
      c(745)=cwell
      c(839)=cwell
      c(933)=cwell
      c(1027)=cwell
      c(1121)=cwell
      c(1215)=cwell
      c(1310)=cwell
      c(1405)=cwell
      c(1500)=cwell
      c(1596)=cwell
      c(1692)=cwell
      c(1789)=cwell
      c(1886)=cwell
      c(1984)=cwell
      c(2082)=cwell
      c(2182)=cwell
      c(2281)=cwell
      c(2382)=cwell
      c(2487)=cwell
      c(2486)=cwell
      c(2485)=cwell
      c(2484)=cwell
      do 515 i=0,93
      i1=2590+106*i
      c(i1)=co
  515 continue
      do 520 i=12449,12552
      c1=a1*cold(i)+a2(i+1)*cold(i+1)+a3(i-1)*cold(i-1)
      c2=a4(i-106)*cold(i-106) +a5(i-106)*cold(i-106)
       c(i)=c1+c2
      c1=a1*cold(12553)+(a2(12553)+a3(12553))*cold(12552)
      c2=(a4(12477)+a5(12477))*cold(12477)
      c(12553)=c1+c2
  520 continue
      do 530 i=2,92
      c1=a1*cold(i)+a2(i+1)*cold(i+1)+a3(i-1)*cold(i-1)
      c2=a4(i+93)*cold(i+93) +a5(i+93)*cold(i+93)
       c(i)=c1+c2
  530 continue
      c1=a1*cold(186)+a2(186-1)*cold(186-1)+a3(186-1)*cold(186-1)
      c2=a4(186+93)*cold(186+93) +a5(186-93)*cold(186-93)
       c(186)=c1+c2
      c1=a1*cold(279)+a2(279-1)*cold(279-1)+a3(279-1)*cold(279-1)
      c2=a4(279+93)*cold(279+93) +a5(279-93)*cold(279-93)
       c(279)=c1+c2
      c1=a1*cold(372)+a2(372-1)*cold(372-1)+a3(372-1)*cold(372-1)
      c2=a4(372+93)*cold(372+93) +a5(372-93)*cold(372-93)
       c(372)=c1+c2
      c1=a1*cold(465)+a2(465-1)*cold(465-1)+a3(465-1)*cold(465-1)
      c2=a4(465+93)*cold(465+93) +a5(465-93)*cold(465-93)
```

```
 c(465)=c1+c2
c1=a1*cold(558)+a2(558-1)*cold(558-1)+a3(558-1)*cold(558-1)
c2=a4(558+93)*cold(558+93) +a5(558-93)*cold(558-93)
 c(558)=c1+c2
c1=a1*cold(651)+a2(651-1)*cold(651-1)+a3(651-1)*cold(651-1)
c2=a4(651+93)*cold(651+93) +a5(651-93)*cold(651-93)
 c(651)=c1+c2
c1=a1*cold(744)+a2(744-1)*cold(744-1)+a3(744-1)*cold(744-1)
c2=a4(744+94)*cold(744+94) +a5(744-93)*cold(744-93)
 c(744)=c1+c2
c1=a1*cold(838)+a2(838-1)*cold(838-1)+a3(838-1)*cold(838-1)
c2=a4(838+94)*cold(838+94) +a5(838-94)*cold(838-94)
 c(838)=c1+c2
c1=a1*cold(932)+a2(932-1)*cold(932-1)+a3(932-1)*cold(932-1)
c2=a4(932+94)*cold(932+94) +a5(932-94)*cold(932-94)
 c(932)=c1+c2
c1=a1*cold(1026)+a2(1026-1)*cold(1026-1)+a3(1026-1)*cold(1026-1)
c2=a4(1026+94)*cold(1026+94) +a5(1026-94)*cold(1026-94)
 c(1026)=c1+c2
c1=a1*cold(1120)+a2(1120-1)*cold(1120-1)+a3(1120-1)*cold(1120-1)
c2=a4(1120+94)*cold(1120+94) +a5(1120-94)*cold(1120-94)
 c(1120)=c1+c2
c1=a1*cold(1214)+a2(1214-1)*cold(1214-1)+a3(1214-1)*cold(1214-1)
c2=a4(1214+95)*cold(1214+95) +a5(1214-94)*cold(1214-94)
 c(1214)=c1+c2
c1=a1*cold(1309)+a2(1309-1)*cold(1309-1)+a3(1309-1)*cold(1309-1)
c2=a4(1309+95)*cold(1309+95) +a5(1309-95)*cold(1309-95)
 c(1309)=c1+c2
c1=a1*cold(1404)+a2(1404-1)*cold(1404-1)+a3(1404-1)*cold(1404-1)
c2=a4(1404+95)*cold(1404+95) +a5(1404-95)*cold(1404-95)
 c(1404)=c1+c2
c1=a1*cold(1499)+a2(1499-1)*cold(1499-1)+a3(1499-1)*cold(1499-1)
c2=a4(1499+96)*cold(1499+96) +a5(1499-95)*cold(1499-95)
 c(1499)=c1+c2
c1=a1*cold(1595)+a2(1595-1)*cold(1595-1)+a3(1595-1)*cold(1595-1)
c2=a4(1595+96)*cold(1595+96) +a5(1595-96)*cold(1595-96)
 c(1595)=c1+c2
c1=a1*cold(1691)+a2(1691-1)*cold(1691-1)+a3(1691-1)*cold(1691-1)
c2=a4(1691+97)*cold(1691+97) +a5(1691-96)*cold(1691-96)
 c(1691)=c1+c2
c1=a1*cold(1788)+a2(1788-1)*cold(1788-1)+a3(1788-1)*cold(1788-1)
c2=a4(1788+97)*cold(1788+97) +a5(1788-97)*cold(1788-97)
 c(1788)=c1+c2
c1=a1*cold(1885)+a2(1885-1)*cold(1885-1)+a3(1885-1)*cold(1885-1)
c2=a4(1885+98)*cold(1885+98) +a5(1885-97)*cold(1885-97)
 c(1885)=c1+c2
c1=a1*cold(1983)+a2(1983-1)*cold(1983-1)+a3(1983-1)*cold(1983-1)
c2=a4(1983+98)*cold(1983+98) +a5(1983-98)*cold(1983-98)
 c(1983)=c1+c2
c1=a1*cold(2081)+a2(2081-1)*cold(2081-1)+a3(2081-1)*cold(2081-1)
c2=a4(2081+99)*cold(2081+99) +a5(2081-98)*cold(2081-98)
 c(2081)=c1+c2
c1=a1*cold(2180)+a2(2180-1)*cold(2180-1)+a3(2180-1)*cold(2180-1)
c2=a4(2180+100)*cold(2180+100) +a5(2180-99)*cold(2180-99)
 c(2180)=c1+c2
c1=a1*cold(2280)+a2(2280-1)*cold(2280-1)+a3(2280-1)*cold(2280-1)
c2=a4(2280+101)*cold(2280+101) +a5(2280-100)*cold(2280-100)
 c(2280)=c1+c2
c1=a1*cold(2381)+a2(2381-1)*cold(2381-1)+a3(2381-1)*cold(2381-1)
c2=a4(2381+102)*cold(2381+102) +a5(2381-101)*cold(2381-101)
 c(2381)=c1+c2
c1=a1*cold(2483)+a2(2483-1)*cold(2483-1)+a3(2483-1)*cold(2483-1)
c2=a4(2483+106)*cold(2483+106) +a5(2483-102)*cold(2483-102)
 c(2483)=c1+c2
c1=a1*cold(2589)+a2(2589-1)*cold(2589-1)+a3(2589-1)*cold(2589-1)
c2=a4(2589+106)*cold(2589+106) +a5(2589-106)*cold(2589-106)
```

```
       c(2589)=c1+c2
      c1=a1*cold(2695)+a2(2695-1)*cold(2695-1)+a3(2695-1)*cold(2695-1)
      c2=a4(2695+106)*cold(2695+106) +a5(2695-106)*cold(2695-106)
       c(2695)=c1+c2
      do 550 j=1,92
      j1=2695+106*j
      c1=a1*cold(j1)+a2(j1-1)*cold(j1-1)+a3(j1-1)*cold(j1-1)
      c2=a4(j1+106)*cold(j1+106) +a5(j1-106)*cold(j1-106)
       c(j1)=c1+c2
 550  continue
c
c Put new calcs. into cold:
c
      do 1000 i=1,12553
      cold(i)=c(i)
 1000 continue
c
c End of time step.
c
 5000 continue
c
c Section IV: Writing out solution at selected nodes.
c
c Define cwell points (not in boundary but in well).
       cc(1,1)=cwell
       cc(1,2)=cwell
       cc(1,3)=cwell
       cc(1,4)=cwell
       cc(1,5)=cwell
       cc(2,1)=cwell
       cc(2,2)=cwell
       cc(2,3)=cwell
       cc(2,4)=cwell
       cc(2,5)=cwell
       cc(3,1)=cwell
       cc(3,2)=cwell
       cc(3,3)=cwell
       cc(3,4)=cwell
       cc(4,1)=cwell
       cc(4,2)=cwell
       cc(4,3)=cwell
       cc(5,1)=cwell
       cc(5,2)=cwell
       do 6100 i=0,33
       xx(i+1)=i*6.0
 6100  continue
       do 6110 i=0,20
       yy(i+1)=i*6.0
 6110  continue
       do 6120 i=0,28
       j=3+i*3
       cc(i+6,1)=c(j)
 6120  continue
       do 6130 i=0,28
       j=561+i*3
       cc(i+6,2)=c(j)
 6130  continue
       do 6140 i=0,29
       j=1121+i*3
       cc(i+5,3)=c(j)
 6140  continue
       do 6150 i=0,30
       j=1692+i*3
       cc(i+4,4)=c(j)
 6150  continue
       do 6160 i=0,31
```

```
      j=2282+i*3
      cc(i+3,5)=c(j)
 6160 continue
      do 6170 i=0,33
      j=2908+i*3
      cc(i+1,6)=c(j)
 6170 continue
      ib=0
      do 6190 ii=1,15
      ib=ib+636
      do 6180 i=0,33
      j=ib+2908+i*3
      cc(i+1,6+ii)=c(j)
 6180 continue
 6190 continue
c
c Write out solution
c
      do 6400 i=1,21
      ii=22-i
      write(6,6350)(cc(j,ii),j=1,34)
 6350 format(/,34(1x,f8.6,2x))
 6400 continue
      do 6500 i=1,21
      write(6,6450)(cc(j,i),j=1,34)
 6450 format(/,34(1x,f8.6,2x))
 6500 continue
      end
```

11. References

Ackerman, D. G., **Destruction and Disposal of PCB's by Thermal and Nonthermal Methods**, Noyes Data Corporation: Park Ridge, N.J., 1983.

Anderson, Mary P., "Using Models to Simulate the Movement of Contaminants Through Groundwater Flow Systems," **CRC Critical Reviews in Environmental Control**, Chemical Rubber Company: Cleveland, Ohio, 1979, pp.97-156.

Bakr, Adel A.; Gelhar, Lynn W.; Gutjahr, Allan L.; and MacMillan, John R., "Stochastic Analysis of Spatial Variability in Subsurface Flows: 1. Comparison of One- and Three-Dimensional Flows," **Water Resources Research**, Vol. 14, No. 2, 1978, pp.263-271.

Baltus, R. E. and Anderson, J. L., "Hindered Diffusion of Ashpaltenes Through Microporous Membranes," **Chem. Eng. Sci.**, Vol. 38, 1983, p.1959.

Bear, Jacob, **Dynamics of Fluids in Porous Media**, Dover Publishers: New York, N. Y., 1972.

Beck, R. E. and Schultz, J. S., "Hindrance of Solute Diffusion Within Membranes as Measured with Microporous Membranes of Known Pore Geometry," **Biochim. Biophys. Acta**, Vol. 255, 1972, p.273.

Bitter, J. G. A., **Transport Mechanisms in Membrane Separation Processes**, Plenum Press: New York N. Y., 1991, p.4.

Bird, R. B.; Stewart, W. E.; and Lightfoot, E. N., **Transport Phenomena**, John Wiley and Sons: New York, N. Y., 1960.

Bohon, Robert L. and Claussen, W. F., "The Solubility of Aromatic Hydrocarbons in Water," **JACS**, Vol. 73, 1951, pp.1571-1578.

Bohrer, M. P.; Patterson, G. D.; and Caroll, P. J., "Hindered Diffusion of Dextran

and Ficoll in Microporous Membranes," **Macromolecules**, Vol. 17, 1984, p. 1170.

Breton, M., **Treatment Technologies for Solvent Containing Wastes**, Noyes Data Corporation: Park Ridge, N. J., 1988.

Brink, L. E. S. and Romijn, D. J., "Reducing the Protein Fouling of Polysulfone Surfaces and Polysulfone Ultrafiltration Membranes: Optimization of the Type of Presorbed Layer," **Desalination**, Vol. 71, 1990, pp.209-233.

Bungay, P. M. and Brenner, H., "The Motion of a Closely Fitting Sphere in a Fluid-Filled Tube," **Int. J. of Multiphase Flow**, 1973, p.25.

Carberry, James J., **Chemical and Catalytic Reaction Engineering**, McGraw Hill: New York, N. Y., 1976, pp.364-366.

Cline, Patricia V.; Delfino, Joseph J.; and Rao, P. S. C., "Partitioning of Aromatic Constituents into Water from Gasoline and Other Complex Solvent Mixtures," **Env. Sci. Tech.**, Vol. 25, 1991, pp. 914-920.

Codell, R. B.; Key, K. T.; and Whelan, G., **A Collection of Mathematical Models for Dispersion in Surface Water and Groundwater**, U. S. Nuclear Regulatory Commission, Paper No. NWREG-0868, 1982.

Cotruvo, Joseph A. and Vogt, Craig D., "Rationale for Water Quality Standards and Goals," in Pontius, F. W., ed, **Water Quality and Treatment**, 4th ed., McGraw-Hill, Inc.: New York, N. Y., 1990, pp.1-62.

Crawford, Mark, "DOE Calls in the Labs for Defense Waste Cleanup," **Science**, Vol. 246, 1989, pp.24-25.

Deen, W. M.; Bohrer, M.P.; and Epstein, N.B., "Effects of Molecular Size and Configuration on Diffusion in Microporous Membranes," **AIChE Journal**, Vol. 27, 1981, p.952.

Edwards, D. A.,; Luthy, R. G.; Liu, Z., "Solubilization of Polycyclic Aromatic

Hydrocarbons in Micellar Nonionic Surfactant Solutions," **Env. Sci. Tech.**, Vol. 25, 1991, pp.127-133.

Fessenden, R. J. and Fessenden, J. S., **Organic Chemistry**, 3rd ed., Wadsworth, Inc.: Monterey, California, 1986.

Freeze, R. Allan and Cherry, John A., **Groundwater**, Prentice Hall, Inc.: Englewood Cliffs, N.J., 1979.

Gelhar, Lynn W.; Gutjahr, Allan L.; and Naff, Richard L., "Stochastic Analysis of Macrodispersion in a Stratified Aquifer," **Water Resources Research**, Vol. 15, No. 6, 1979, pp.1387-1397.

Grane, F. E. and Gardner, G. H. F., "Measurements of Transverse Dispersion in Granular Media," **Journal of Chemical and Engineering Data**, Vol. 6, No. 2, 1961, pp.283-287.

Haggin, Joseph, "Membrane Technology Has Achieved Success, Yet Lags Potential," **Chemical and Engineering News**, Oct. 1, 1990, pp.22-26.

Hansch, C. and Leo, A., **Substituent Constants for Correlation Analysis in Chemistry and Biology**, Wiley: New York, N. Y., 1979.

Hatton, T. A. and Lightfoot, E. N., "On the Significance of the Dispersion Coefficient in Two-Phase Flow," **Chemical Engineering Science**, Vol. 37, No. 9, 1982, pp.1289-1307.

Houghton, Patrick A. and Hatton, T. Alan, "Transient Effects in the Description of Axial Dispersion in Polydisperse Two-phase Systems," **Physico-Chemical Hydrodynamics**, Vol. 11, No. 2, 1989, pp.129-166.

Hurter, P. N. and Hatton, T. A., "Solubilization of Polycyclic Aromatic Hydrocarbons by Poly(ethylene oxide-propylene oxide) Block Copolymer Micelles: Effects of Polymer Structure," **Langmuir**, Vol. 8, 1992, pp.1291-1299.

James, Stephen C. and Sanning, Donald E., "Summary of the NATO/CCMS Conference: The Demonstration of Remedial Action Technologies for Contaminated Land and Groundwater, " **JAPCA**, Vol. 39, No. 9, 1989, pp.1178-1184.

Kakac, S. and Yener, Y., **Heat Conduction**, Hemisphere Publishing Corp.: Washington, D. C., 1985.

Karickoff, Samuel W.; Brown, David S.; and Scott, Trudy A., "Sorption of Hydrophobic Pollutants on Natural Sediments," **Water Research**, Vol. 13, 1979, pp.241-248.

Lageman, Reinout; Pool, Wieberent; and Seffinga, Geert, "Electro-Reclamation: Theory and Practice," **Chemistry and Industry**, Sept. 1989, pp.597-602.

Lion, Leonard W.; Stauffer, Thomas B.; and MacIntyre, William G., "Sorption of Hydrophobic Compounds on Aquifer Materials: Analysis Methods and the Effect of Organic Carbon," **Journal of Contaminant Hydrology**, Vol. 5, 1990, pp.215-234.

Lyman, W. J.; Reehl, W. F.; and Rosenblatt, D. H., **Handbook of Chemical Property Estimation Methods**, American Chemical Society: Washington, D. C., 1990.

Mackay, Douglas M. and Cherry, John A., "Groundwater Contamination: Pump-and-treat Remediation," **Environmental Science and Technology**, Vol. 23, No. 6, 1989, pp.630-636.

Mackay, D. and Medir, M., "Industrial Effluent Treatment (Nonmetals)," in **Handbook of Solvent Extraction**, John Wiley and Sons: New York, N.Y., 1983.

Magee, Brian R.; Lion, Leonard W.; and Lemley, Ann T., "Transport of Dissolved Organic Macromolecules and Their Effect on the Transport of Phenanthrene in Porous Media," **Environmental Science and Technology**, Vol. 25, 1991, pp.323-331.

Malone, D. M. and Anderson, J. L., "Hindered Diffusion of Particles Through Small Pores," **Chem. Eng. Sci.**, Vol. 33, 1978, p.1429.

May, Willie E.; Wasik, Stanley P.; and Freeman, David H., "Determination of the Solubility Behavior of Some Polycyclic Aromatic Hydrocarbons in Water," **Analytica Chemistry**, Vol. 50, 1978, pp.997-1000.

Modell, M. and Reid, R. C., **Thermodynamics and Its Applications**, 2nd ed., Prentice-Hall, Inc.: Englewood Cliffs, N. J., 1983.

Molyneaux, P., **Water Soluble Synthetic Polymers: Properties and Behavior, Volume 1**, CRC Press, Inc.: Boca Raton, Florida, 1984, p.146.

Nystrom, Marianne, "Fouling of Unmodified and Modified Polysulfone Ultrafiltration Membranes by Ovalbumin," **Journal of Membrane Science**, Vol. 44, 1989, pp.183-196.

Patterson, D.; Tewari, Y. B.; Schreiber, H. P.; and Guillet, J. E., "Application of Gas-Liquid Chromatography to the Thermodynamics of Polymer Solutions," **Macromolecules**, Vol. 4, 1971, pp. 356-359.

Prausnitz, J. M.; Lichtenthaler, R. N.; and deAzevedo, E. G., **Molecular Thermodynamics of Fluid-Phase Equilibrium**, Prentice-Hall, Inc.: Englewood Cliffs, N. J., 1986.

Renaud, P. C. and Probstein, R. F., "Electoosmotic Control of Toxic Wastes," **J. PhysicoChemical Hydrodynamics**, Vol. 9, 1987, pp. 345-360.

Robertson, Bruce C. and Zydney, Andrew L., "Hindered Protein Diffusion in Asymmetric Ultrafiltration Membranes with Highly Constricted Pores," **Journal of Membrane Science**, Vol. 49, 1990, pp. 287-303.

Ryan, C. R., "Slurry Cut-off Walls Methods and Applications," Geo-Con, Inc.: Pittsburgh, PN, March 1980.

Schwarzenbach, Rene P. and Westall, John, "Transport of Nonpolar Organic Compounds from Surface Water to Groundwater. Laboratory Sorption Studies," **Environmental Science and Technology**, Vol. 15, 1981, pp. 1360-1367.

Scientific Polymer Products, Inc., 1991 Price List, Ontario, New York.

Spooner, Philip A.; Wetzel, Roger S.; and Grube, Walter E. Jr., **Management of Uncontrolled Hazardous Waste Site**, Hazardous Materials Control Research Institute: Silver Springs, Maryland, 1982, pp.191-197.

Staps, Sjef, "Biorestoration of Contaminated Soil and Groundwater," **Chemistry and Industry**, 1989, p.588.

Stephenson, R. M. and Malanowski, S., **Handbook of the Thermodynamics of Organic Compounds**, Elsevier Science Publishing Co., Inc.: New York, N. Y., 1987.

Streeter, Victor L. and Wylie, E. Benjamin, **Fluid Mechanics**, 8th ed., McGraw Hill: New York, N. Y., 1985.

Tester, J. W.; Holgate, H. R.; Armellini, F. J.; Webley, P. A.; Killilea, W. R.; Barner, H. E.; Hong, G. T., **Supercritical Water Oxidation Technology: A Review of Process Development and Fundamental Research,** In **Emerging Technologies in Hazardous Waste Management III;** Tedder, D. W. and Pohland, F. G., eds., No. 518, ACS Symposium Series, American Chemical Society: Washington, D. C., 1993.

Thomas, E. R.; Newman, B. A.; Long, T. C.; Wood, D. A.; Eckert, C. A., "Limiting Activity Coefficients of Nonpolar and Polar Solutes in Both Volatile and Nonvolatile Solvents by Gas Chromatography," **J. Chem. Eng. Data,** Vol. 27, 1982, p.399.

Tolman, A. L. et al., "Guidance Manual for Minimizing Pollution from Work Disposal Sites," EPA-60012-78-142, U.S. Environmental Protection Agency: Cincinnati, Ohio, August 1978.

Treybal, R. E., **Mass Transfer Operations**, McGraw Hill: New York N. Y., 1987.

Valsaraj, K. T. and Thibodeaux, L. J., "Relationships Between Micelle-Water and Octanol-Water Partition Constants for Hydrophobic Organics of Environmental Interest," **Water Research**, Vol. 23, 1989, pp.183-189.

Volk, William, **Applied Statistics for Engineers**, McGraw-Hill: New York, N. Y., 1958.

Wauchope, R. Donald and Getzen, Forrest W., "Temperature Dependence of Solubilities in Water and Heats of Fusion of Solid Aromatic Hydrocarbons," **J. Chem. Eng. Data**, Vol. 17, 1972, pp.38-41.

Wong, H. J. and Quinn, J. A., "Hindered Diffusion of Macromolecules in Track-Etched Membranes," in **Colloid and Interface Science, Vol. 5**, M. Kerker, ed., Academic Press: New York, N.Y., 1976, p.169.